A STUDY OF THE STRUCTURE, PROPERTIES AND SYNTHESIS OF BLOCK COPOLYMERS.

by

A.S. TAN

Supervisor:

Dr. R.E. WETTON

Submitted for the Degree of Doctor of Philosophy
of Loughborough University of Technology.

December, 1970. Department of Chemistry.

ACKNOWLEDGEMENTS

The author wishes to express his gratitude to: Dr. R.E. Wetton for supervising this work and for his help and encouragement throughout, Professor R.F. Phillips for providing the facilities, The Malayan Rubber Fund Board for the award of a Research Scholarship.

The author also wishes to thank Mr. A.G. Thomas and Mr. C.J. Derham for valuable discussions concerning the research work carried out during a six month visit in 1969 to the Natural Rubber Producers Research Association, Welwyn Garden City, Herts.

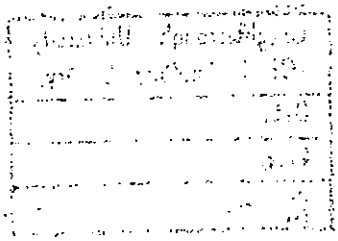

ORIGINALITY

All the work presented in this thesis has been carried out by the author, except where otherwise acknowledged and has not previously been presented for a degree at this University or any other institution.

ABSTRACT

The mechanical properties of a styrene-butadiene-styrene block copolymer (Shell Cariflex K101) have been found to be dependent upon the morphology of the polymer, which could be altered by thermal or solvent treatments. Films cast from toluene, methylene chloride and methyl cyclohexane and moulded samples are compared.

Small angle X-ray scattering, electron microscopic and swelling techniques have been used to determine the morphology of the samples. Macro-lattice models based on the microphase separation of the two chemical species into domains and matrix have been proposed for the toluene and methylene chloride cast samples.

Properties which have been found to differ are the dynamic mechanical spectra, stress-strain behaviour, stress relaxation and creep. The dynamic mechanical apparatus as described by Bowman (161) has been improved and modified and has been used to measure the Young's moduli and loss tangent of the samples over a wide temperature (-150 to +120^{o}C) and frequency range (0·01 to 1000 Hz).

The network characteristic of this system has been attributed to the entanglements of the polybutadiene chains, the physical adsorption of the polybutadiene chains onto the domain surface and the polybutadiene-polystyrene junctions. The ultimate properties have been shown to be those of the rubbery matrix but are highly enhanced by the polystyrene domains acting as reinforcing fillers.

Preliminary work has been carried out in the synthesis of the XYX type of block copolymer where X is a crystalline segment (Poly 3,3-bis(chloromethyl) oxetane) and Y is an elastomeric segment (tetrahydrofuran/3,3-bis(chloromethyl) oxetane copolymer.)

CONTENTS

CHAPTER 1. INTRODUCTION.

1.1. DEVELOPMENT OF COMMERCIAL BLOCK COPOLYMERS

The earlier work on block copolymers had centered on design of materials with novel or improved mechanical properties and an extensive literature (1-3) on the preparation and characterization of block copolymers developed. In terms of commercial success, the return has been meagre in comparison to many other areas of endeavour. This was partly due to inherent synthetic difficulties, but probably also because no major physical property improvement over simple polymer blends had been observed. The block copolymers had been synthesized by a variety of ionic and free radical reactions induced by heat, catalysts, radiations and mechanical stressing. These older methods of preparation are often inefficient and give block copolymers in low yields, accompanied by large amounts of homopolymers. Fractionation of these mixtures, even in analytical quantities, is difficult, often impossible.

The development of anionic polymerization techniques, particularly with living systems, was the first breakthrough in the synthesis of block copolymers. (4,5). Anionic methods and organometallic methods (6-8) of polymerization are now widely applied to block copolymer synthesis. Although these new methods are not without unsolved problems, mainly because they require starting materials of extreme purity, they have the potential of overcoming the two major deficiencies of previous methods of preparation: low yield and undefined structure.

The molecules of block copolymers consist of two or more chemically dissimilar segments, covalently bonded end to end. The latter feature distinguishes them from graft copolymers. Each segment or block is usually a long sequence of units of a single monomer (A or B or C etc.), but it may also be a long sequence of randomly copolymerized units (A plus B or C etc.). Therefore even with only two monomers, A and B, there can be many combinations, some of which are given below.

A - B	AAAAAAAA - BBBBBBBB
A/B - B	AABAAABBA - BBBBBBBB
A - B - A	AAAAAA - BBBBBB - AAAAAA
A - A/B - A	AAAAAA - BAABBBAA - AAAAAA
B - A - B	BBBBBB - AAAAAA - BBBBBB
B - A/B - B	BBBBBB - AABABBAAB - BBBBBB
$(A - B)_n$	-AAAAA - BBBBB - AAAAA - BBBBB - AAAAA - BBBBB -

In the last type $(A - B)_n$, as the block length becomes smaller and smaller the polymer becomes more nearly a kind of alternating copolymer.

It was the discovery of the thermoplastic elastomers (9) that spurred intensive work in the block copolymer field. The thermoplastic elastomers are novel in that they can be processed as thermoplastics at elevated temperatures, while at ambient temperatures, they exhibit most of the useful properties of vulcanized rubber without any chemical vulcanization (10). These materials are triblocks of the type A - B - A, where A is a thermoplastic block polymer and B is an elastomeric block polymer. Choice of monomers, block length, and the weight fraction of A and B are crucial in achieving elastomeric performance.

Thermoplastic elastomers can best be appreciated as a class when the properties are placed in the context of those of other polymeric materials. Such materials can be characterized as either thermosetting or thermoplastic and also as either hard, flexible or rubbery. As shown in Fig. 1.1. of the six classes, the first five are well known. Thermoplastic elastomers constitute the sixth class.

FIG. 1.1. Classification of Polymers

	Thermosetting	Thermoplastic
Rigid	Epoxy Phenol-formaldehyde Hard rubber	Polystyrene Polyvinyl Chloride Polypropylene
Flexible	Highly loaded and/or Highly vulcanized rubbers	Polyethylene Plasticized PVC Ethylene-vinyl acetate copolymer
Rubbery	Vulcanized rubbers (Natural rubber, polyisoprene, styrene- butadiene rubber)	Thermoplastic elastomers

In the past few years, most of the attention in block copolymers has been confined to those of styrene and butadiene or isoprene, because these block copolymers have found commercial applications.

They are marketed by the Shell Chemical Company under the trade names THERMOLASTIC and KRATON (11,12). However there are many other block copolymers that have created theoretical as well as commercial interest. (13).

Copper and co-workers (14-17) published recently a series of papers on the physical behaviour of SPANDEX and ESTANE urethane elastomers. (18,19). These poly(ester - urethane) elastomers have been shown to be segmented linear polymers with two glass transitions and to behave like filled crosslinked rubbers.

The poly(ethylene oxide) - polystyrene - poly(ethylene oxide) block copolymers display marked differences in the properties and behaviour of the individual components. While poly(ethylene oxide) is crystallizable, polar and hydrophilic; polystyrene is glassy, non-polar and hydrophobic. Because of their hydrophilic-hydrophobic nature, these materials can be regarded as "macromolecular surfactants" (20-22).

A thermoplastic elastomer with a higher use temperature has been obtained by replacing the polystyrene blocks with poly α-methylstyrene blocks in the polystyrene-polyisoprene - polystyrene copolymer. (23,24).

Alternating block copolymers having the structure $(A-B)_n$, where A is a polycarbonate and B is a polyether have been prepared and found to be both thermoplastic and elastomeric. (25-27). These block copolymers contain either crystalline units or bulky three-dimensional polycyclic groups in the hard segment, which act as crosslinks for the elastomers.

Other block copolymers that have been synthesized, include those based on ethylenic monomers-propylene sulphide, siloxane and cyclic imino-ethers. (13,28).

1.2. STRUCTURAL PARAMETERS OF THERMOPLASTIC ELASTOMERS

A block copolymer of the type A-B-A where A is a thermoplastic segment and B is an elastomeric segment forms a stable network. This structural formation is due to the phase separation of the two dissimilar polymers into glassy domains of A segments, dispersed in the elastomeric matrix. The glassy domains act as multiple crosslinks and fillers for the elastomeric chains. Above the softening temperature of the thermoplastic segment, the system becomes a viscoelastic fluid and thus may be processed like any conventional thermoplastic. On cooling, it behaves like a rubber vulcanizate again, and the thermal cycle can be repeated indefinitely.

An uncrosslinked, amorphous polymer will show dynamic modulus-temperature behaviour as depicted in curve A of Fig. 1.2. The drop of a factor of 10^3 in modulus through the glass transition, Tg, is typical of linear amorphous polymer. The rubbery plateau region (10^6-10^7 dynes/cm^2) is sensitive to the molecular weight of the polymer and to crosslinking which extends it to higher temperatures (curve B.). Semi-crystalline polymers, for which data are shown as curve C, generally have a very high plateau modulus above Tg which extends to the melting point, Tm, of the crystallites. The region between Tg and Tm possesses high impact strength and high rigidity.

A thermoplastic elastomer displays glass transitions at two temperatures, corresponding to the Tg for the respective homopolymers. The dynamic modulus-temperature curve (D) exhibits a two-step feature analogous to that of a semicrystalline polymer. However, the modulus in the plateau region of a useful thermoplastic elastomer is generally close to the modulus of the rubbery region of a conventional vulcanizate.

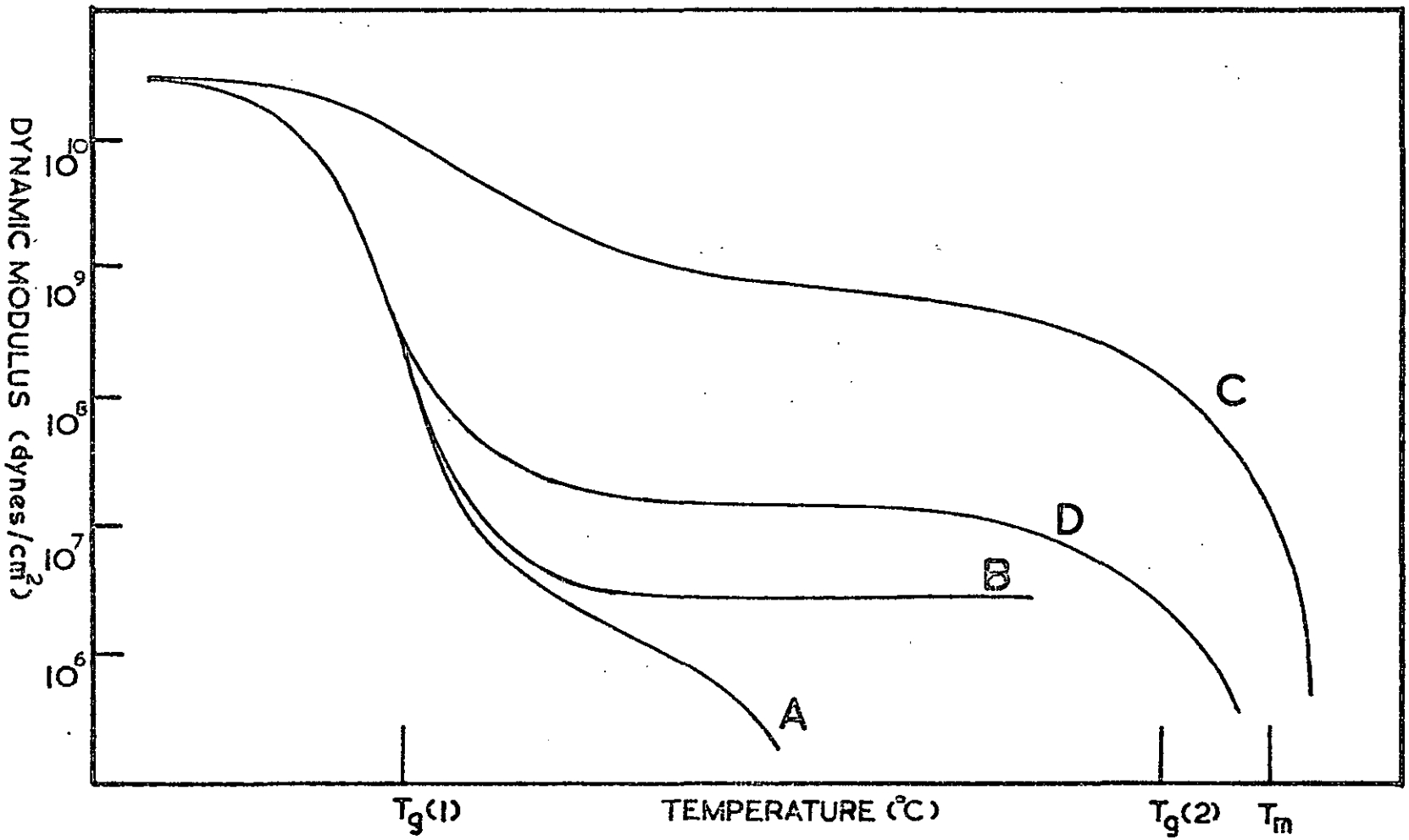
DYNAMIC MODULUS (dynes/cm²)
10⁹
10⁸
10⁷
10⁶
A
B
C
D
Tg(1)
TEMPERATURE (°C)
Tg(2)
Tm

FIG. 1.2.

At temperatures above the Tg of the elastomeric homopolymer, rubbery and liquid flow is suppressed by the presence of the glassy domains. The thermoplastic elastomer behaves as a rubber vulcanizate in the region between the two Tg's. Commercial applications of the thermoplastic elastomer require that the terminal blocks remain rigid up to temperatures well in excess of service temperatures, while the central block remains flexible down to low temperatures.

The morphology of the A-B-A block copolymer is dependent upon the weight fractions of A and B. At low A content, the thermoplastic may be the domains in the elastomeric matrix. At intermediate compositions of A and B, either A or B can be the disperse phase. Inversion of domains into matrix can be effected by thermal or solvent treatment, At high content of A, the system is that of rubbery domains in a rigid matrix.

The stress-strain behaviour of the A-B-A polymer at very low A content is similar to that of an undercured gum vulcanizate. On the other extreme, at high A content, the stress-strain curve approaches that of the thermoplastic homopolymer. However, since the stress-strain properties change gradually with increasing A contents, there is a range of weight fractions of A and B such that the A-B-A polymers display stress-strain curves approximate those of conventional vulcanizates.

The range of molecular weights of A and B that can give a good balance between processing performance and elastomeric character is set at the lower limit by the minimum A chain length required to ensure the formation of a heterogeneous phase. The upper limit is set by the high viscosity of both blocks which might seriously hamper domain formation.

A block copolymer of the type B-A-B where A is a thermoplastic segment and B is an elastomeric segment undergoes phase separation but does not form a network. For in this sequential arrangement only one end of B segment is attached to the glass-forming A segment. Such polymers are similar in behaviour to that of a blend of A and B.

1.3. INTRODUCTION TO THE PRESENT WORK.

The fundamental principles regarding homogeneous anionic polymerization of block copolymers are well established (5, 29-31). It is possible to synthesize block copolymers of the A-B-A type, such as polystyrene-polybutadiene-polystyrene having a precise and predictable structure. However, at the commencement of this study, the basic principles concerning the relationship between morphology and mechanical behaviour are still unresolved.

It has been suggested that each segment of A-B-A block copolymers have characteristic conformation in solution depending on the nature of interaction between solvent and polymer. And that the conformation in solution is retained, at least partly in the bulk copolymer, which are produced by slow evaporation of solvent.(32-34) Therefore the morphology and properties of a bulk copolymer prepared by casting from different solvents can be expected to differ from each other and also to differ from a compression-moulded sample. In this studv it will be demonstrated that the dgree of phase separation and the morphological details of a polystyrene-polybutadiene -polystyrene block copolymer (S-B-S) is dependent on the thermal or solvent treatment used in its fabrication.

X-rays are reflected by inhomogeneities of matter. If the inhomogeneities are of colloidal dimensions, the effect will be confined to very small angles with respect to the primary beam of incident x-rays. The details of this scattering will depend upon the morphological structure of the system. It was decided to use small angle x-ray scattering to observe the morphology of the various samples. However detailed information on the size, shape and arrangement of the domains in the matrix of the various samples cannot be obtained from small angle x-ray scattering alone. As such electron microsopy studies will provide a complement to the small angle x-ray scattering measurements.

The dynamic mechanical properties of A-B-A block copolymers, such as the two distinct peaks in the loss modulus-temperature relation curve and the two-step character of the dynamic modulus-temperature relation as well as the high elasticity have been explained in terms of a two phase structure originating from microphase separation of the block segments. (35-37). It was decided to relate the dynamic mechanical behaviour of each sample to its morphology. In order to obtain more information on the transitions observed, the dynamic mechanical properties will have to be measured over a wide temperature and frequency range.

The S-B-S block copolymers have been shown to possess high tensile strength and high ultimate elongation. (10). High tensile strength is usually associated with rubbers modified by the addition of reinforcing filler, or in rubbers which have the ability to crystallize when stretched (e.g. Natural rubber). Because of this, it was thought that a study of the stress strain properties of the S-B-S block copolymer will provide an interesting comparision with those of conventional rubber vulcanizate.

There are few references to block copolymers syntheses through cationic polymerization. M.P. Dreyfuss and P. Dreyfuss (38) have obtained crystalline poly 3, 3-bis(chloromethyl)oxetane (BCMO) and a rubbery random copolymer of BCMO and tetrahydrofuran (THF) using p-chlorophenyldiazonuim hexafluorophosphate as a catalyst. The polymerization mechanism is cationic. T. Saegusa et al (39) have also obtained rubbery random copolymers of BCMO and THF, using various Friedel-Crafts catalysts. An attempt will be made in this work to synthesize an A-B-A block having poly (BCMO) as the end segments and a random copolymer of BCMO and THF as the elastomeric central segment. Such a block copolymer would behave as a vulcanized rubber. Since poly (BCMO) has a melting point of 180° C. (40,41), this block copolymer would have a high effective service temperature. Also a comparative study of the crystalline domains and the glassy polystyrene domains in the S-B-S block copolymer is of interest.

CHAPTER 2. THEORETICAL BACKGROUND

2.1. THE ELASTICITY OF RUBBER NETWORKS

Whereas the Young's modulus of crystalline solids and glasses lies in the range 10^{10} to 10^{13} dynes/cm^2, the Young's modulus of natural rubber and of a tremendous variety of synthetic rubbers lies in the approximate range 10^6 to 10^8 dynes/cm^2. Furthermore, whereas the elastic limit of many crystalline and glassy solids is substantially less than 1%, natural and synthetic rubbers may often be reversibly stretched several hundred per cent.

A typical stress-strain curve for rubber is shown in Figure 2.1. Experimentally the curve is obtained by subjecting a piece of vulcanized rubber to a simple elongation. The features of this curve are (1) an initial bending over towards the extension axis, and (2) a final upward curvature in the region immediately preceding the breaking strain. These characteristic features of rubber are explained by the well-established theory of rubber-like elasticity. There are many excellent reviews of this subject. (42 - 45).

All natural and synthetic rubbers have a common molecular morphology. They are formed from long flexible chain-like molecules occasionally cross-linked to form a three-dimensional network. There is approximately one cross link to every few hundred chain atoms in a typical rubber of good properties. Linear polymers of sufficiently high molecular weight also show rubbery properties in a suitable temperature interval. In these

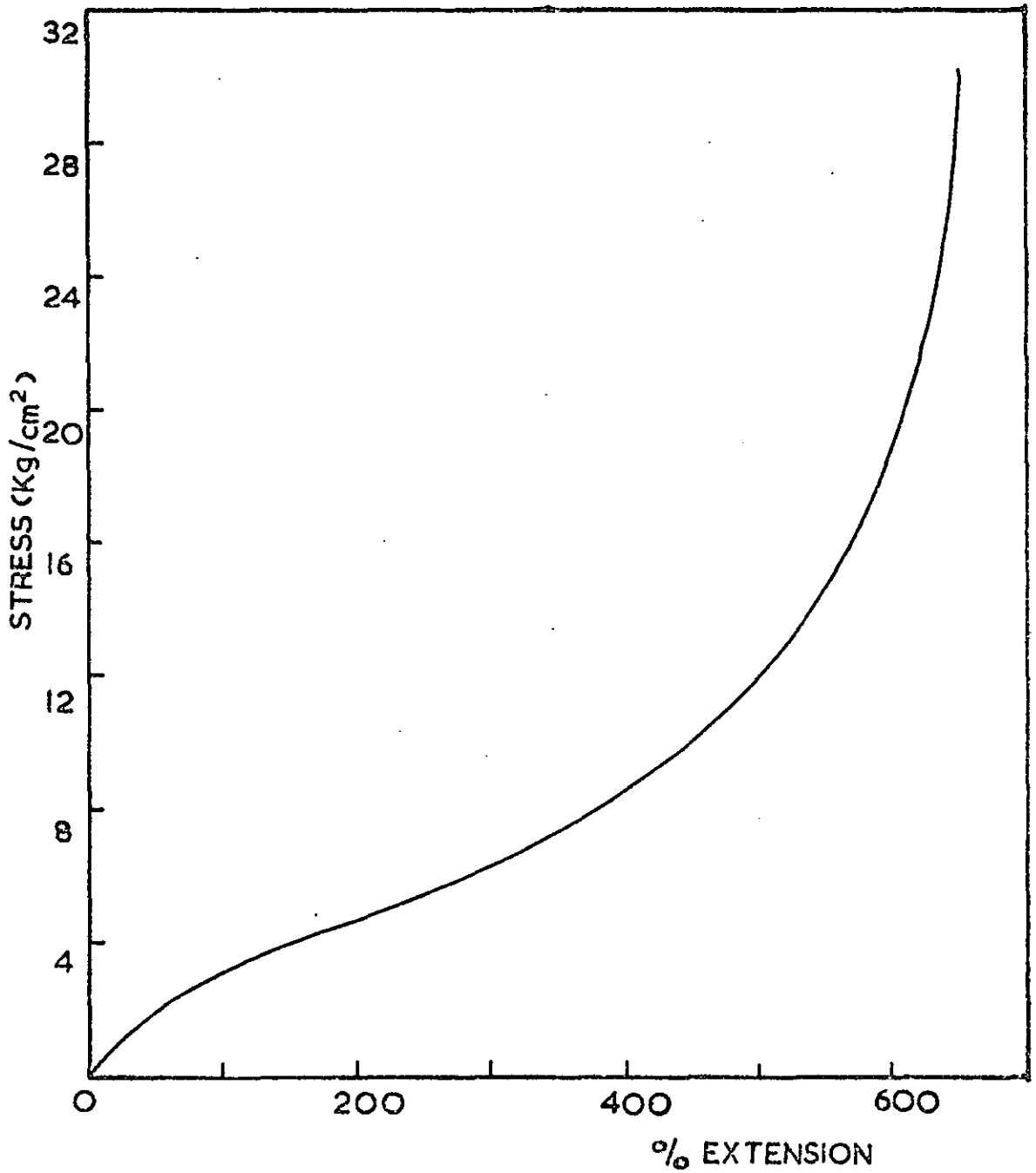

FIG. 2.1.

cases the "entanglements" between the chains act as transient cross links, but the linear polymer will flow at sufficiently high temperatures.

In the unstretched state the network chain is randomly coiled, and is rapidly changing from one conformation to the other, all, however, consistent with the fixed distance between the crosslinks. When the rubber is stretched, the average distance between the crosslinks increases, and the number of possible conformations of the flexible chain between its cross links is reduced from Ω_u to Ω. The change in entropy between the stretched state and the unstretched state is related to the number of configuration in the two states by the relation

$$S-S_u = k \ln \frac{\Omega}{\Omega_u} \tag{2.1}$$

where k is the Boltzmann's constant.

By evaluating the number of configurations Ω_u and Ω using the statistical theory, (43,44,46)

$$S-S_u = -\frac{1}{2} N_o k (\alpha^2 + 2/\alpha - 3) \tag{2.2.}$$

where N_o is the number of network chains in the sample, and α is the extension ratio, defined as extended length L divided by unextended length L_u.

From thermodynamic treatment of simple tension for an ideal rubber, the tensile force X is given as

$$X = -T \left(\frac{\partial S}{\partial L}\right)_T \tag{2.3.}$$

where T is the absolute temperature.

Combining Equations (2.2.) and (2.3.)

$$X = \frac{N_o kT}{L_u} (\alpha - \frac{1}{\alpha^2}) \qquad (2.4.)$$

The stress-strain curve for an ideal rubber is obtained by dividing both sides of Equation (2.4.) by A_u, the cross-sectional area of the unstretched sample.

$$\sigma = \frac{X}{Au} = nRT(\alpha - \frac{1}{\alpha^2}) \qquad (2.5.)$$

Where n is the number of moles of network chains per unit volume (in cubic centimeters) of rubber and R is the gas constant.

The number-average molecular weight of the network chains, Mc, is defined by the relationship

$$nMc = d$$

where d is the density of the rubber.
Thus Equation (2.5.) can be expressed in terms of Mc instead of n.

$$\sigma = \frac{dRT}{Mc} (\alpha - \frac{1}{\alpha^2}) \qquad (2.6.)$$

In general, it has been found that experimental stress-strain data on most rubbers cannot be fitted by Equation (2.6.); but that such data can be fitted at low to moderate elongations, by the Mooney-Rivlin equation(47):

$$\sigma = (2C_1 + 2C_2 \alpha^{-1})(\alpha - \alpha^{-2}) \qquad (2.7.)$$

Many authors (48,49) have shown that C_2 approaches zero with increased swelling in swollen vulcanizates. At the same time, C_1 remains essentially constant and is identified empirically with the $\frac{dRT}{2M_c}$ term of the kinetic theory equation.

2.2. VISCOELASTIC BEHAVIOUR AND DEFINITION OF TERMS

Polymers have mechanical properties that are common to perfect solids and perfect liquids. Various theories have been developed over the past century to describe the behaviour of perfect solids (50) and perfect liquids.(51) The classical theory of elasticity deals with the behaviour of solids for which the stress is directly proportional to the strain. This type of solid is known as Hookean solid or perfect elastic solid. The theory of hydrodynamics describes the behaviour of perfectly viscous liquids for which, in accordance with the Newton's viscosity law, the stress is directly proportional to rate of strain.

A viscoelastic body is intermediate in behaviour and does not maintain a constant deformation under constant stress but slowly deforms with time. (i.e. creeps). When such a body is constrained at constant deformation, the stress required to hold it diminishes with time (i.e. relaxes). Also when subjected to sinusoidally oscillating stress, the strain is neither exactly in phase with the stress (as in the case of a perfectly solid) nor 90^{o} out of phase (as in the case of a perfectly viscous liquid), but somewhere in between. Some of the energy input is stored and recovered in each cycle and some is dissipated as heat.

In many of the materials of interest in classical physics, as well as of physical importance in engineering, viscoelastic anomalies are negligible or of minor importance. In polymeric systems, by contrast mechanical properties are dominated by viscoelastic phenomena which are often truely spectacular.

Mechanical properties are obtained from deformation of the material by applied forces. The three basic types of deformation are simple shear, bulk compression, and simple tensile elongation. Figure 2.2. Simple shear deformation produces a change in shape with no change in volume. This feature facilitates interpretation of the mechanical behaviour in molecular terms. Bulk compression involves a change in volume without change in shape. The simple

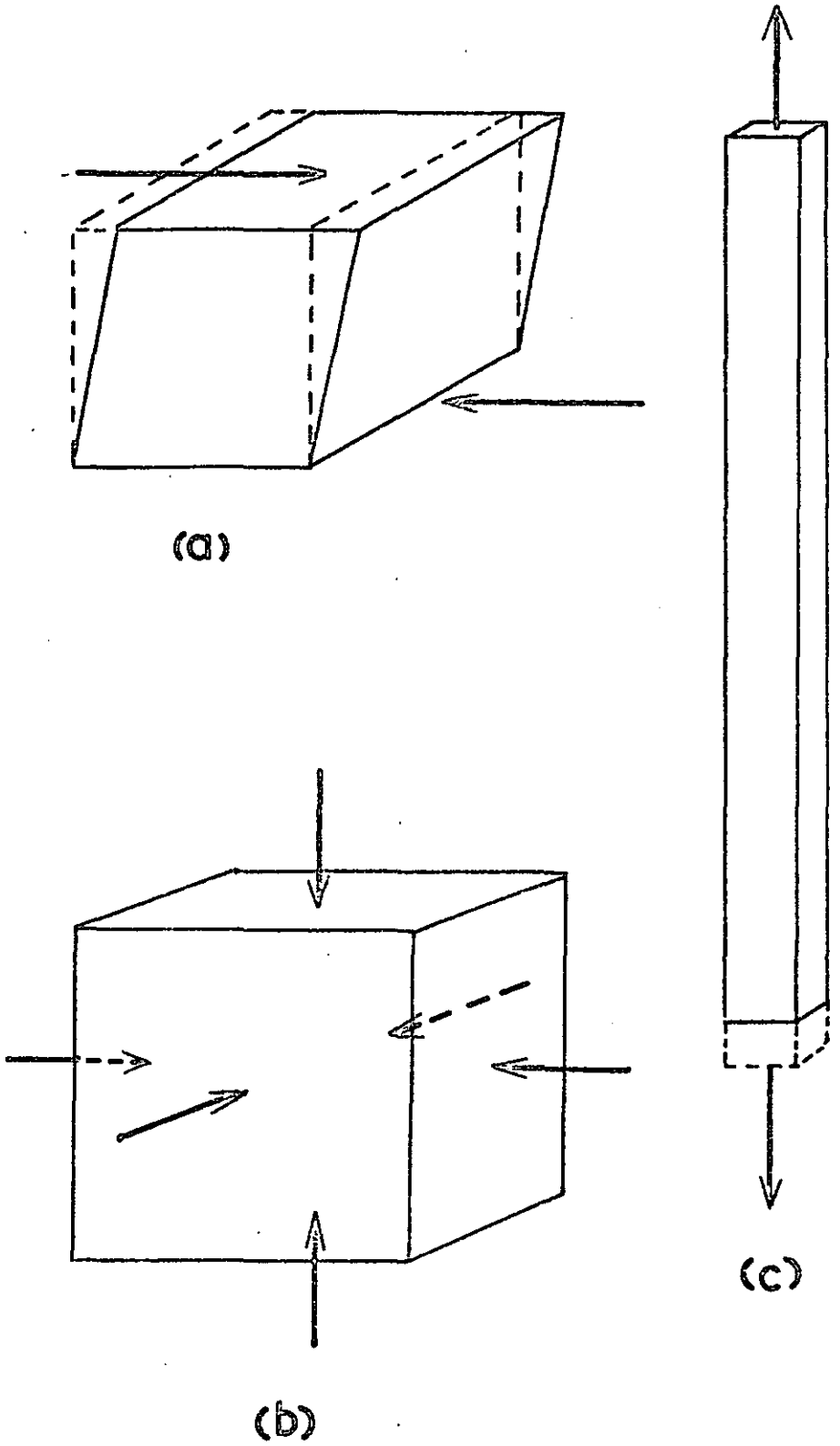

FIG. 2.2. Geometrical arrangement for (a) Simple shear (b) Bulk compression (c) Simple extension.

tensile deformation which can be easily produced in laboratory, has the disadvantage that simultaneous changes in both shape and volume make the behaviour more difficult to interpret on a molecular basis. However, the various moduli are related by the following equations:

$$E(t) = 9G(t)K(t)/\left[G(t) + 3K(t)\right] \qquad (2.8.)$$

$$D(t) = J(t)/3 + B(t)/9 \qquad (2.9.)$$

where E(t) is the tensile relaxation modulus, D(t) is the tensile creep compliance, K(t) is the bulk relaxation modulus, B(t) is the bulk creep compliance, G(t) is the shear relaxation modulus and J(t) is the shear creep compliance.

In polymeric systems, in certain board ranges of time scale, K(t) is often greater than G(t) by two orders of magnitude or more. In this case, Equations (2.8.) and (2.9.) become:

$$E(t) = 3G(t) \qquad (2.10.)$$

$$D(t) = J(t)/3 \qquad (2.11.)$$

Then simple extension gives the same information as simple shear, and the results of the two experiments are interconvertible. Physically, this fact arises because the change in volume caused by the extension is negligible in comparison with the change in shape.

The most important mechanical tests used to study viscoelastic materials include creep, stress relaxation, stress-strain, and dynamic mechanical behaviour.

In a creep experiment a shear stress σ_{xy} is suddenly applied at time zero and held constant during the test. The strain is measured as a function of time. The strain has been found to increase monotonically with time. For a linear viscoelastic solid, creep strain can be related to the stress by

$$\varepsilon_{xy} = J(t)\, \sigma_{xy} \qquad (2.12.)$$

where J(t) is the creep compliance function.
J(t) can be decomposed into three parts corresponding to the observed instantaneous deformation, retarded elastic deformation and flow

$$J(t) = J_o + J\, \Psi(t) + t/\eta_v \qquad (2.13.)$$

where J_o is the glass or initial compliance, J is the decay compliance, $\Psi(t)$ is the retardation function and η_v is the viscosity function.

In figure 2.3. is plotted the logarithm of creep compliance function with the logarithm of time. This kind of plot clearly explains the characteristic features of viscoelastic behaviour in polymers.

At very short times the material behaves as a perfect elastic solid, and is termed "glassy". In this region, the deformation is a function of stress only and is therefore independent of time. As time progresses the material deviates from perfect elastic behaviour. The creep compliance monotonically increases with time until it reaches a constant value again. At this time the material has softened considerably and shows large elastic deformation indicative of the behaviour of a rubbery material. The transition from perfect elastic behaviour to finite behaviour takes place

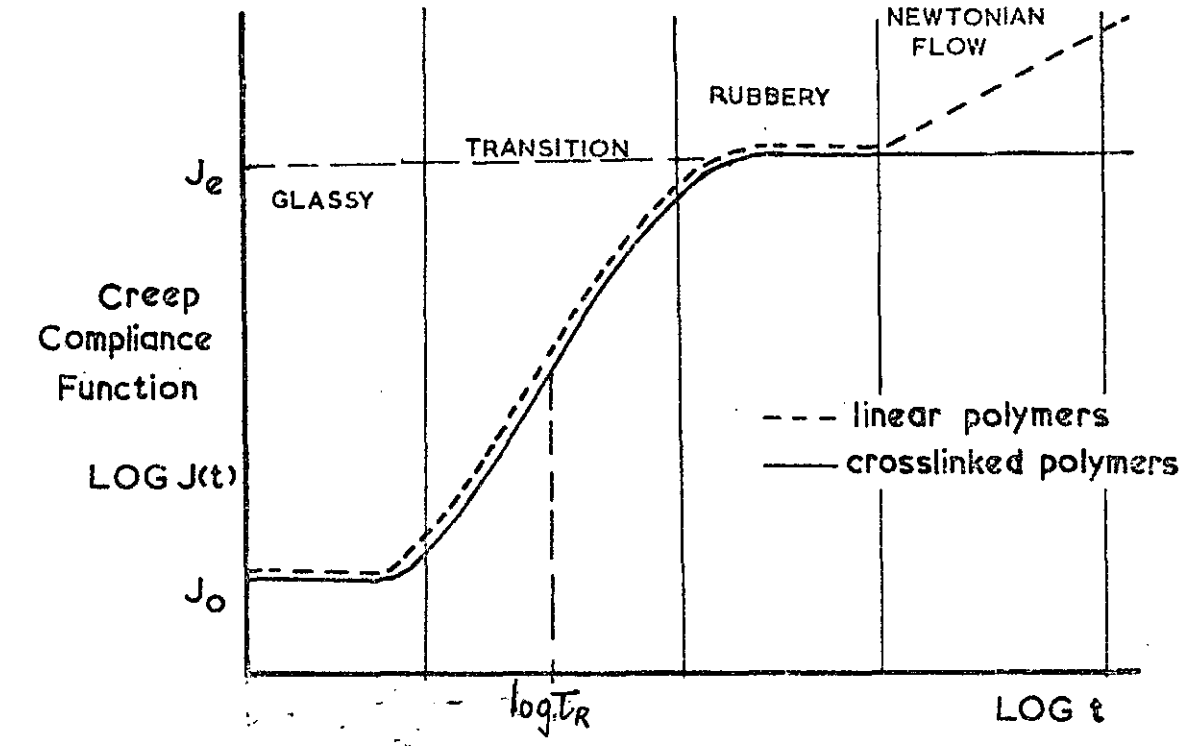

FIG. 2.3. Typical creep compliance curves for linear and crosslinked polymers.

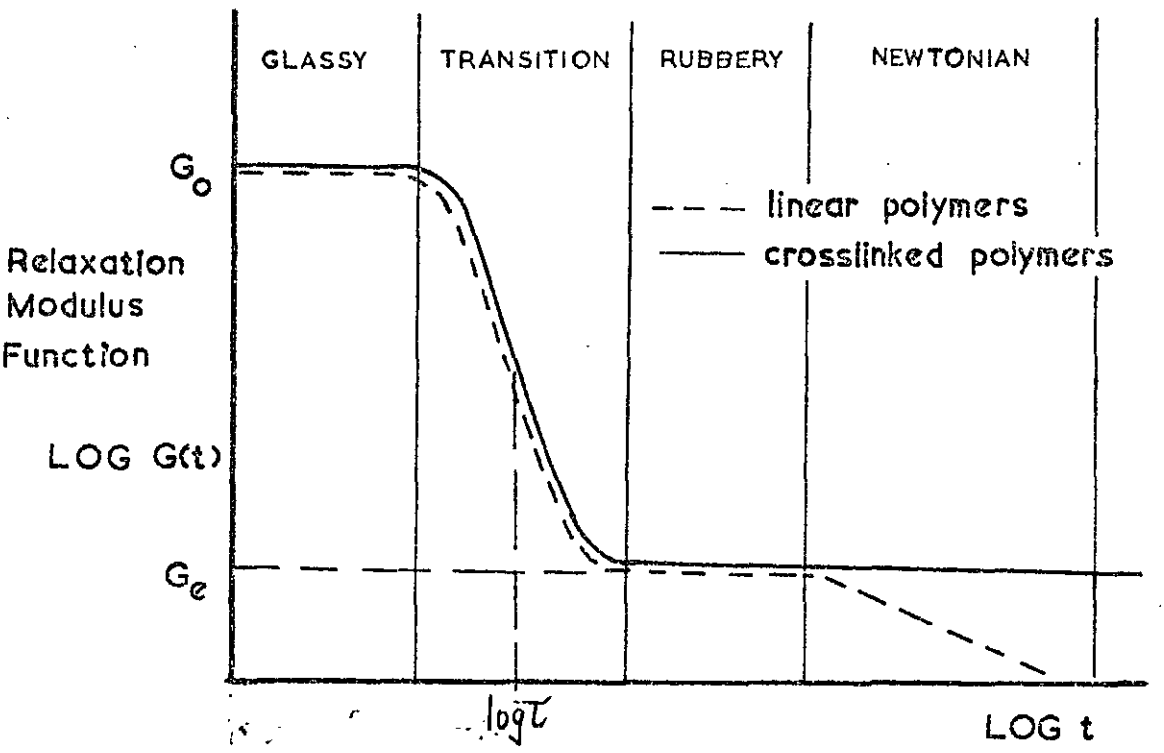

FIG. 2.4. Typical relaxation modulus curves for linear and crosslinked polymers.

over several decades during which the material shows predominant viscoelasticity. This region is characterized by a transition time, τ_R. After still longer times the behaviour of polymers depends upon their chemical structure - that is, whether the polymers are linear or crosslinked. Linear polymers show Newtonian flow and behave almost like viscous liquids, after the rubbery region is exceeded. However, crosslinked polymers do not show Newtonian flow but remain in a rubbery state indefinitely, provided that all chemical bonds maintain their integrity.

When a sample of polymeric material is subjected to an instantaneous strain ε_{xy} that is held constant during the test, the stress is formed to decrease with time and can be expressed by the relation

$$\sigma_{xy} = G(t) \quad \varepsilon_{xy} \tag{2.14.}$$

where G(t) is the relaxation modulus function.

The relaxation modulus function is a monotonically decreasing function of time and can be written as

$$G(t) = G_e + G\,\Psi(t) \tag{2.15.}$$

where $\Psi(t)$ is the relaxation function having the initial and final values.

$$\Psi(0) = 1$$

$$\Psi(\infty) = 0$$

and G_e is the equilibrium modulus

At time t = 0, Equation (2.15.) reduces to

$$G(0) = (G_e + G) = G_o \tag{2.16.}$$

where G_o is the initial modulus.

The stress relaxation behaviour of high polymers can be described by a diagram relating the logarithm of relaxation modulus G(t) to the logarithm of time t(Figure 2.4.)

Dynamic behaviour of polymers can be studied by subjecting a sample to a sinusoidal stress and observing the strain as a function of time or vice versa. Since the applied sinusoidal stress and the resulting sinusoidal strain, or vice versa, are periodic in nature, viscoeleastic parameters are determined as functions of frequency of fluctuations which is the reciprocal of time.

Suppose a specimen is subjected to a stress variation given by

$$\sigma_{xy} = \overline{\sigma}_{xy} \sin \omega t \qquad (2.17.)$$

where $\overline{\sigma}_{xy}$ is the amplitude of stress in any cycle and ω is the angular frequency.

The strain has been observed to vary with the same frequency as the stress but lags behind the stress by an angle δ which is usually termed the phase angle.

$$\varepsilon_{xy} = \overline{\varepsilon}_{xy} \sin (\omega t - \delta) \qquad (2.18.)$$

The variation of stress and strain with time is indicated in Figure 2.5.

The dynamic viscoelastic behaviour can be described by measuring two quantities, namely complex dynamic compliance, $J^*(\omega)$, and the phase angle, δ.

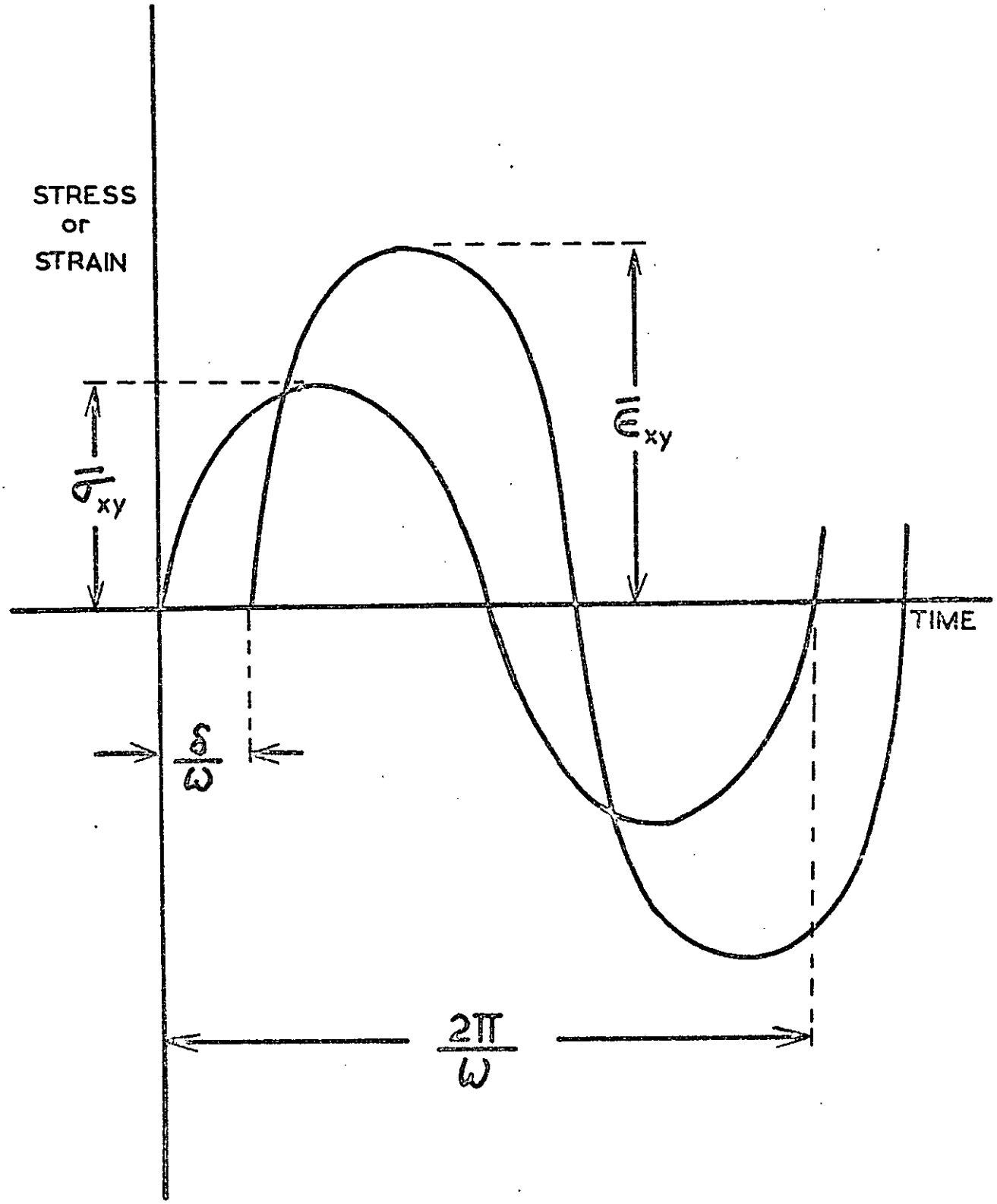
STRESS
or
STRAIN
$\bar{\sigma}_{xy}$
$\bar{\epsilon}_{xy}$
TIME
$\frac{\delta}{\omega}$
$\frac{2\pi}{\omega}$

FIG. 2.5.

The complex dynamic compliance can be expressed in terms of a real part and an imaginary part

$$J^*(\omega) = J_1(\omega) - i\, J_2(\omega) \qquad (2.19.)$$

where $J_1(\omega)$ is the storage compliance and $J_2(\omega)$ is the loss compliance.

The ratio of amplitude of strain to the amplitude of stress is the absolute value of complex dynamic compliance. That is

$$\left|J^*(i\omega)\right| = \bar{\varepsilon}_{xy}/\bar{\sigma}_{xy} \qquad (2.20.)$$

The characteristic features of viscoelastic behaviour under dynamic stress are clearly shown in a diagram relating the logarithm of storage compliance, and the logarithm of loss compliance with the logarithm of frequency of fluatuation. (Figure 2.6.)

If a sample of high polymeric material is subjected to a sinusoidal strain and the resulting stress is measured as function of time, then the stress can be split into two parts

$$\bar{\sigma}_{xy} = \bar{\varepsilon}_{xy}\left[G_1(\omega)\mathrm{Sin}\ \omega t + G_2(\omega)\ \mathrm{Cos}\ \omega t\right] \qquad (2.21.)$$

where $G_1(\omega)$ is the storage modulus and $G_2(\omega)$ is the loss modulus. A complex modulus function can be defined just as in Equation (2.19) That is

$$G^*(i\omega) = G_1(\omega) + iG_2(\omega) \qquad (2.22.)$$

where $\left|G^*(i\omega)\right| = \bar{\sigma}_{xy}/\bar{\varepsilon}_{xy}$, is the absolute value of complex modulus function.

Corresponding to Figure 2.6., the variation of storage and loss moduli with frequency are shown in Figure 2.7.

The relation between these quantities is illustrated in Figure 2.8. It is apparent that the phase angle, δ, can be expressed as

$$\tan \delta = G_2(\omega) / G_1(\omega) = J_2(\omega) / J_1(\omega) \qquad (2.23.)$$

and that

$$J^*(i\omega) = 1 / G^*(i\omega) \qquad (2.24.)$$

It should be noted, however, that neither $G_1(\omega)$ and $J_2(\omega)$, are reciprocally related in a simple manner.

If $G_1(\omega)$ and $J_1(\omega)$ functions are plotted against log $(1/\omega)$, this has the effect of reflecting the curves about the log ω equal to zero. If now G(t) and J(t) curves are plotted against log t to the same scale, it is found that the storage modulus and storage compliance curves coincide with relaxation modulus and creep compliance curves respectively. This is a consequence of linear viscoelastic behaviour.

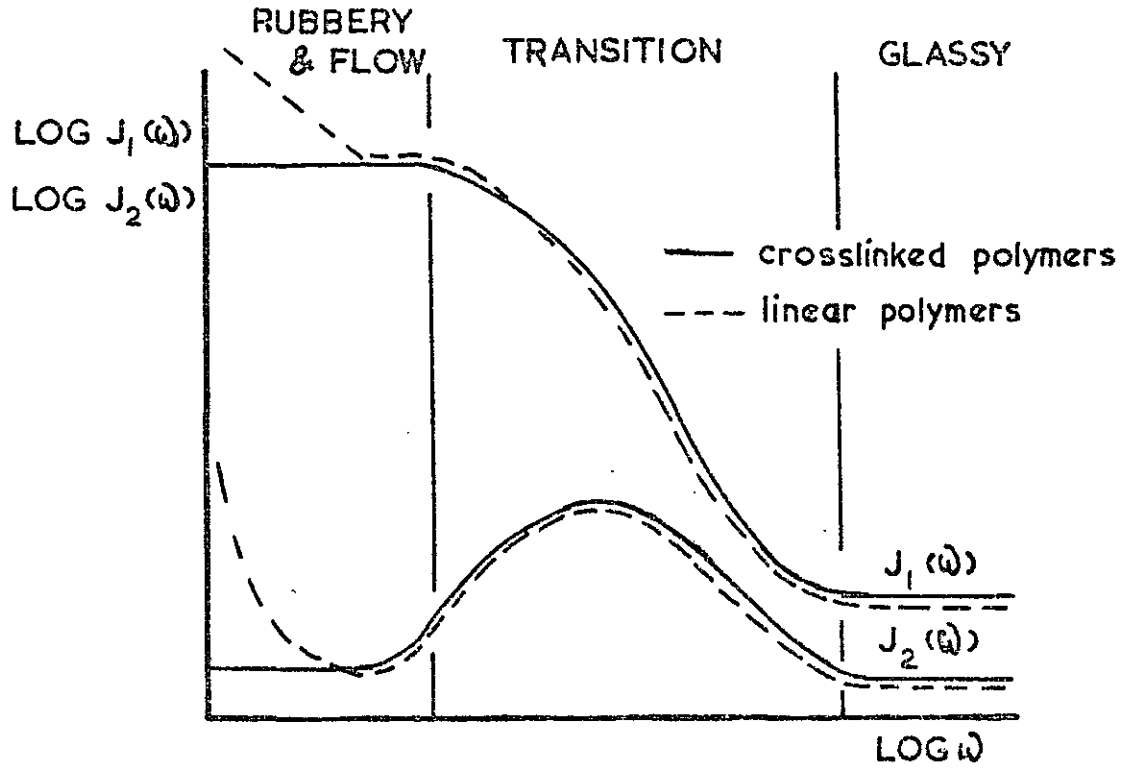

FIG. 2.6. Typical storage and loss compliance curves for linear and crosslinked polymers.

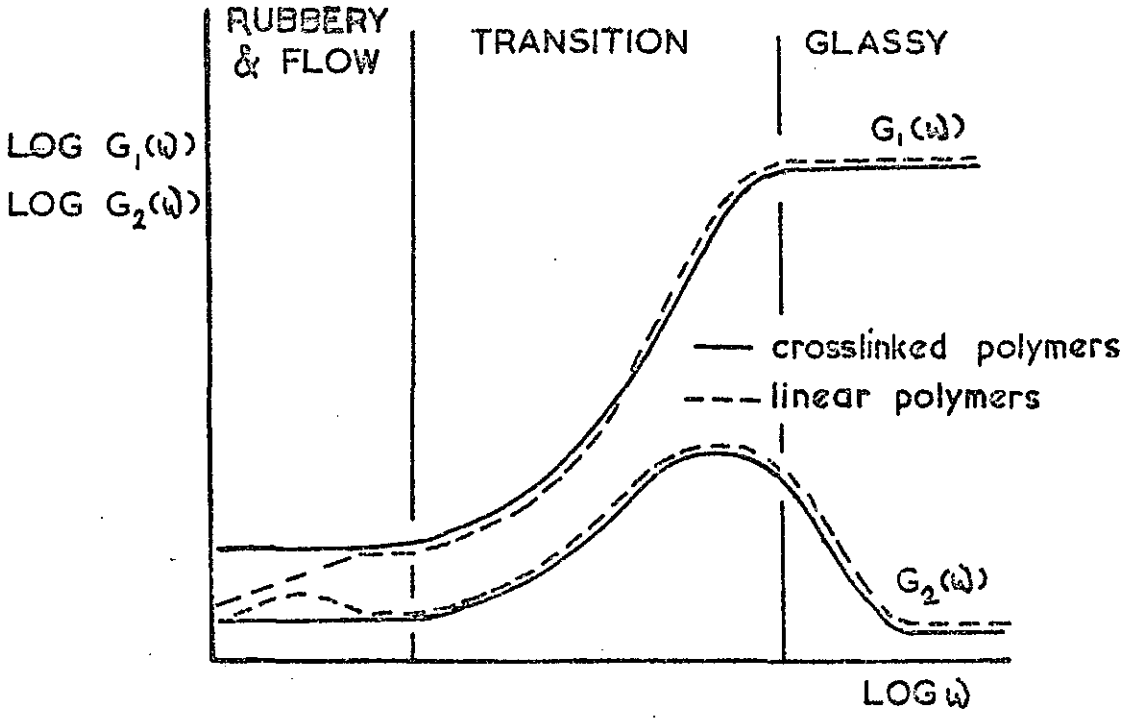

FIG. 2.7. Typical storage and loss modulus curves for linear and crosslinked polymers.

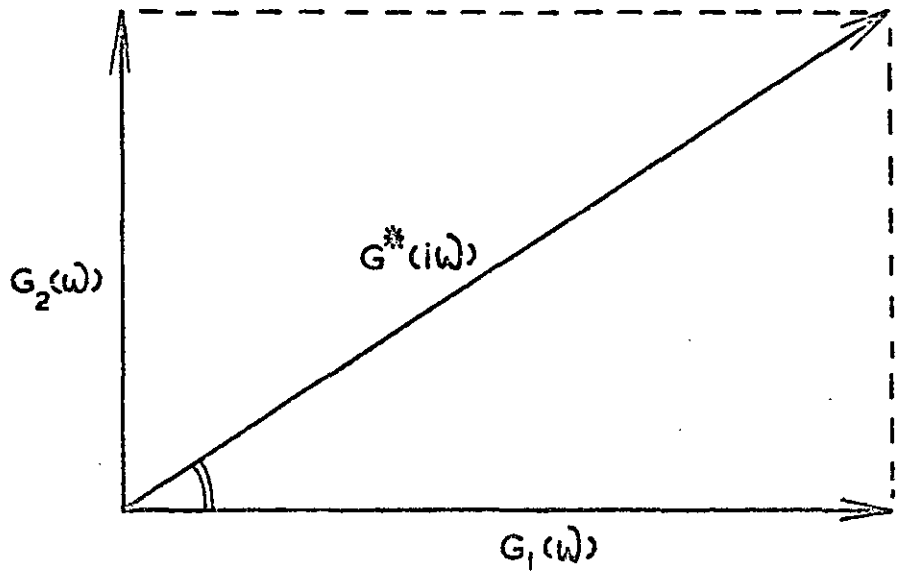

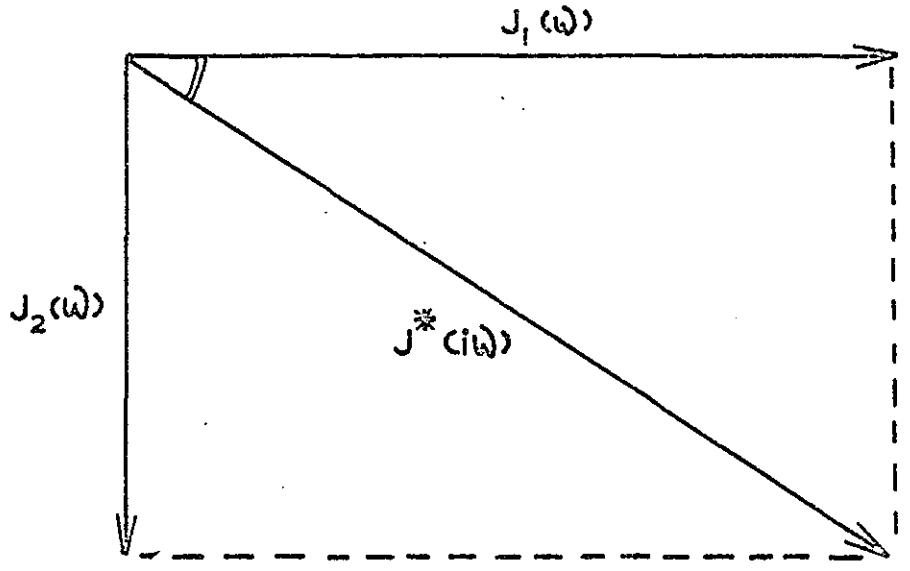

FIG. 2.8.

2.3. PHENOMENOLOGICAL CONCEPTS OF VISCOELASTICITY

In his "principle of superposition", Boltzmann (52) suggested that the mechanical behaviour of a specimen was a function of its entire previous loading history. He further postulated that the effect of each deformation was independent of the others and that the behaviour of a specimen could be calculated by a simple addition of the effects that would occur when the deformations took place singly. This implies a linear mechanical response of the material. It is upon such linear viscoelastic behaviour that the phenomenological theory of viscoelasticity has been developed.

The theory gives a purely mathematical description of the stress-strain behaviour of a body. It is concerned solely in establishing the mathematical characteristics of a given viscoelastic response, and the exact prediction, from these characteristics, of all other viscoelastic behaviour. In this objective the theory is essentially complete. The various mathematical forms of linear viscoelastic theory are discussed in a number of works. (52 - 56)

The phenomenological approach has developed with the aid of mechanical models which are pictorial representations of certain equations of motion, but the theory is of general applicability with most discrepancies arising in the choice of a particular model.

The two simplest mechanical models are the Maxwell model and the Voigt or Kelvin model. These are shown in Figure 2.9. The Maxwell model has a spring of modulus E_m, connected in series with a dashpot of viscosity η_m. The Voigt model has a spring of modulus E_v, connected in parallel with a dashpot of viscosity η_v.

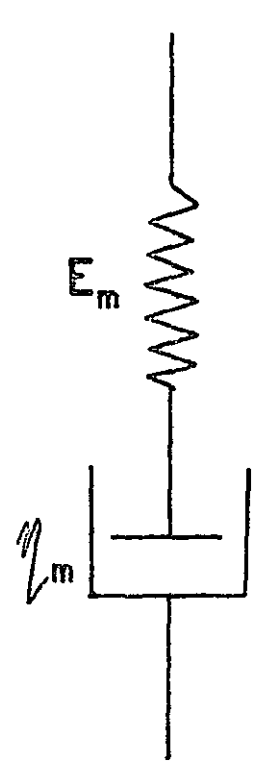

MAXWELL MODEL

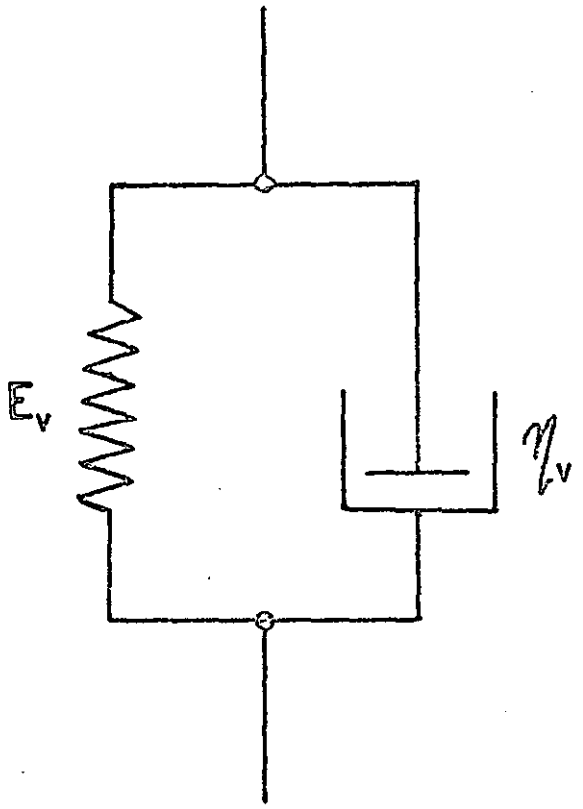

VOIGT MODEL

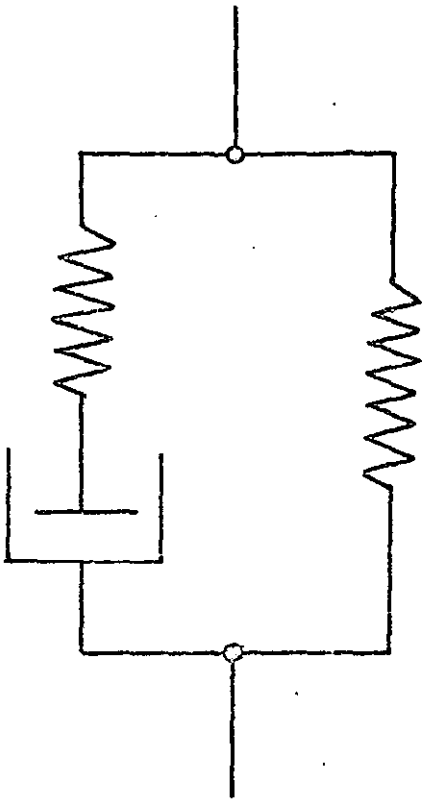

STANDARD LINEAR SOLID

FIG. 2.9.

Denoting the load applied to such a model by σ and the extension by ε, the relation for the Maxwell model is

$$\sigma + \tau d\sigma/dt = \eta_m \, d\varepsilon/dt \qquad (2.25.)$$

where $\tau = \eta_m/E_m$ and is called the "relaxation time" of the model.

Similarly, for the Voigt model, the load-extension relation is

$$\sigma = E_v\varepsilon + E_v\tau_R d\varepsilon/dt \qquad (2.26.)$$

where $\tau_R = \eta_v/E_v$, and is here termed the "retardation time" of the model.

However most real viscoelastic solids do not behave even approximately like the Maxwell or Voigt models, and more complicated models have been used in attempts to simulate the behaviour of real materials.

The model shown in Figure 2.9. consisting of a Maxwell body with another spring in parallel, is known as the "Standard linear body". It possesses single relaxation and retardation times. As such, its response is the archetype of all real linear viscoelastic responses.

The responses of a standard linear body are in fact those of an ideal polymer with a single relaxation. Thus, if the instantaneous modulus is G_o, the equilibrium modulus, G_e, and the relaxation time τ, then Equations (2.27-2.29.) represent the behaviour of both a standard linear body and an ideal polymer.

$$G(t) = G_e + (G_o - G_e) \exp.(-t/\tau) \qquad (2.27.)$$

where G(t) is the relaxation modulus at time t.

$$G_1(\omega) = G_e + [(G_o - G_e)\omega^2\tau^2] / (1 + \omega^2\tau^2) \qquad (2.28.)$$

$$G_2(\omega) = (G_o - G_e)\omega\tau / (1 + \omega^2\tau^2) \qquad (2.29.)$$

where $G_1(\omega)$ and $G_2(\omega)$ are the storage and loss moduli, as defined in Section 2.2. , at the angular frequency ω.

The complianaces of the system (defined in Section 2.2.) will be given by equations of a similar type to the moduli, but with a retardation time, τ_R, in place of the relaxation time.

A real relaxation process can usually be considered as the superposition of numerous smaller, ideal relaxations. Each contributory relaxation has its own relaxation and retardation time, so that a relaxation (and retardation) time spectrum has to be introduced. This approach was first used by Wiechert (57) and Thomson (58) and many empirical and theoretical forms of spectra have since been suggested.

In general, a continuous relaxation time spectra can be conveniently defined as $H(\tau)$ where $Hd(\ell n\tau)$ is the contribution to the rigidity modulus of relaxation times whose logarithms lie between $(\ell n\tau)$ and $(\ell n\tau + d\ell n\tau)$.

A corresponding relaxation time spectra, $L(\tau)$, may be defined as a similar contribution to the compliance. The expressions for the dynamic moduli, analogous to Equations (2.28.) and (2.29.), but in terms of the relaxation spectra H, and of the retardation time spectra L, are thus.

$$G_1(\omega) = G_\epsilon + \int_{-\infty}^{+\infty} \frac{H(\tau)\omega^2\tau^2 d(\ell n\tau)}{1 + \omega^2\tau^2} \qquad (2.30.)$$

$$G_2(\omega) = \int_{-\infty}^{+\infty} \frac{H(\tau)\omega\tau d(\ell n\tau)}{1 + \omega^2\tau^2} \qquad (2.31.)$$

$$J_1(\omega) = J_o + \int_{-\infty}^{+\infty} \frac{L(\tau)\, d(\ell n\tau)}{1 + \omega^2\tau^2} \qquad (2.32.)$$

$$J_2(\omega) = \int_{-\infty}^{+\infty} \frac{L(\tau)\omega\tau d(\ell n\tau)}{1 + \omega^2\tau^2} \qquad (2.33.)$$

In principle, the phenomenological approach enables a spectrum to be determined and allows all other viscoelastic behaviour to be obtained from this spectrum. (52,55,59,60)

2.4. MOLECULAR INTERPRETATION OF VISCOELASTIC BEHAVIOUR OF POLYMERS

The mechanical models used in the phenomenological approach can provide little insight into the molecular origins of the observed viscoelastic behaviours. This may be confirmed from the fact that many quite different arrangements of springs and dashpots could be imagined which would represent an observed phenomena. Therefore in the molecular approach, the aim is to explain the observed behaviour in terms of an assumed structural model for the material which is some approximation of the real molecular structure.

One molecular approach is the consideration of a ladder network in which the molecules are represented as springs moving in a viscous medium (61-63). A typical ladder network suitable for the discussion of relaxation phenomena, consists of a linear succession of N identical springs connected to a common ground through (N-1) identical dashpots attached at the (N-1) junction points of N springs. If the total unstrained length of the springs is finite the relaxation spectrum of such a model is discontinuous and contains N discrete lines. A continuous spectrum is obtained only with a model of infinite length. These ladder networks bear a close structural similarity to the molecular models of Rouse (65) and Bueche (64) in their theories of polymer viscoelasticity.

Rouse (65) has considered a polymer molecule in dilute solution. If a force is applied to the solution the molecule will be disturbed from its equilibrium configuration. The viscoelastic properties of the system are then related to the manner in which the molecule returns to equilibrium. Thermal motion will do this, but will be opposed by viscous forces between the solvent and the polymer molecule, and by intra-molecular effects.

The polymer molecule is treated as a succession of equal submolecules, each long enough to obey the Gaussian distribution function for random chain configuration. Each submolecule contains q monomer units. The root-mean-square distance between two points separated by q monomer units is given by, $\sigma = a\sqrt{q}$, where a is a geometric parameter. The root-mean-square end-to-end distance of the entire molecule equals $a\sqrt{z}$, where z is the degree of polymerization. The resistance to motion caused by viscous forces is concentrated at the junctions between submolecules and is characterized by a friction coefficient, f_o. This is related to q by ξ_o, the monomeric friction coefficient. Each junction is assumed to be hydrodynamically independent, and intramolecular friction is assumed to be zero. The response to an applied stress may be described by a series of co-operative modes, p. Each mode represents motion away from a given instantaneous configuration and corresponds to a discrete contribution to a relaxation spectrum, H, characterized by a relaxation time, τ_p. In these terms H is given by:

$$H = nkT\sum_{p=1}^{N} \tau_p \delta(\tau - \tau_p) \qquad (2.34.)$$

$$\tau_p = \sigma^2 N^2 f_o / 6\pi^2 p^2 kT \qquad (2.35.)$$

where n is the number of polymer molecules per cc. and δ is the Dirac delta. Thus, a line spectrum is predicted in which each contribution to the modulus equal nkT and the relaxation times become progressively more closely spaced at shorter times. This theory appears to give a very reasonable correlation with experimental data (66) but the modification by Zimm (67) to account for hydrodynamic intersection is not so satisfactory. (68). Ferry et al (69) have modified the theory for undiluted polymers on the grounds that the same kind of motions occur in an amorphous polymer as in solution, although very much slower.

They obtained the following expression for $H(\tau)$ and $L(\tau)$,

$$H(\tau) = (a\rho N_o/2\pi M_o)(\xi_o kT/6)^{\frac{1}{2}}\tau^{-\frac{1}{2}} \qquad (2.36.)$$

$$L(\tau) = (2M_o/\pi a\rho N_o)(6/\xi_o kT)^{\frac{1}{2}}\tau^{\frac{1}{2}} \qquad (2.37.)$$

where p is the polymer density, N_o is Avogadro's number, and M_o is the monomeric molecular weight.

Bueche (64) formulated a theory to apply both to a linear polymer and to a cross-linked network. In this case, however, thermal motion is only inferred by the introduction of an entropy spring constant. Like the ladder networks, this also suffers from the criticism that actual molecular parameters are not being used. However, the expressions obtained for $H(\tau)$ and $L(\tau)$ are very similar to those obtained from the Rouse theory:

$$H(\tau) = 2^{\frac{1}{2}}H(\tau)(\text{Rouse}) \qquad (2.38.)$$

$$L(\tau) = 2^{-\frac{1}{2}}L(\tau)(\text{Rouse}) \qquad (2.39.)$$

The best agreement between experimental data and theoretical calculations of the viscoelastic functions is found when the modulus of the material is less than 10^7 dynes/cm^2, i.e. when it is in the rubbery state. Thus, the theory gives a good approximation to experiment on the low frequency side of the glass transition. As the frequency increases the theory breaks down because modes of motion corresponding to rearrangements within the submolecule must be considered.

Inspection of equations (2.36.) and (2.37.) shows that a change of temperature changes only a, ξ_o and T and consequently multiplies both $H(\tau)$ and $L(\tau)$ by a factor independent of τ. Thus on a logarithmic plot a change of temperature simply translates the curves along the log time axis. This agrees with the time-temperature superposition principle.

2.5. TIME-TEMPERATURE SUPERPOSITION PRINCIPLE AND MASTER CURVES

The practical range of time scale for creep, stress relaxation and dynamic mechanical measurements is limited. At a given temperature, the complete range in viscoelastic properties is certainly not covered by this limited range of four or five decades of log time. Hence a satisfactory method of extrapolation is obviously necessary.

Such a method was first suggested by Leaderman (55,70) who observed that, for some polymeric materials, creep recovery curves obtained at different temperatures could be superposed by a translation along the logarithmic time axis. Hence the effect of temperature on the creep relaxation properties appears simply to be to multiply the time scale by a constant A_T which will depend on the temperature in question. This factor A_T can be experimentally determined simply by noting the amount of shift on the logarithmic time scale required to bring the creep curve at temperature T into coincidence with that at some reference temperature T_o. Then if the creep compliance at the temperature in question is plotted, not against time but against the reduced variable (t/A_T), all the creep curves obtained at various temperatures will superpose to give the master curve for T_o. Thus the complicated time-temperature dependence is effectively reduced to a separate time dependence (at some reference temperature T_o) and a separate temperature dependence, the latter showing up only in the variation of the factor A_T with temperature. Furthermore, if linear viscoelastic theory is obeyed by the material in question, similar alteration in the time or frequency variable will also effectively superpose stress relaxation time curves (71,72) or dynamic modulus frequency curves. (73,74).

The method of reduced variables is generally applied only to the behaviour of materials in the transition region between glass-like behaviour and rubber-like behaviour. In the transition region amorphous polymers are assumed to obey the laws of rubber elasticity, and hence the contribution to the modulus should be proportional to absolute temperature. Since the density of a polymer changes with temperature, it is appropriate also to consider this effect. The reduced relaxation modulus is now $G(t)(T_o/T)(\rho_o/\rho)$

and the reduced creep compliance is $J(t)(T/T_o)(\rho/\rho_c)$, where T_o is some reference temperature and ρ_o is the value of the density at this temperature. Similarly, for the dynamic experiments the appropriate reduced variables are $G_1(T_o/T)(\rho_o/\rho)$ and $G_2(T_o/T)(\rho_o/\rho)$ plotted against the reduced frequency (ωA_T). The reduction factors A_T, for temperatures other than the standard temperature T_o, are found empirically so as to make the data superpose when plotted in terms of the reduced variables.

Williams, Landel and Ferry (75) have defined the factor A_T as the ratio of the relaxation times at temperature T to the relaxation times at temperature T_o. The relaxation time τ is related to the viscosity η. Hence A_T can also be expressed in terms of the steady flow viscosity (η_T) at temperature T and the steady flow viscosity at the reference temperature (η_{To}). The relation is

$$A_T = (T_o/T)(\rho_o/\rho)(\eta_T/\eta_{T_o}) = \tau/\tau_o \qquad (2.40.)$$

and, if measurements of steady flow viscosity have been made, A_T as a function of temperature can be found directly.

For many polymeric materials (75-79) in the softening range the data are found to superpose quite well when plotted in the form of the reduced modulus or compliance versus the reduced time or frequency. For dynamic experiments in which both G_1 and G_2 are measured, it is essential that the same values of A_T superpose both sets of data.

The variation of A_T with temperature is usually exponential and an activation enthalpy for the relaxation process can be obtained from the expression

$$\Delta H_a = R\, d\ell nA_T / d(1/T) \qquad (2.41.)$$

However a plot of log A_T vs 1/T is frequently not a straight line and hence the activation enthalpy may itself be a function of temperature.

2.6. MODELS FOR TWO-PHASE SYSTEMS

GUTH-GOLD EQUATION

There have been several attempts to derive formulas giving the apparent modulus due to a dispersion of particles in rubber. The earliest of these attempts was by Smallwood (80) using an analogy to Einstein's viscosity equation (81),

$$E = E_o\ (1 + 2.5\phi) \qquad (2.42.)$$

where E is the modulus of the filled rubber, E_o that of the rubber matrix, and ϕ the volume concentration of filler.

However, this equation holds only for low concentrations of filler and amendments were derived (82-85). That of Guth and Gold (84), by considering the interactions between pairs of particles, added the term involving the square of the concentration of filler to Smallwood's equation and obtained

$$E = E_o(1 + 2.5\phi + 14.1\phi^2) \qquad (2.43.)$$

For nonspherical particles, Guth (86) introduced a shape factor, f and proposed

$$E = E_o(1 + 0.67f\phi + 1.62f^2\phi^2) \qquad (2.44.)$$

where f is expressed as the ratio of diameter to width of particles.

These equations were derived on the assumptions that that medium wets the filler particles, but does not chemically reacts with the filler surface

Cohan (85) applied these last equations to data obtained for a variety of fillers in several rubbers by measuring the initial stress required for extension to 400%, and found that the shape factor f thus deduced corresponded closely to values observed directly in the electron microscope. In general the relation for these complex systems is only useful as an empirical description.

KERNER'S EQUATION

Kerner (87) has derived an equation relating the modulus of a filled material to the elastic constants of the matrix and filler, assuming that the dispersed phase is in the shape of spherical particles randomly dispersed and that there is perfect adhesion between the two phases. Kerner's equation for the shear modulus is:

$$G_o = G_1 \left[\frac{\dfrac{v_2 G_2}{(7-5\nu_1)G_1 + (8-10\nu_1)G_2} + \dfrac{v_1}{15(1-\nu_1)}}{\dfrac{v_2 G_1}{(7-5\nu_1)G_1 + (8-10\nu_1)G_2} + \dfrac{v_1}{15(1-\nu_1)}} \right] \qquad (2.45.)$$

where G_o is the shear modulus of the two-phase system, G_1 and G_2 are the shear moduli of the continuous phase and the dispersed phase, respectively, v_1 and v_2 are the volume fractions of the matrix and filler respectively, and ν_1 is the Poisson's ratio of the matrix.

For rigid fillers which have moduli much greater than that of the polymer, Kerner's equation may be simplified at low volume fraction of filler to

$$G_o = G_1 \left[1 + \frac{v_2}{v_1} \left\{ \frac{15(1-\nu_1)}{8-10\nu_1} \right\} \right] \qquad (2.46.)$$

The quantity $15(1-\nu_1)/(8-10\nu_1)$ varies between 2.00 and 2.50 as Poisson's ratio changes from 0.2 to 0.5.

THE TAKAYANAGI MODEL

The viscoelastic properties of two-phase systems have been described with considerably success by the use of "mechanically equivalent models". (88-91). In principle, these assign various amounts of parallel and series coupling to the two-phase structure. The model of Takayanagi is shown in Figure 2.10. The two parameters ϕ and λ represent the state of mixing of the two phases, but only one is independent. The two phases in the model are assumed to be perfectly bonded to each other. In Figure 2.10 are schematic representations of the mixing state of the two-phase system and their equivalent models. The upper figure shows a homogenously dispersed system and the lower figure a heterogeneously dispersed system. The product $\phi\lambda = \nu_2$, the volume fraction of the disperse phase.

The solution for the Takayanagi model is

$$E^* = \left[\frac{\phi}{\lambda E_2^* + (1-\lambda)E_1^*} + \frac{1-\phi}{E_1^*} \right]^{-1} \qquad (2.47.)$$

where E^* is the complex modulus of the blend and E_1^*, and E_2^* are the complex moduli of the components. To obtain separate mixture rules for E' and E", one substitutes the complex moduli into Equation (2.47.) and separates E^* into its real and imaginary parts.

When the particles are spheres, λ and ϕ depend on the volume fraction of the dispersed phase, ν_2, as follows. (92).

$$\lambda = (2 + 3\nu_2)/5 \qquad (2.48.)$$

$$\phi = 5\nu_2/(2 + 3\nu_2) \qquad (2.49.)$$

These equations have been derived from the condition that Kerner's equation (2.46.) and equation (2.47.) should hold at the same time.

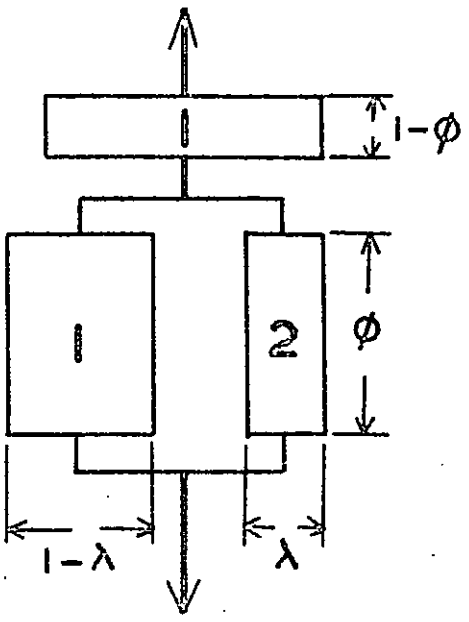

(a)

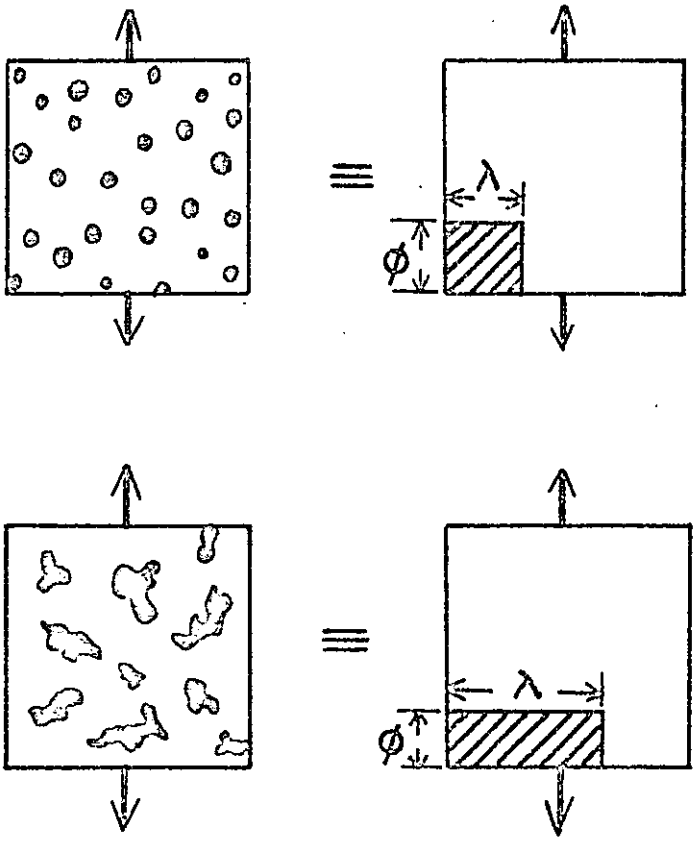

(b)

FIG. 2.10.

2.7. RELATION BETWEEN THE RATES OF STRESS RELAXATION AND CREEP

A general relation (93) for the creep rate may be formulated as

$$C = \frac{1}{e}\left(\frac{\partial e}{\partial t}\right)_{\sigma} \qquad (2.50.)$$

where e is the strain under a constant stress, σ, and t is an arbitrary monotonically-increasing function of time. Similarly the rate of stress relaxation S at a constant deformation, may be expressed as

$$S = \frac{1}{\sigma}\left(\frac{\partial \sigma}{\partial t}\right)_{e} \qquad (2.51.)$$

The rate of creep is then given by

$$C = AS \qquad (2.52.)$$

where

$$A = \frac{\sigma}{e}\left(\frac{\partial e}{\partial \sigma}\right)_{t} \qquad (2.53.)$$

σ is the stress corresponding to the strain e; $\left(\frac{\partial \sigma}{\partial e}\right)_{t}$ is the slope of the stress-strain behaviour, A is unity, and the rates of creep and stress relaxation are then numerically identical.

For unfilled vulcanizates under moderate deformations, the relation between stress and strain is predicted by the Mooney form of stored energy function, (48,94).

$$\sigma = 2(c_1 + c_2\,\alpha^{-1})(\alpha - \alpha^{-2}) \qquad (2.54.)$$

where $\alpha = 1 + e$, and c_1, c_2 are elastic constants for the rubber, such that the ratio $T = c_2/c_1$ lies generally within the range 0.5 to 1.0 for soft vulcanizates of rubber-like polymers.

The factor A can thus be expressed in terms of the amount of extension and the ratio c_2/c_1, explicitly.

$$A = \frac{\alpha(\alpha^2+\alpha+1)(\alpha+T)}{\alpha^4+2\alpha+3T} \qquad (2.55.)$$

Generally, however, A may be calculated at any extension from the experimentally determined relation between stress and extension by graphical means.

The decay of stress is found to occur approximately in proportion to the logarithm of the time spent in the deformed state, for vulcanized rubbers and other materials (95-101). For this reason, the rates of stress relaxation and creep can often be conveniently expressed as a percentage change per decade of time. The time t in Equations (2.50) and (2.51) is replaced by log t.

2.8. THERMODYNAMIC ASPECTS OF POLYMERIC PHASE SEPARATION

With every few exceptions, mixtures of polymers are heterogeneous, because polymers of different chemical structure are usually incompatible. The entropy to be gained by intermixing of the polymer molecules is very small owing to the small numbers of molecules involved. The small entrophy can readily be counteracted by a small positive heat of mixing. Since mixing of a pair of polymers or of pairs of solutions of different polymers, is usually endothermic, incompatibility of polymers usually occurs. This phenomenon was first demonstrated by Dobry and Boyer-Kawenoki (102) who studied some thirty-five pairs of homopolymers and found only three pairs were definitely compatible up to moderate concentration. Scott (103) and Tompa(104,105) have presented theoretical treatment of phase separation of polymers, and Flory(106) added theoretical consideration which make clear that incompatibility of different polymers is expected to be the rule, and compatibility is a rare exception. Stockmayer and co-workers (107) pointed out that interaction, which are in their net effect repulsive, must be considered even between different units in random copolymers and Molau (108) has shown that such interactions are strong enough to cause phase separation even within a series of random copolymers of identical monomers, but of different composition. Repulsive polymer-polymer interactions and an intramolecular phase separation within molecules of block and graft copolymers have been postulated by a number of authors (5,109,110), and experimental studies with regard to the problem have appeared in the recent literature. (111-116). The intramolecular phase separation or microphase separation of block and graft copolymers occurs both in the solid state and in solution.

Block and graft copolymers have sequences of different homopolymers in the same molecule. Selective solvents can often be found which are good with respect to one of the homopolymer sequences, but are poor with respect to the other types of sequences. Merrett (117) has shown

that two modifications, a "hard form" and a "soft form", can be prepared from the same sample of a graft copolymer of natural rubber and polymethyl methacrylate. He dissolved the graft copolymer and precipitated it from solution choosing the solvent-nonsolvent system so that either the rubber chains or the polymethyl methacrylate chains collapse first, when the non-solvent is added. In order to explain the observed behaviour, Merrett postulated the formation of micelles during the precipitation. The cores of the micelles would be formed by those polymer chains that collapse first in the precipitation process. The opposite polymer chains, which are still soluable at that point, would form the shells of micelles and would fuse together forming a continuous phase, when all of the graft copolymer has been precipitated. This continuous phase determines the over-all appearance of the formed modification, which is either hard and rigid or soft and rubbery.

Inoue et al (118) have described the mechanism of domain formation in A-B type block copolymers of styrene and isoprene, in terms of thermodynamic and molecular parameters, such as the incompatibility between A and B segments, the solvation power of solvent for the segments, the casting temperature, the total chain length of the block copolymer and the weight fraction of the block segments within the block copolymer. There is a critical concentration at which each segment of the block copolymers undergoes phase separation and aggregates into characteristic molecular micelles. The micelle structures thus formed is maintained as a whole at higher concentration until the solid structure are formed. There are three types of micelles, spherical, rodlike and alternating lameller micelles, which correspond to the three types of fundamental domain structure that can form the domain structure at the critical concentration by hexagonal close packing (spherical and rodlike micelles) or by piling up (lamellar micelles). The relative values of the minimum free energies involved in the formation of each type of micelles are plotted as a function of the whole range of weight fraction ϕ_A of A-blocks from zero to unity. The plot indicates that the type of micelle formed varies from spherical (A dispersed in B) to rodlike (A dispersed in B), to alternating lameller (A and B), to rodlike (B dispersed in A) and to spherical (B dispersed in A) with increasing ϕ_A, and that the limiting fraction ϕ_i for each type of micelles shifts towards

lower values with decreasing relative solvation power, σ_B/σ_A. Furthermore, the type of micelles formed is found to be insensitive to the casting temperature and the size of the micelle is expected to change with temperature. Such morphological effects have also been shown by Matso et al (119) in A-B, A-B-A and A-B-A-B block copolymers of styrene with butadiene.

2.9. CATIONIC POLYMERIZATION OF CYCLIC ETHERS

Although certain polyethers can be obtained by polymerization of aldehydes and other carbonyl components, the most convenient method for obtaining high polymers of the type $\{(CH_2)_x\text{-}O\}_n$ is by ring-opening polymerization of cyclic ethers. (40,120-123)

Conversion of cyclic monomer to linear high polymer is only feasible when the reaction involves a decrease in free energy and when there is a suitable reaction mechanism to induce the ring opening process. The thermodynamic factors affecting polymerizability were first rationalized by Dainton, Devlin, and Small (124) who used semiempirical methods to calculate free energy changes for hypothetical polymerization of pure liquid cycloalkanes. Small (125) extended the earlier calculations to cyclic ethers and show that since the bond lengths of C-C and C-O bonds do not differ very much, replacement of a carbon atom in a cycloalkane by a heteroatom such as oxygen would affect the free energy change only slightly. Data for cycloalkane can therefore be taken to represent roughly, the free energy involved in cyclic ether polymerization. The following generalizations emerge:

1. In any one graph of derivatives, the thermodynamic feasibility of the ring opening process decreases with increasing ring size in the order 3 > 4 > 5 > 6, at which ring size the free energy change has become positive. With further increase in ring size, ring opening again becomes possible, the free energy change favouring the reaction in the order 8 > 7 > 6.

2. For any one size of ring, the thermodynamic feasibility of ring opening decreases in the order unsubstituted derivative > monomethyl derivative > 1,1-dimethyl derivative.

3. The thermodynamic criterion for a spontaneous process, that the

free energy changes must be negative, is of importance only in the case of the six-membered rings and substituted five-membered rings. In all these cases the attendant free energy change is positive, thereby precluding their participation in the ring opening polymerization.

The cyclic ethers usually homopolymerize or copolymerize by homogeneous cationic mechanisms. The relative efficiency of the various initiator systems varies in an as yet unpredictable way for one ring system to another and in copolymerization of various mixtures. Initiation of cyclic ether polymerization requires reaction between the ether oxygen atom and an ion pair comprising a highly electrophilic cation (X^+) and a gegenion of low nuclearphilicity (Y^-), forming a cyclic oxonium ion.

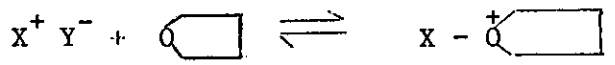

(2.56.)

Meerwein and co-workers have carried out an extensive study of the polymerization of tetrahydrofuran using various initiator systems. (126 - 129). The initiator systems used include trialkyl oxonium salts e.g. $Et_3\overset{+}{O}\ BF_4^-$; protonic acids e.g. $HCl\ O_4$; carbonium ion salts, e.g. $[CH_3\overset{+}{O} = CH_2]AlCl_4^-$ (prepared in situ) and acylium ion salts, e.g. $CH_3CO^+AlCl_4^-$.

In recent years, a number of initiator systems in cyclic ether polymerization have been introduced. Bawn et al (130,131) have found that the triphenyl methyl cation (Ph_3C^+) and cycloheptatrienyl cation ($C_7H_7^+$) are readily isolated in the form of crystalline salts having stable anions such as BF_4^-, ClO_4^-, $SbCl_6^-$, PF_6^-, etc. The triphenyl methyl cation salts are very good initiators for cyclic ether polymerization and are very convenient to handle. Especially useful are triphenyl methyl

hexachloroantimonate and the corresponding hexafluorophosphate. In general the efficient production of high polymers requires stable gegenion.

Dreyfuss and Dreyfuss first showed that p-chlorophenyl diazonium hexafluorophosphate was a very effective initiator for tetrahydrofuran polymerization. (132). Extremely high molecular weights were obtained and the system was apparently free from termination reactions. The initiation is thought to occur by hydride abstraction as shown in Reaction (2.57.). These authors

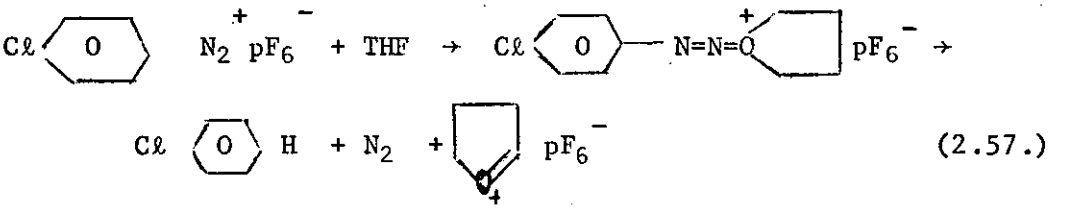

(2.57.)

propose (38) that the cyclic carbononium so formed reacts further with tetrahydrofuran to give an aldehyde endgroup in the polymer chains, viz:

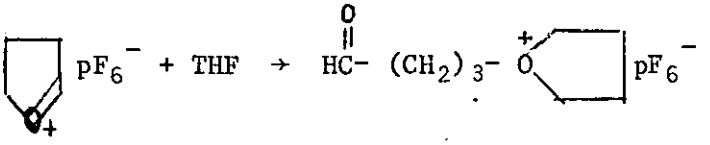

(2.58.)

It has been reported that THF and other cyclic ethers can be polymerized using BF_3(133), SiF_4(134), pF_5(135,136). $SbCl_5$ (137,127-129) and WCl_6 (138). The initiator PF_5 gives rise to a very high molecular weight polymer (in the case of THF) although there is considerable doubt as to whether the simple halide is a true initiator. Polymerizations induced by PF_5 are very similar to those initiated by p-chlorophenyldiazonium hexafluorophosphate.

The chain growth processes in cyclic ether polymerization are best represented by Reaction (2.59.). Evidence for the

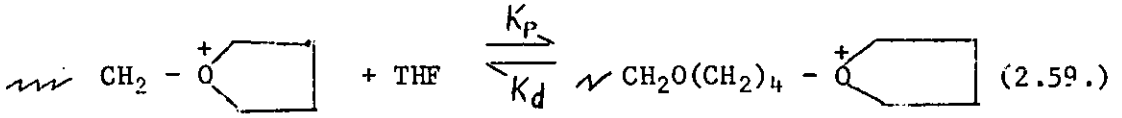

(2.59.)

reversibility of these polymerizations is provided by the very rapid depolymerization of polymer to monomer under the influence of, for example, $SbCl_5$ (139). Early work by Meerwein (126-128) had shown that for a given temperature, there was an upper limit to the percentage conversion of monomeric THF to polymer. The other cyclic ethers behave similarly (121) and this type of behaviour is typical of polymerizations exhibiting so-called ceiling temperature phenomena.

The propagation reaction in cyclic ether polymerization may be regarded as involving mucleophilic attack by the monomer ether oxygen atom on the alpha carbon of the cyclic oxonium ion. The depropagation reaction can similarly be considered as a nucleophilic attack by the penultimate oxygen atom followed by explusion of monomer. At

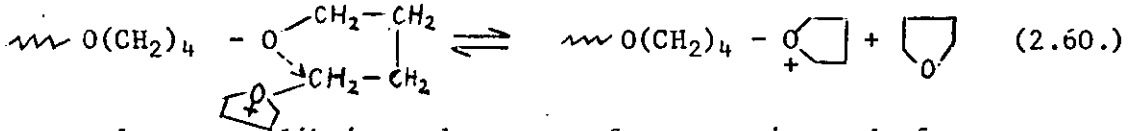

(2.60.)

monomer-polymer equilibrium, the rates of propagation and of depropagation become equal. In addition to reaction with monomer oxygen and penultimate polymer chain oxygen, the polymeric, cyclic oxonium ion should also be capable of reacting with other ether oxygen atoms distributed randomly in the system. So the possibility of intermolecular reaction exists as shown in reaction (2.61.)

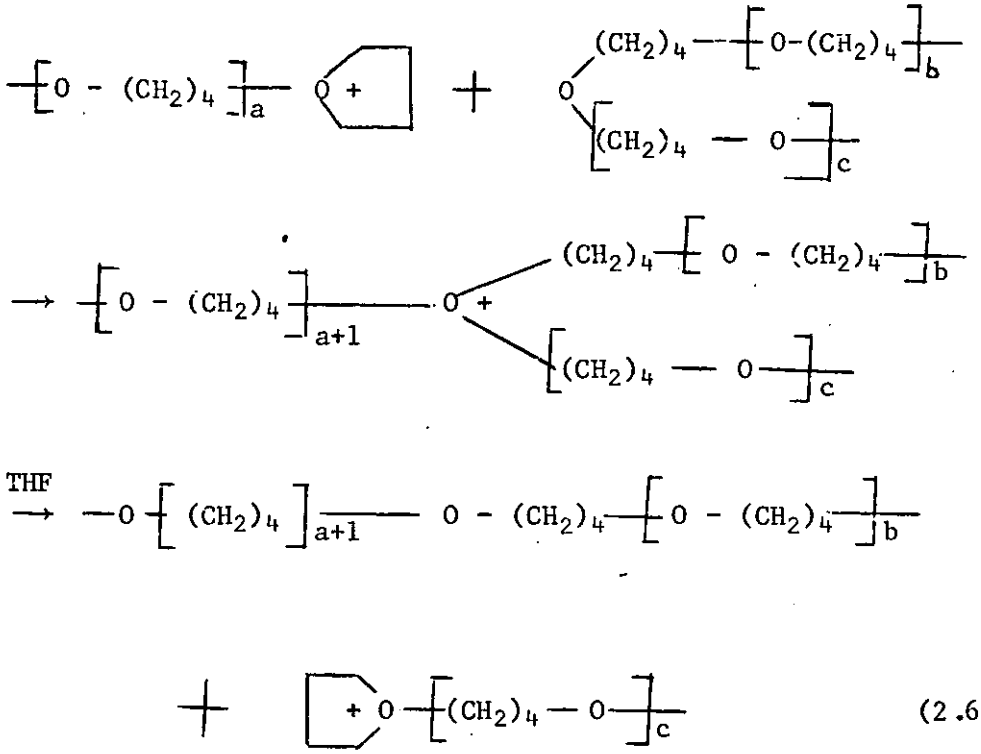

(2.61.)

An analysis of the consequences of this reaction reveals that the only result is an alteration of the molecular weight distribution.

However, if an acyclic ether is present the analogous reaction (2.62.) leads to chain transfer and the formation of new short chains.

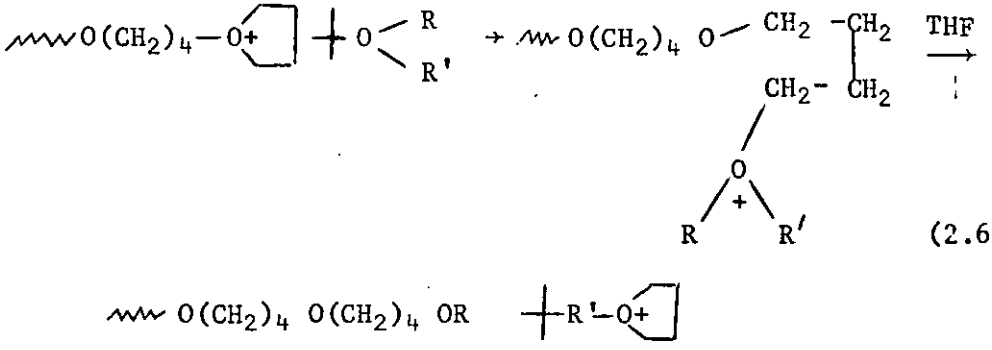

(2.62.)

The new short chains can be formed even at equilibrium. They will enter into the propagation - depropagation reaction and they can also react with polymer oxygen. Both of these reactions will lead to a decrease in overall molecular weight; the first results in growth of new chains at the expense of longer ones and the second brings about chain cleavage.

The destruction of active centers, rather than transfer of charge to another chain, is not a simple process. Perhaps the most obvious method for chain termination during polymerization would be by anion recombination, i.e.,

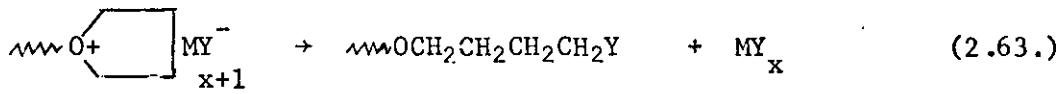

(2.63.)

With certain systems in cyclic ether polymerization, it is possible to demonstrate lack of termination and thus establish a "living" cationic polymerization. (38,132,140, 141). Polymerising systems having perfluoro axions such as BF_4^-, PF_6^-, SbF_6^- appear to be the most stable and demonstration of "living" character in the system is achieved by waiting until the system reaches equilibrium and adding extra monomer, with a consequent increase in molecular weight. Alternatively, addition of a second monomer results in block copolymer formation.

Many examples of copolymerization of cyclic ethers are known (40,142,145). Quantitative estimation of relative reactivities in polymerization for cyclic ethers is very difficult because of the complications arising from equilibrium depolymerizations and the likelihood of block copolymer formation. However, the relative basicities of cyclic ethers have been estimated by several different techniques. (142, 146). The results show that for cyclic ethers the basicity varies with ring size in the order: 4 > 5 > 6 > 3.

2.10. SMALL-ANGLE SCATTERING OF POLYMERS

X-ray scattering and interference effects can be considered as due to the variations in electron density from one point to another in the material.' In a perfect crystal, in which the atoms are regularly arranged according to a space lattice, the scattering angle 2θ is related to the interplanar spacing d by the Bragg equation $n\lambda = 2d \sin\theta$. Because of the reciprocity between interatomic distance and sin θ, inhomogeneities of colloid dimensions generate x-ray scattering and interference effects at very small angles, typically less than 2^{o} with the wavelength of CuK_{α}, $1.542A^{o}$. This small-angle scattering has little dependence except via density effect on the inhomogeneities of atomic dimensions that give rise to the wide-angle diffraction. It is only the fluatuations in electron density over distances, typically 30 to 1000 A^{o} that determine the nature of the small-angle scattering. Therefore rather perfect single-crystals, pure phases in general and other homogeneous substances do not scatter x-rays at very small angles.

The two kinds of inhomogeneity that are most likely to be responsible for small-angle x-ray scattering from solid polymers are (a) alteration of crystalline and amorphous regions, which in general will possess different electron densities, and (b) the presence of microvoids or microdomains dispersed throughout the solid polymer matrix. The intensity of small-angle scattering increases with the degree of contract between the elecron densities of the two or more kinds of region that produce the heterogeneity. For a two-phase system with volume fractions ϕ_1 and ϕ_2 and with the respective electron densities ρ_1 and ρ_2, the scattering power is defined as

$$\overline{I_2} = \overline{(\rho_1 - \rho_2)^2}\ \phi_1\phi_2 \qquad (2.64.)$$

Thus the intensity of small-angle scattering is relatively large for a system of discrete particles dispersed in matrix, but relatively small for a heterogeneous system of crystalline and amorphous regions that differ but slightly in density.

An inhomogeneous system exhibits two types of x-ray effects at small angles: diffuse scattering and discrete diffraction. Diffuse scattering usually has a maximum intensity at an angle of 0° and it decreases in intensity up to $1\text{-}2^{\circ}$; whereas discrete diffraction is most frequently found as a single maximum corresponding to a Bragg spacing of $75A^{\circ}$ to $200A^{\circ}$, although second or third order maxima have been observed in some cases.

The diffuse small-angle scattering pattern is not subjected to an unequivocal structural interpretation on the basis of the x-ray data taken alone due to the following ambiguities.

1. As a consequence of the Babinet principle of reciprocity in optics it is not possible to distinguish the scattering by a system of particles in space from the scattering by a complementary system of micropores in a solid continum. Other evidence must be used to distinguish between these possible causes of the scattering.

2. It is not possible to differentiate without some degree of uncertainty the effect due to particle shape from those due to polydispersity.

3. It is frequently difficult to determine to whatextent the scattering curve is determined by the isolated particles and to what extent by the interparticle interferences. Whereas dilute systems yield only particulate scattering, in close packed systems interparticle interferences cannot be neglected.

Excellent reviews on the theory of small-angle x-ray scattering and on the application of x-ray diffraction methods in polymer science exist. (147 - 152).

As mentioned above, the atoms in a crystal are regularly arranged according to a space lattice. There are 14 possible types of space lattice, one triclinic, two monoclinic, four orthorhombic, one rhombohedral, one hexagonal, two tetragonal and three cubic.

The simplest cubic lattice is that in which the lattice points lie at the corners of cubes. The three primitive translations are all equal, and at right angles and this is the true cubic space lattice (P). The other cubic lattices are the face-centred cube(F), having a point at each corner of a cube and one on the middle of each face; and the body-centred cube (B), having a point at each cube corner and one at the cube centre.

In face-centered cubic crystals, x-ray reflection will only occur when h,k and ℓ are all odd or all even. (h, k, ℓ are the Miller indices). In body-centered cubic crystals, reflection will occur when the sum of the Miller indices is even. All reflections are allowed for a primitive lattice. Table 2.1. gives the allowed reflections in the cubic system for $h^2+k^2+\ell^2$ = 1 to 10.

TABLE 2.1 ALLOWED REFLECTIONS IN THE CUBIC SYSTEM

$h^2+k^2+\ell^2$	$(h^2+k^2+\ell^2)^{\frac{1}{2}}$	Allowed, for lattice	{hkℓ}
1	1.000	P	100
2	1.414	PB	110
3	1.732	PF	111
4	2.000	PBF	200
5	2.236	P	210
6	2.449	PB	211
7	not allowed		
8	2.828	PBF	220
9	3.000	P	300,221
10	3.162	PI	310

CHAPTER 3. EXPERIMENTAL

3.1 DETAILS OF THE POLYMERS MEASURED

The polymer used in this work was a polystyrene-polybutadiene-polystyrene (S-B-S) block copolymer, marketed by the Shell Chemical Company under the name KRATON 101.

Table 3.1 Properties of the S-B-S Block Copolymer

	Experimental	Literature (153, 154)
Density	0·94 g./c.c.	0·94 g./c.c
Weight % Styrene	28	28
$\overline{Mn}$	78,000	76,000
	Diene microstructure	
cis-1,4		41%
trans-1,4		51%
1,2 (vinyl)		8%

Molecular Weight Determination

The number-average molecular weight was determined with a Hewlett-Packard 502 High Speed Membrane Osmometer, using toluene as solvent, at 25°C.

Chemical Analysis for Polystyrene

The method of Kolthoff et al (155) was used to determine the weight fraction of polystyrene in the S-B-S block coplymer. It is

based on the degradation of the butadiene portion of the molecule by tert-butylhydroperoxide in p-dichlorobenzene, catalysed by osmium tetroxide. The resulting small molecular fragments (low molecular weight aldehydes) are soluble in ethanol, while the unattached polystyrene is not. The polystyrene is isolated by pouring the reaction mixture into ethanol and filtering out the polymer.

Table 3.2 Solubility Parameter for Polymers and Solvents (156)

Polymer/Solvent	δ $(cal./c.c)^{\frac{1}{2}}$
polystyrene	9·1
polybutadiene	8·6
n-hexane	7·3
methyl-cyclohexane	7·8
toluene	8·9
methylene chloride	9·7

Cast Samples

Films ranging in thickness from about 0·05 cm to 0·2 cm were cast from methyl cyclohexane, toluene and methylene chloride. The polymer was weighed and dissolved in the solvent. The concentration of the solution was about 10%. After the polymer was dissolved, the solution was poured into clean mercury, contained in a large crystallising dish.

The solvent was allowed to evaporate slowly at room temperature and atmospheric pressure. Complete evaporation of solvent took about a week. The films after being removed from the mercury were air-dried for at least ten days before being used in a test.

Moulded Samples

The polymer was compression moulded into strips, 10 cm long, 0·6 cm wide and 0·3 cm thick, and disc of 5 cm in diameter. The mouldings were carried out at 150°C for twenty minutes. The moulded samples were allowed to cool slowly to ambient temperature under pressure.

Swollen-Deswollen (S/D-S) Samples

The apparatus used in preparing the S/D-S samples is shown in Figure 3.1. Strips of films cast from toluene and methylene chloride were swollen with n-hexane at ambient temperature to about 50% extension. The swollen strips were then deswollen and dried by removing the solvent under vacuum. However, the strips did not completely recover their original dimensions. The amount of set was generally 6%, being greatest at the clamped end and very small at the lower end. The clamped end of each strip was cut off and the remaining piece was used as a test sample.

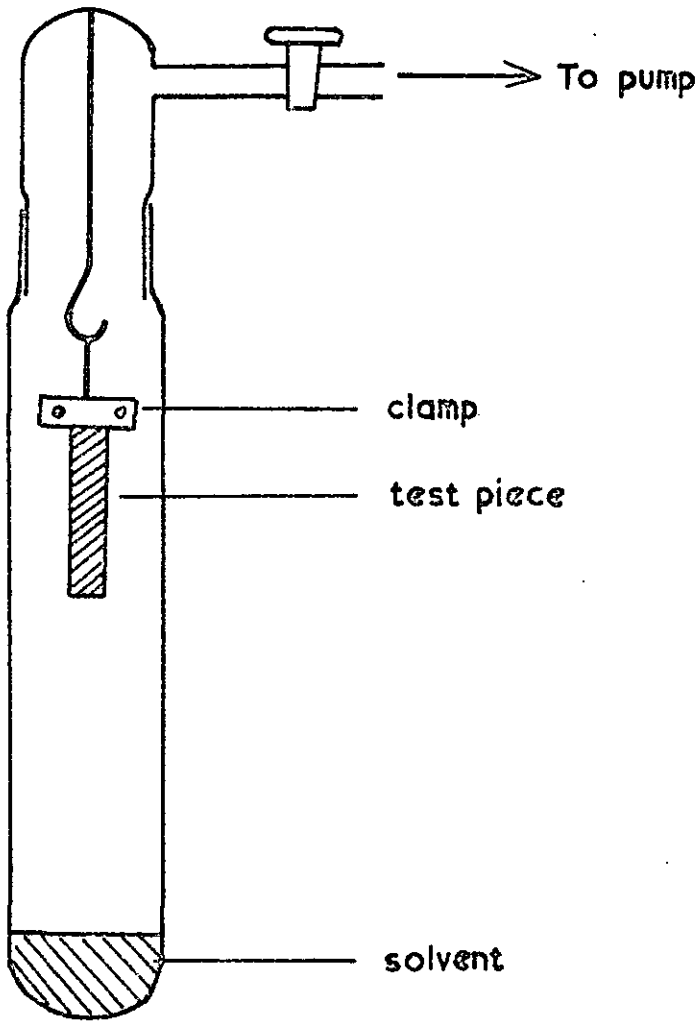

FIG. 3.1.

3.2 SMALL ANGLE X-RAY SCATTERING AND ELECTRON MICROSCOPY STUDIES

Samples of approximately 1 mm thick were used in the SAXS studies. The samples were mounted in a temperature-controlled cell on a Rigaku-Denki SAXS goniometer (2202). Slit collimation in conjunction with Geiger counting, was used to study the scattering from unstretched samples. The effect of temperature on unstretched samples in the range $-100^{\circ}C$ to $+125^{\circ}C$ was also studied. The Geiger counting was operated by automatic scanning at very slow rates, approximately half a degree per hour. The scanning time was about an hour. Scanning was done both to the right and to the left of the axis, in order to check the zero alignment. The effect of stretching up to 600% extension on the samples was investigated with pin-hole optics and film detection. Pin-hole optics were also used to determine the lattice structure of more regular morphologies. By use of long exposure, higher order reflections were observed. The exposure time in this case was two days. The instrumental variables were optimised to give a maximum resolution at 1000 Å (157).

The domain structures of K101 were observed by electron microscopy. Films of about 0·1 mm thick were cast from an approximately 1% toluene solution. The solvent was allowed to evaporate off at room temperature in vacuo. The dry films were stained with osmium tetroxide, to provide sufficient contrast between polystyrene and polybutadiene phases. The stained films were then embedded in Araldite, and ultrathin sectioning carried out by an ultramicrotome to a thickness of about 500 Å.

3.3 EQUILIBRIUM SWELLING AND EXTENSION STUDIES

SWELLING MEASUREMENTS

Rectangular specimens were cut from moulded and toluene cast samples. The specimens were weighed on an analytical balance, and allowed to swell in n-heptane for one day at 25°C. The swollen specimens were blotted with filter paper and transferred quickly to weighing bottles. The volume of imbibed solvent was obtained by dividing the difference between the weight of the swollen specimen and the weight of the dry specimen (dried for two days at room temperature in vacuo). Next the dry specimens were weighed in methanol and their volumes calculated. From this volume was substracted the volume of the polystyrene 'fillers', giving the volume of rubber (polybutadiene). The latter was used to calculate the volume fraction of rubber in the swollen polymer (V_r).

Using the value of V_r from equilibrium swelling measurements, an estimation of the molecular weight between 'effective crosslinks' for conventional vulcanizates is given by the Flory-Rehner Equation (158).

$$M_c = \frac{\rho_2 \bar{V}_1 (V_r^{1/3} - V_r/2)}{\ell_n(1-V_r) + V_r + \chi_1 V_r^2} \qquad (3.1)$$

where χ_1 is the polymer-solvent interaction parameter,

ρ_2 is the density of the unswollen elastomer phase,

and $\bar{V}_1$ is the molar volume of the swelling agent.

This treatment assumes the network to contain no imperfections or free chain ends and to have a cross link functionality of four.

MODULUS DETERMINATION ON UNSWOLLEN SAMPLES

Samples of dimensions approximately 6·0 × 0·5 × 0·1 cm were

clamped at both ends. The upper clamp was fixed rigidly to a vertical scale, while the lower clamp was free to slide along the scale and can be locked at any position. The specimen was then stretched to about 30% extension and a stress-strain curve was determined at decreasing elongation. About twenty minutes were allowed for the stress to attain equilibrium at each elongation. The load was measured with the Autobalance Universe Bridge B641, in term of inductance. From the load/inductance calibration curve and the cross-sectional area of the unstretched sample, the stress corresponding to each elongation was calculated.

The values obtained were plotted according to a modified equation of the kinetic theory of rubber elasticity (159), taking in consideration the presence of fillers in the network (86).

$$\sigma = \frac{\rho RT}{M_c}(\lambda - \lambda^{-2})(1 + 2{\cdot}5\phi_s + 14{\cdot}1\phi_s^{2}) \qquad (3.2)$$

where σ is the tensile stress based on the cross-sectional area of the unstretched sample,

ϕ_s is the volume fraction of the polystyrene 'fillers' in the rubber network,

ρ is the density of the elastomer phase,

R is the gas constant,

T is the absolute temperature,

M_c is the molecular weight between 'cross-links',

and λ is the extension ratio.

MODULUS DETERMINATION ON SWOLLEN SAMPLES

Rectangular specimens were swelled in Nujol (castor oil). The swollen specimens were allowed to equilibrate at room temperature for overnight. Using one of the swollen specimens, the volume fraction of rubber in the swollen polymer V_r was determined. Nujol was used

as the swelling agent because it swells the polybutadiene phase, but does not affect the polystyrene domains. Also Nujol is a non-volatile solvent. The swollen specimens were stretched using a step loading technique by adding 50 gm. weight every twenty minutes. The extensions were measured with a cathetometer on two bench marks made on the unstretched swollen sample.

The molecular weight between 'crosslinks' was calculated from the stress-strain relation for a swollen, filled rubber network (86, 159).

$$\sigma = \frac{\rho RT}{M_c} V_r^{-1/3}(\lambda - \lambda^{-2})(1 + 2{\cdot}5\phi_f + 14{\cdot}1\phi_f^2) \qquad (3.3)$$

where σ is the tensile stress based on the cross-sectional area of the unstretched, swollen specimen,

ϕ_f is the volume fraction of polystyrene 'fillers' in the swollen specimen,

and λ is based on the unstretched, swollen length.

3.4 STRESS-STRAIN BEHAVIOUR

Tensile stress-strain curves for each sample were determined to the rupture point over a temperature range of +30°C to +70°C and at 5 strain rates. Stress-strain data were obtained with an Instron tester at crosshead speeds between 0·5 and 50 cm per minute.

The Instron tester was equipped with a temperature controlled box, which allowed the attainment of temperature from ambient to 100°C. Temperature control in the range studied was ±0·5°C.

Tensile tests were made on ring-type specimens which were cut from films of the various solvent cast samples, using a special ring cutter. The rings had an inside diameter of about 1·54 cm, and an outside diameter of about 1·73 cm. The dimensions of each ring were calculated from the weight of a ring, the weight of the disc from the centre of a ring, the thickness of the disc, and the density of the block copolymer. A ring was tested by placing it over hooks attached to the load cell and movable crosshead of the Instron.

Stress-strain data were obtained from the dimensions of a ring and the load-time trace obtained during a test. The average stress at any instant was obtained by dividing the observed load by twice the cross-sectional area of an unstretched ring; average strain was obtained from the crosshead displacement and the average diameter of an unstretched ring.

Hystersis loops of about 250% extension for the various ring-type specimens were also obtained from the Instron.

3.5 CREEP

A diagram of the apparatus is shown in Figure 3.2. Strips of the films cast from toluene were subjected to constant tensile loads and the resulting extensions measured by means of a cathetometer. Brench marks were made on the stretched strips with small droplets of ink and the distance between them measured. The strips were generally 6 cm long, 6 mm wide and 1 mm thick. They were allowed to equilibrate in the temperature controlled chamber at the requisite temperature before the load was applied. The first measurement was made one minute after the load was applied and subsequent ones at convenient intervals during the test.

Creep data were obtained over a temperature range of +30°C to +50°C at four stress levels, corresponding approximately to 14%, 45%, 100% and 300% extensions at one minute, after the application of the load. All tests were carried out on freshly cut pieces.

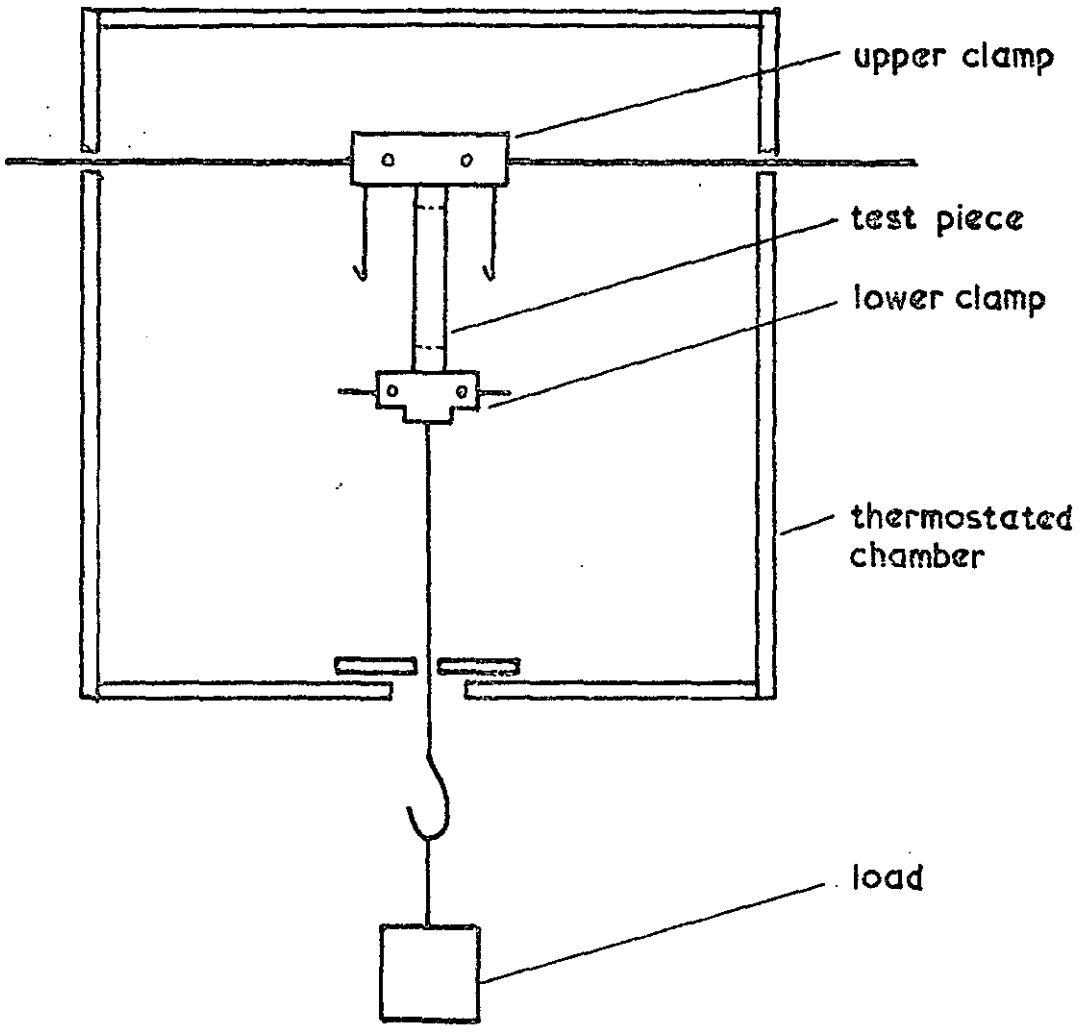

FIG. 3.2. TENSILE CREEP APPARATUS

3.6 STRESS RELAXATION

The stress relaxation apparatus is shown in Figure 3.3. Stress relaxation data were obtained for films cast from toluene and methylene chloride. The measurements were taken over a temperature range from +30°C to +70°C, and for fixed elongations of 14%, 45%, 100% and 300%. The time for each test was generally 300 minutes.

Test strips of about 7 mm wide, 3 mm thick and 3 to 10 cm in length were suspended in the chamber, which was air-thermostated. A period of about an hour was allowed for the strips to attain the test temperature before they were extended.

The ends of the strips were gripped in metal clamps, the upper one being fastened to a stiff spring whose deflection was used to measure the stress in the sample. The spring deflection was negligibly small in comparison with the deformation of the sample. The lower clamp was displaced vertically away from the upper one to a fixed stop, positioned so that the required degree of extension was imposed on the sample. It was then secured in this position.

The stress relaxation data were obtained from the dimensions of a strip and the load-time trace obtained during a test. The average stress at any instant was obtained by dividing the observed load by the cross-sectional area of the unstretched strip. The stress σ, after a period of time, t, in the deformed state is then expressed as a fraction of the stress σ_i, after 0·5 minutes in the deformed state.

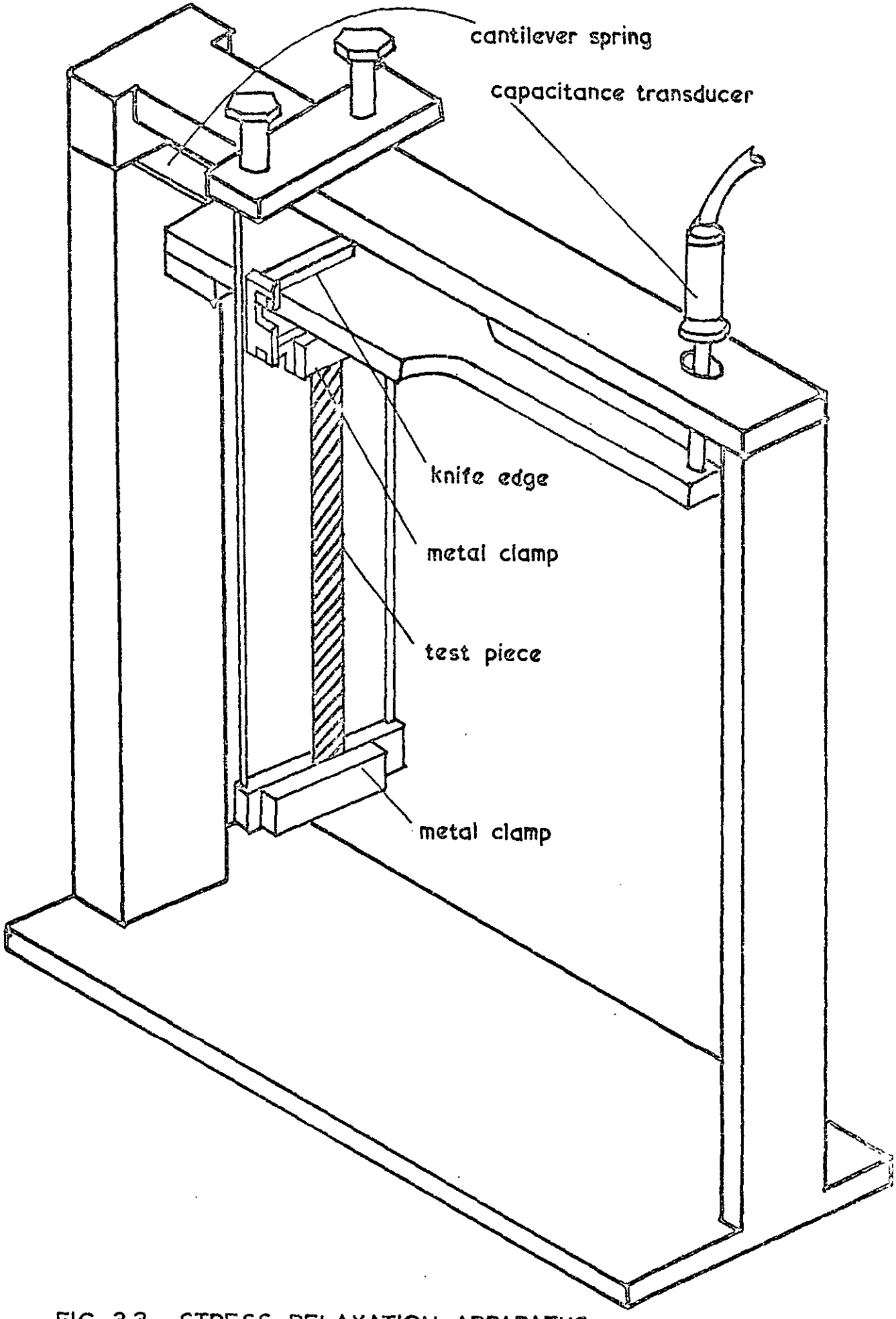

FIG. 3.3. STRESS RELAXATION APPARATUS

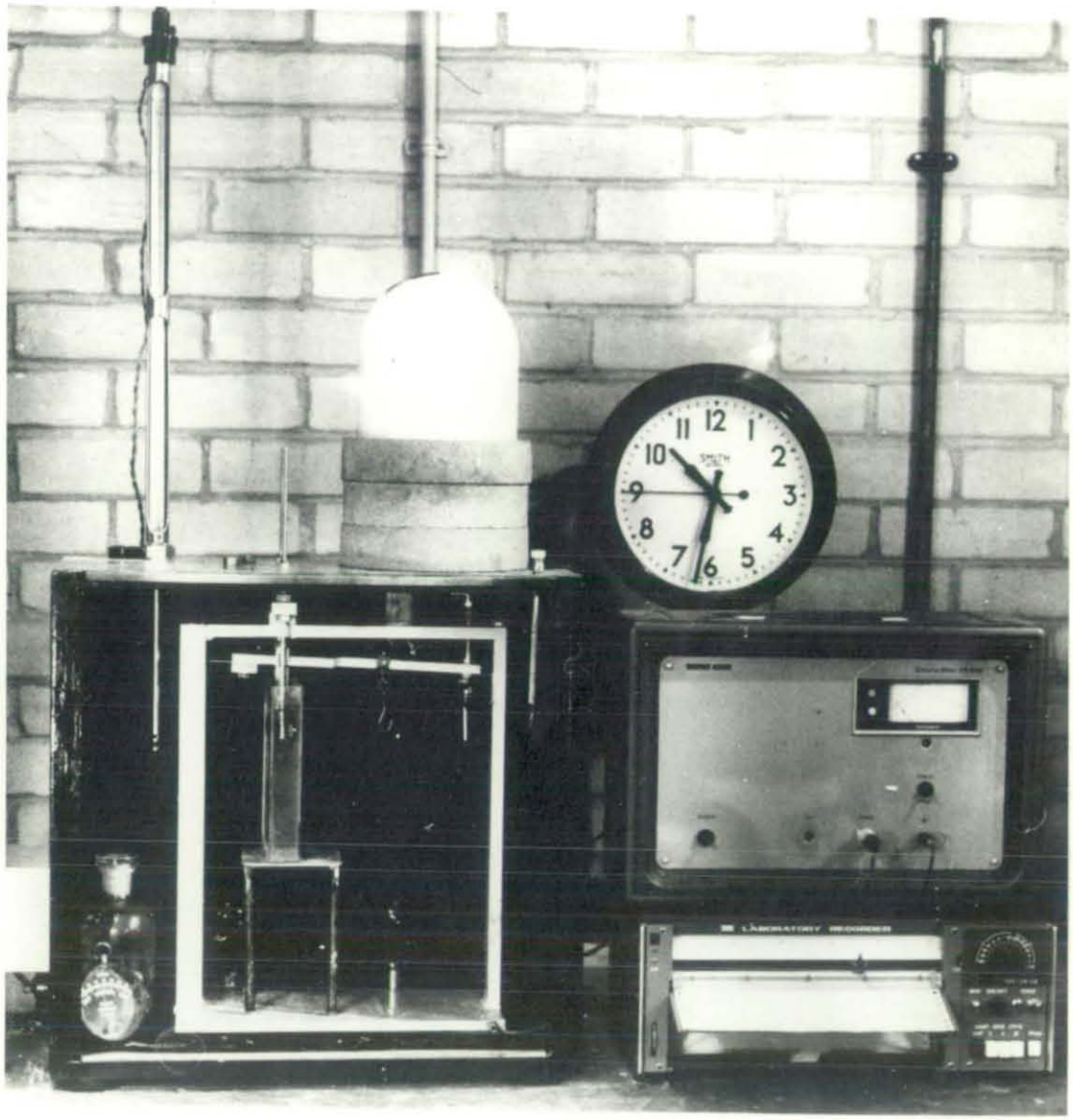

FIG. 3.3.

3.7 PRINCIPLE OF THE DYNAMIC MECHANICAL APPARATUS

The dynamic mechanical apparatus, which is described in the following section, can be used to measure either Young's or shear rigidity moduli, depending on the deformation applied to the test specimen. For Young's moduli, a rectangular beam specimen is clamped rigidly at both ends and is oscillated in bending geometry by a central clamp. Wherelse for shear moduli, two disc specimens are oscillated, in shear sandwich geometry, by a central plate. The central clamp and the central plate are interchangeable and are driven by a magnet suspended on thin wires in the centre of a coil.

The force is produced by the action of a sinusoidal current in the coil of the magnet. It is resisted by the mass of the moving system, the rigidity of the specimen and the rigidity of the suspension wires. The equation of motion for such a system is:

$$M\ddot{x} + kE^*x + Ax = F_o \exp(i\omega t) \qquad (3.4)$$

where M is the mass of the vibrating system
x is the linear displacement of the driven clamp,
E^* is the complex rigidity modulus ($E' + iE''$) of the specimen,
F_o is the maximum driving force,
ω is the angular frequency of the driving current,
t is the time,
A is a term for the rigidity of the suspension wires,
and k is a geometrical factor, which for bending geometry is given as:

$$k = 2bh^3/\ell^3 \qquad (3.5)$$

where b is the width, h the thickness and ℓ the length of each half of the specimen between each rigid clamp and the central clamp. (See Appendix I)

For shear sandwich geometry, E* is replaced by G* in Equation (3.4) and k, the geometrical factor, equals:

$$\begin{aligned} k &= Q_1/\ell_1 + Q_2/\ell_2 \\ &= 2Q/\ell, \quad \text{if samples are identical.} \end{aligned} \tag{3.6}$$

where Q is the cross-sectional area and ℓ the length of the specimens.

It has been shown (160) that the solution to this differential equation is:

$$x = \frac{F_o \exp. i(\omega t - \beta)}{\left[(kE' + A - M\omega^2)^2 + k^2E''^2\right]^{\frac{1}{2}}} \tag{3.7}$$

where

$$\beta = \tan^{-1}\left[\frac{kE''}{kE' + A - M\omega^2}\right] \tag{3.8}$$

If only peak force and peak amplitude are considered Equation (3.7) becomes:

$$\frac{F_o}{x_o} = \left[(kE' + A - M\omega^2)^2 + k^2E''^2\right]^{\frac{1}{2}} \tag{3.9}$$

where x_o is the peak linear displacement.

Solving the simultaneous equations (161) (3.8) and (3.9) for E' and E'' gives:

$$E' = \frac{1}{k}\left[\frac{F_o}{x_o}\cos\beta - A + M\omega^2\right] \tag{3.10}$$

$$E'' = \frac{1}{k}\,\frac{F_o}{x_o}\sin\beta \tag{3.11}$$

The $M\omega^2/k$ term can usually be neglected when ω is less than one-fifth of the resonant frequency. The suspension rigidity term, A, will have a value equal to $M\omega^2_{(V)}$, where $\omega_{(V)}$ is the resonant frequency of the vibrating system without samples. A will be small when $\omega_{(V)} << \omega_{(S)}$, where $\omega_{(S)}$ is the resonant frequency of the vibrating system with sample.

Therefore Equation (3.10) becomes:

$$E' = \frac{1}{k}\left[\frac{F_o}{x_o}\cos\beta\right] \tag{3.12}$$

This simplifies the calculation considerably since from Equations (3.11) and (3.12):

$$\tan\delta = \tan\beta \tag{3.13}$$

and

$$E^* = E' + iE'' = \frac{F_o}{kx_o} \tag{3.14}$$

At some high frequency, depending on the rigidity of the sample, the vibrating system will possess an amplitude resonance. From Equation (3.9) the condition for a maximum in x_o with varying frequency is (160):

$$kE' = M\omega_o^2 \tag{3.15}$$

where ω_o is the resonant frequency. Measurement of the resonant frequency thus gives an accurate value of E' at that frequency.

An essential step in the measuring process is the conversion of the linear displacement into a proportional voltage. This is done with a Bently transducer, operating in conjunction with a Bently Proximator circuit and a power supply. The Bently system produces

an output voltage proportional to gap and gap variation from the probe face to the observed surface. That is,

$$x_o = BV \tag{3.16}$$

where x_o is the peak linear displacement,
V is the R.M.S. value of the output voltage,
and B is a constant of the transducer system.

In principle, the dynamic properties of a specimen are given in terms of quantities which are measurable.

The peak driving force is proportional to the R.M.S. value of the driving current i. Thus:

$$F_o = Ni \tag{3.17}$$

where N is a constant dependent on the strength of the magnet and the properties of the coil. Similarly, the peak displacement is proportional to the output voltage as given by Equation (3.16).

Combining Equations (3.10) and (3.11) with Equations (3.16) and (3.17) gives E' and E" in terms of actual measurements.

$$E' = \frac{N}{kB}\left[\frac{i}{v}\cos\beta\right] - \frac{A}{k} + \frac{M\omega^2}{k} \tag{3.18}$$

$$E'' = \frac{N}{kB}\left[\frac{i}{v}\sin\beta\right] \tag{3.19}$$

3.8 IMPROVED VERSION OF THE DYNAMIC MECHANICAL APPARATUS

The dynamic mechanical apparatus described by Bowman (161) has been modified and improved. A general description of the modified apparatus (with reference to Figure 3.4) as a whole is given initially, followed by more detailed descriptions of those components which have been modified.

The two magnets (M) are suspended in the centre of the system of coils (C) by two sets of three stainless steel wires (W) (38 gauge). The coils are supported on a metal bobbin (B). The magnets are connected to the drive clamp (D) by an aluminium spacer (A) and a 6BA threaded aluminium rod (R). The rectangular beam specimen (S) is clamped at both ends to two brass plates (P), and is attached at the centre to the drive clamp. Each of the brass plates is struck with "Araldite" to a brass three-quarter cylinder (T) which is free to move in a vertical direction. This allows the length of the specimen to be varied. The movement of the cylinders is controlled by the two 2BA screws (E). A brass cylindrical tube, $1\frac{3}{4}$" in length and 2" in diameter, is screwed to the main body of the apparatus. This supports the coil bobbin and provides anchor points for the suspension wires. A brass case slides tightly into the open end of the cylindrical tube. This holds a brass cylindrical rod (G), with a probe (F) at one end. The probe and the soft-iron disc (I), on the vibrating system form the transducer unit.

The apparatus is attached to a thick, flanged, brass plate by two L-shaped brackets. The whole instrument is thus supported vertically by its top end, so that it may be placed in a brass container and evacuated.

The vibrating system is shown schematically in Figure 3.5. It consists of the aluminium drive clamp (D), the 6BA threaded aluminium rod (R), four soft-iron nuts, the aluminium spacers (A), the magnets (M)

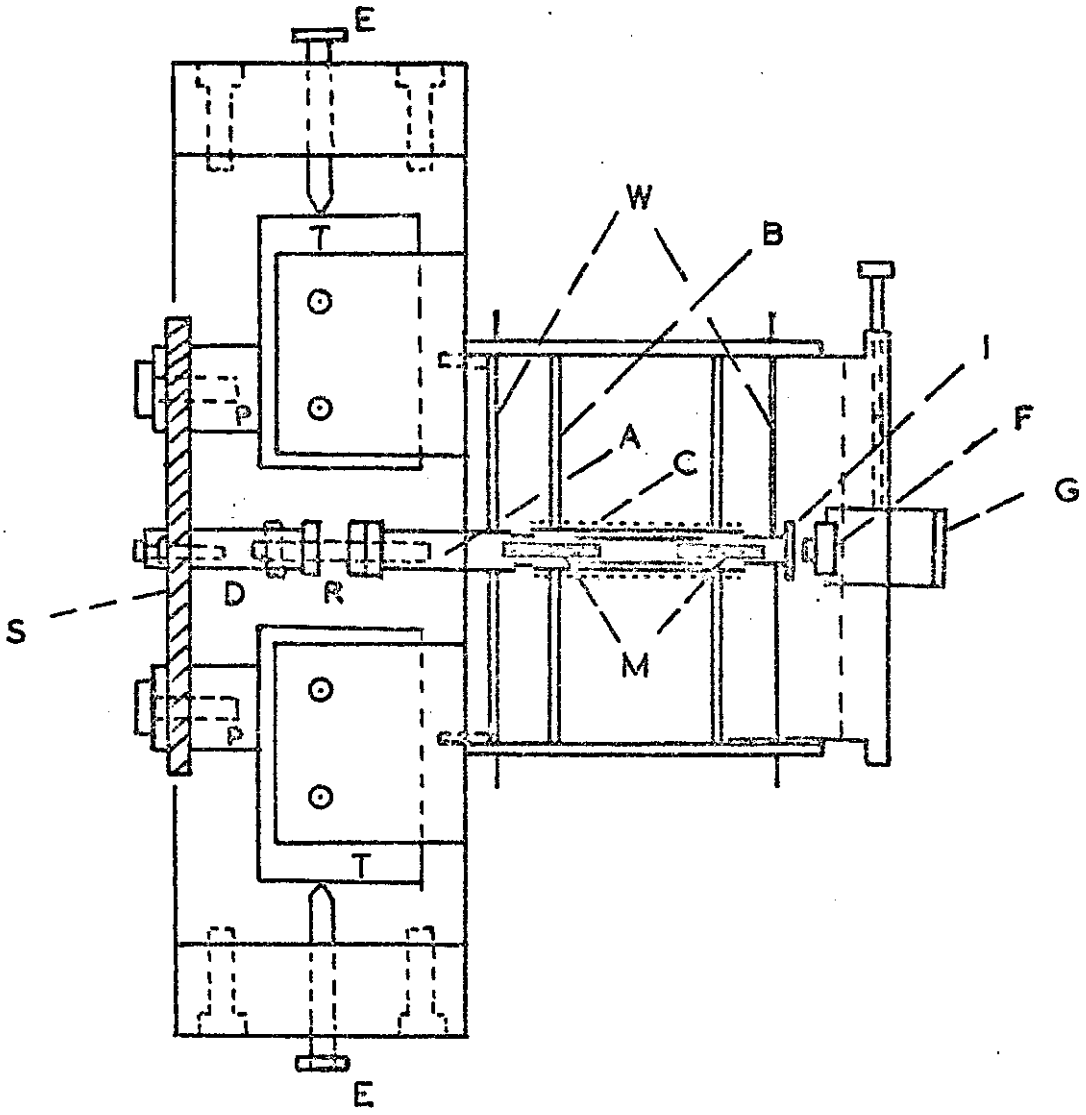

FIG. 3.4.

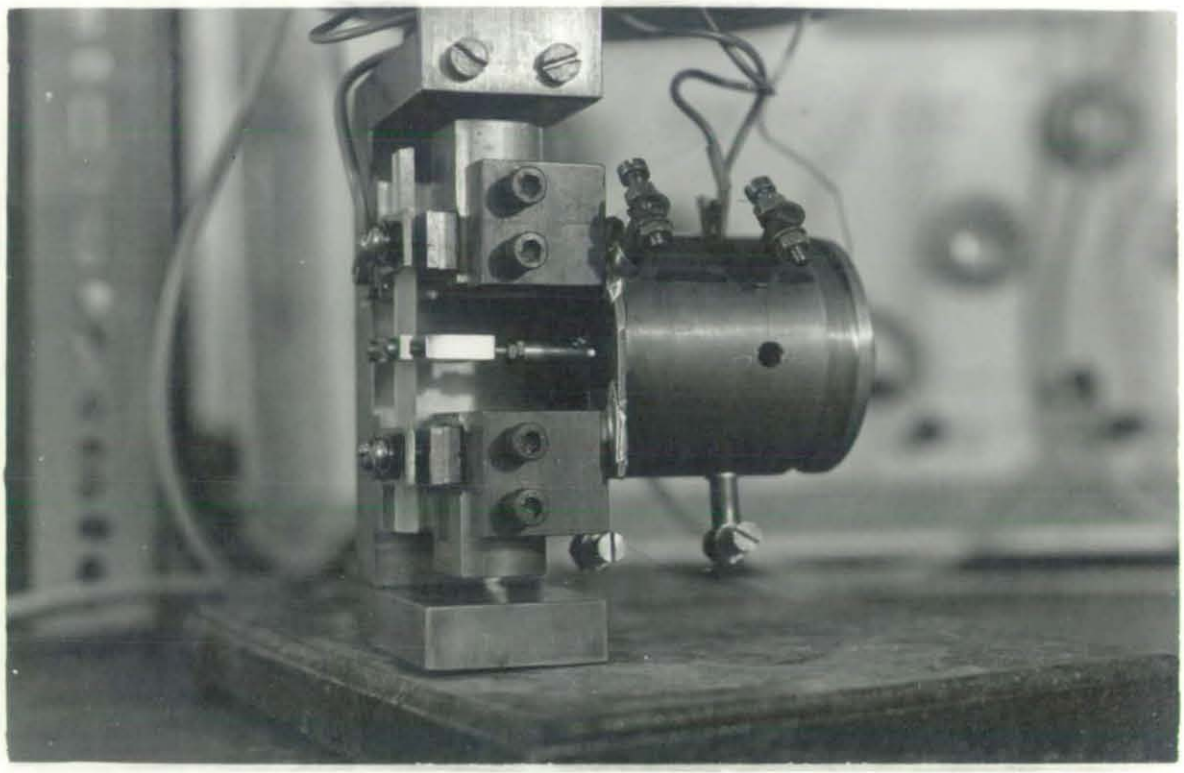

FIG . 3.4.

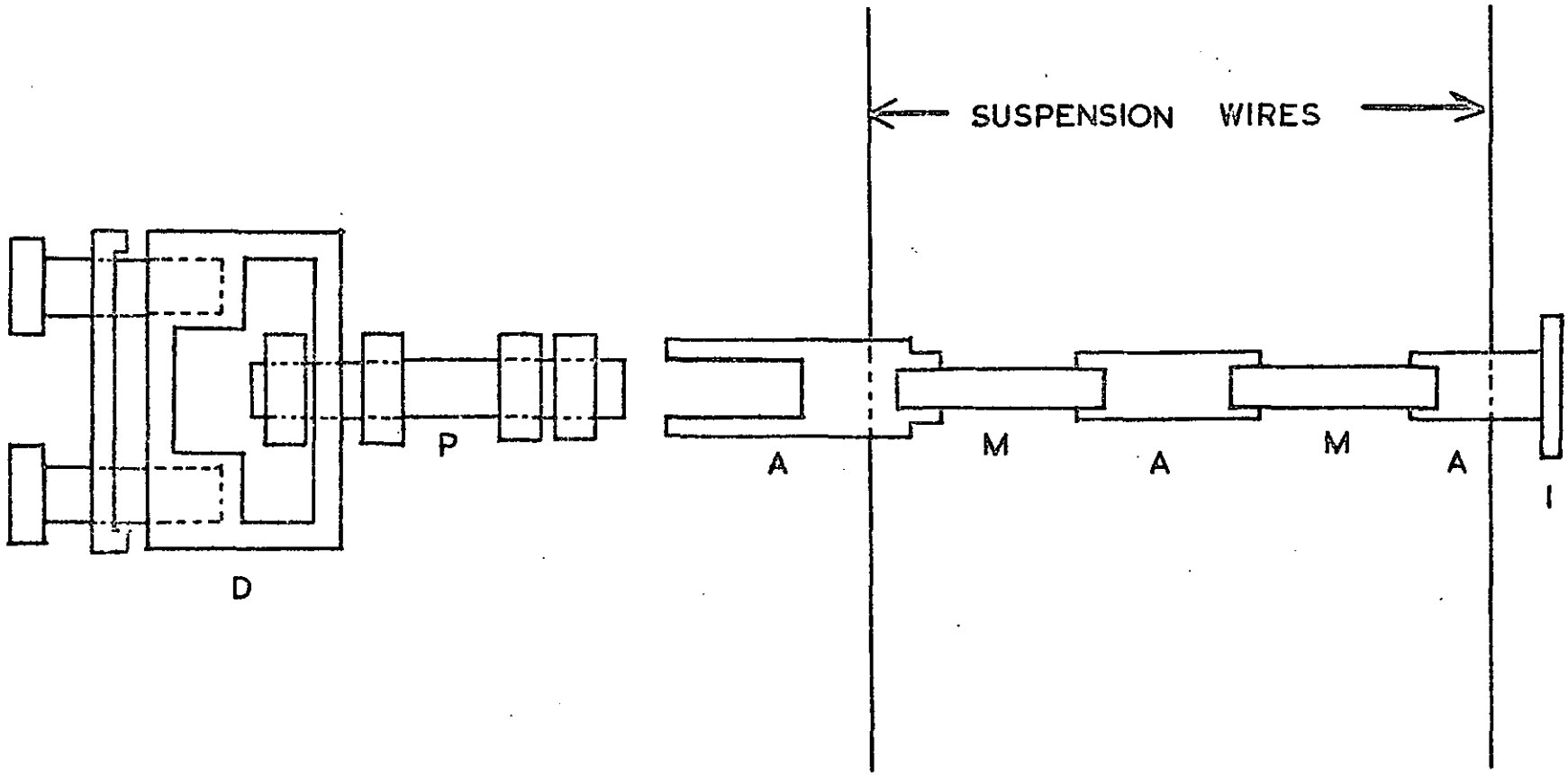

FIG. 3.5.

and the soft-iron disc (I). The drive clamp is free to move in the horizontal direction and is locked in position by two 6BA nuts. The drive clamp and threaded rod can be replaced by a drive plate. Two similar disc specimens could then be oscillated in shear sandwich geometry as described by Bowman (161).

The soft-iron disc was found to provide the most sensitive electrically conductive surface for the Bently Probe to sense. The disc is of ½" diameter and 1/16 inch thickness and is struck to the vibrating system with "Araldite". Alternative metals like tin, copper, stainless steel and aluminium gave less sensitivity.

The Bently probe is fitted onto the end face of the one inch long brass cylindrical rod. The rod is free to slide in a horizontal direction, through the centre of the thick cover of the brass case and is solidly locked in position by a screw pressing against it. The probe and the soft-iron disc are parallel to each other. The initial gap between them is adjusted by moving the rod, to give the highest output voltage commensurate with good linearity for the range of the displacement of the vibrating system.

Figure 3.6 shows the tensioning device used in tightening the suspension wires. Each wire is anchored to the vibrating system by a soldered-knot. The wire then passes through the fine hole in the centre of the tensioning device. The wires are tightened and locked in tension by two 4BA nuts, turning in opposite directions. The tensioning device sits in a hole through the supporting brass cylindrical tube and is clamped tightly by a 4BA nut.

The block diagram and the photograph (Figures 3.7) show the arrangement of the electronic apparatus. The variable frequency (0·01 c/s to 11·1 kc/s) oscillator (Solartron O.S. 103·3) is capable of supplying an unbalanced, attenuated alternating voltage of 10 volts r.m.s. maximum. The output voltage from the oscillator is fed into a power amplifier (AIM WPA.116). The power amplifier

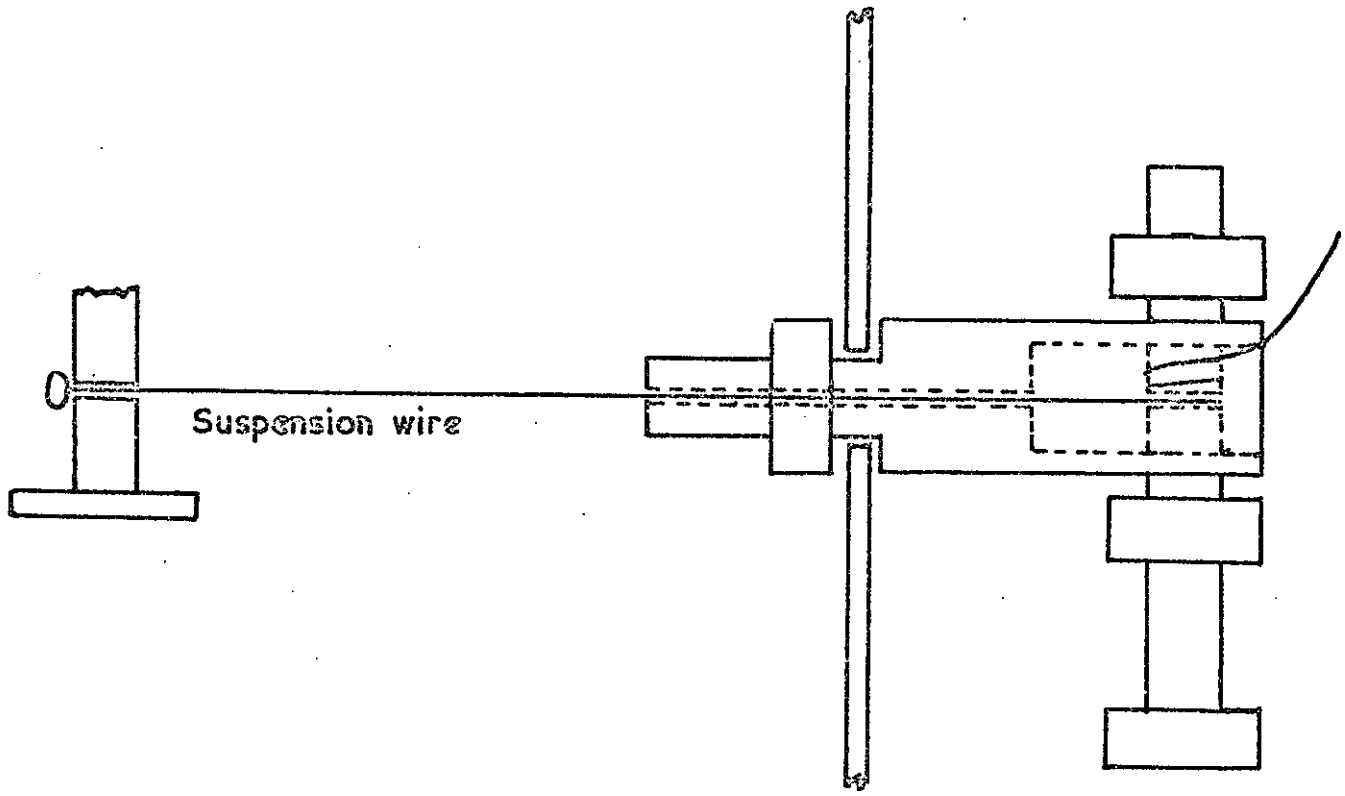

FIG. 3.6.

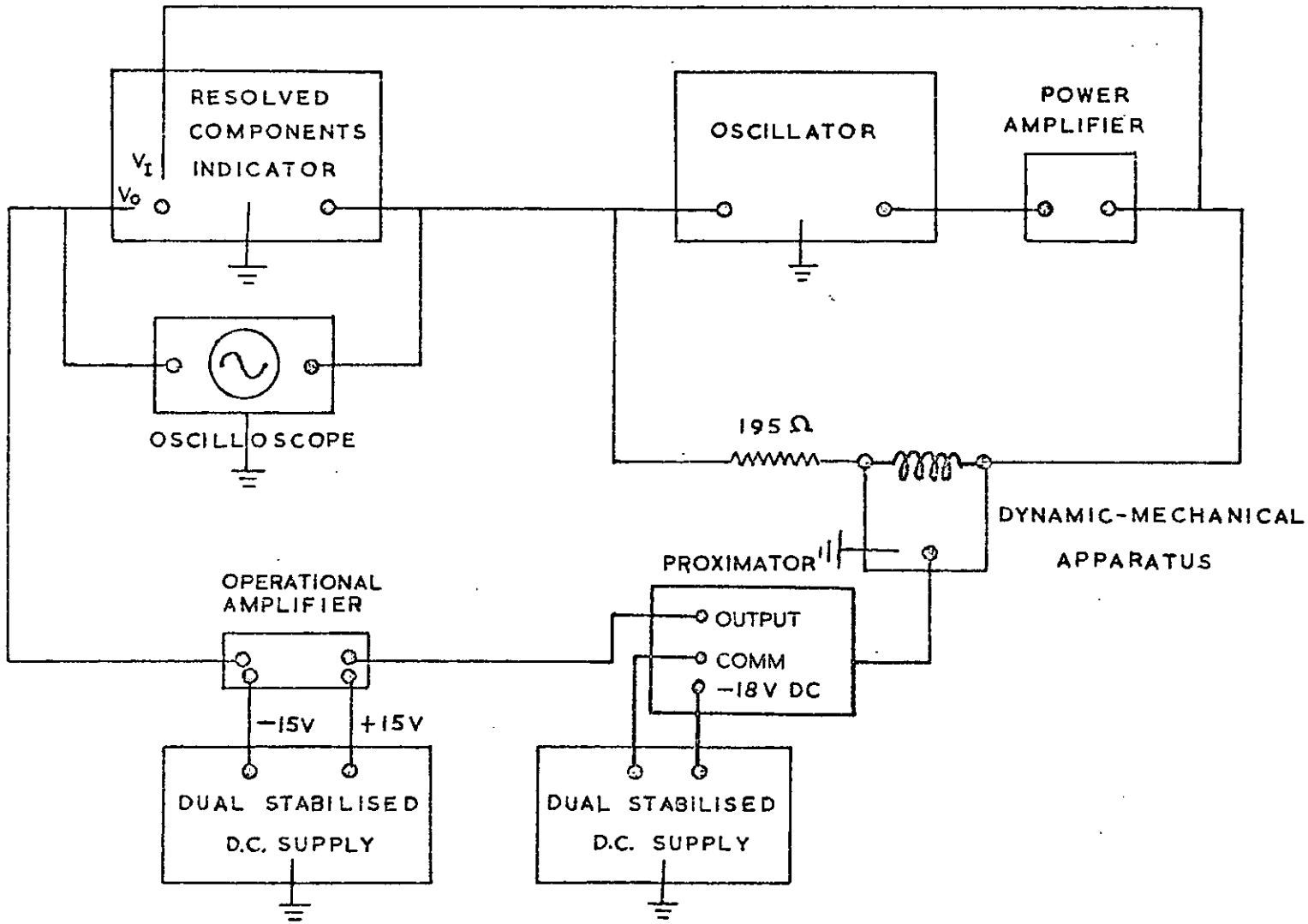
RESOLVED
COMPONENTS
INDICATOR
V_I
V_o
OSCILLATOR
POWER
AMPLIFIER
OSCILLOSCOPE
195 Ω
DYNAMIC-MECHANICAL
APPARATUS
PROXIMATOR
OPERATIONAL
AMPLIFIER
OUTPUT
COMM
−18V DC
−15V
+15V
DUAL STABILISED
D.C. SUPPLY
DUAL STABILISED
D.C. SUPPLY

FIG. 3.7.

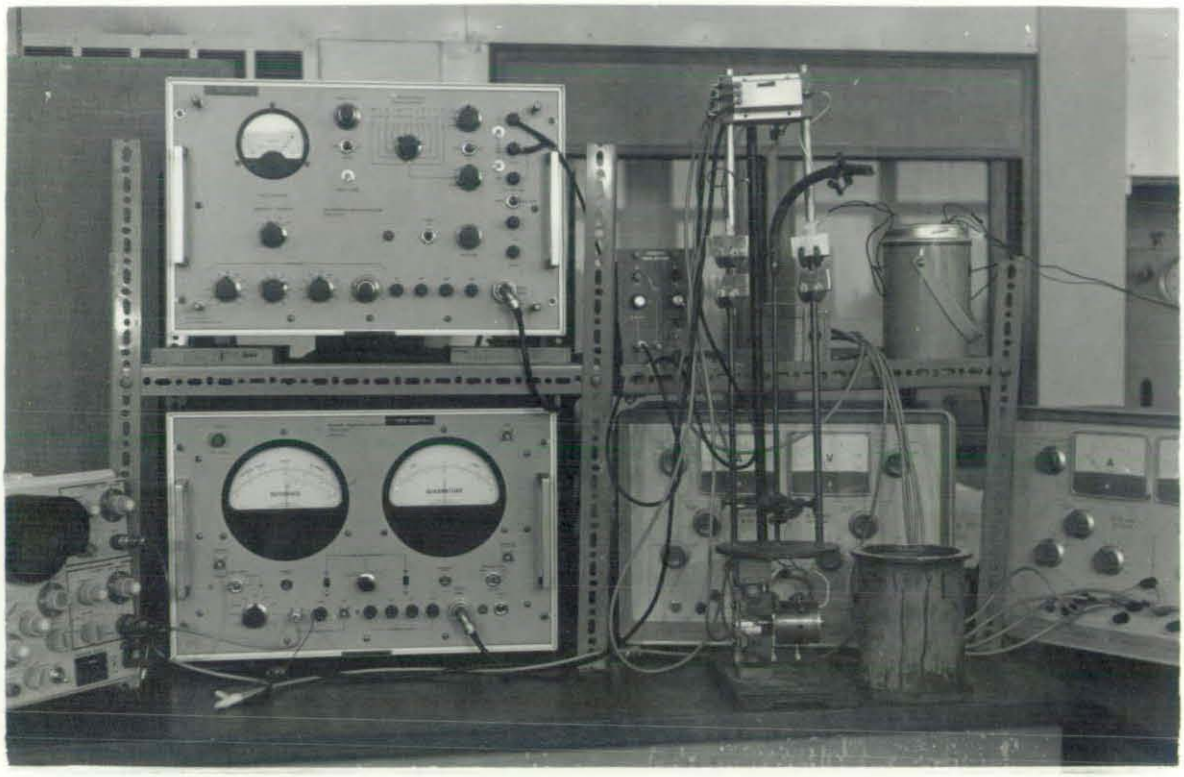

FIG. 3.7.

supplies a voltage to a 195 ohms resistance (consisting of 4 resistors in parallel) in series with the driving coil.

The probe (Bently Nevada 304) operates in conjunction with a proximator (Bently Nevada 3106) and a power supply (Advanced Dual Stabilised D.C. supply PP3). The proximator supplies electrical energy from the power supply to the probe and senses the signal return from the probe to provide a voltage signal that is proportional to the displacement variation of the vibrating system detected by the probe. The transducer system which works on an eddy current principle has a sensitivity of $\sim$ 8 volts per millimetre of motion and applies negligible stress to the vibrating elements. The voltage from the proximator is fed into an Operational amplifier (Burr-Brown 1632A/16). The operational amplifier has switch-selected gains of 1, 10 and 100. It operates with regulated ±15 V D.C. power supply (Advance Dual Stabilised D.C. Supply PP3). The amplified voltage output is resolved into in-phase and in quadrature with a 10-volt reference signal from the oscillator, by means of a resolved components indicator (Solartron V.P. 253.3). This measurement thus yields the absolute amplitude of the output voltage (V_o) and also its phase relative to the driving voltage.

The input voltage (V_I) from the oscillator after amplification is also given by the in-phase voltage on the resolved component indicator. The input signal from the oscillator and the output signal from the transducer circuit are monitored on a double beam oscilloscope (Solarscope CD 1014.2) to ensure that they are undistorted sine waves.

The Bently probe and proximator operates with a regulated -18V dc power supply. This voltage supply to the proximator from the Advanced Dual Stabilised D.C. supply is balanced to obtain output signal about earth. This allows the probe gap to be monitored on the oscilloscope.

3.9 DYNAMIC MECHANICAL MEASUREMENTS

The dynamic mechanical behaviour of the S-B-S block copolymer (Cariflex K101), fabricated under various thermal or solvent treatments were studied with the apparatus described in Sections 3.8 and 3.9.

The size of the specimens used in these experiments was such that the resonant frequency of the apparatus with specimens in position, was sufficiently high to give a reasonable range of measurement below it, and that the samples were being periodically bent rather than sheared, i.e. the Young's moduli were being measured (see Appendix II). The shape of the specimens was that of a rectangular beam.

The stationary upper and lower clamps and the central drive clamp were adjusted with two aims in mind. Firstly that their faces were in the same vertical plane. Secondly that the gaps between the drive clamp and the two rigid clamps were equal and were that of the decided length for the test specimen. The clamps were then locked in position by the respective screws. The adjustment was carried out with the use of the cathetometer. The beam specimen was then placed in position and clamped at both its end and at its centre.

The gap between the soft-iron disc and the probe was adjusted to obtain a measurable signal, bearing in mind the change in modulus of the test specimen over the temperature and frequency range to be measured.

The apparatus was placed in its cylindrical brass container. The ground flange of the plate attached to the top of the apparatus and the similar flange of the container, with a tinfoil gasket between them, were pulled together by twelve 2BA socket-head screws.

The screws passed through both flanges and the gasket to a steel backing ring on the underside of the container flange. The apparatus was then evacuated.

Measurements were obtained at the resonant frequency, and frequencies of 30, 10, 3, 1, 0·3 and 0·1 c/s, at selected constant temperatures. The apparatus was placed in a vacuum thermosflask and cooled from room temperatures at intervals of 7° or $8^{\circ}C$ to about $-70^{\circ}C$ by a mixture of solid carbon dioxide and methanol. Cooling from $-70^{\circ}C$ to $-120^{\circ}C$ or lower was effected using liquid Nitrogen as the coolant. The temperature inside the apparatus was measured with a copper-constantin thermocouple. The apparatus was left overnight to warm up to room temperature.

Measurements from room temperature to about $+120^{\circ}C$ was carried out in a thermostat liquid paraffin bath. Again each set of measurements was obtained at temperature intervals of 7° or $8^{\circ}C$.

As part of the setting-up procedure the resonant frequency of the vibrating system without specimen was determined. If this had fallen much below 70 c/s the suspension wires were tightened. The output signal was examined on the oscilloscope to ensure that it was an undistorted sine wave. Any distortion or abnormally high resonant frequency indicated that the drive mechanism was not vibrating freely.

As part of the calibration procedure, a steel blade was clamped in place of the specimen in the apparatus. The 'tan δ' for steel at room temperature is in the order of 10^{-4}, thus any measured phase shift (α_o) between the output and input voltages under these conditions is presented in the instrument and in particular, in the electrical circuitry. Numerous determination of α_o against frequency showed that any instrumental phase shift in the power amplifier, the proximator or the operational amplifier can be neglected up to frequency of 10 c/s.

The conversion of the measured terms to absolute values of dynamic moduli is now considered. In all the experiments carried out the applied stress was kept constant for each set of measurements at constant temperature, i.e., the driving current was constant. Equations (3.18) and (3.19) therefore become:

$$E' = \frac{Ni}{kB}\left[\frac{1}{v}\cos\beta - \frac{A}{k} + \frac{M\omega^2}{k}\right] \tag{3.20}$$

$$E'' = \frac{Ni}{kB}\left[\frac{1}{v}\sin\beta\right] \tag{3.21}$$

In order to convert the amplitude of the output voltage (V) to absolute values it is necessary to know the value of the constant Ni/kB. If the transducer system could be calibrated, at varying settings of transducer sensitivity, the constant B could be obtained. Then, knowing the values of N, k and i, the constant Ni/kB could be calculated.

It is not possible to calibrate the transducer as in practice it was not quite linear and it proved difficult to exactly reproduce a particular sensitivity setting. Also with change of temperature slight distortion of the samples occurred, thus altering the transducer setting.

The results were therefore converted to absolute values in the following way. Equation (3.15) states that $kE' = M\omega_o^2$. The geometrical factor, k, is determined by direct measurement of the specimen and the mass, M, of the vibrating system by weighing. The resonant frequency may be determined accurately and thus the absolute value of E' can be obtained at this frequency.

At a given temperature the time required to take measurements over the complete frequency range is about 30 minutes. The transducer setting remains constant at a constant temperature. Thus the

term Ni/kB in Equations (3.20) and (3.21) is constant for a set temperature, and it only remains to determine its absolute value. A plot of 1/V' is made against the logarithm of frequency in the region where the inertial term is negligible. V' is the in-phase component of the output voltage and equals V cos β. This plot is extrapolated to the resonant frequency where the exact value of E' is known. Thus the 1/V' curve is calibrated, i.e. a value is given to the constant Ni/kB. In fact, changes with temperature are also small, typical variations of transducer sensitivity with the appropriate power supply voltage (sensitive to gap setting) to give signals about earth are shown in Figure 3.8.

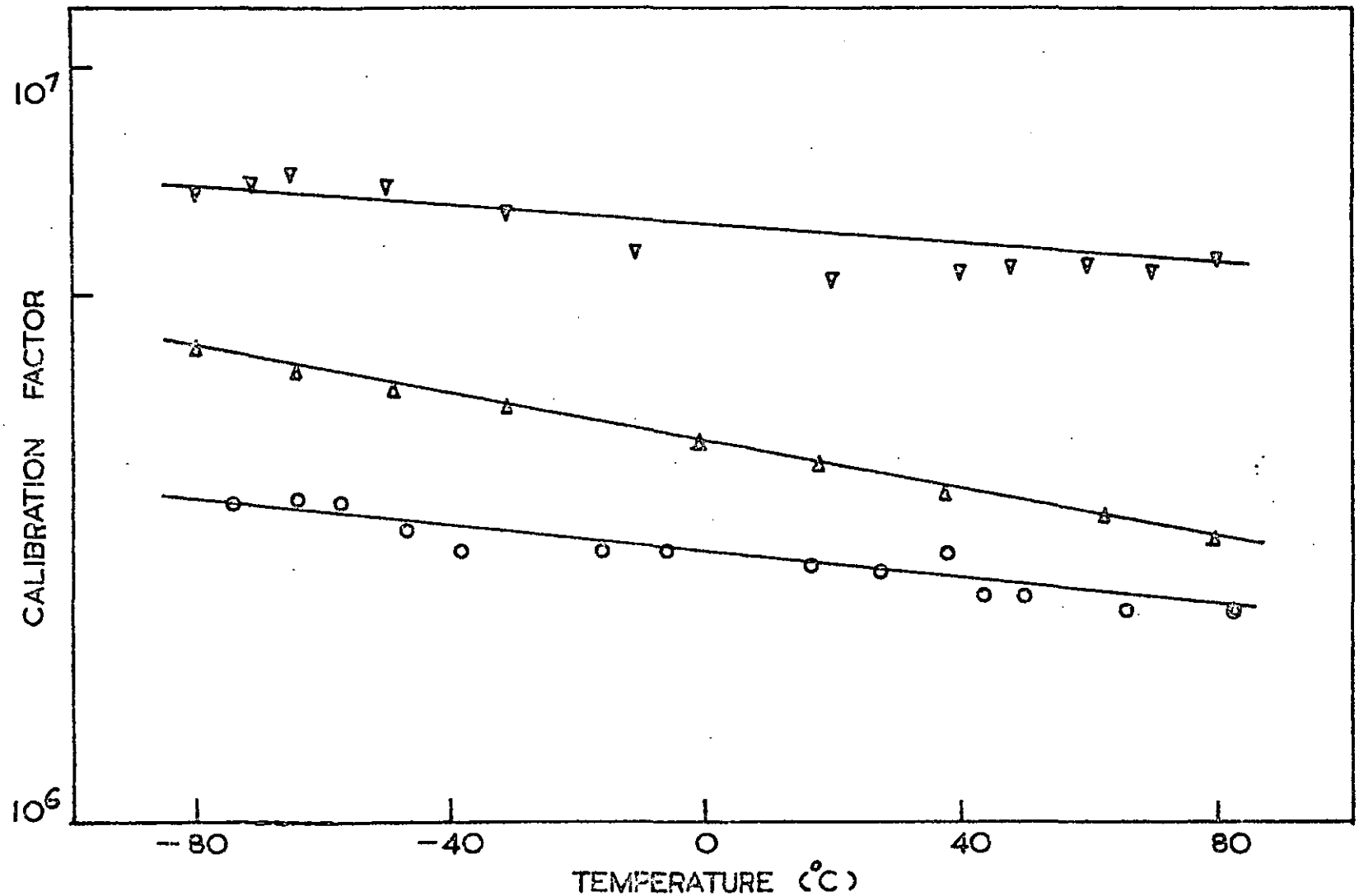

FIG. 3.0. Variation of transducer sensitivity with temperature at various gap settings.

3.10 VIBRATING REED MEASUREMENTS

The vibrating reed apparatus (162,163) was used to measure the Young's modulus E' and the mechanical loss factor tan δ of S-B-S/ polystyrene and polystyrene/polybutadiene blends.

Table 3.3. Composition of the blends by weight

Blend	S-B-S (%)	Polystyrene (%)	Polybutadiene (%)
M I	60	40	-
M II	40	60	-
M III	26·7	73·3	-
M IV	16·9	83·1	-
M V	-	79	21
M VI	-	88	12
M VII	-	100	-
S I	60	40	-
S II	40	60	-
S III	26·7	73·3	-
S IV	16·9	83·1	-

Samples M I to M VI were obtained by mechanically blending the polymer mixtures in an internal blender. Samples S I to S IV were prepared by dissolving the polymers in A.R. benzene. The 10% solutions were then freeze-dried in vacuo at $0^{\circ}C$ for four days.

The vibrating reed apparatus is capable of measuring six polymer specimens simultaneously. The specimens were compression moulded into rectangular beam of approximate dimensions 6·4 × 1·0 × 1·5 cm. Each polymer specimen was mounted vertically in the apparatus by a clamp at its upper end so that it could be

stressed as a cantilever. The polymer beam was vibrated by energising a coil with a soft-iron core adjacent to a small permanent magnet attached to the free end of the specimen. The amplitude of vibrations of each sample was detected by a small ceramic piezoelectric pressure transducer, which was clamped against the upper end of the sample (Figure 3.9).

The measurements were carried out in vacuo over the temperature range of $-120^{\circ}C$ to $+120^{\circ}C$. Cooling down to $-70^{\circ}C$ was effected by using a mixture of solid carbon dioxide and methanol. For temperatures below $-70^{\circ}C$, liquid nitrogen was used as the coolant. For temperatures above room temperature, the apparatus was placed in a thermostat-controlled oil bath. About forty minutes were required for the apparatus to achieve thermal equilibrium at each measurement. Measurements were usually taken at intervals of 7° or $8^{\circ}C$.

The mechanical loss factor, tan δ, is calculated (164) as

$$\tan \delta = \Delta f / f_o \qquad (3.22)$$

where f_o is the resonant frequency of the polymer beam and Δf is the resonance-curve frequency width at the half-power points.

Young's modulus E' for the 'loaded' polymer beam (because of the magnet) is calculated (165) as

$$E' = \frac{4\pi^2 \ell^3 f_o^2}{35 t^3 x} (140 M_L + 33 \rho x t \ell) \qquad (3.23)$$

where ρ, ℓ, t and x are the density, length, thickness and width of the polymer specimen respectively. M_L is the mass of the magnet attached to the free end of the specimen.

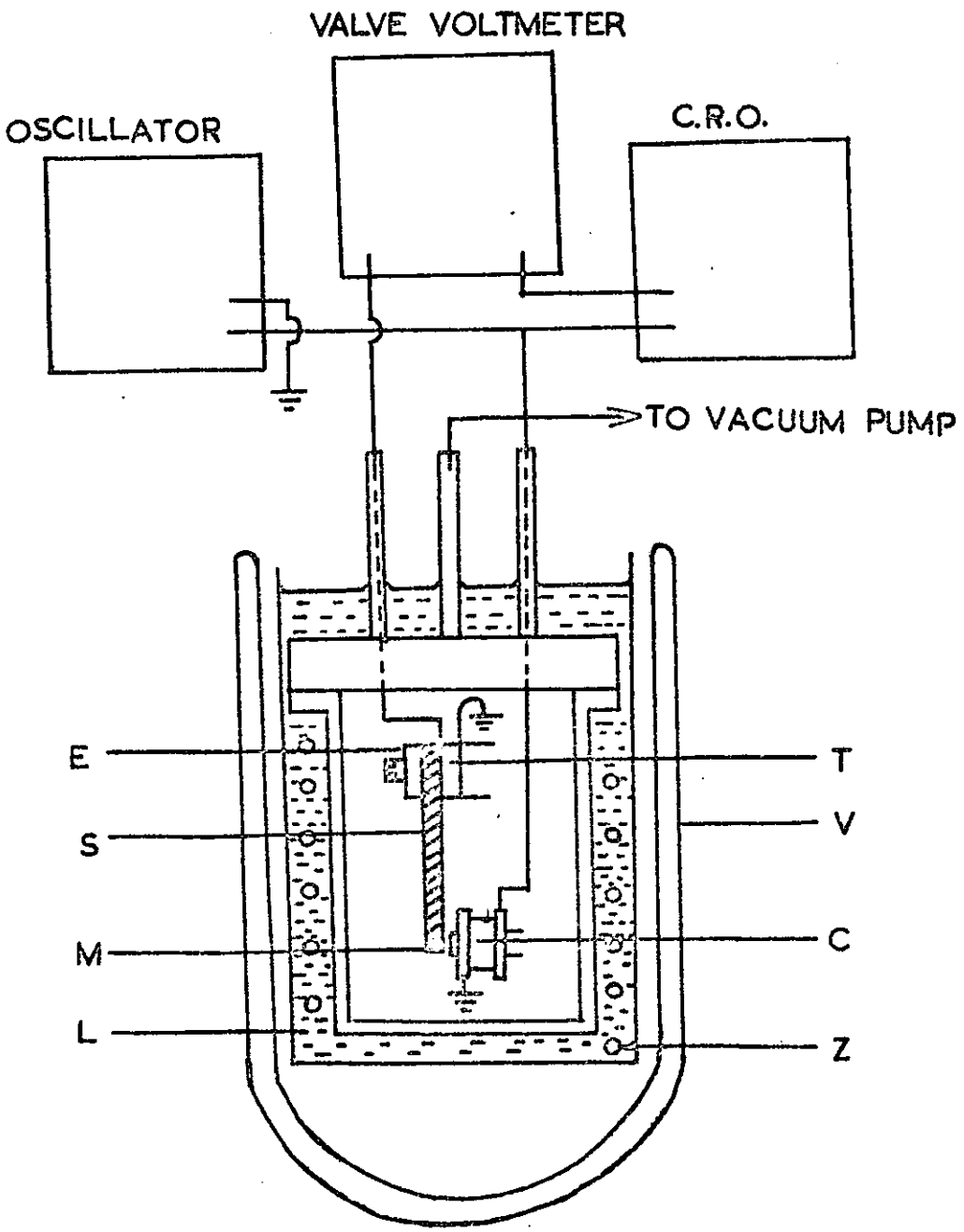

FIG. 3.9.

C energizing coils E screw clamps
L liquid coolant M magnet
S polymer samples T transducer
V Dewar vessel Z copper cooling coil

3.11 SYNTHESES OF HOMOPOLYMERS AND COPOLYMERS

High-Vacuum Apparatus

A high vacuum apparatus as shown in Figure 3.10 was used. High vacuum techniques (5,31,166,167) permit the attainment of the rigorous experimental conditions necessary to prevent termination of a reaction by the presence of impurities. The vacuum apparatus is composed of a GeneVac High Vacuum Pumping unit comprising of a rotary pump ($\sim 10^{-2}$ Torr) (A) and a fractionating, water-cooled diffusion pump ($\sim 10^{-6}$ Torr) (B). In a leak-free system, pressures in the range of 10^{-5} to 10^{-6} Torr are obtainable. The other units include a liquid nitrogen trap (C) to condense any condensable gases, the main manifold (D) and the pressure release (E) which is a tube over 76 cm in length with one end connected to the vacuum apparatus and the other end submerged in a mercury pool. The vacuum gauge (F) registers the pressure of the system.

Monomers

B.D.H. tetrahydrofuran (THF) was refluxed over, and distilled from potassium and a centre cut (b.p. 65·0°- 65·5°C) was collected and stored over sodium wires.

Hercules Incorporated 3,3-bis(chloromethyl)oxetane (BCMO) was distilled at reduced pressure, in the presence of dry nitrogen. A centre cut (m.p. 19°C) was collected and stored over calcium hydride.

Initiator

Phosfluorogen A (p-chlorodiazonium hexafluorophosphate) (38,168) was obtained from the Ozark Mahoning Company, Oklahoma. 10 gm of Phosfluorogen A was dissolved in 650 ml of distilled water by stirring

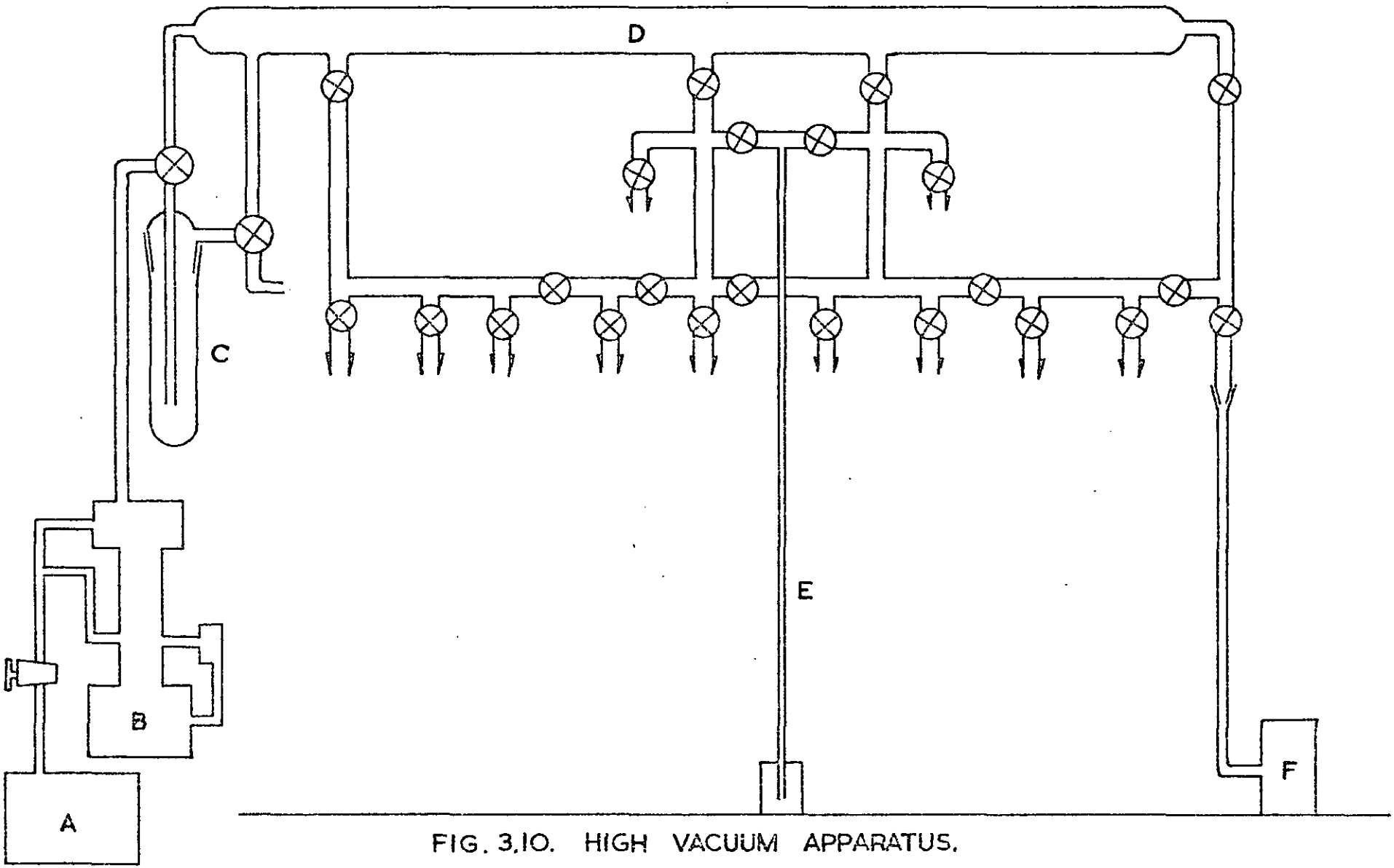

FIG. 3.10. HIGH VACUUM APPARATUS.

at temperatures of 28^{o} - 32^{o}C for one hour. The solution was filtered to remove the remaining dark red solids, and the clear colourless filtrate was cooled in ice water to effect srystallisation. It was dried in vacuo at room temperature. 5 gm of white plates was obtained. They were stored over anhydrous calcium chloride in vacuo.

Solvents

Benzene, cyclohexanone and o-dichlorobenzene were refluxed over and distilled from calcium hydride and a centre cut was stored over fresh calcium hydride.

Bulk Polymerisation of THF

About 10 ml of the THF was further dried over CaH_2 in a flask on the high vacuum line, and stirred with a magnetic stirrer for two days. The liquid was then degassed properly and vacuum-distilled onto a complex of Na-K alloy and α-methylstyrene.

The complex was prepared as follows. The flask containing the two alkali metals ($\frac{3}{4}$ gm Na, $\frac{1}{4}$ gm K), the covering solvent (purified, dry benzene) and a glass enclosed iron nail was placed on the vacuum line. The apparatus was carefully evacuated and the covering solvent distilled off. After the attainment of a good vacuum (~10^{-5} Torr), the flask was heated with an electric dryer until the alkali metals melted and fused together. About 1 ml of dried α-methylstyrene was then vacuum-distilled onto the alloy at room temperature.

The THF/Na-K alloy/α-methylstyrene complex was stirred overnight and the red complex was then ready for use as a reservoir of exceedingly dry THF free from any hydroxyl impurities. A measured amount of THF was vacuum-distilled into an ampoule (Figure 3.11)

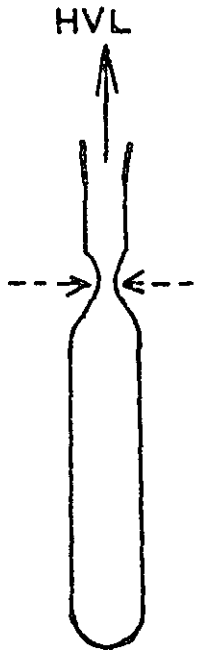

FIG. 3.11.

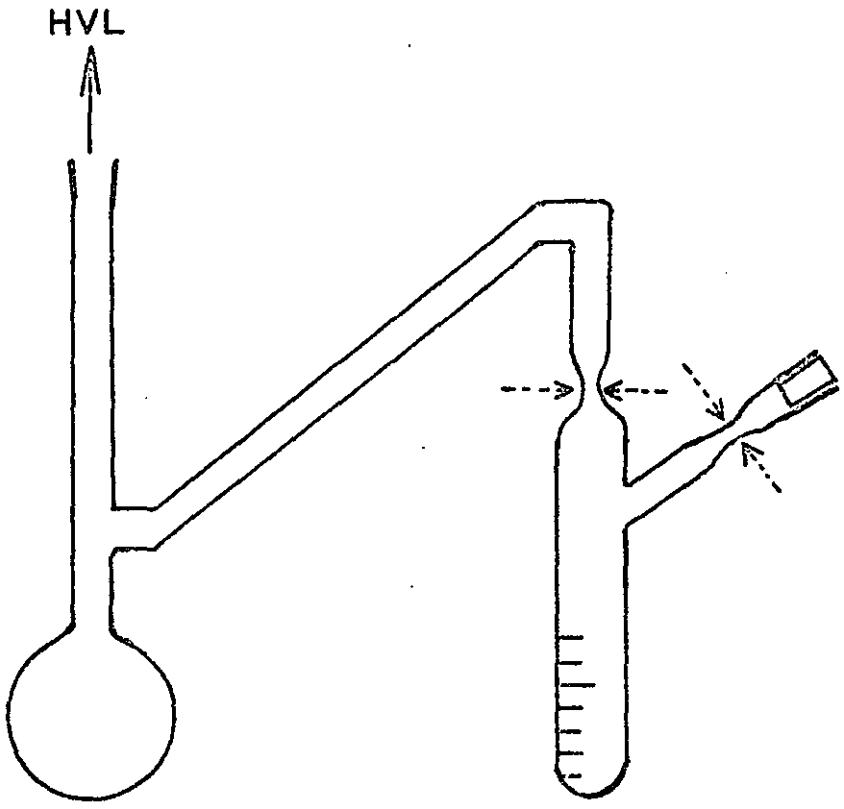

FIG. 3.12.

containing the initiator. The ampoule was sealed off in vacuo and heated for thirty minutes at 50°C. The polymerisation was carried out at 25°C for twenty hours.

The solution of monomer and initiator turned viscous and then solidified. The ampoule was broken and the light purple polymer mass was stirred into a solution of THF containing 10% acetic acid to terminate the polymerisation. The polymer was precipitated out with water and dried overnight in vacuo at 25°C.

Bulk Polymerisation of BCMO

It was difficult to vacuum-distil BCMO. The distillate tends to solidify along the vacuum line connecting the flask and the ampoule.

An apparatus consisting of a flask, a delivery tube and an ampoule with a constricted side 'arm' and a B14 stopper was used, (Figure 3.12). The ampoule was calibrated to read in millilitres. About 10 ml of BCMO was dried over calcium hydride in the flask on the vacuum line and stirred for two days. The apparatus was then opened to atmospheric pressure and the initiator introduced into the ampoule through the side arm. The flask was immersed in a bath of solid carbon dioxide and methanol and the apparatus evacuated. The constricted side arm was sealed off. The BCMO was degassed and vacuum distilled into the ampoule. The delivery tube and the neck of the flask was heated with a heating tape. After the required amount of BCMO was collected, the ampoule was sealed off in vacuo.

The ampoule was placed in water bath at 50°C for thirty minutes and then transferred to another water bath at 25°C and left to polymerise for twenty hours.

Solution polymerisation of BCMO

BCMO and the solvent, o-dichlorobenzene was collected in ampoules shown in Figure 3.13. The ampoules are calibrated and have a break-seal. The ampoules were then sealed onto the polymerisation reactor (Figure 3.14). The initiator was introduced through the side arm attached to the reactor. The whole apparatus was thoroughly evacuated and the side arm sealed off. After the attainment of a good vacuum of 10^{-5} torr, the whole apparatus was removed from the high vacuum line by sealing off at the constriction.

The breakseal connecting the solvent ampoule and the reactor was broken by means of a hammer (iron nail enclosed in a glass) and a magnet. Similarly the breakseal in the monomer ampoule was also broken. The polymerisation was carried out at $60^{\circ}C$. After five hours, the reactor was broken and the polymerisation was terminated with methanol.

Copolymerisation of THF and BCMO

The breakseal arrangement described above was found unsatisfactory, as it was difficult to transfer completely, the monomer and the solvent from the ampoules to the reactor.

The monomer BCMO and THF were collected in the ampoules shown in Figures 3.15 and 3.16 respectively. Each ampoule has a B14 ground glass socket with a taper end. The polymerisation reactor (Figure 3.17) has as many arms as the number of ampoules to be used. Each arm has a B14 ground glass socket and is constricted just below the socket at one side. The ampoule is broken at its taper end, by twisting it against the constricted side of the side arm.

Polymerisations of different ratios of BCMO monomer to the

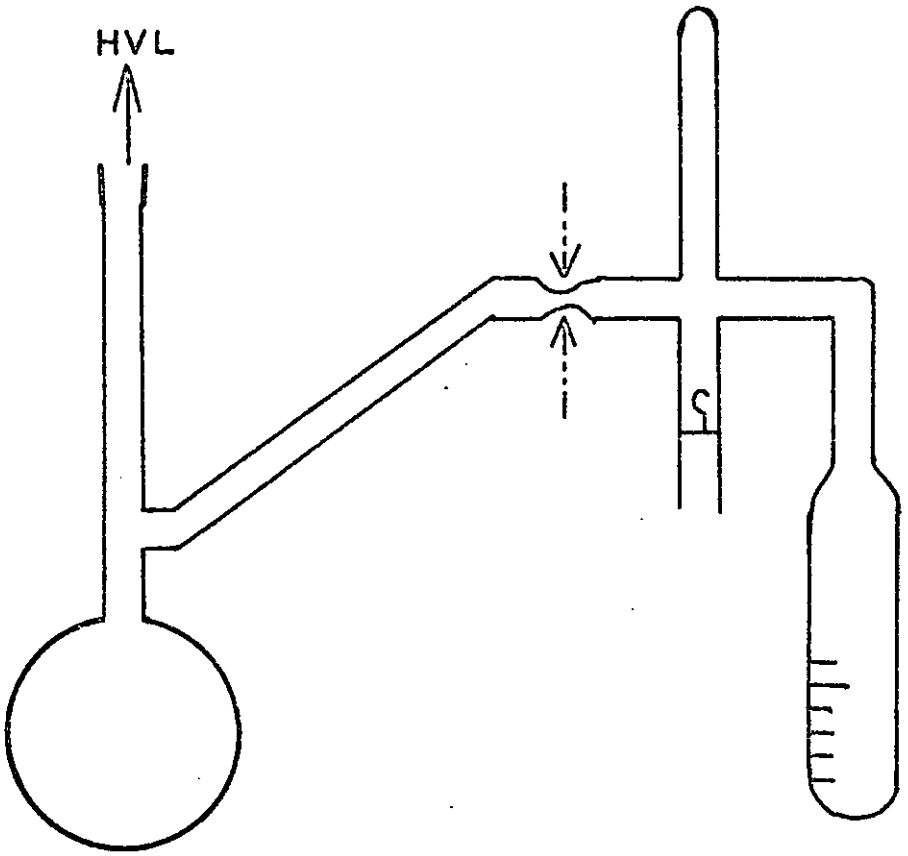

FIG. 3.13.

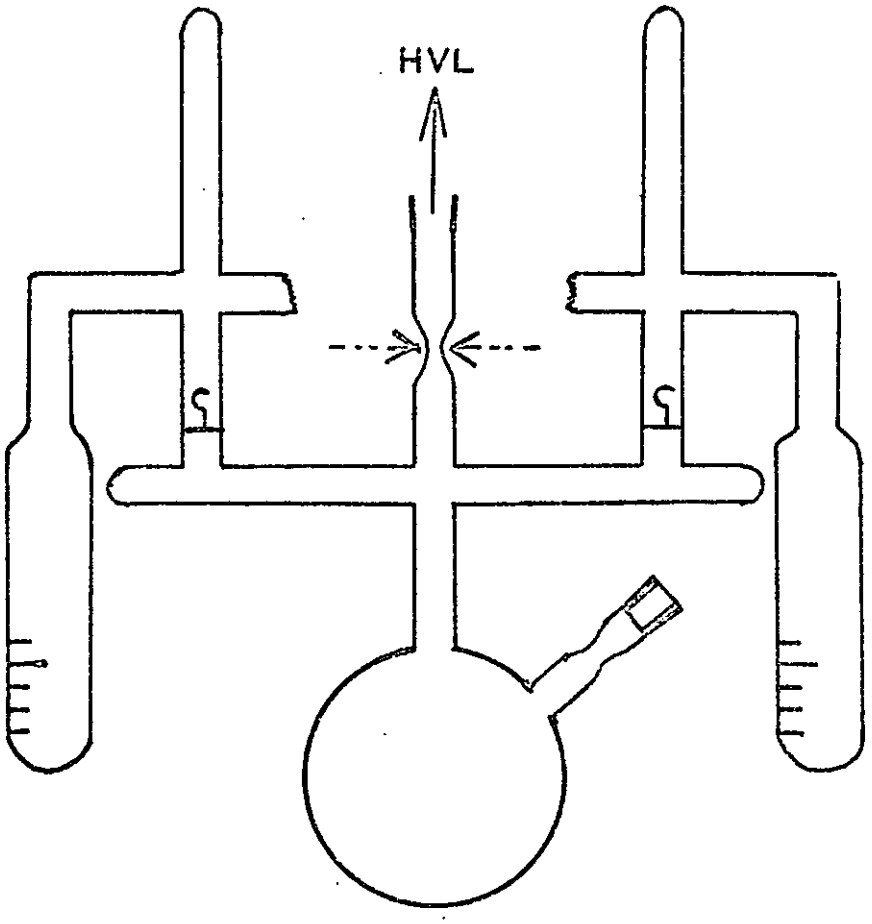

FIG. 3.14.

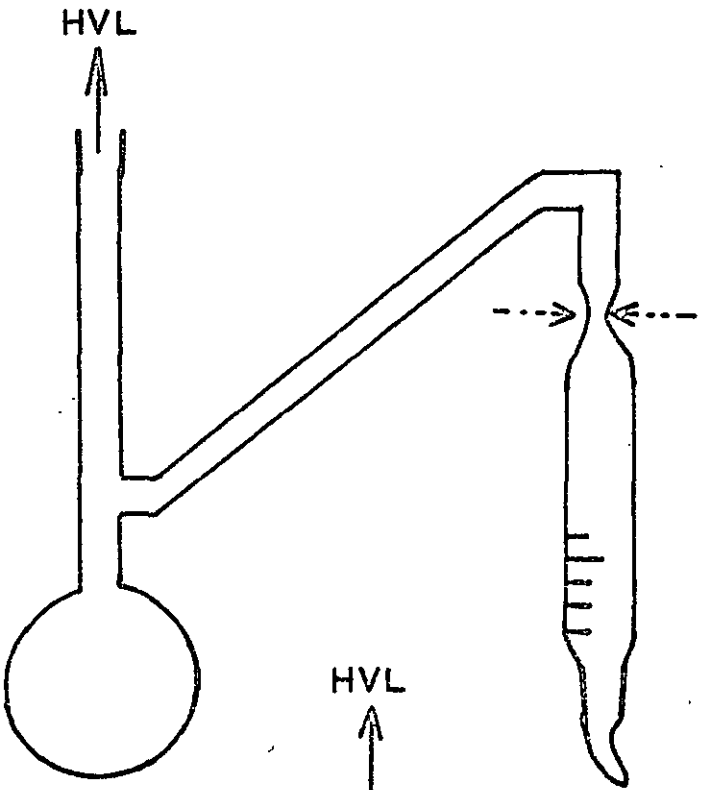

FIG. 3.15.

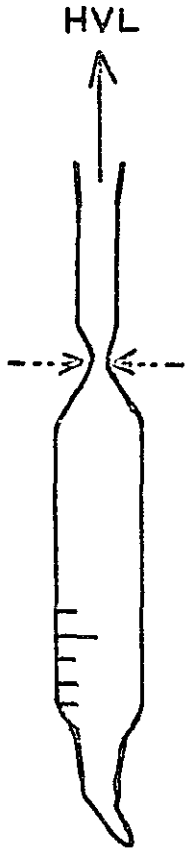

FIG. 3.16.

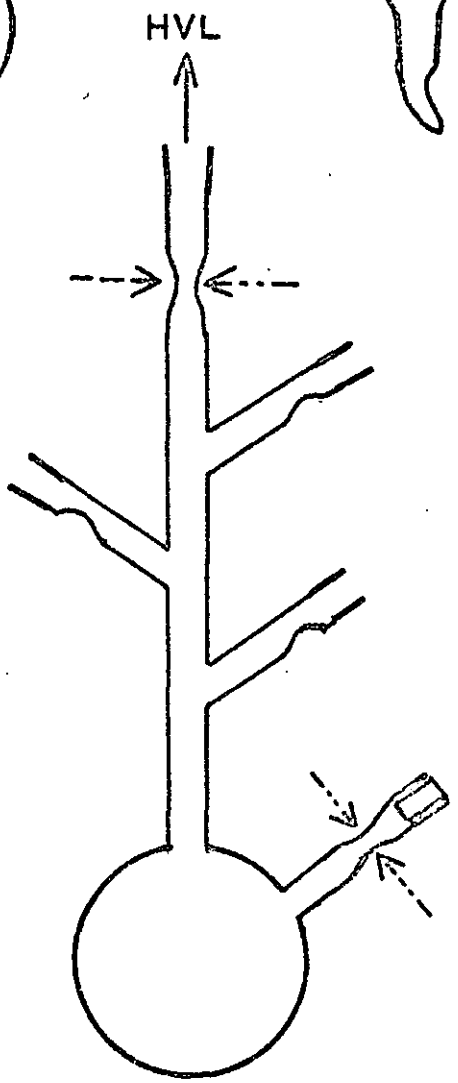

FIG. 3.17.

THF monomer were carried as described in above section.

With extension of these techniques, block polymerisation is feasible, but there are many basic difficulties, as will be discussed later (Section 5.7). Time did not allow the preparative work to progress beyond this point.

CHAPTER 4. RESULTS

The results are presented in the same order as the experimental works described in Chapter 3.

4.1. SMALL ANGLE X-RAY SCATTERING AND ELECTRON MICROSCOPY

A comparison of the small angle x-ray scattering patterns for the various unstretched samples of K101 at room temperature, using a Geiger detector are shown in Figure 4.1. Table 4.1. gives the details of K101 morphology from the x-ray scattering.

For the toluene cast sample, the principle Bragg spacing obtained is 300Å. Two higher order diffraction peaks of weak intensity are observed at angles corresponding to Bragg spacings of 208Å and 130Å respectively, when film detection and long exposure times were employed.

The x-ray scattering from unstretched and 600% stretched toluene-cast samples using pin-hole optics and photographic detection are shown in Figures 4.2. (a) and (b).

The effect of temperature and extension on morphology of toluene cast samples are summarized in Table 4.2. and Table 4.3.

Electron micrographs of a toluene cast sample are shown in Figures 4.3. (a) and (b). The figures seem to be composed of regularly arranged, well defined particles, and oriented strips of non-uniform intensity. The particle sizes are in the range of 180 - 220Å. The interparticle distance is approximately 325Å.

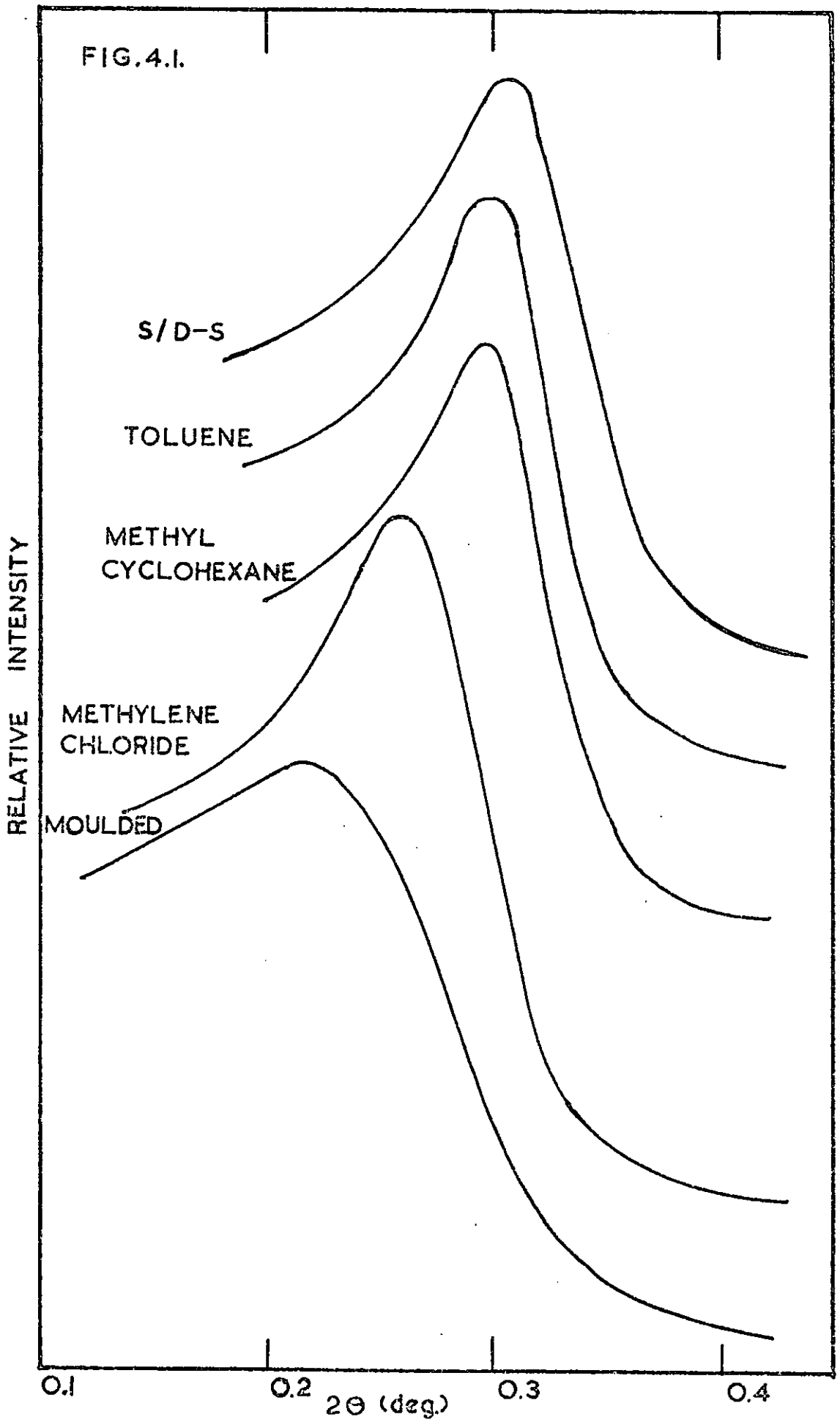
FIG. 4.1.
S/D-S
TOLUENE
METHYL CYCLOHEXANE
METHYLENE CHLORIDE
MOULDED
RELATIVE INTENSITY
0.1
0.2
0.3
0.4
2Θ (deg.)

FIG. 4.2a.

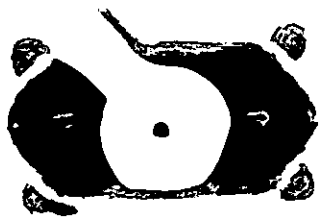

FIG. 4.2b.

FIG. 4.3a.

FIG. 4.3b.

TABLE 4.1.

Details of Cariflex K101 Morphology from Low Angle X-ray Scattering

	Sample	Nearest neighbour spacing	Half-width
1.	Moulded	412 Å	98 Å
2.	Methylene Chloride-Cast	348 Å	52 Å
3.	Methyl Cyclohexane-Cast	302 Å	34 Å
4.	Toluene-Cast	300 Å	32 Å
5.	Toluene-swollen/deswollen	294 Å	32 Å
6.	Methylene Chloride-swollen/deswollen	290 Å	34 Å

TABLE 4.2.

Effect of Temperature on Morphology of Toluene-cast K101

Temperature	Nearest neighbour spacing	Half-width
$-100^{\circ}c$	300 Å	28 Å
$+20^{\circ}c$	305 Å	32 Å
$+65^{\circ}c$	314 Å	30 Å
$+125^{\circ}c$	318 Å	31 Å

TABLE 4.3.

Effect of Extension on Morphology of Toluene-cast K101

Extension	Nearest neighbour spacing	Half-width
0%	300 Å	33 Å
15% (Relaxed)	301 Å	32 Å
100% (Relaxed)	305 Å	34 Å
400% (Relaxed)	300 Å	33 Å
600% (relaxed)	300 Å	34 Å

4.2. EQUILIBRIUM SWELLING AND EXTENSION STUDIES

According to Holden and coworkers (10), the dominant factors contributing to the elastic moduli of SBS block copolymers, are the "entanglement crosslinks" between the elastomer chains and the filler effect of the polystyrene domains. Using the above concept, the elastic properties of a moulded sample of K101 are expressed by Equation (3.2.).

$$\sigma = \frac{PRT}{Mc} (\lambda - \lambda^{-2})(1 + 2.5\phi_5 + 14.1\phi_5^2) \qquad (3.2.)$$

The quantity σ is plotted against $(\lambda - \lambda^{-2})$ as in Figure 4.4. where a linear relationship is obtained. λ, the extension ratio is based on the length of the sample, after the load is removed. The amount of set is 2%. The values used in the plot were the mean of measurements at $288^{o}K$, on three replicate test pieces.

From the slope of the line through the experimental points in Figure 4.4., a value of about 2.64×10^3 is obtained for Mc.

In the equilibrium swelling measurements, Vr, the volume fraction of rubber in the swollen sample is determined to be 0.111. The interaction parameter used for SBS in n-heptane is given by

$$\chi_1 = 0.37 + 0.52\ Vr.$$

The value for the polybutadiene-n-heptane system is that determined by Kraus (169).

The Mc value for K101 samples swollen in n-heptane is then calculated using the Flory-Rehner equation (Equation 3.1.) and is found to be approximately 2.80×10^4.

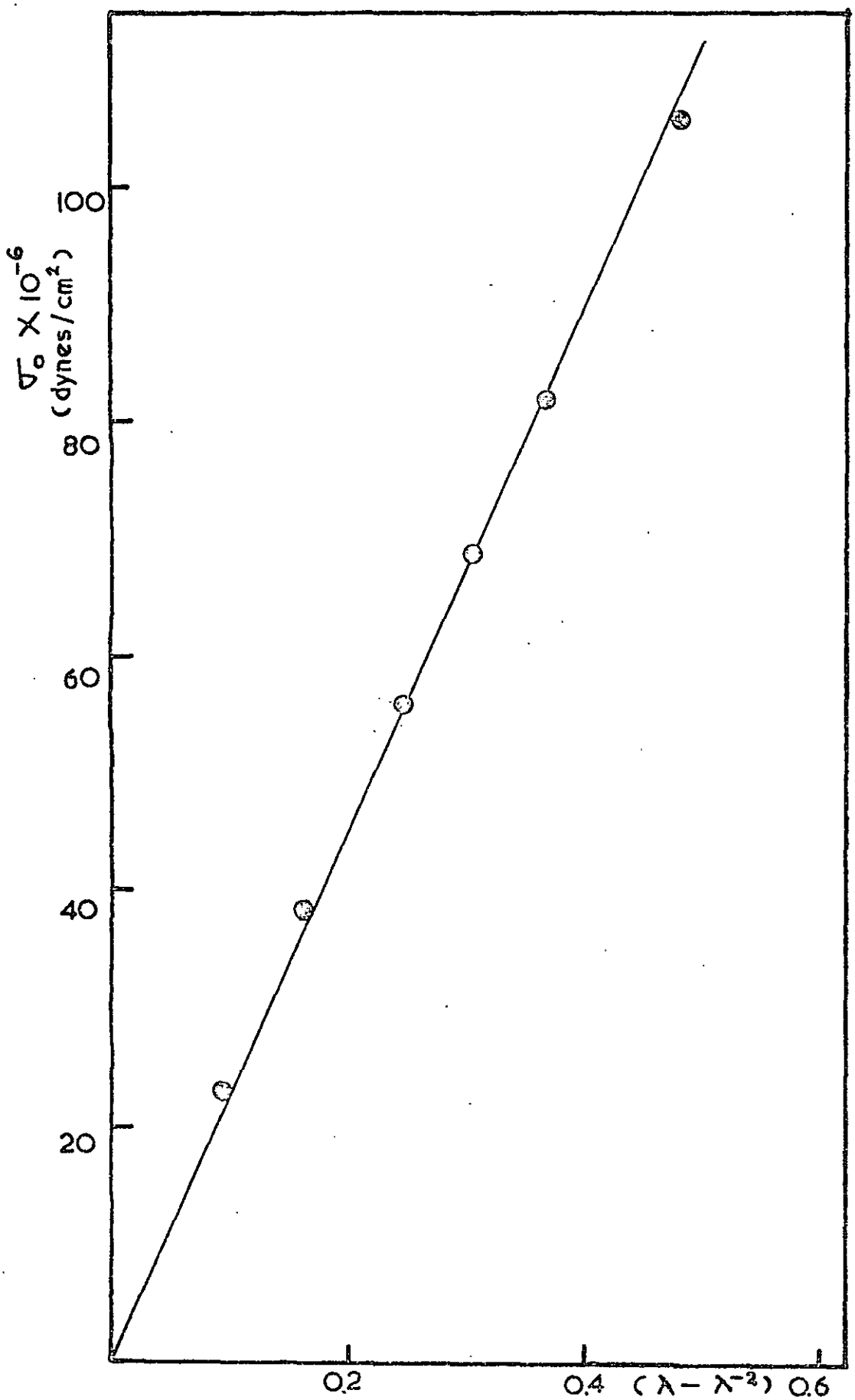

FIG. 4.4. STRESS-STRAIN OF UNSWOLLEN SAMPLE.

The equilibrium swelling time of one day was chosen on the basis of test results on several samples which showed no signifcant increase in swelling after one day of immersion in n-heptane.

The stress-strain relationship for a swollen, filled rubber network as given by Equation (3.3.) is used to calculate Mc from the stress-strain data on the swollen sample of K101 in Nujol. A linear plot of σ versus $(\lambda-\lambda^{-2})$ is obtained. (Figure 4.5.). The value of Vr on a duplicate test sample of K101 is determined to be 0.288. From the gradient of the graph (Figure 4.5.), a value of about 6.6×10^3 is obtained for Mc.

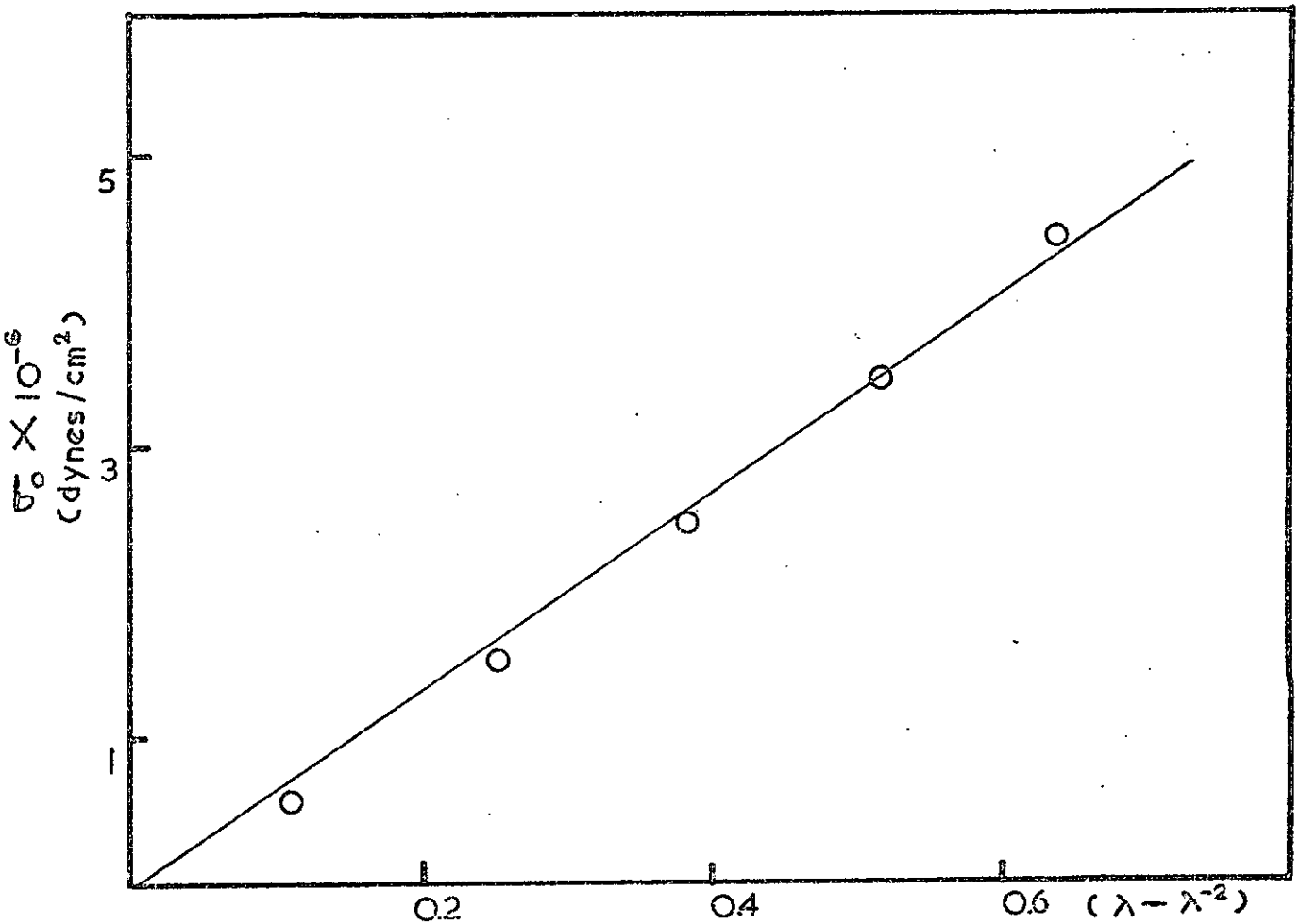

FIG. 4.5. STRESS STRAIN OF SWOLLEN SAMPLE.

4.3. STRESS-STRAIN BEHAVIOUR

Figures 4.6. to 4.10 show stress-strain curves for toluene cast samples, determined at 30, 40, 50, 60 and 70°c., at strain rates of 0.196, 0.392, 1.96, 3.92 and 19.6 % per minute. Figures 4.11. and 4.12. show the stress-strain curves for methylene chloride cast and methyl cyclohexane for temperatures of 30, 40, 50, 60 and 70°c., at a strain rate of 1.96% per minute. The stress value, σ_o, is based on the unextended cross-sectional area of the sample.

From the stress-strain curves for the toluene cast samples, values of the stress were obtained at three preselected strains of λ = 1.45, 2.0 and 4.0. (These strain values were used in the stress relaxation measurements, described in Section 3.6.). Figures 4.13 to 4.15. show the plot of log $\lambda\sigma$ 313/T versus log time, where each curve represents the stress at a single strain; the time, t, equals the strain divided by the strain rate. The quantity $\lambda\sigma$ is the tensile stress based on the dimensions of the stretched sample, and is reduced to the reference temperature, 313°K.

The ultimate properties of the various samples are given in Tables 4.4 and 4.5., in terms of the maximum extension λ_b and the corresponding tensile stress at break σ_b. The values of λ_b and σ_b are given by the rupture points in the stress-strain curves. Figures 4.16. and 4.17. show the dependence of the temperature-reduced true rupture stress, $\lambda_b\sigma_b$ 313/T and $\lambda_b - 1$ on the strain rate. The tensile strength $\lambda_b\sigma_b$ is based on the cross-sectional area of the deformed sample.

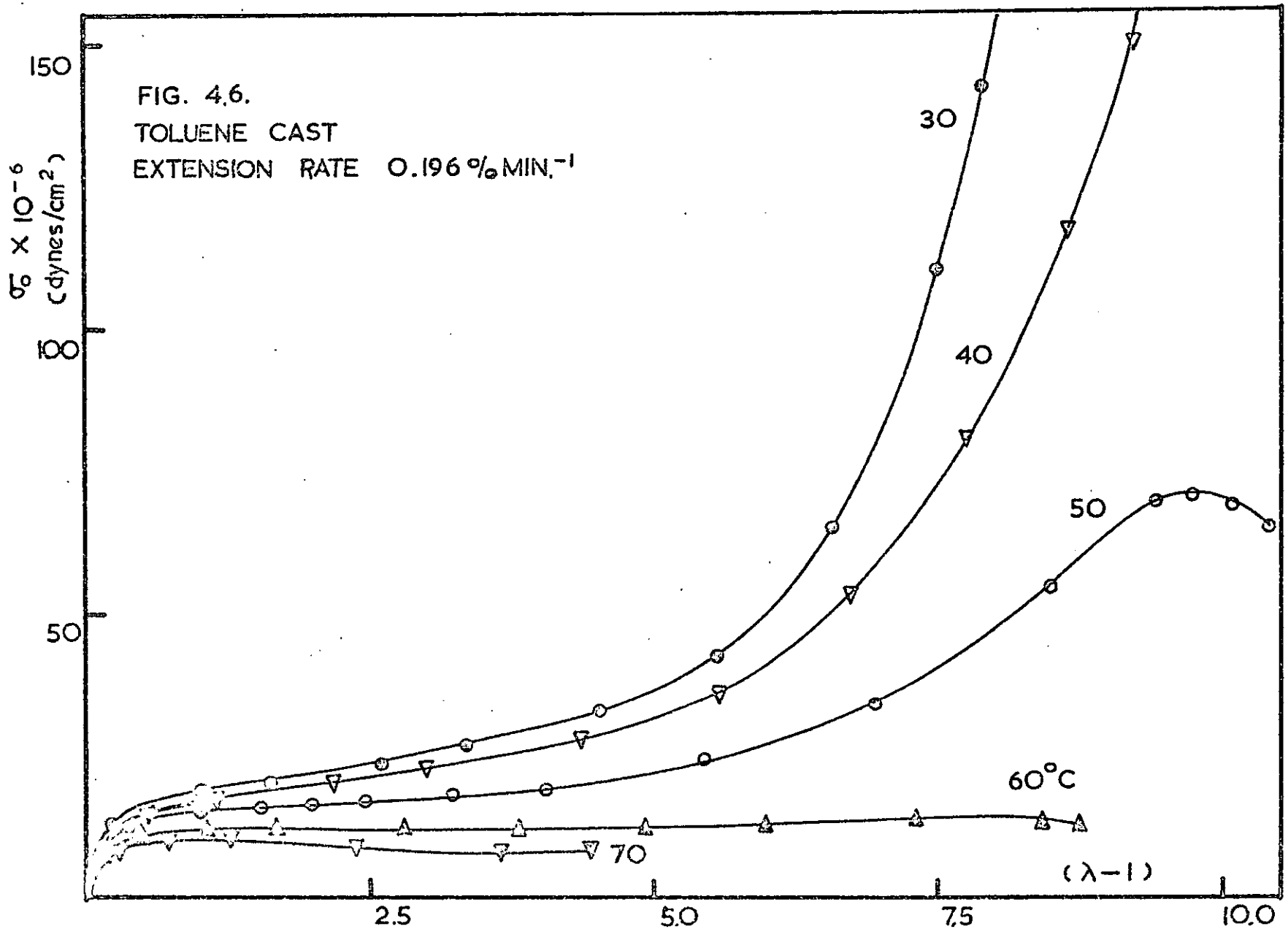
FIG. 4.6.
TOLUENE CAST
EXTENSION RATE 0.196 % MIN.⁻¹
σ₀ × 10⁻⁶ (dynes/cm²)
150
100
50
30
40
50
60°C
70
(λ−1)
2.5
5.0
7.5
10.0

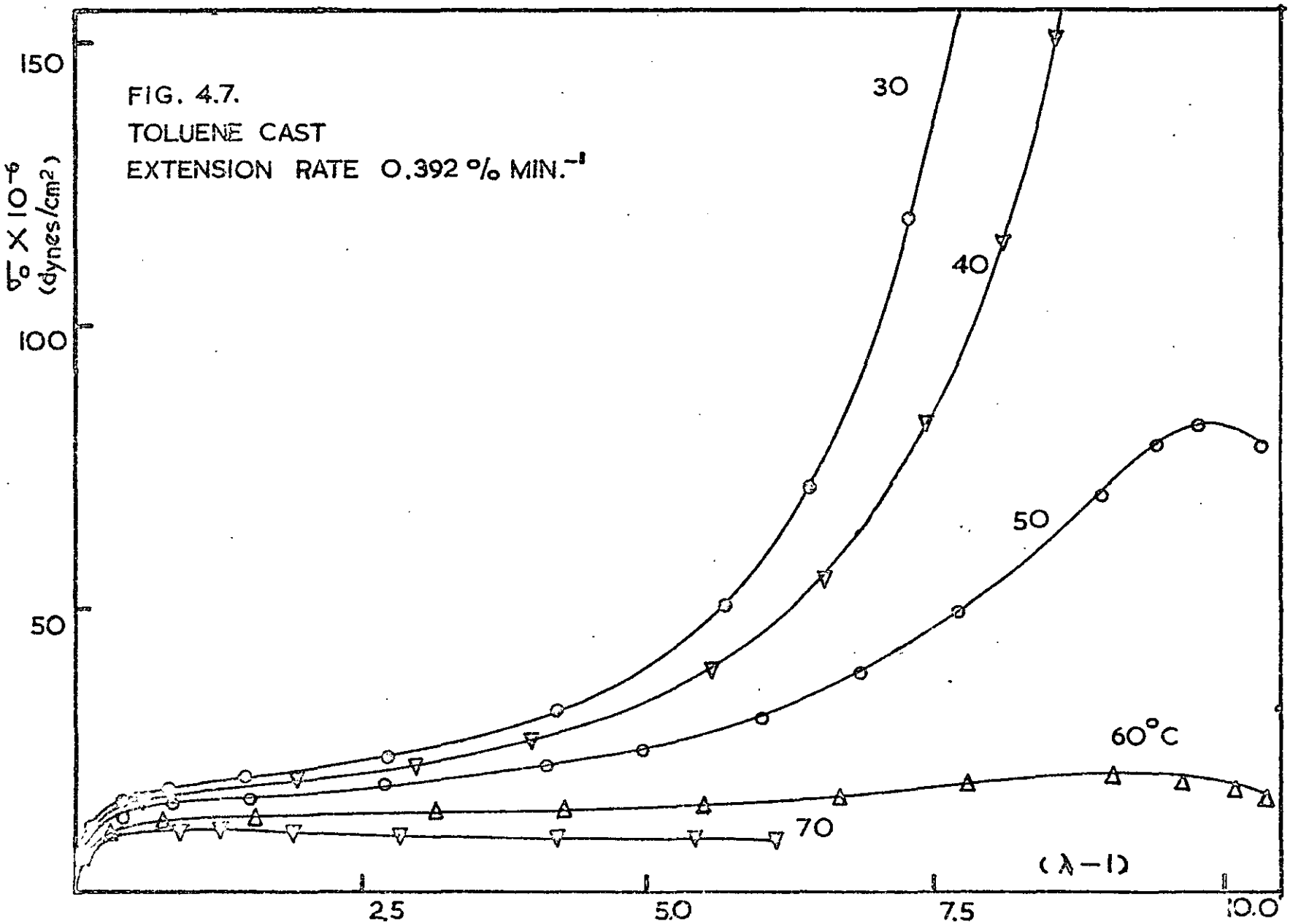
FIG. 4.7.
TOLUENE CAST
EXTENSION RATE 0.392 % MIN.⁻¹
$\sigma_0 \times 10^{-9}$ (dynes/cm²)
150
100
50
30
40
50
60°C
70
(λ−1)
2.5
5.0
7.5
10.0

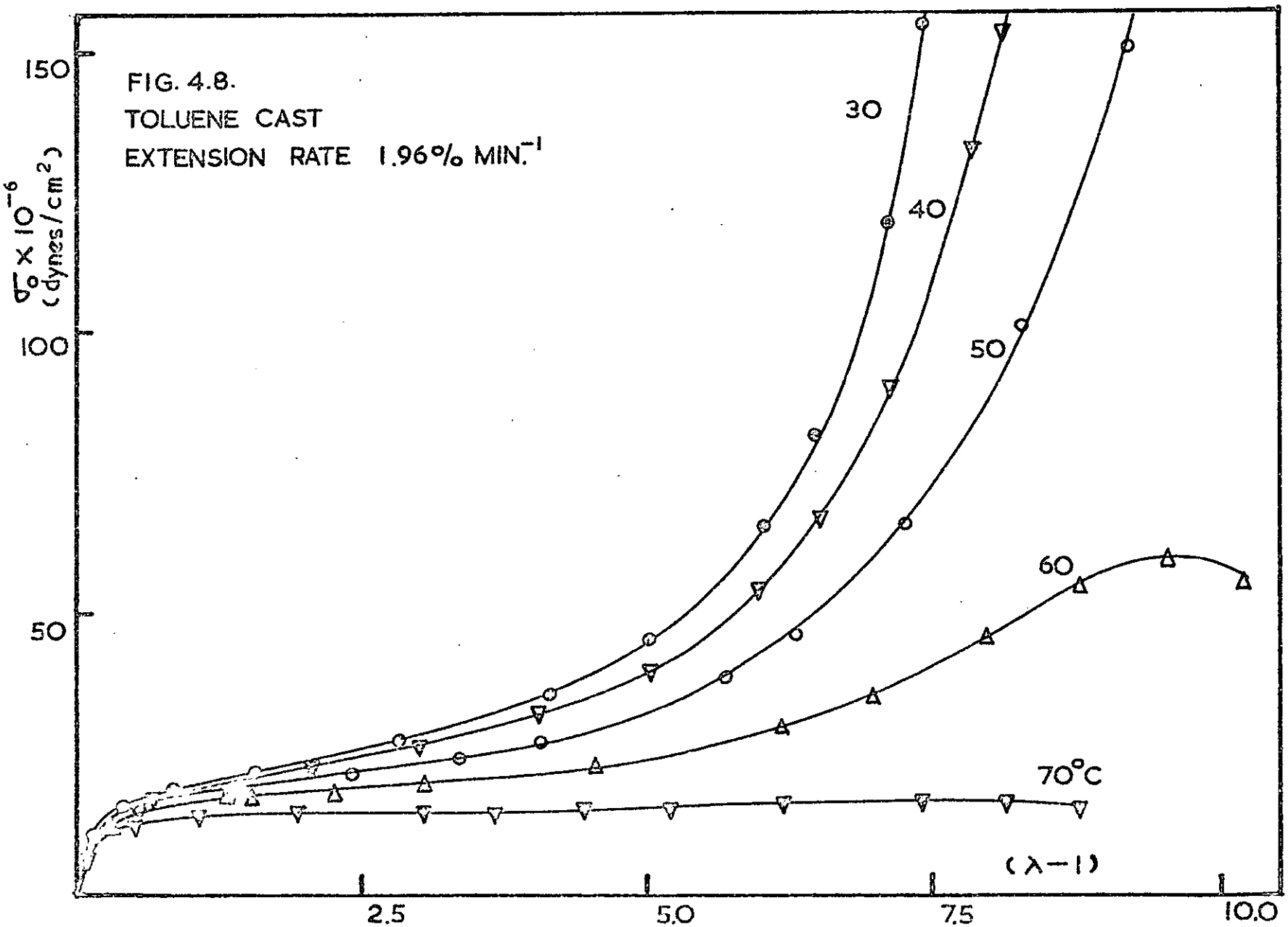
FIG. 4.8.
TOLUENE CAST
EXTENSION RATE 1.96% MIN.$^{-1}$
$\sigma_o \times 10^{-6}$ (dynes/cm^2)
150
100
50
30
40
50
60
70°C
(λ−1)
2.5
5.0
7.5
10.0

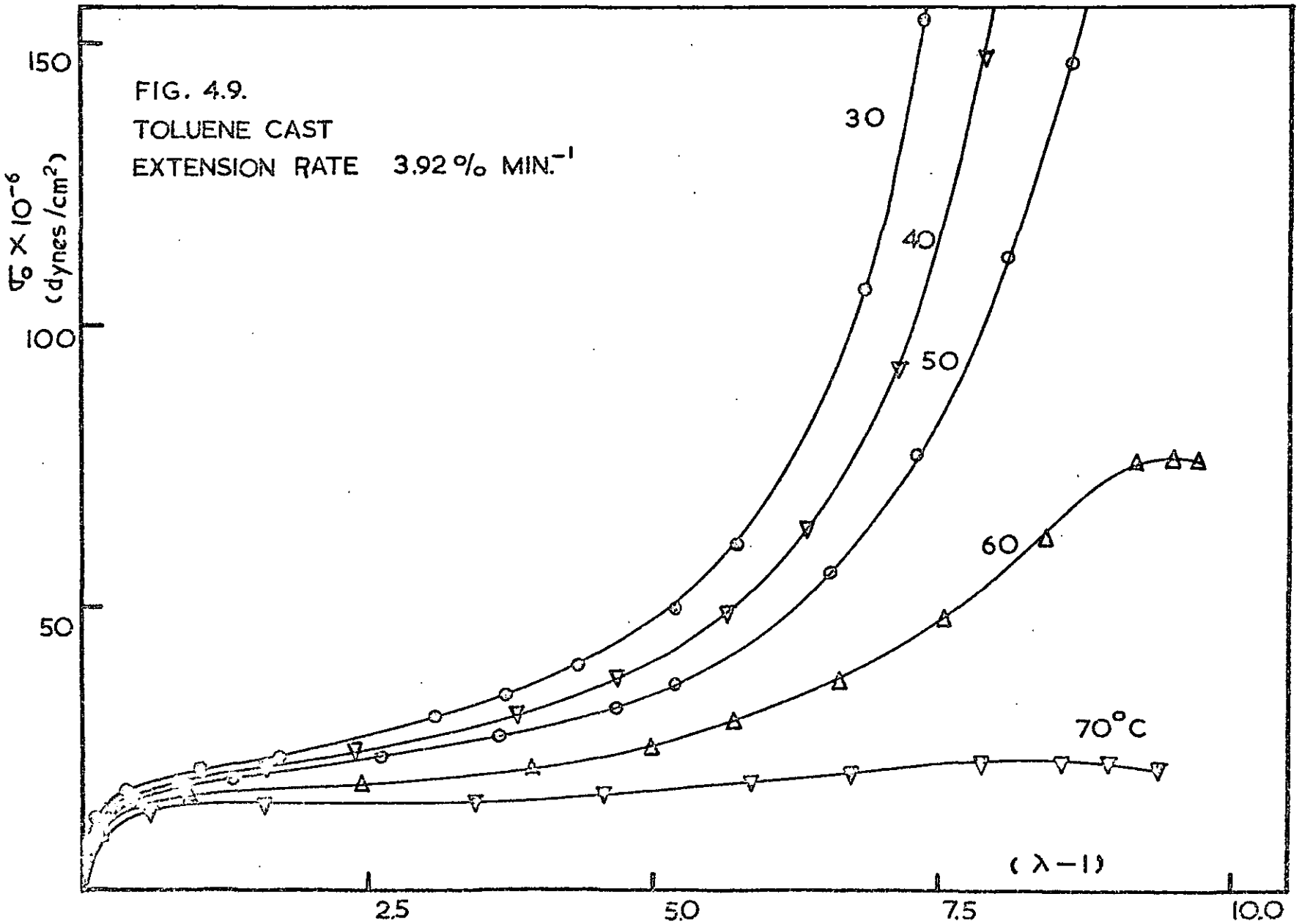
FIG. 4.9.
TOLUENE CAST
EXTENSION RATE 3.92 % MIN.⁻¹
σ₀ X 10⁻⁶ (dynes/cm²)
150
100
50
30
40
50
60
70°C
(λ−1)
2.5
5.0
7.5
10.0

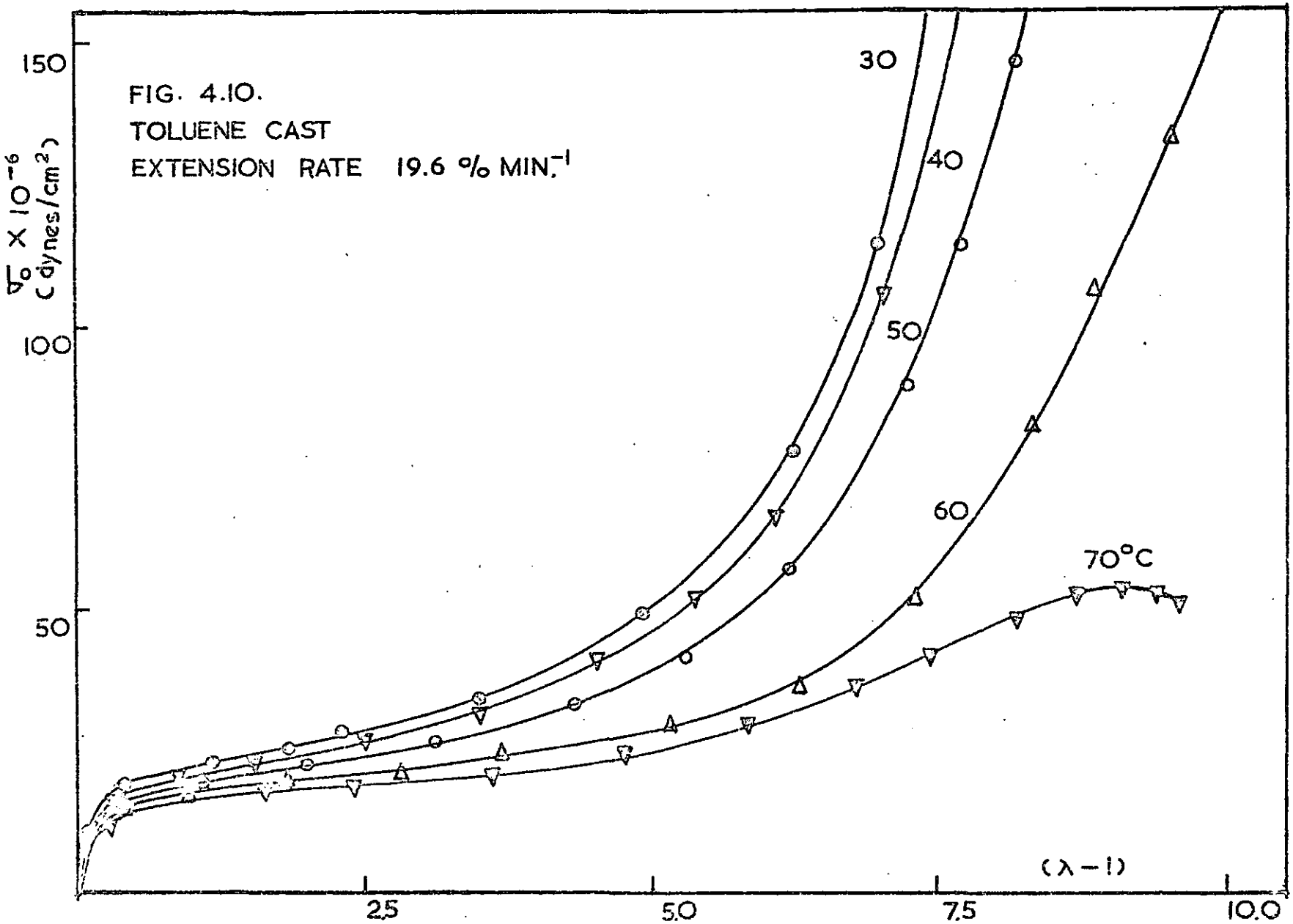
FIG. 4.10.
TOLUENE CAST
EXTENSION RATE 19.6 % MIN.$^{-1}$
$\sigma_o \times 10^{-6}$ (dynes/cm^2)
150
100
50
30
40
50
60
70°C
(λ − 1)
2.5
5.0
7.5
10.0

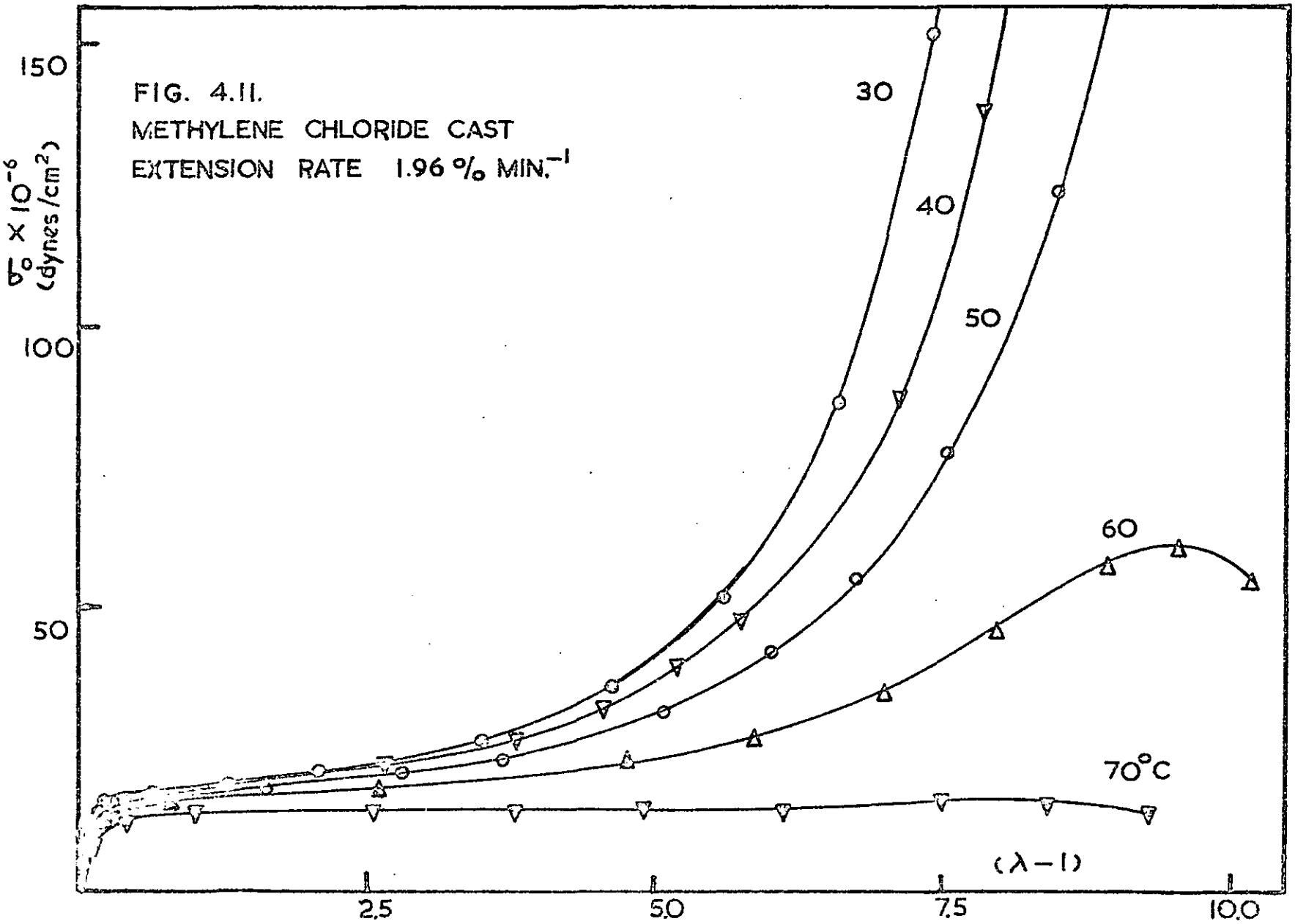
FIG. 4.11.
METHYLENE CHLORIDE CAST
EXTENSION RATE 1.96 % MIN.$^{-1}$
$\sigma_0 \times 10^{-6}$ (dynes/cm^2)
150
100
50
30
40
50
60
70°C
(λ − 1)
2.5
5.0
7.5
10.0

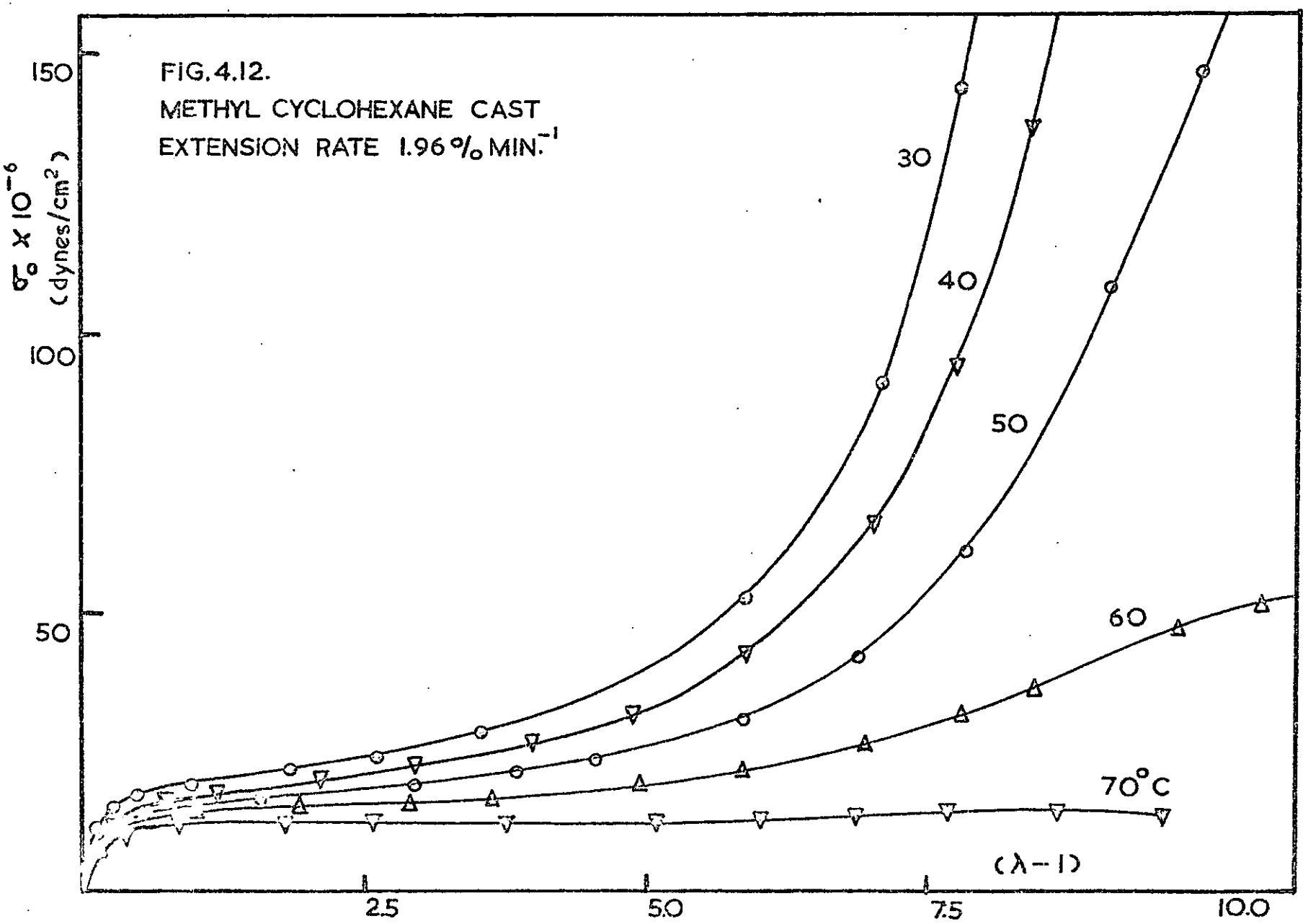
FIG. 4.12.
METHYL CYCLOHEXANE CAST
EXTENSION RATE 1.96 % MIN.$^{-1}$
$\sigma_0 \times 10^{-6}$ (dynes/cm^2)
150
100
50
30
40
50
60
70°C
(λ − 1)
2.5
5.0
7.5
10.0

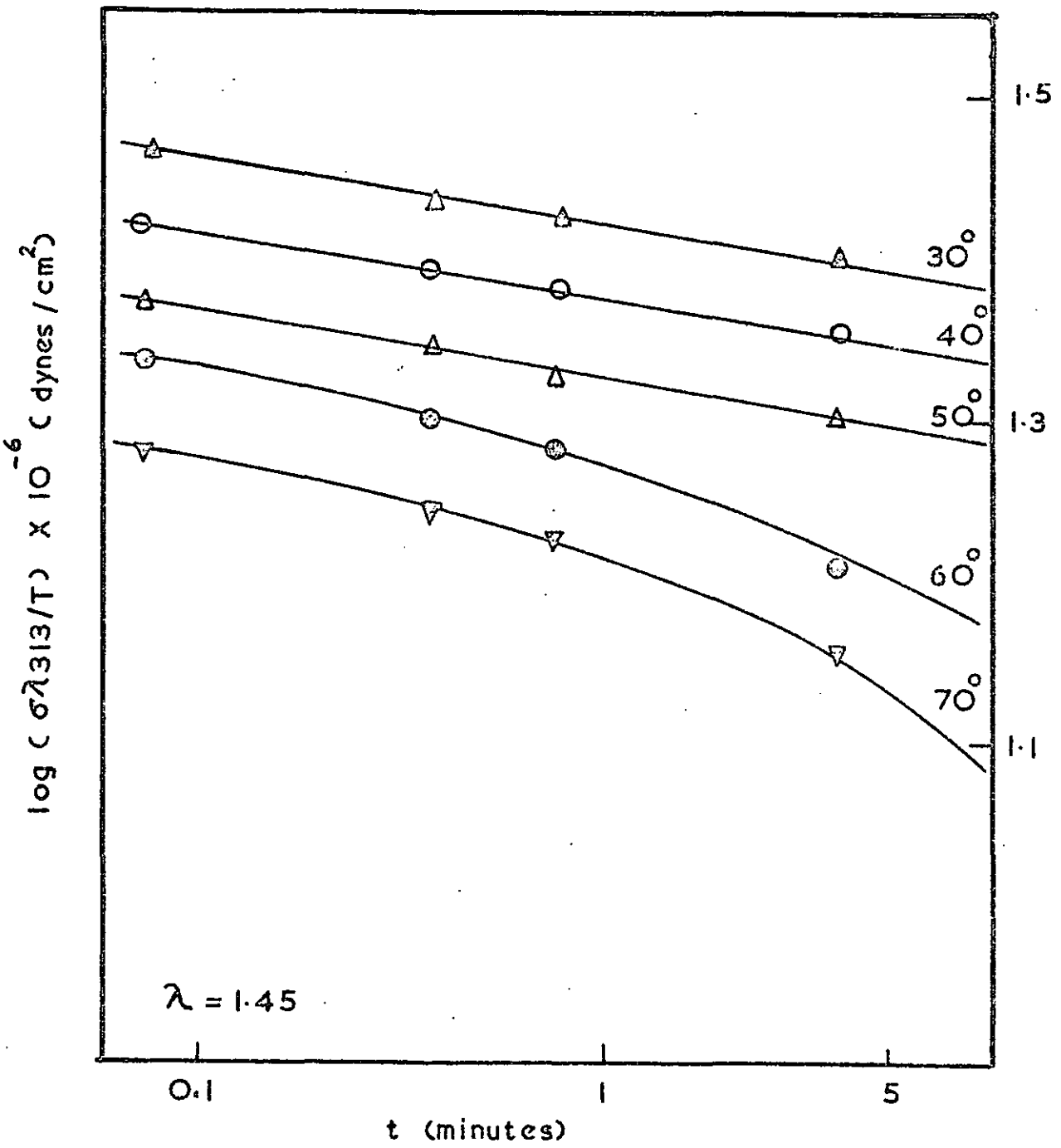

FIG. 4·13. STRESS-STRAIN DATA

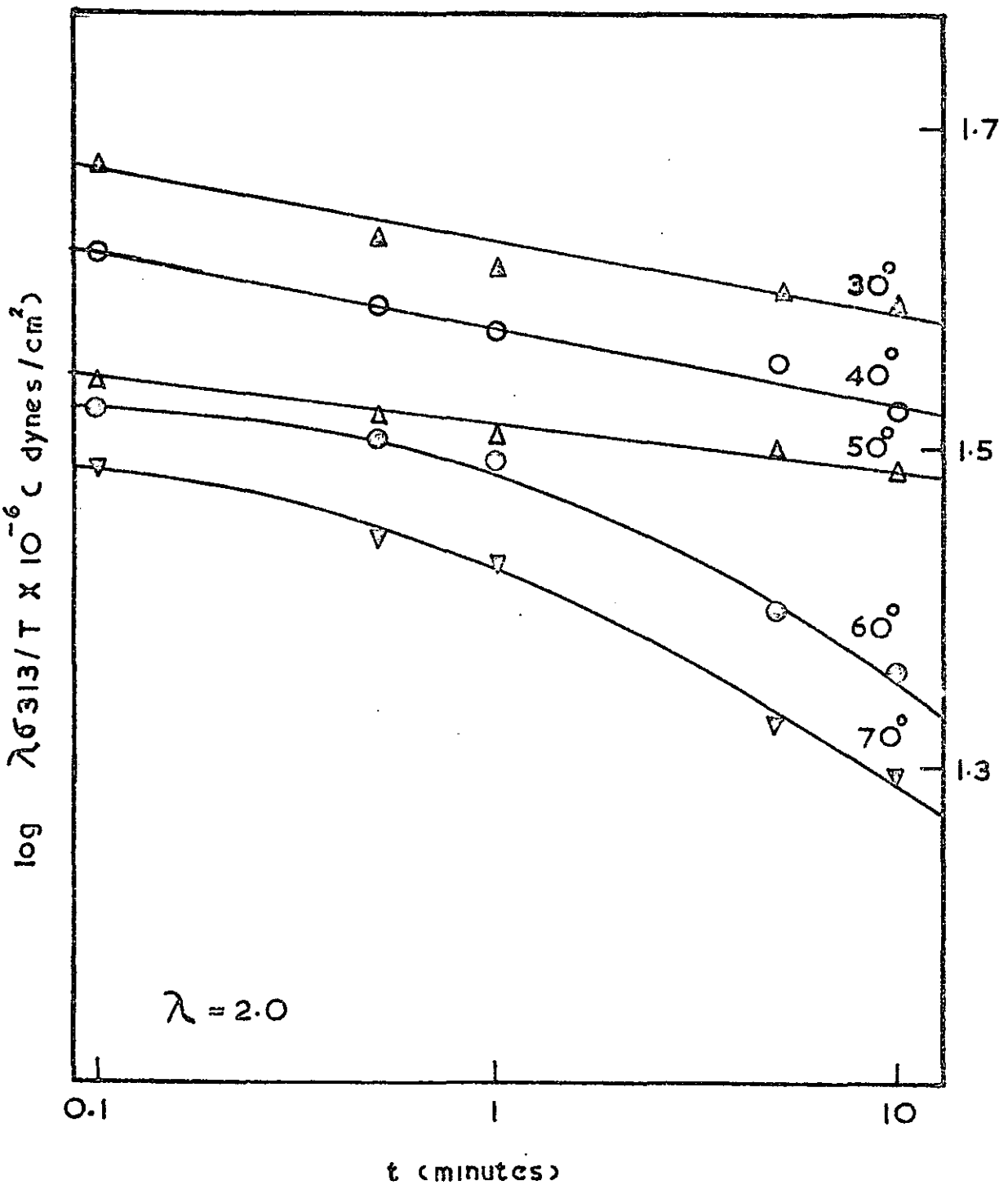

FIG. 4.14 STRESS-STRAIN DATA

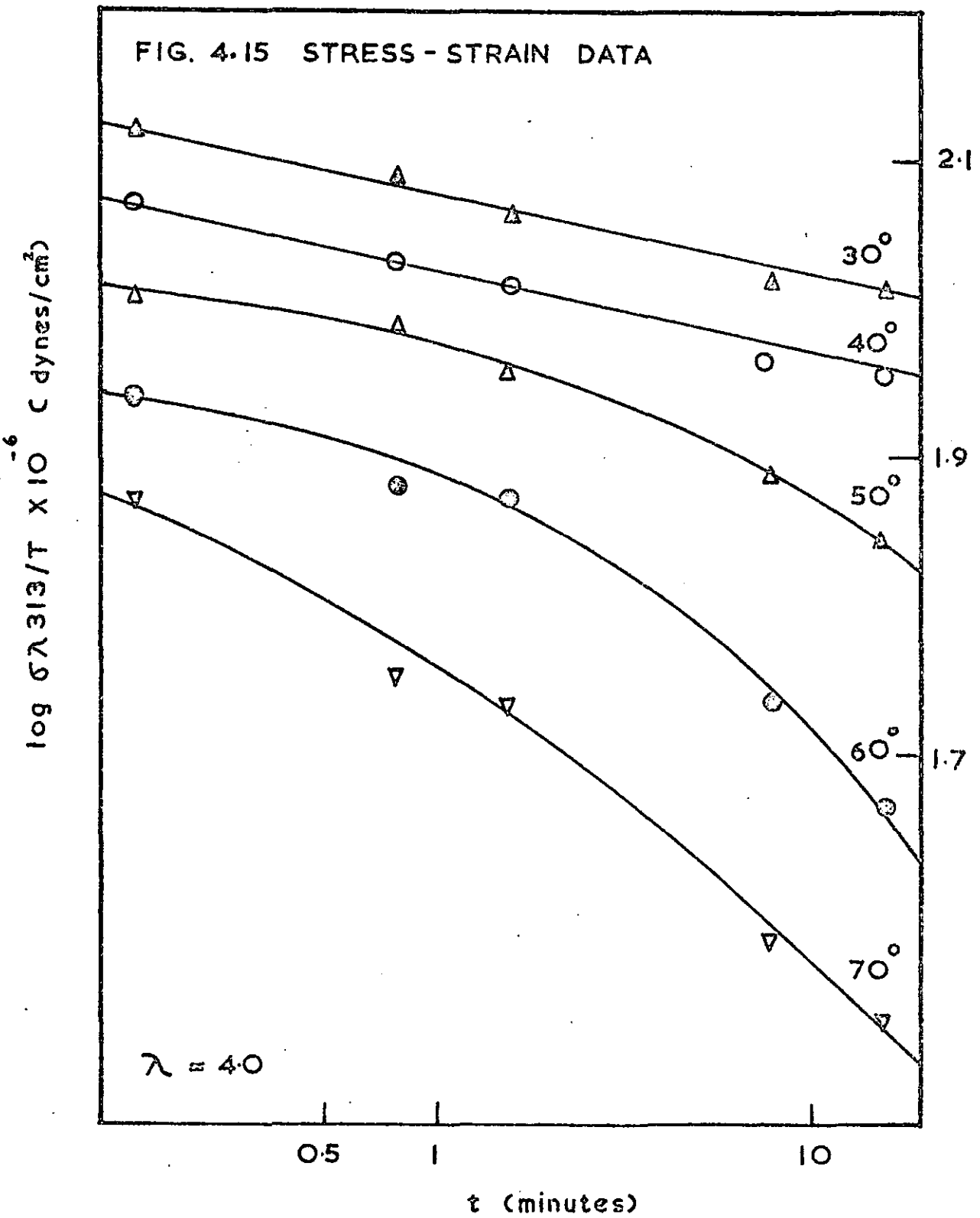
FIG. 4.15 STRESS - STRAIN DATA
log σλ 313/T X 10^-6 C dynes/cm^2
2·1
1·9
1·7
30°
40°
50°
60°
70°
λ = 4·0
0·5
1
10
t (minutes)

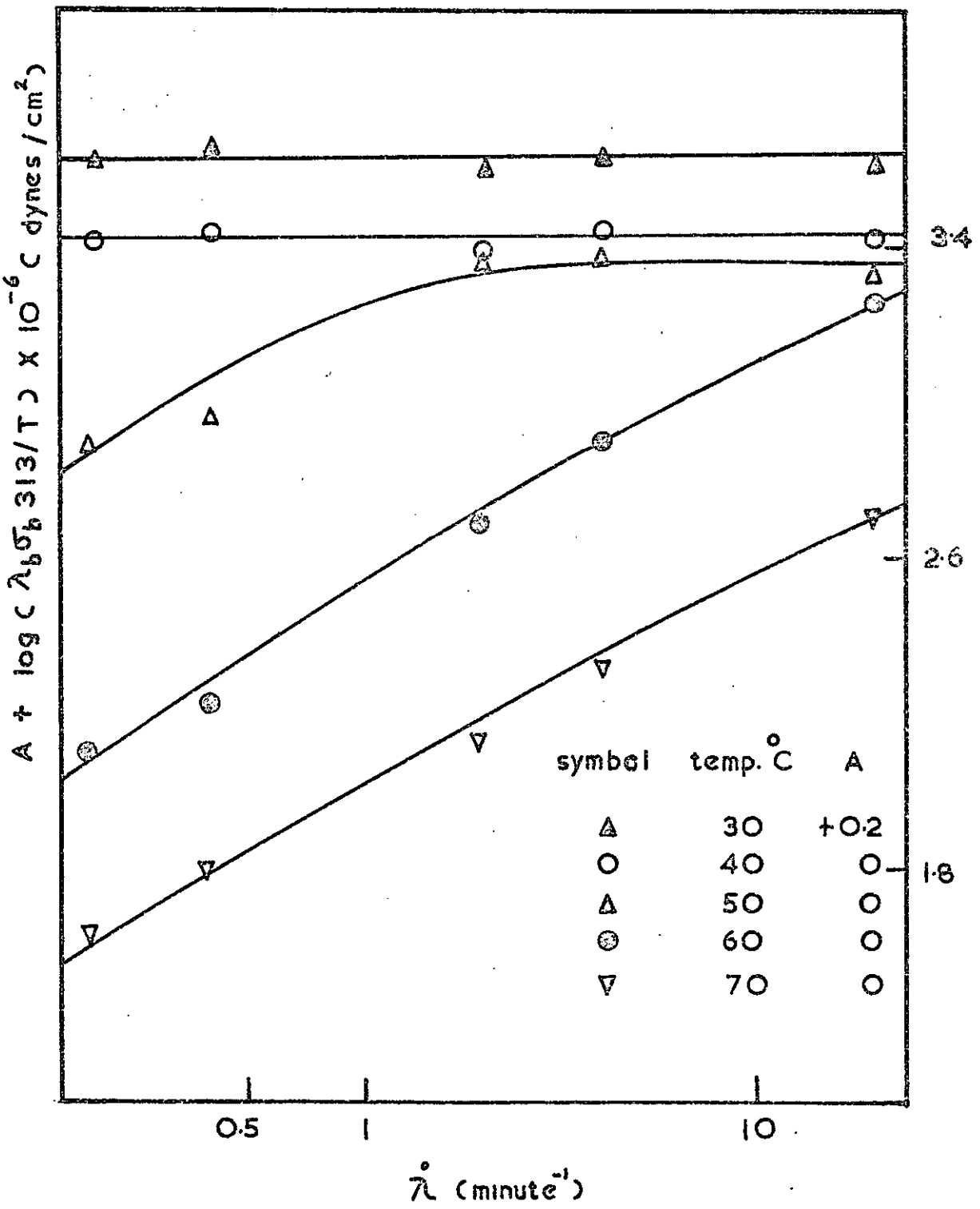
A + log C λb σb 313/T) X 10⁻⁶ C dynes / cm²)
3·4
2·6
1·8
symbol
temp. °C
A
30
+0·2
40
0
50
0
60
0
70
0
0·5
1
10
λ̇ (minute⁻¹)

FIG. 4·16

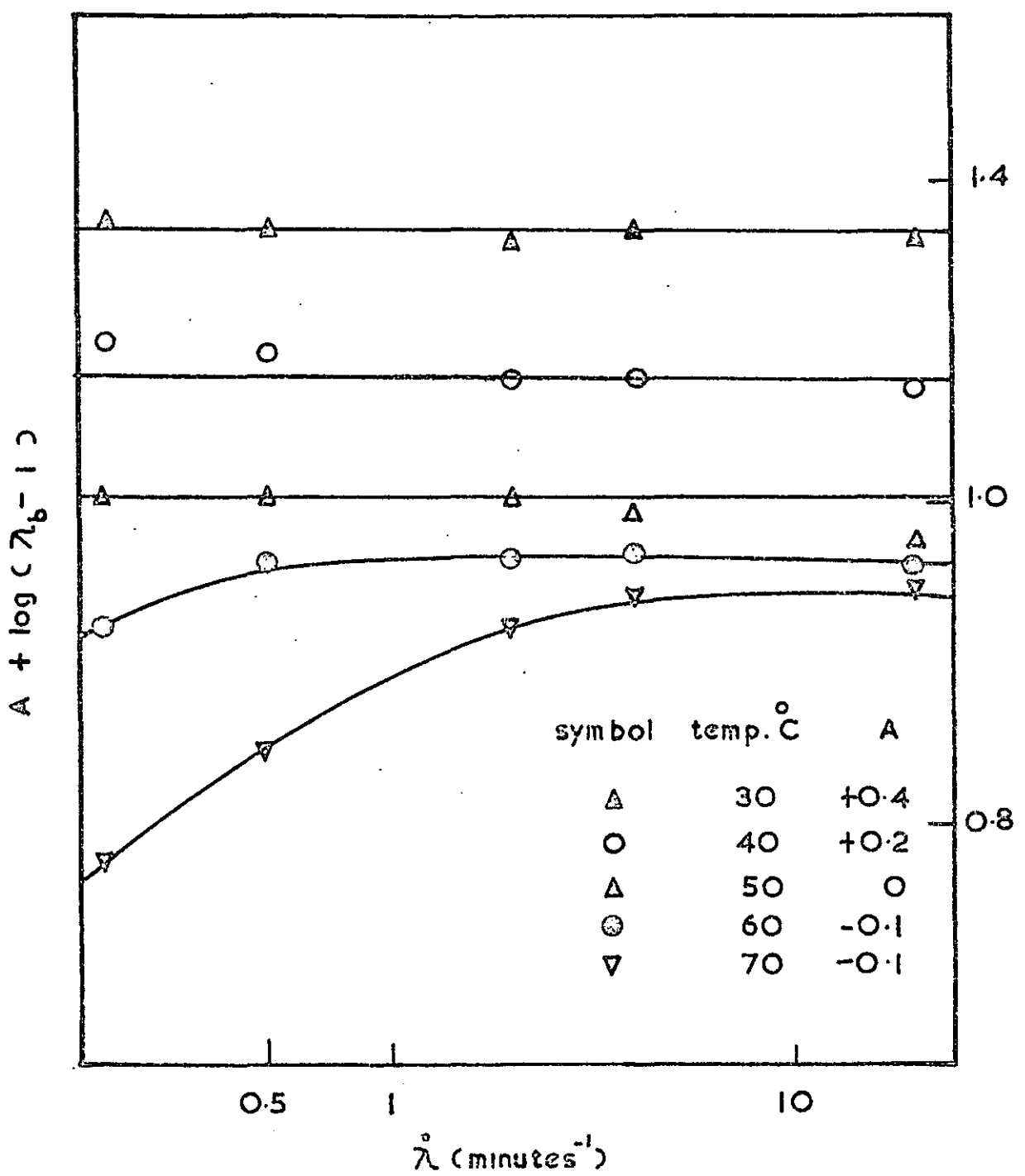
1·4
1·0
0·8
A + log (λ_b − l)
symbol
temp. °C
A
30
+0·4
40
+0·2
50
0
60
-0·1
70
-0·1
0·5
1
10
λ (minutes⁻¹)

FIG. 4·17

The area under the stress-strain curve represents the work which has been performed during the extension of the sample. Because stress-softening occurs in the K101 samples, not all of the work which was put into their extension is recovered as the samples are returned to zero stress level. In such a cyclic stress-strain experiment the energy which is nonrecoverable is dissipated as heat in the stress-softening process, and is represented by the area enclosed in the hysteresis loop.

Table 4.6. summarizes the details of the hysteresis loops obtained for the solvent cast samples at temperatures from 30^{o} to 70^{o}c. The hysteresis loops over two cycles, for toluene and methylene chloride cast samples at 30^{o}c and 60^{o}c, are shown in Figures 4.18. and 4.19. respectively.

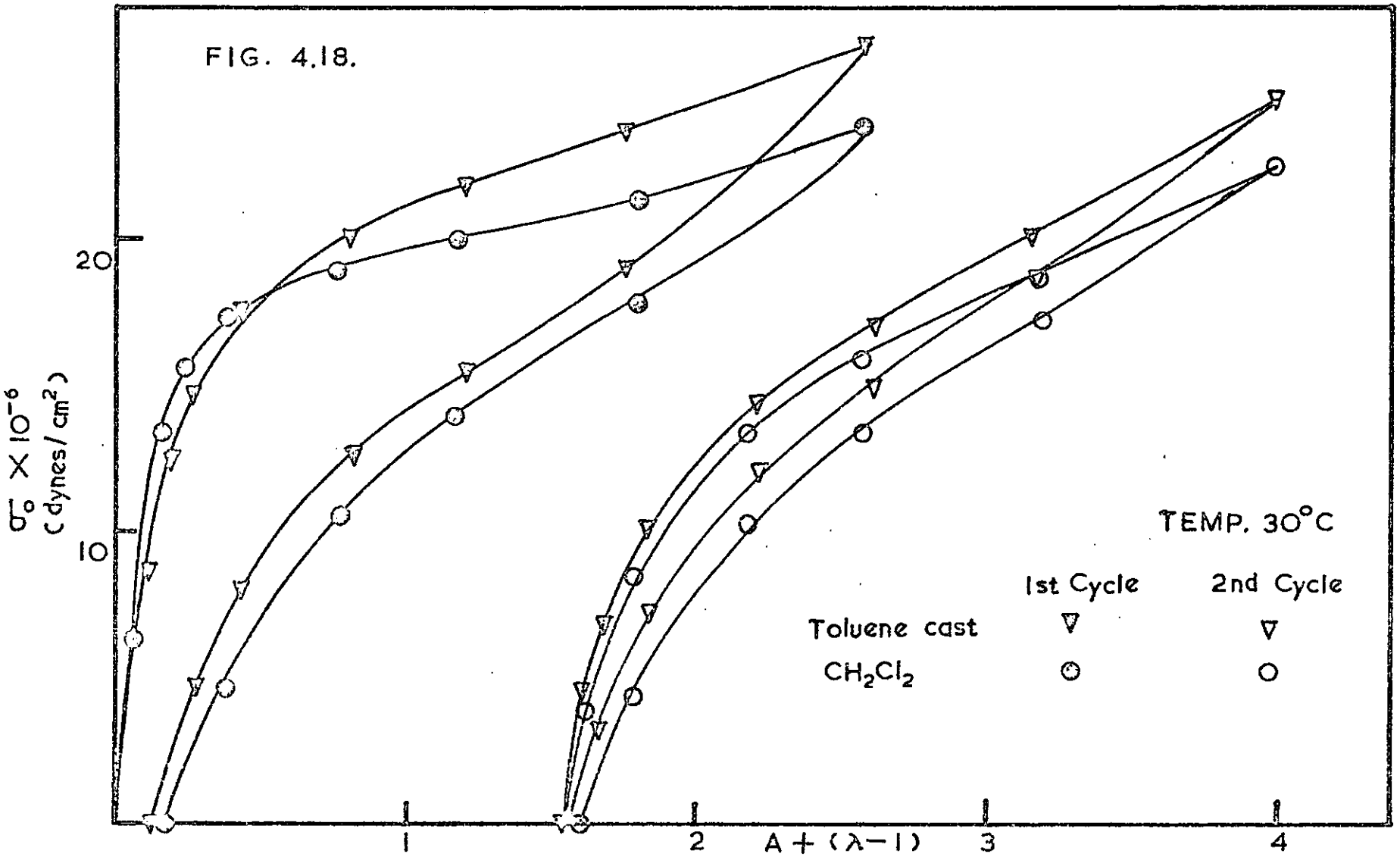
FIG. 4.18.
20
10
$\sigma_o \times 10^{-6}$ (dynes/cm²)
1
2
A + (λ−1)
3
4
TEMP. 30°C
1st Cycle
2nd Cycle
Toluene cast
CH_2Cl_2

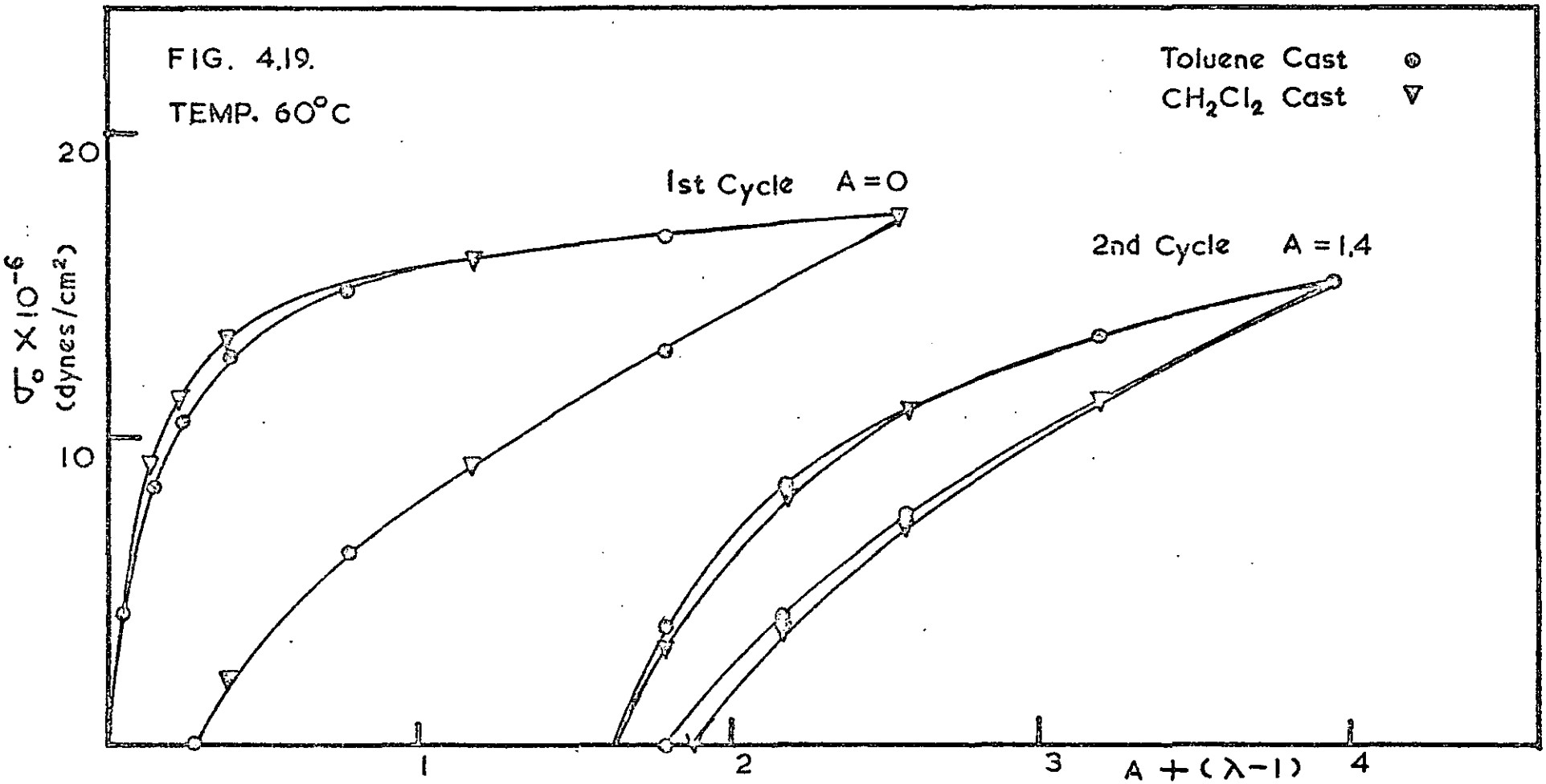
FIG. 4.19.
TEMP. 60°C
Toluene Cast
CH_2Cl_2 Cast
1st Cycle A=0
2nd Cycle A=1.4
$\sigma_o \times 10^{-6}$ (dynes/cm²)
20
10
1
2
3
A + (λ−1)
4

TABLE 4.4.

ULTIMATE PROPERTIES OF TOLUENE CAST K101

Strain Rate ($\% \text{ min}^{-1}$)	Temp (^{o}c)	λ_b	$\sigma_b \times 10^{-6}$ (dynes/cm^2)
0.196	30	9.9	256
	40	11.1	227
	50	11.3	55.1
	60	9.8	13.8
	70	5.4	8.5
0.392	30	9.7	286
	40	10.6	253
	50	11.3	78.5
	60	11.5	15.3
	70	7.1	9.3
1.96	30	9.3	260
	40	9.8	230
	50	11.3	240
	60	11.7	44.7
	70	9.7	14.5
3.92	30	9.7	277
	40	10.0	267
	50	10.6	225
	60	10.7	76.2
	70	10.4	20.8
19.6	30	9.3	264
	40	9.7	262
	50	9.9	218
	60	11.2	172
	70	10.6	50.7

TABLE 4.5.

ULTIMATE PROPERTIES OF METHYLENE CHLORIDE AND METHYL CYCLOHEXANE CAST SAMPLES

Strain Rate (% min^{-1})	Temp (^{o}c)	λ_b	$\sigma_b \times 10^{-6}$ (dynes/cm^2)
1.96	30	9.2	265
	40	9.5	213
	50	11.0	249
	60	11.1	54.5
	70	10.3	14.3
1.96	30	10.0	288
	40	10.9	296
	50	12.1	233
	60	12.1	51.4
	70	10.6	13.5

TABLE 4.6.

DETAILS OF THE HYSTERESIS LOOP

Sample	Temp (°c)	1st Cycle			2nd Cycle		
		E.P.* (%)	$\sigma_p \times 10^{-6}$ (dynes/cm^2)	Set (%)	E.P.* (%)	$\sigma_p \times 10^{-6}$ (dynes/cm^2)	Set (%)
Toluene cast	30	25.2	26.9	13.7	9.8	25.0	7.1
	40	25.6	25.3	15.7	11.1	23.7	8.8
	50	27.9	22.9	19.6	15.0	20.2	10.3
	60	36.3	17.4	33.3	20.5	15.3	14.3
	70	46.3	13.7	51.0	27.5	11.9	20.3
$CH_2C\ell_2$ cast	30	29.2	24.1	23.5	13.8	22.8	10.2
	40	29.4	22.8	23.5	14.5	21.6	10.2
	50	32.2	20.1	31.4	18.3	18.3	12.7
	60	39.0	17.3	39.2	23.9	15.1	14.0
Methyl cyclohexane	30	28.6	23.8	13.7	13.6	22.1	7.0
cast	40	28.5	22.3	21.6	14.0	20.5	10.3
	50	31.8	20.1	23.5	18.2	18.2	11.9
	60	40.1	15.3	39.2	24.7	13.6	19.0

* % Energy dissipation in cyclic stress-strain test to approximately 250% strain level.

4.4. STRESS RELAXATION AND CREEP

The stress σ after a period of time t in the deformed state is expressed as a fraction of the stress σ_i after 0.5 minutes in the deformed state. This percentage decrease in stress was then plotted against the logarithm of the time after extension, as shown in Figures 4.20. to 4.27. for toluene cast and methylene chloride cast samples at extensions e = 0.14, 0.45, 1.00 and 3.00 and temperatures of 30, 40, 50 and 60°c. The relaxation is not accurately proportional to the logarithm of the period in the deformed state. However, an approximately linear relation could be fitted to the experimental points over the limited time range of 0.5 to 10 minutes. The slope S of this linear relation is taken as a convenient measure of the rate of relaxation. It should be noted that such values should not be used to predict relaxation during considerable longer intervals of time.

Plots of the experimentally determined rates of stress relaxation against the imposed extension for toluene cast and methylene chloride cast samples are given in Figures 4.28. and 4.29.

For the toluene cast samples, $\log(\sigma\lambda\ 313/T)$ is plotted against log t at $\lambda = (1 + e) = 1.45$, 2.0 and 4.0, for each test temperature as given by Figures 4.30. to 4.32. These plots correspond to those shown in Figures 4.13. to 4.15. of Section (4.3.).

The tensile creep curves for the toluene cast samples, at various loading are shown in Figures 4.33. to 4.35. Plots of the percentage increase in elongation against the logarithm of time after loading are linear up to 10 minutes in all cases. At longer times, the creep becomes faster than a linear relation would suggest. The slope of the initial linear relationship of such plots is taken as the creep rate

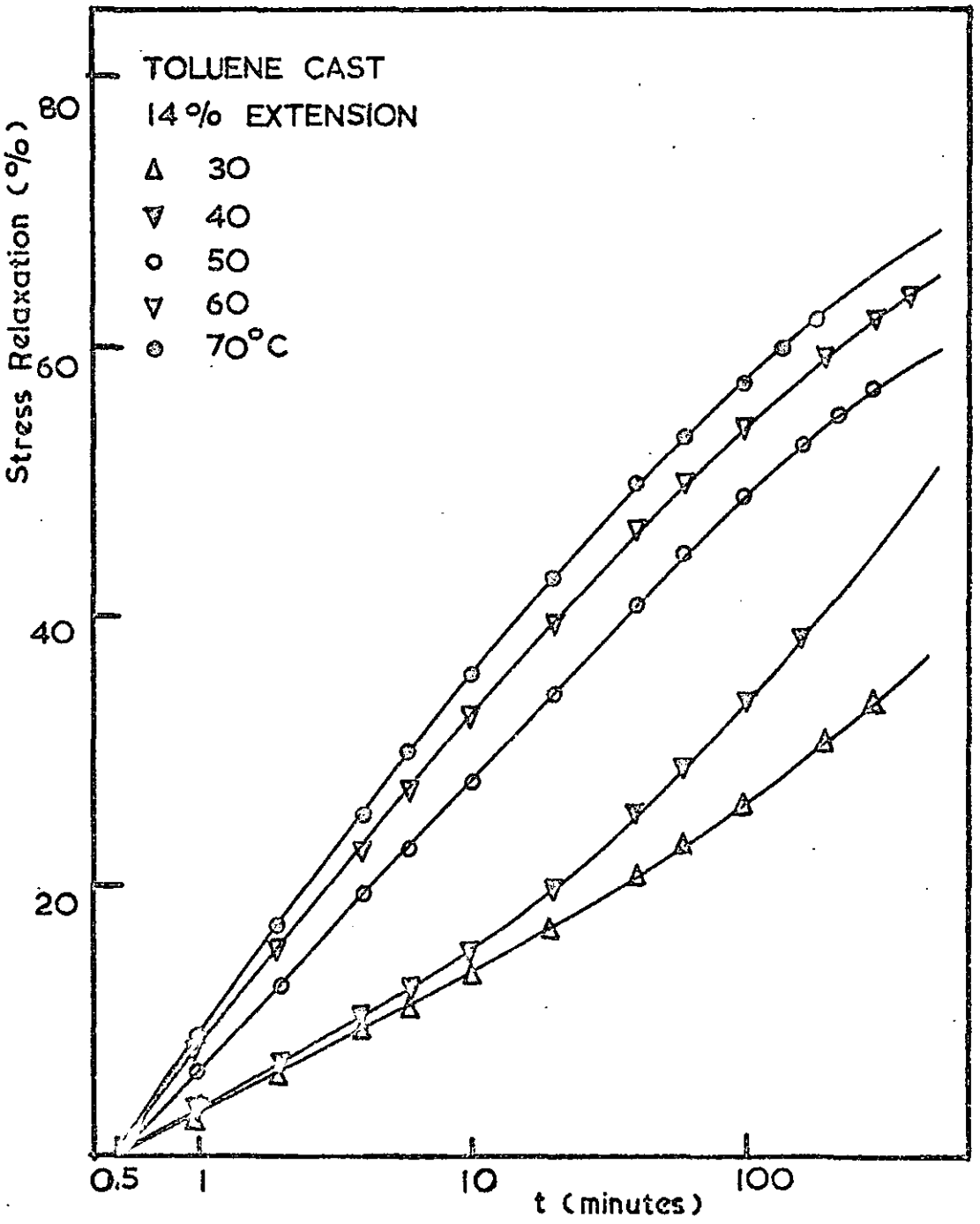
TOLUENE CAST
14 % EXTENSION
Δ 30
▽ 40
o 50
▽ 60
⊙ 70°C
Stress Relaxation (%)
80
60
40
20
0.5
1
10
100
t (minutes)

FIG. 4.20.

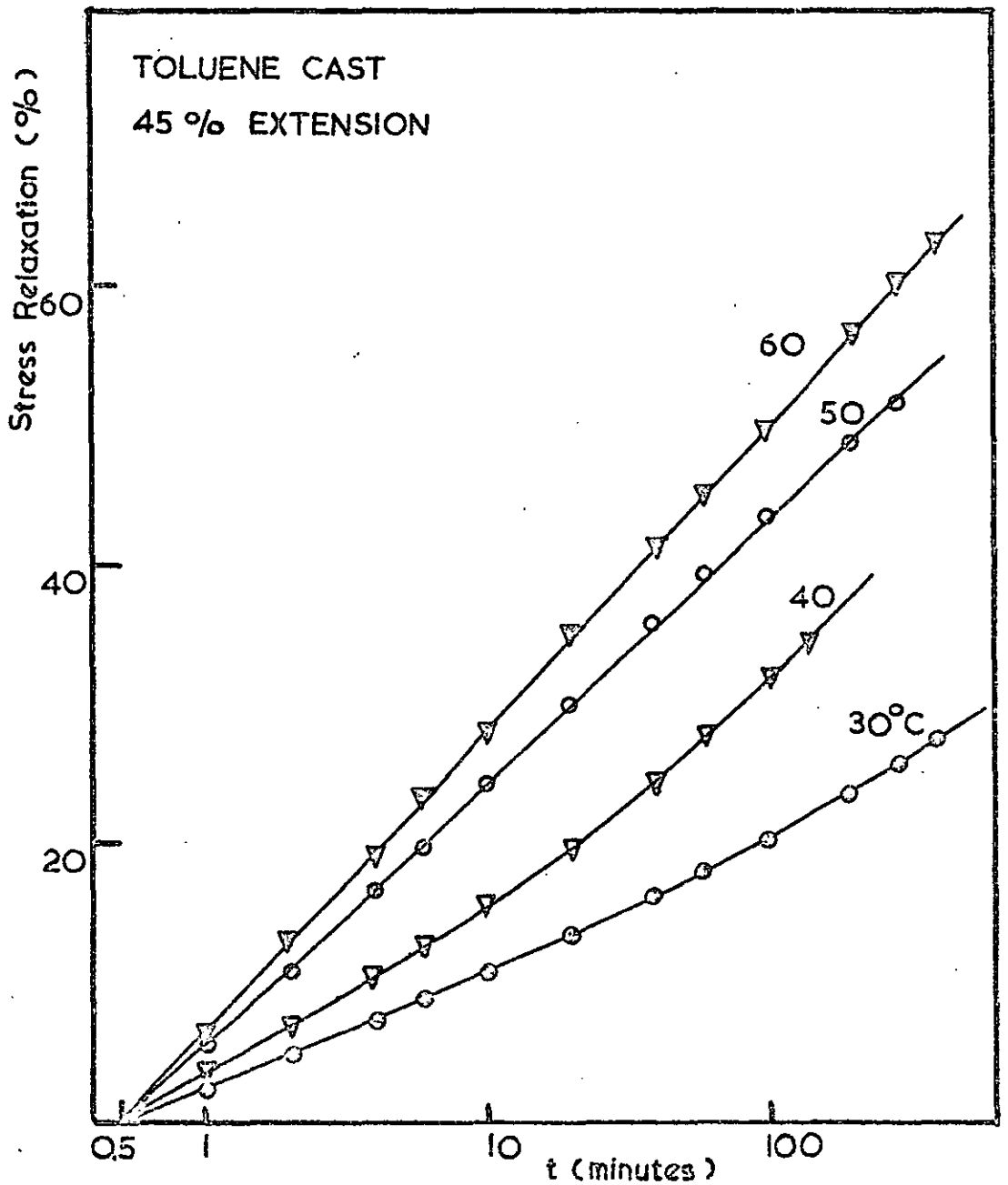
TOLUENE CAST
45 % EXTENSION
Stress Relaxation (%)
60
40
20
60
50
40
30°C
0.5
1
10
100
t (minutes)

FIG. 4.21.

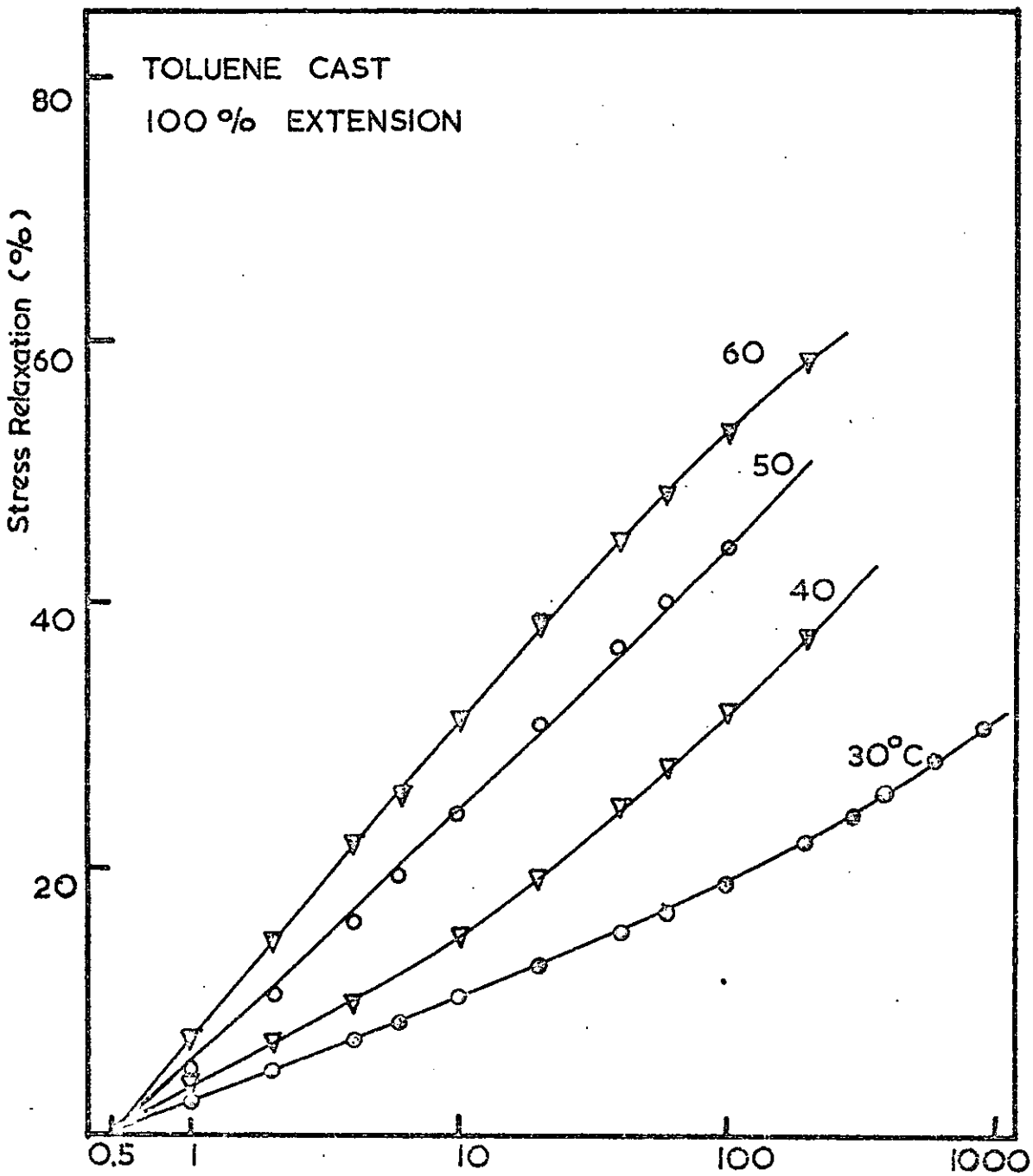
TOLUENE CAST
100 % EXTENSION
Stress Relaxation (%)
80
60
40
20
60
50
40
30°C
0.5
1
10
100
1000

FIG. 4.22.

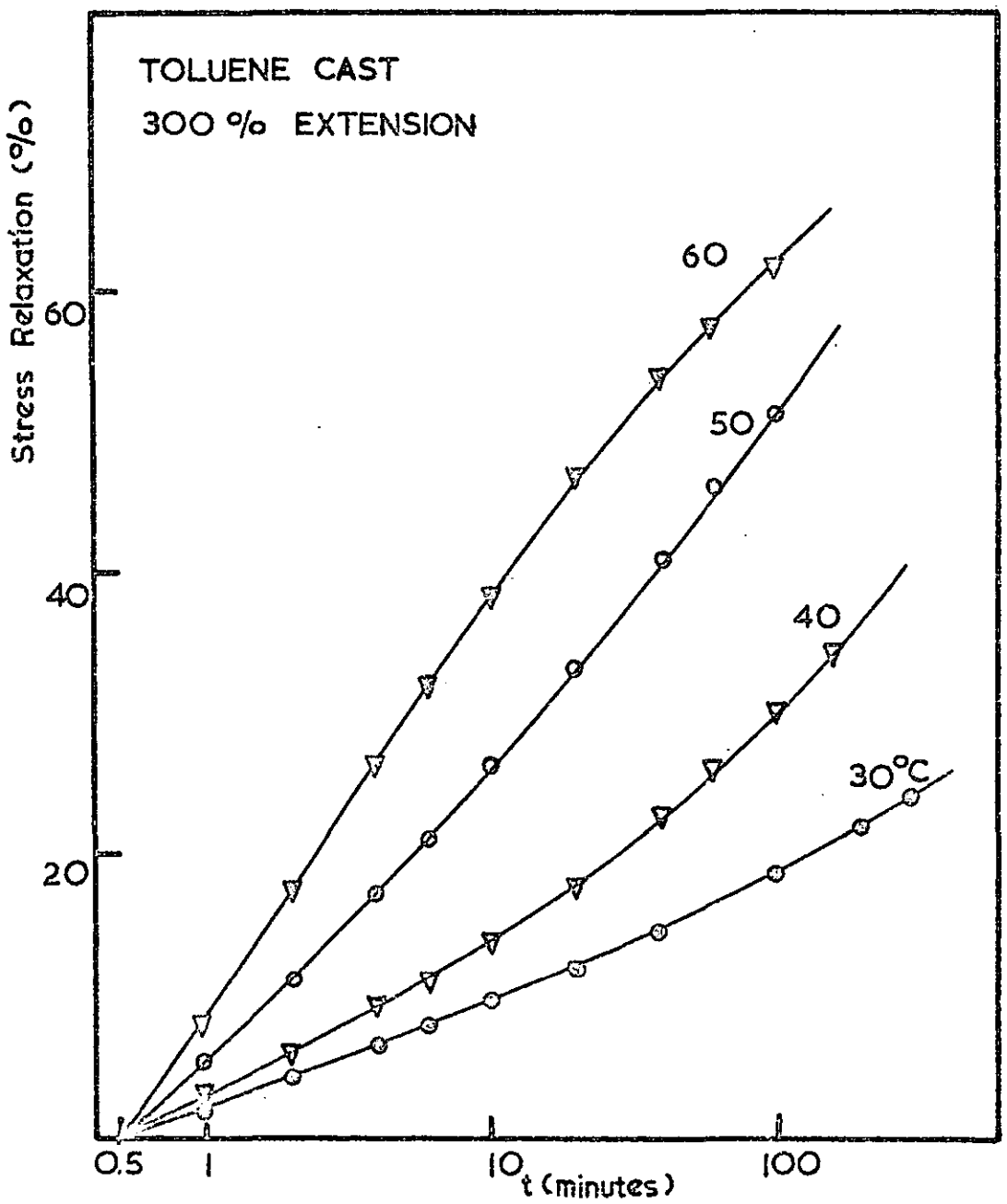
TOLUENE CAST
300 % EXTENSION
Stress Relaxation (%)
60
40
20
60
50
40
30°C
0.5
1
10
100
t (minutes)

FIG. 4.23.

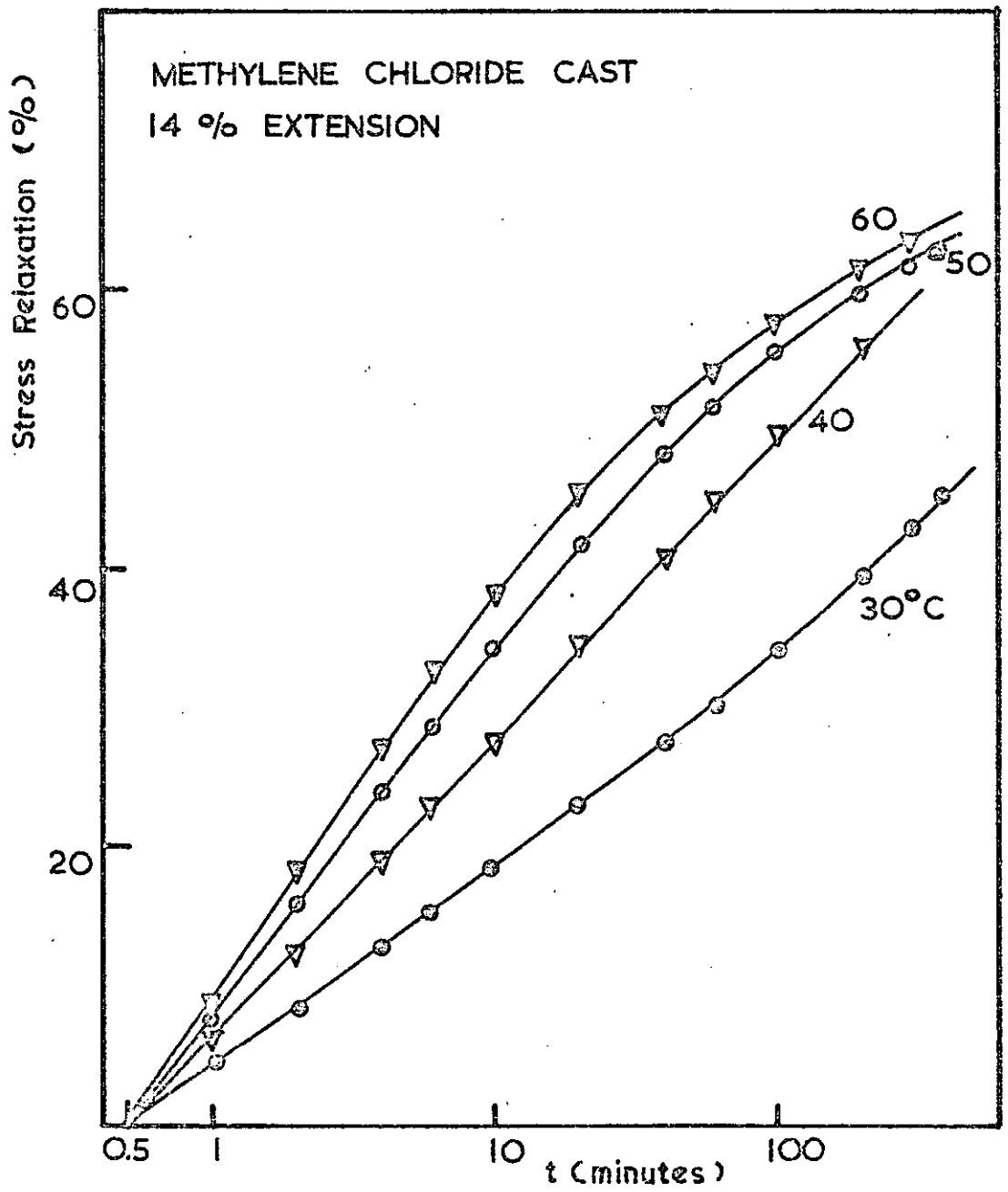
METHYLENE CHLORIDE CAST
14 % EXTENSION
Stress Relaxation (%)
60
40
20
60
50
40
30°C
0.5
1
10
100
t (minutes)

FIG. 4.24.

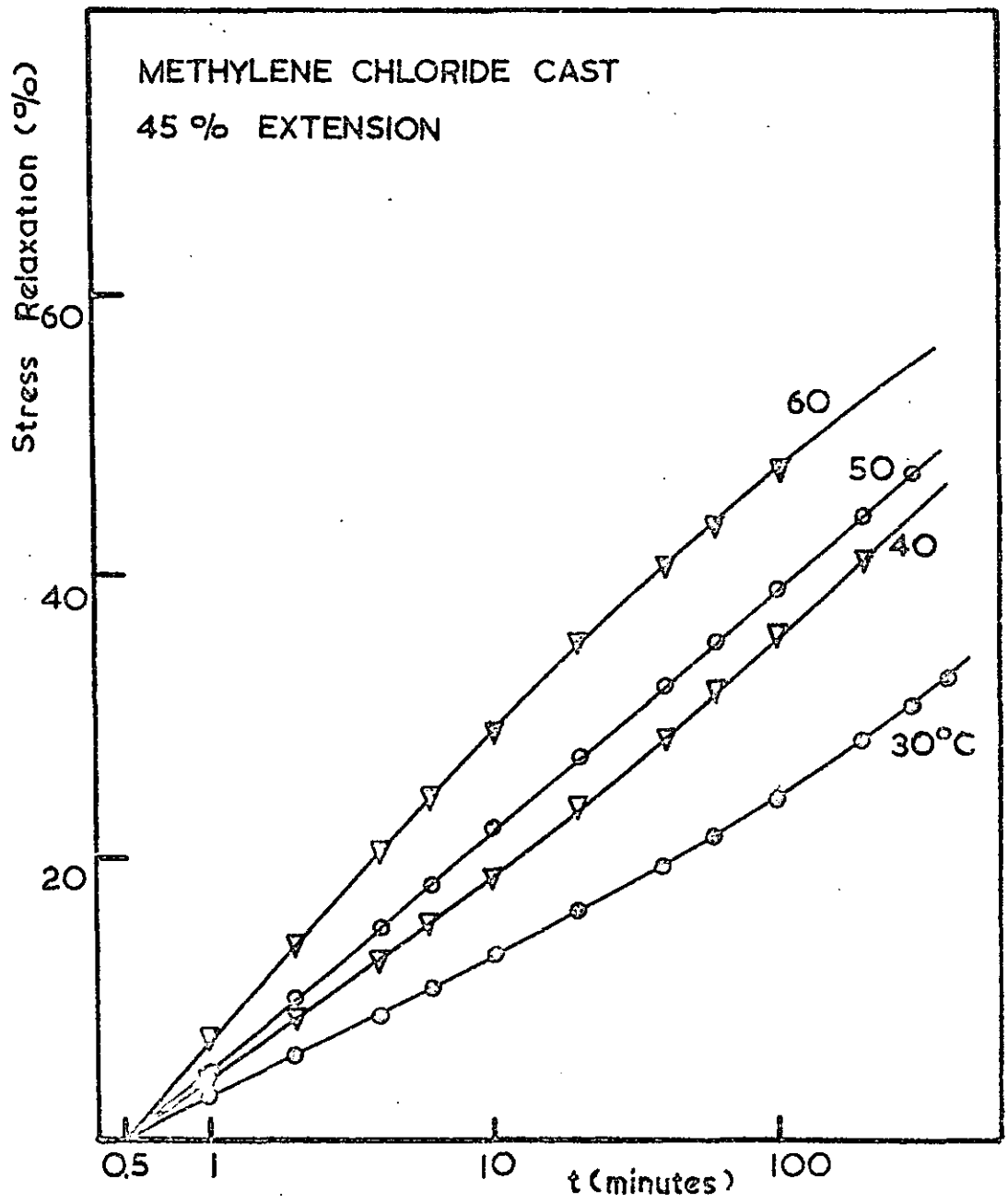
METHYLENE CHLORIDE CAST
45 % EXTENSION
Stress Relaxation (%)
60
40
20
60
50
40
30°C
0.5
1
10
100
t (minutes)

FIG. 4.25.

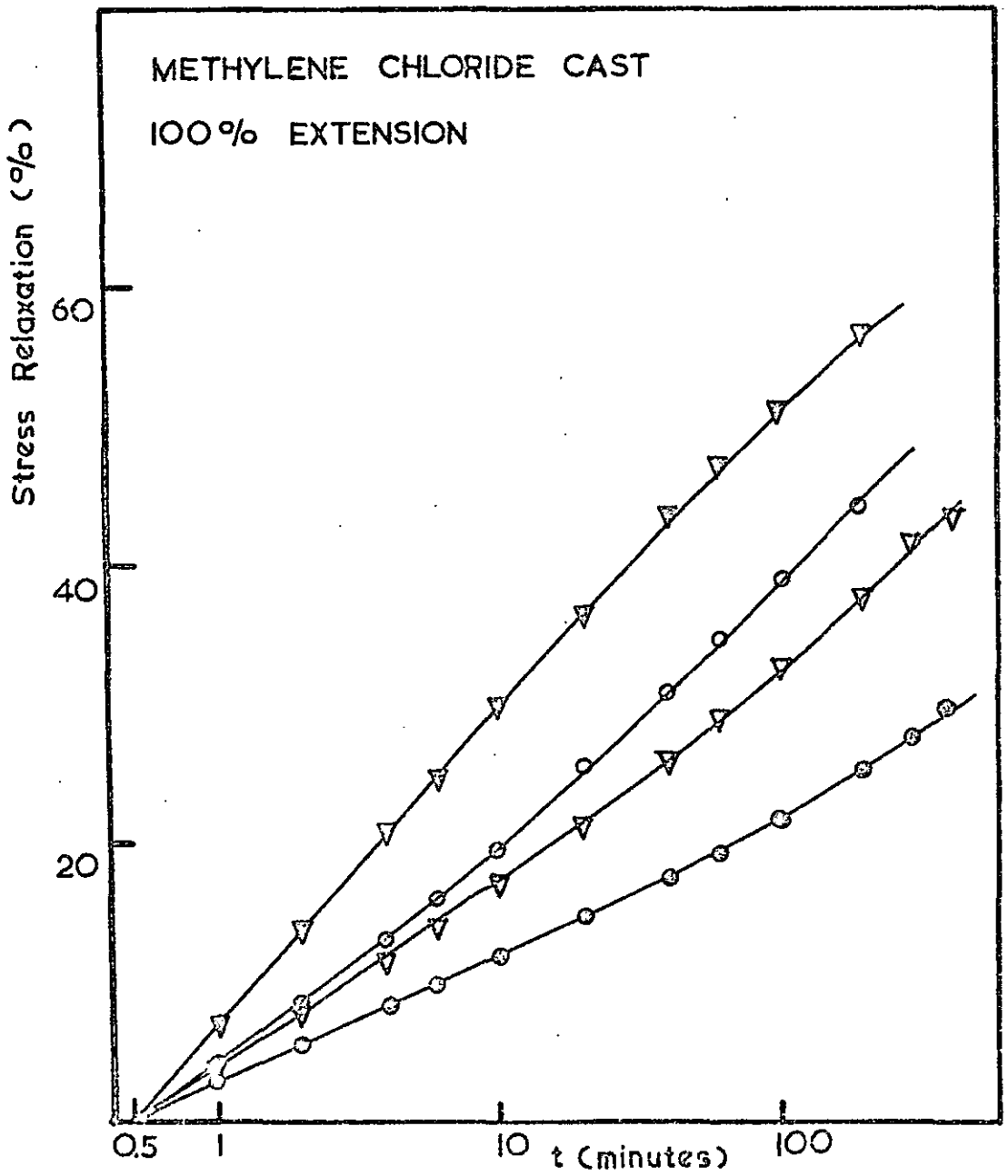
METHYLENE CHLORIDE CAST
100% EXTENSION
Stress Relaxation (%)
60
40
20
0.5
1
10
100
t (minutes)

FIG. 4.26.

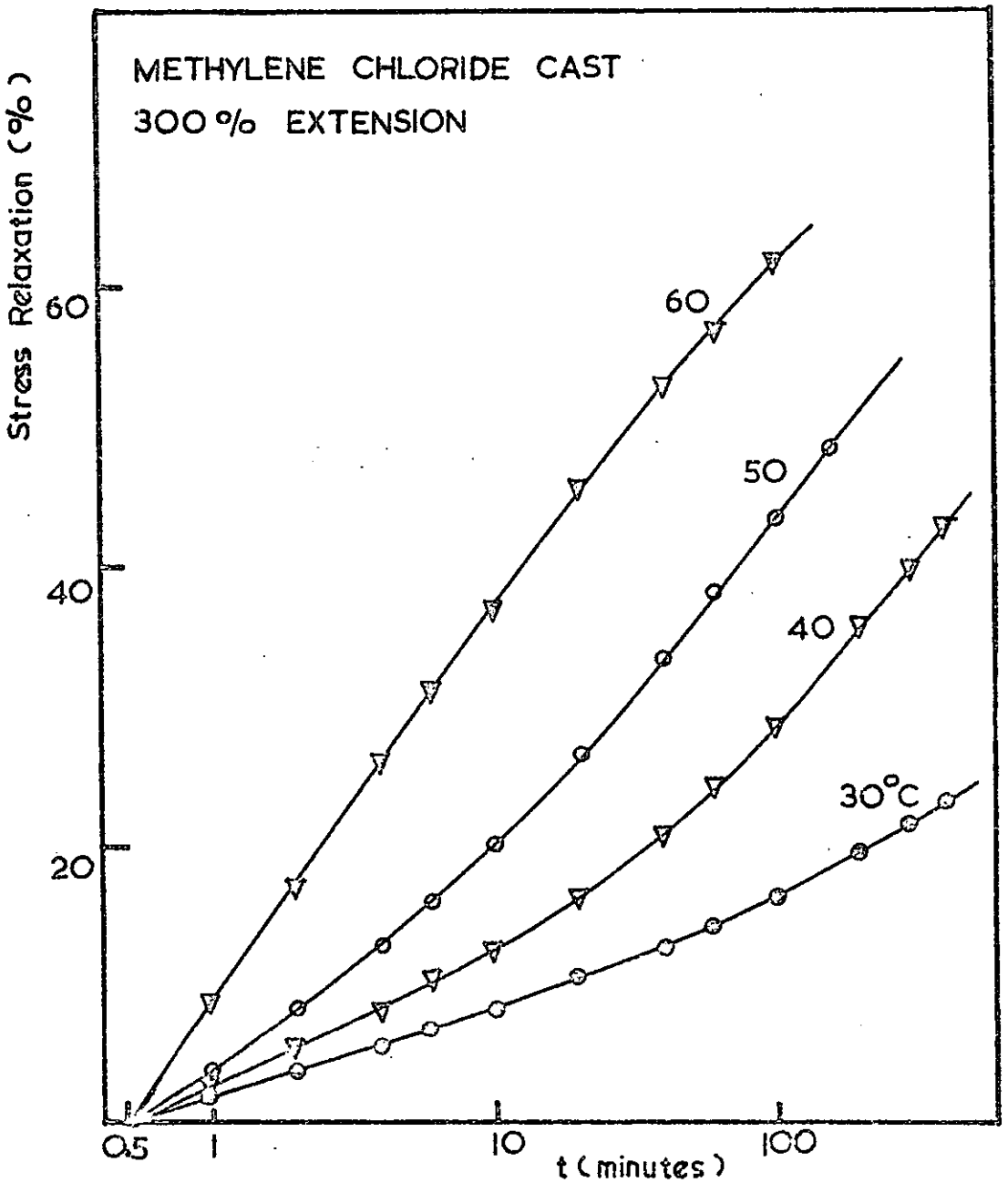
METHYLENE CHLORIDE CAST
300 % EXTENSION
Stress Relaxation (%)
60
40
20
60
50
40
30°C
0.5
1
10
100
t (minutes)

FIG. 4.27

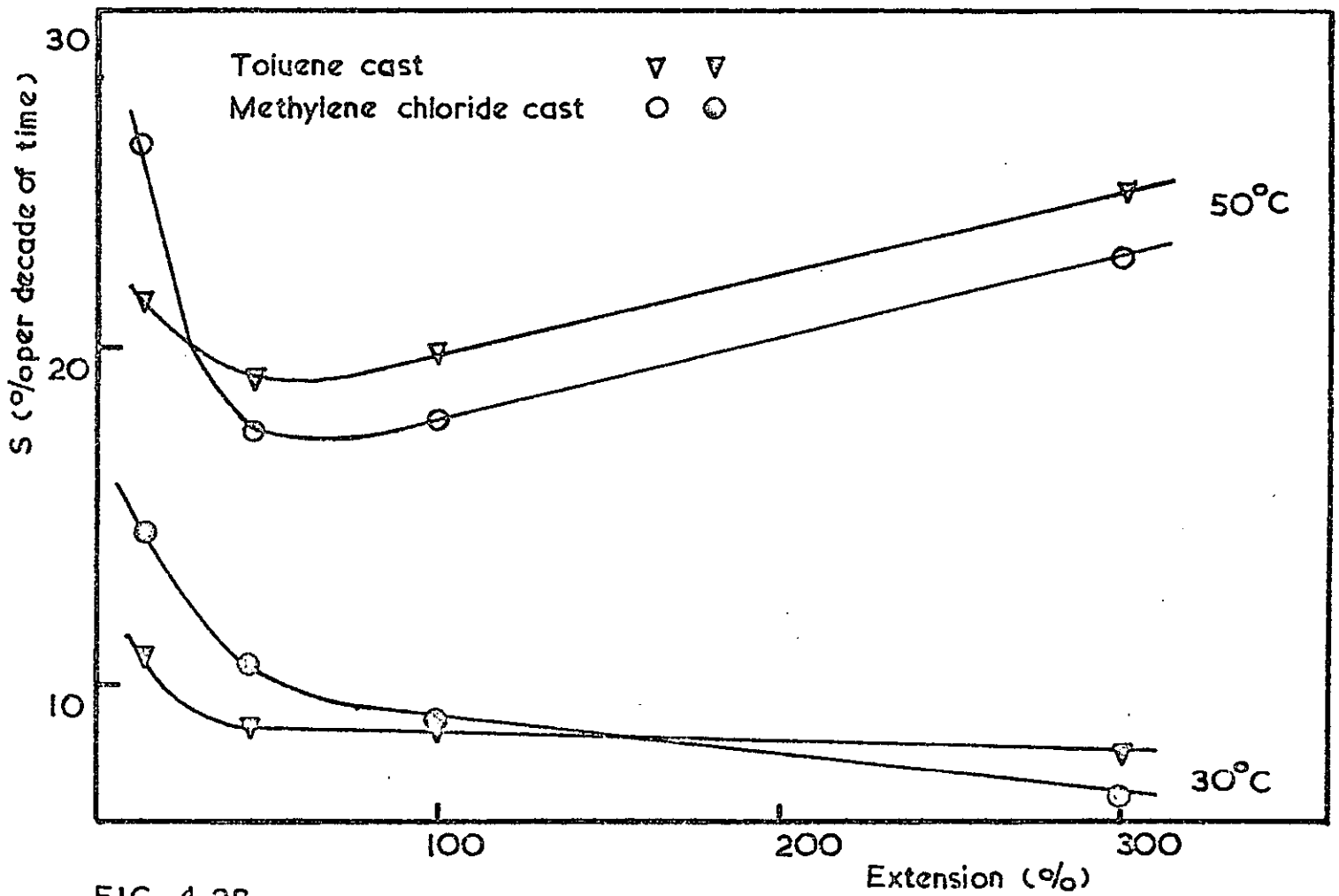
Toluene cast
Methylene chloride cast
S (%per decade of time)
30
20
10
50°C
30°C
100
200
300
Extension (%)

FIG. 4.28.

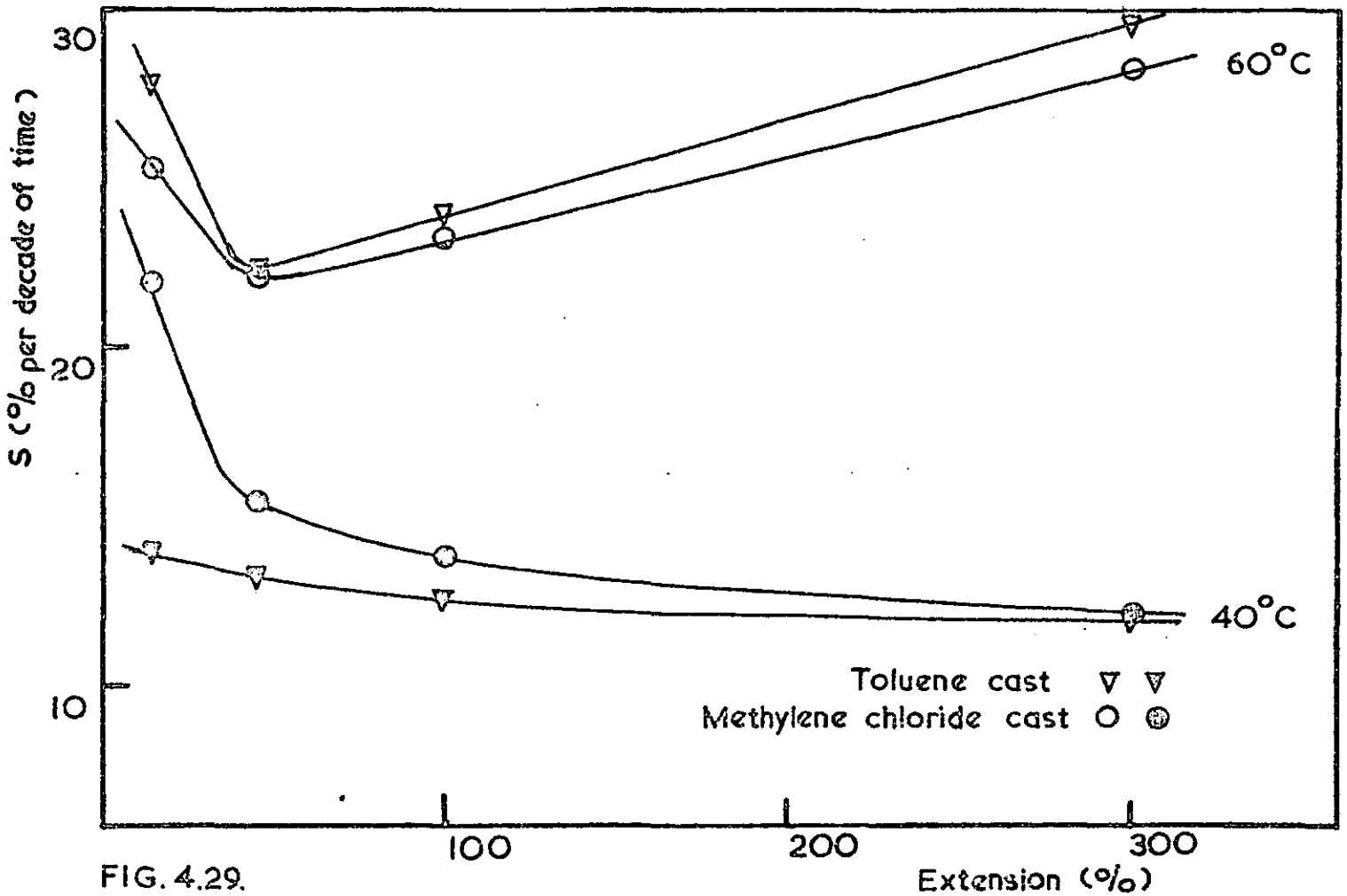
30
20
10
S (% per decade of time)
60°C
40°C
Toluene cast
Methylene chloride cast
100
200
300
Extension (%)

FIG. 4.29.

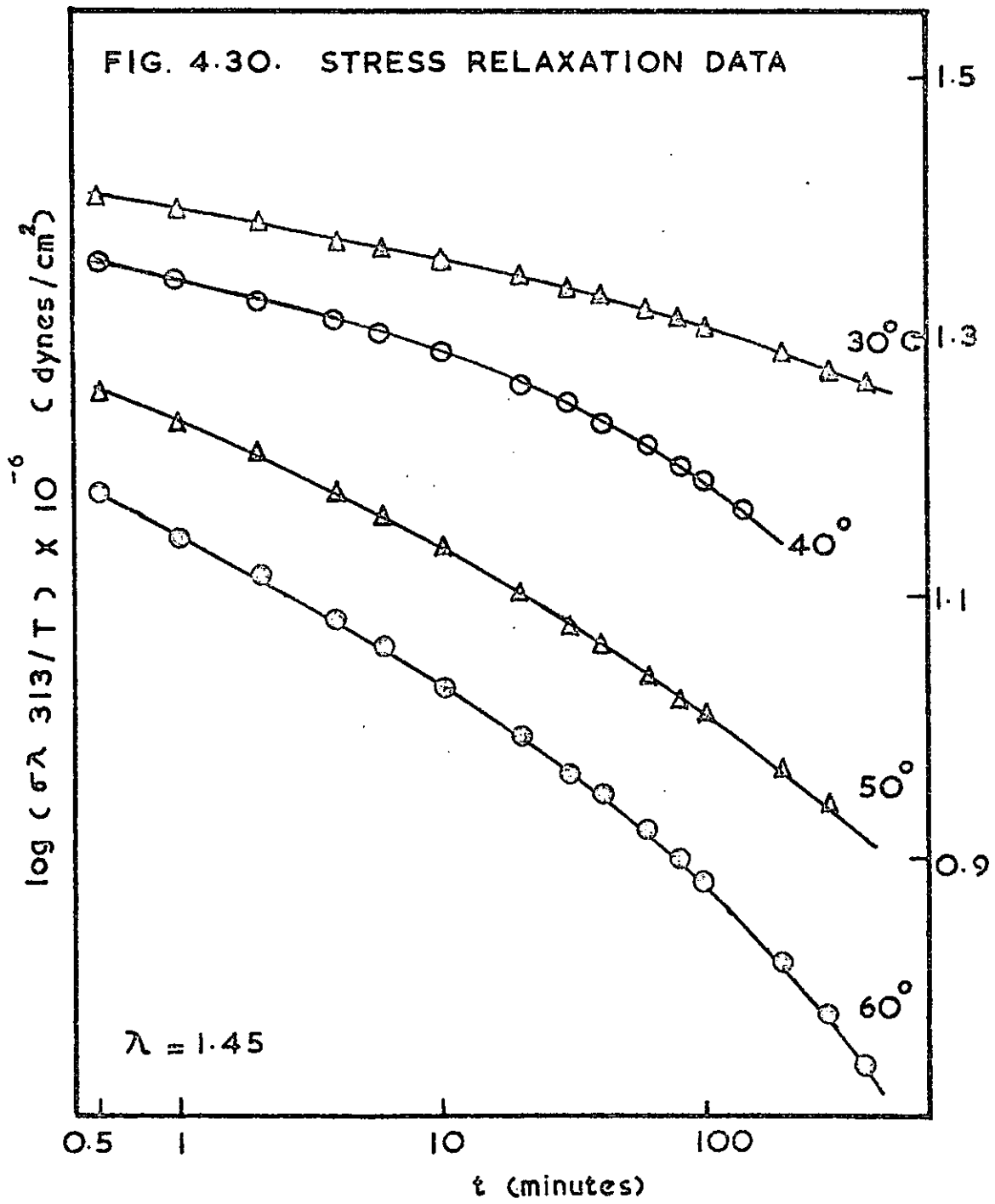
FIG. 4·30. STRESS RELAXATION DATA
log (σλ 313/T) X 10^-6 (dynes/cm^2)
1.5
1.3
1.1
0.9
30°C
40°
50°
60°
λ = 1·45
0.5
1
10
100
t (minutes)

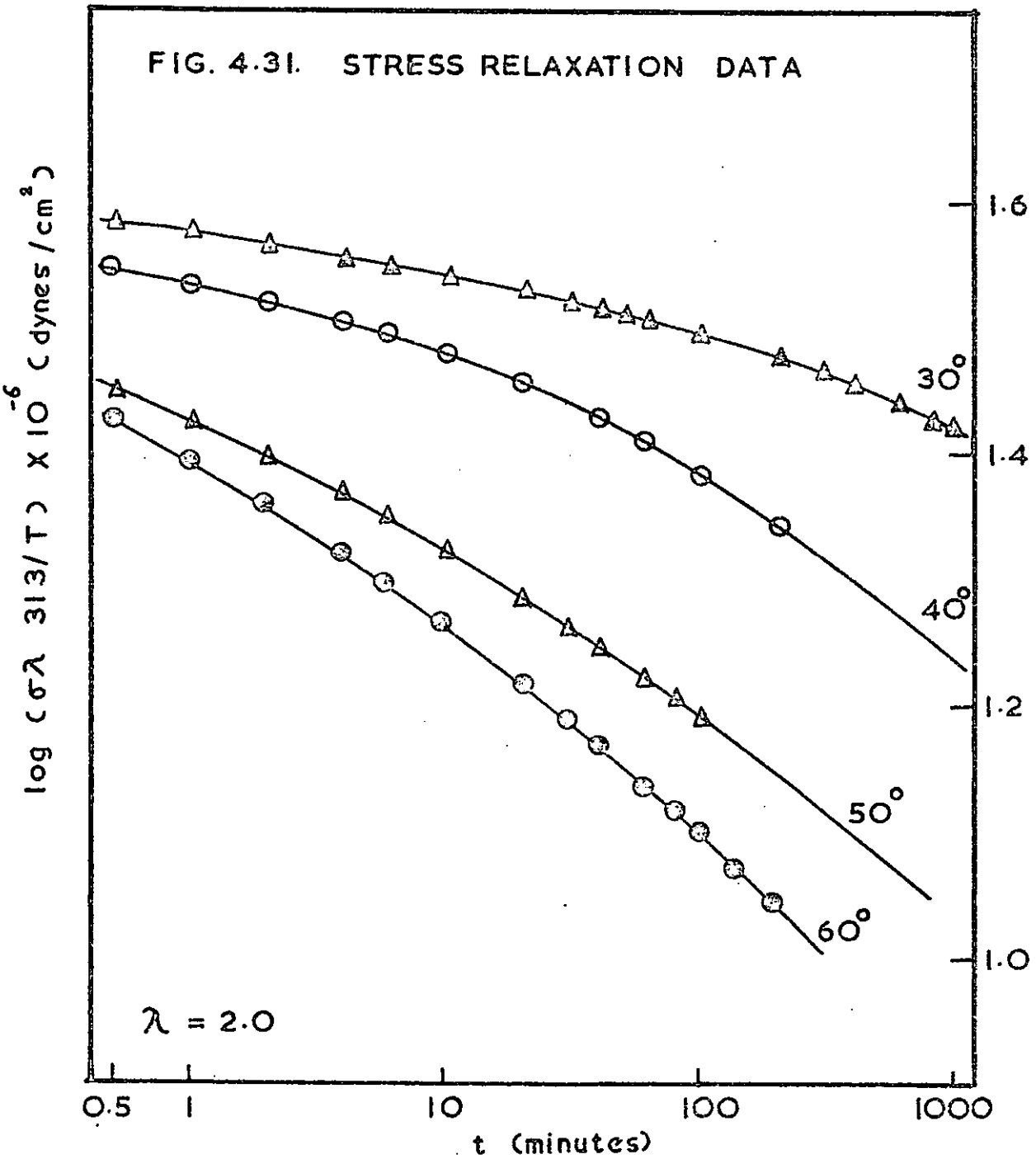
FIG. 4.31. STRESS RELAXATION DATA
log (σλ 313/T) X 10^-6 (dynes/cm^2)
1.6
1.4
1.2
1.0
30°
40°
50°
60°
λ = 2.0
0.5
1
10
100
1000
t (minutes)

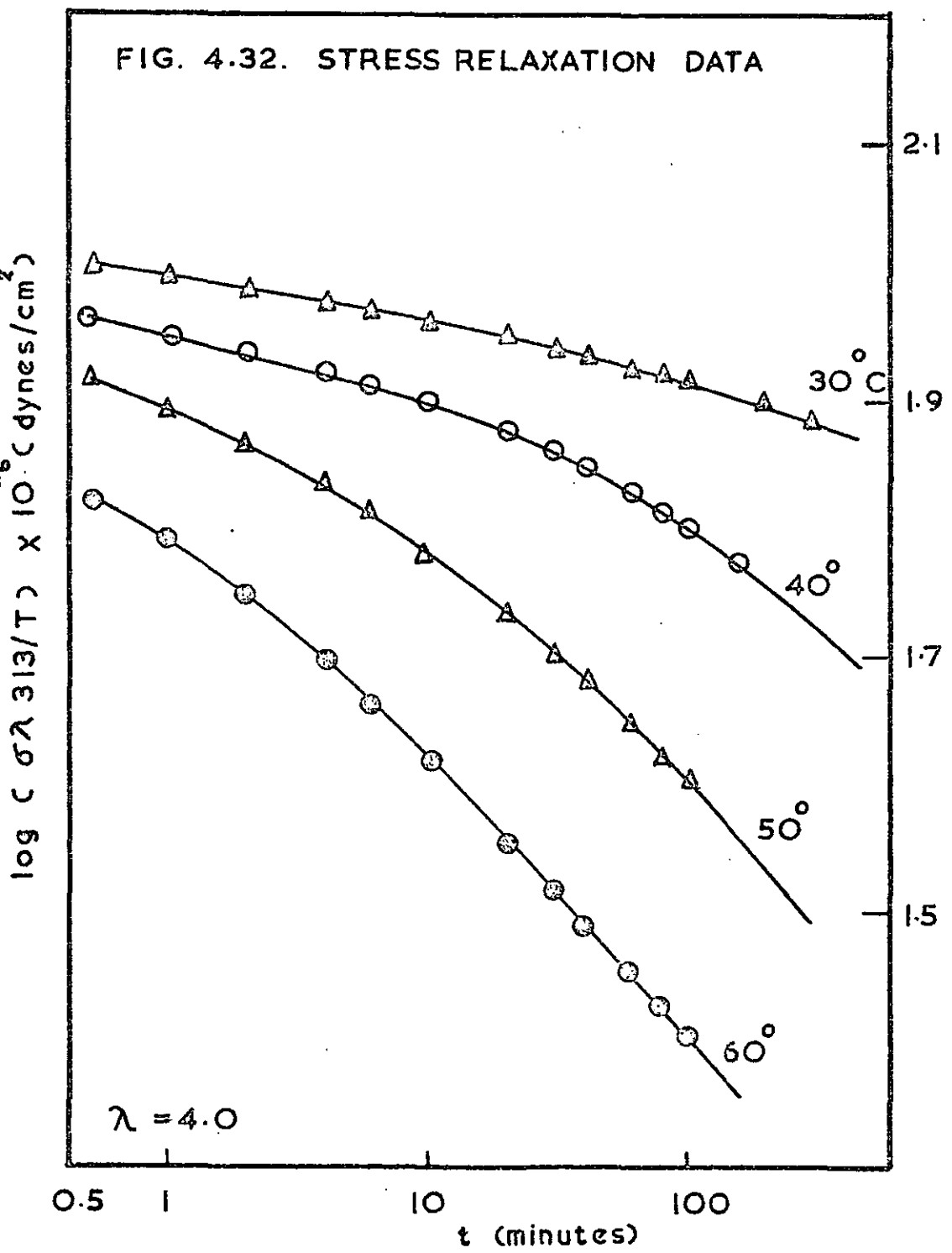
FIG. 4.32. STRESS RELAXATION DATA
log (σλ 313/T) X 10^-6 (dynes/cm^2)
2·1
1·9
1·7
1·5
30° C
40°
50°
60°
λ = 4.0
0.5
1
10
100
t (minutes)

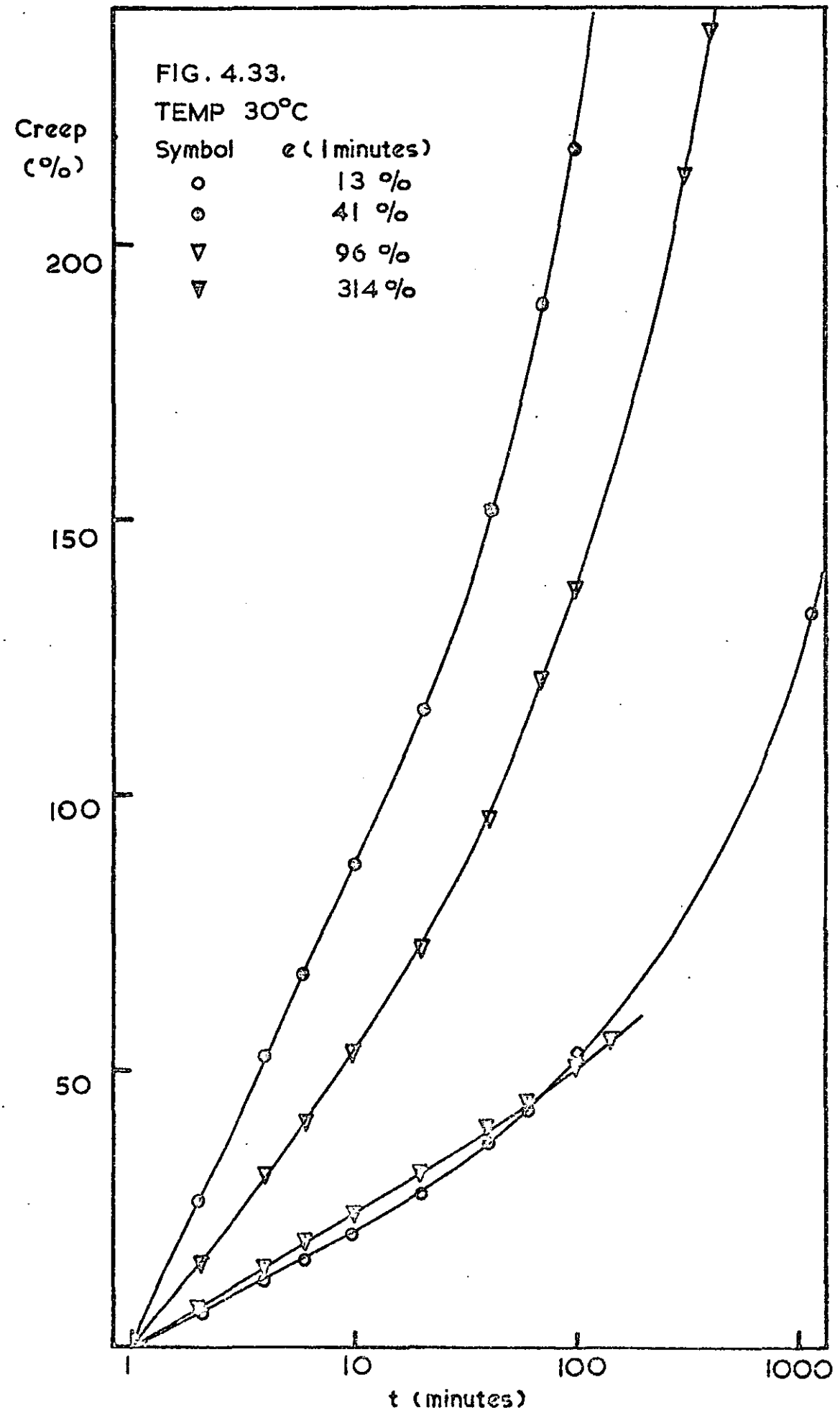
FIG. 4.33.
TEMP 30°C
Symbol e (minutes)
13 %
41 %
96 %
314 %
Creep (%)
200
150
100
50
1
10
100
1000
t (minutes)

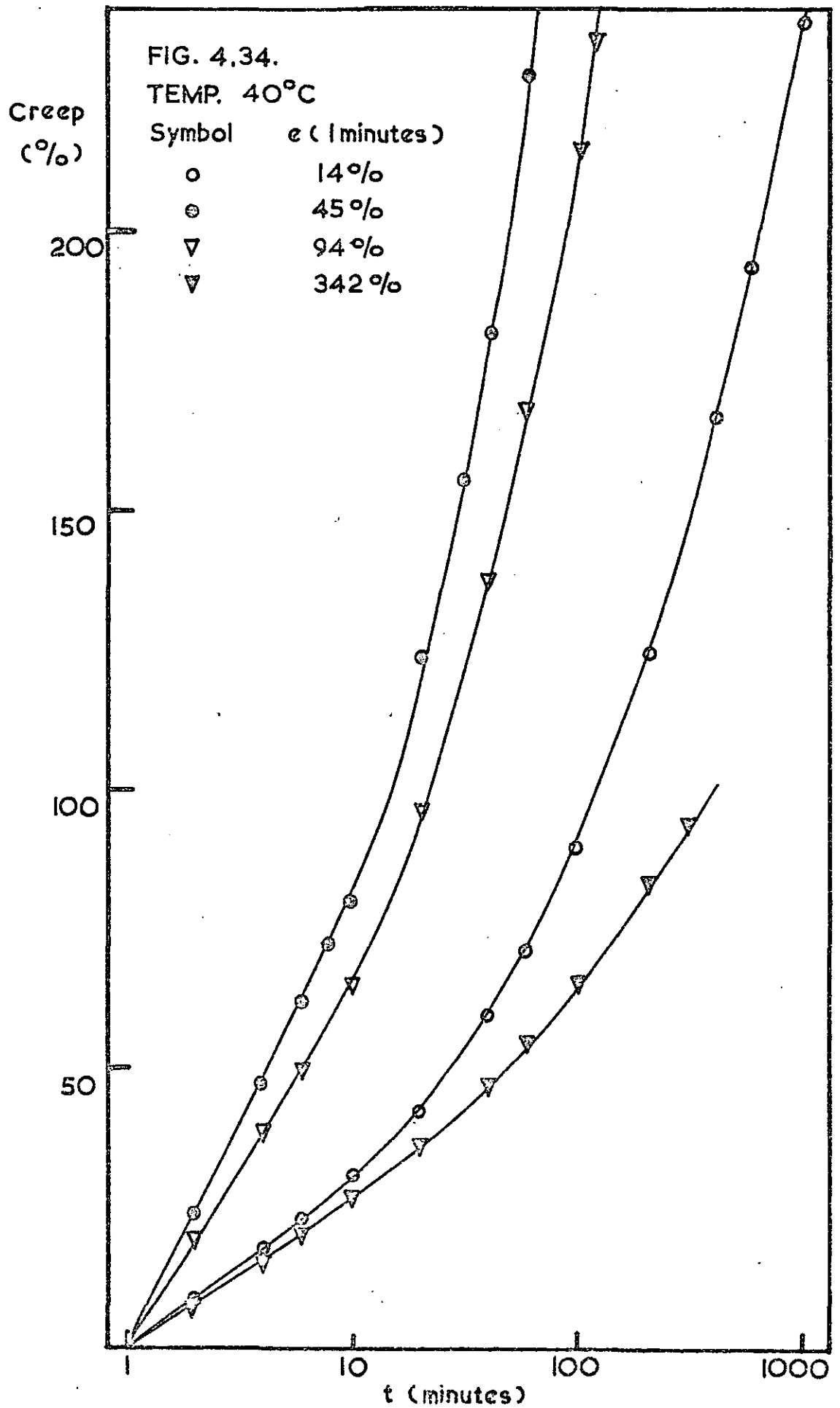
FIG. 4.34.
TEMP. 40°C
Symbol
e (I minutes)
14 %
45 %
94 %
342 %
Creep
(%)
200
150
100
50
1
10
100
1000
t (minutes)

FIG. 4.35.

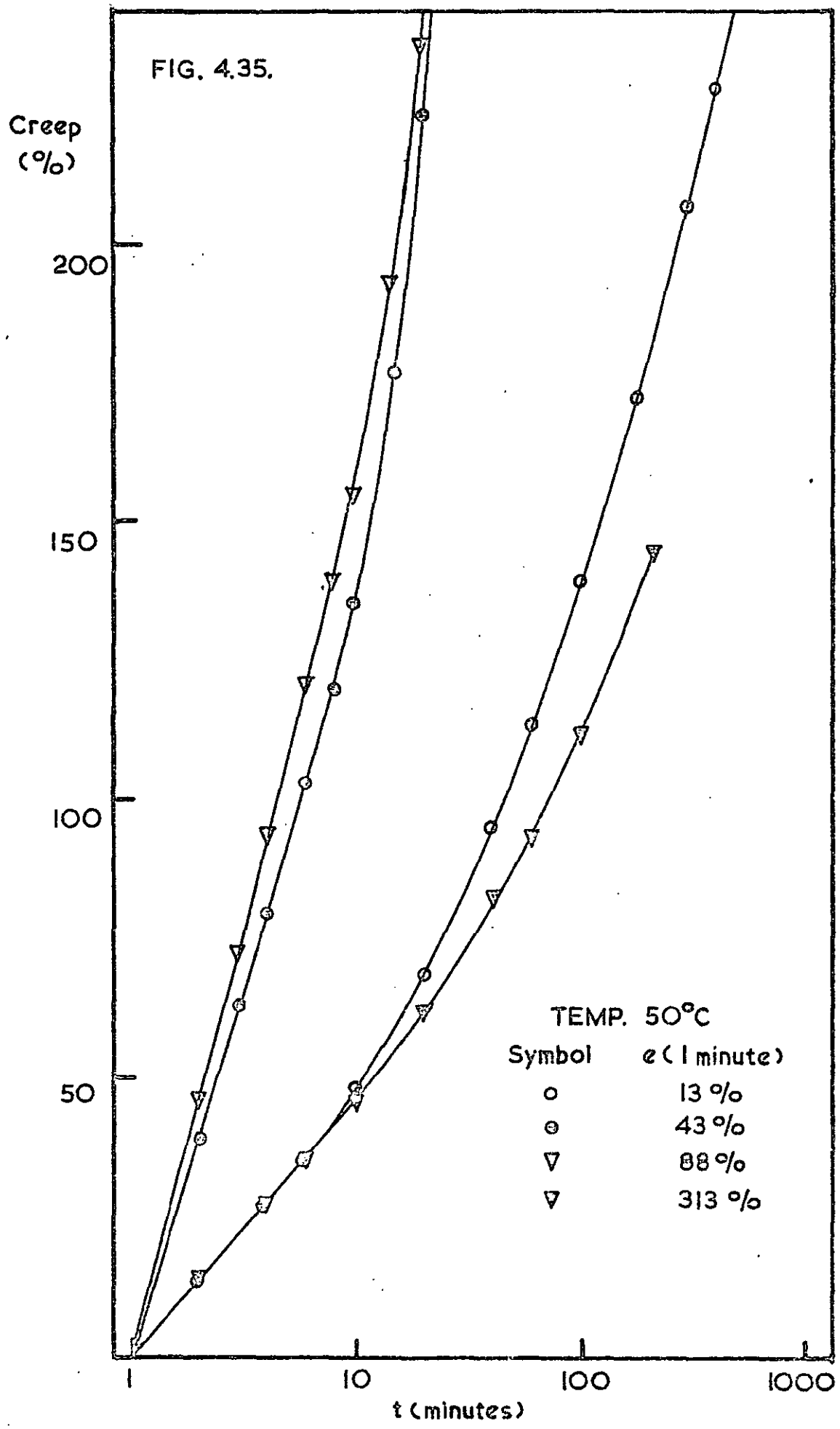
Creep (%)
200
150
100
50
1
10
100
1000
t (minutes)
TEMP. 50°C
Symbol
e (1 minute)
13 %
43 %
88 %
313 %

C, where $C = (1/e)(\partial e/\partial \log t)_{\sigma}$ and e is the elongation after one minute. The creep rate is expressed as % per decade of time and is given in Table 4.7. together with the corresponding extension one minute after imposing the constant applied stress σ, for various loading and temperatures. The stress is based on the dimensions of the unstretched sample.

TABLE 4.7.

Creep properties of toluene cast K101

Temp (^{o}c)	e(1 minutes) (%)	C (% per decade)	$\sigma_o \times 10^{-7}$ (dynes/cm^2)
30	13	20.1	1.05
	41	87.5	1.75
	96	51.8	2.05
	314	23.5	2.93
40	14	27.6	1.02
	45	79.7	1.66
	94	63.8	1.78
	342	25.8	2.62
50	13	46.8	0.86
	43	133.4	1.45
	88	154.8	1.75
	313	45.6	2.36

4.5. DYNAMIC MECHANICAL STUDIES

The results of the dynamic mechanical measurements made on the various samples of K101, fabricated under different thermal or solvent treatments are given in this section.

Each set of data is summarized by plotting the following graphs.

(a) Log E' against temperature at frequencies of 10,1, 0.3 and 0.1 Hz. For the toluene cast sample, the test frequencies are 10,1, 0.1 and 0.01 Hz. (Figures 4.36. to 4.40.). E' is the storage Young's modulus and is expressed as dynes/cm^2.

(b) Tan δ against temperature at frequencies of 10,1, 0.3 and 0.1 Hz. For the toluene cast sample, the test frequencies are 10,1, 0.1 and 0.01 Hz. (Figures 4.41. to 4.45.). Tan δ is the mechanical loss factor. Experimentally it is obtained directly from the ratio of $V_{lag}/V_{inphase}$, given by the resolved component indicator. (See section 3.8.)

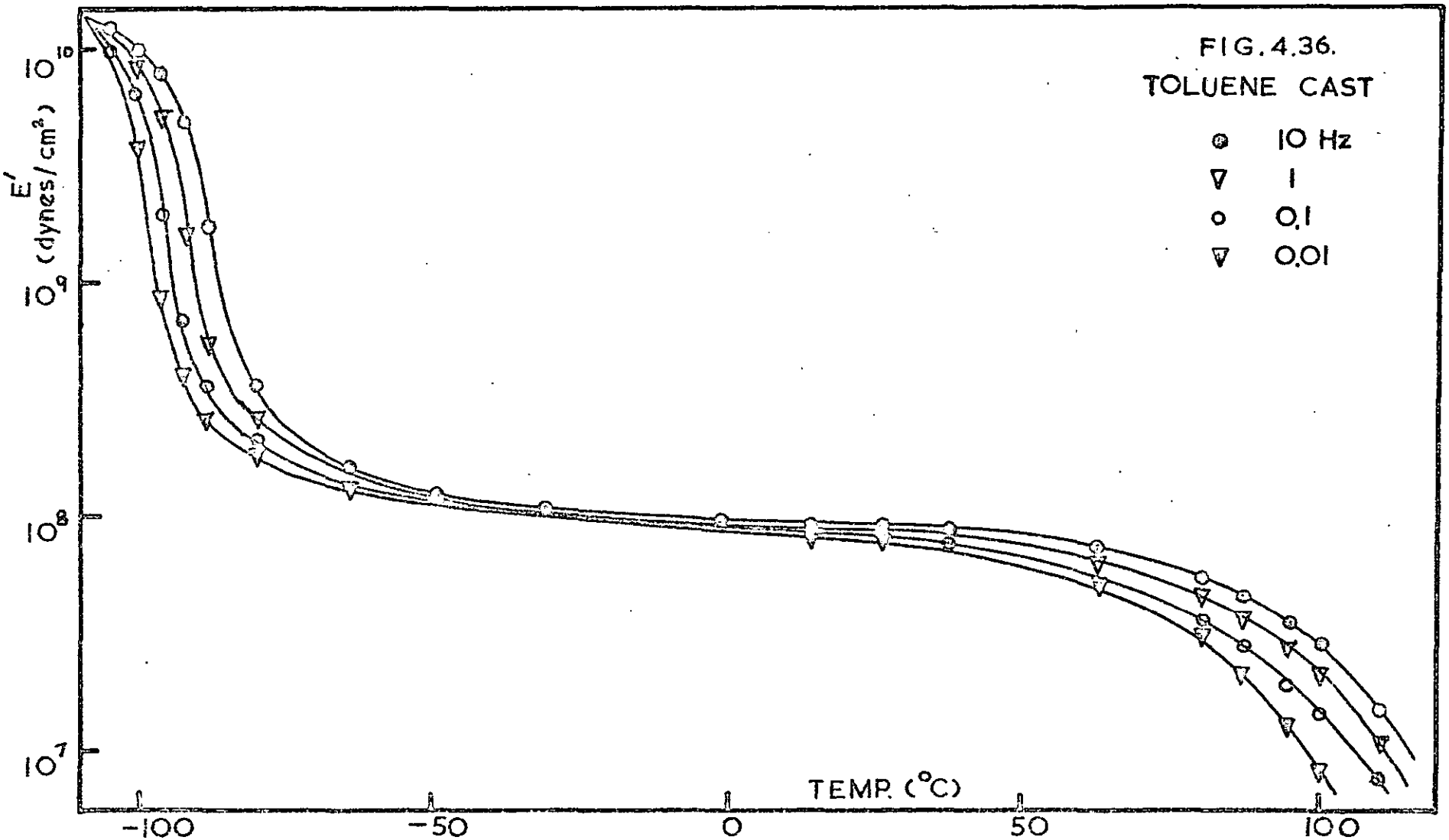
FIG. 4.36.
TOLUENE CAST
10 Hz
1
0.1
0.01
E' (dynes/cm²)
10¹⁰
10⁹
10⁸
10⁷
TEMP. (°C)
-100
-50
0
50
100

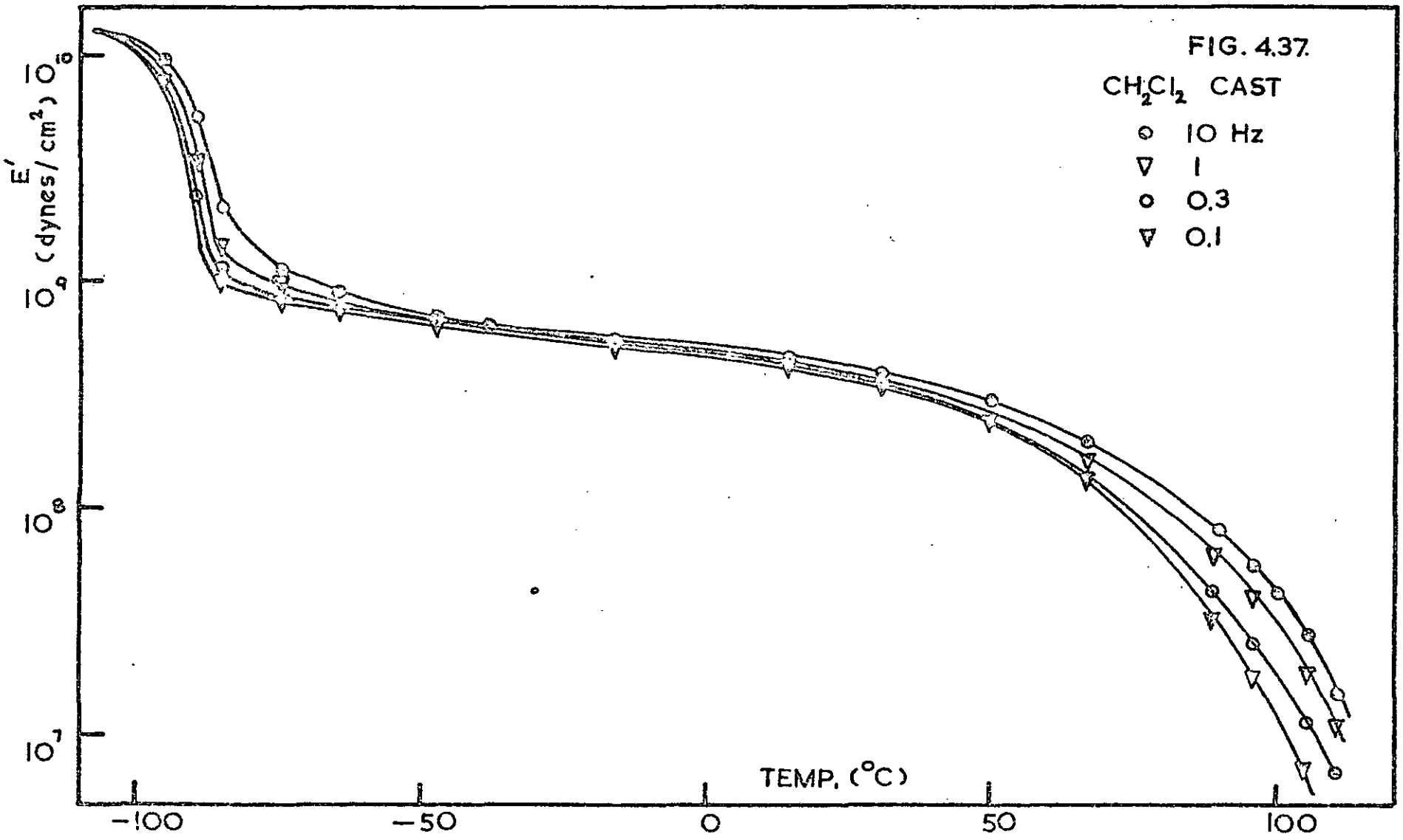
FIG. 4.37.
CH_2Cl_2 CAST
10 Hz
1
0.3
0.1
E' (dynes/cm²)
10^{10}
10^{9}
10^{8}
10^{7}
TEMP. (°C)
-100
-50
0
50
100

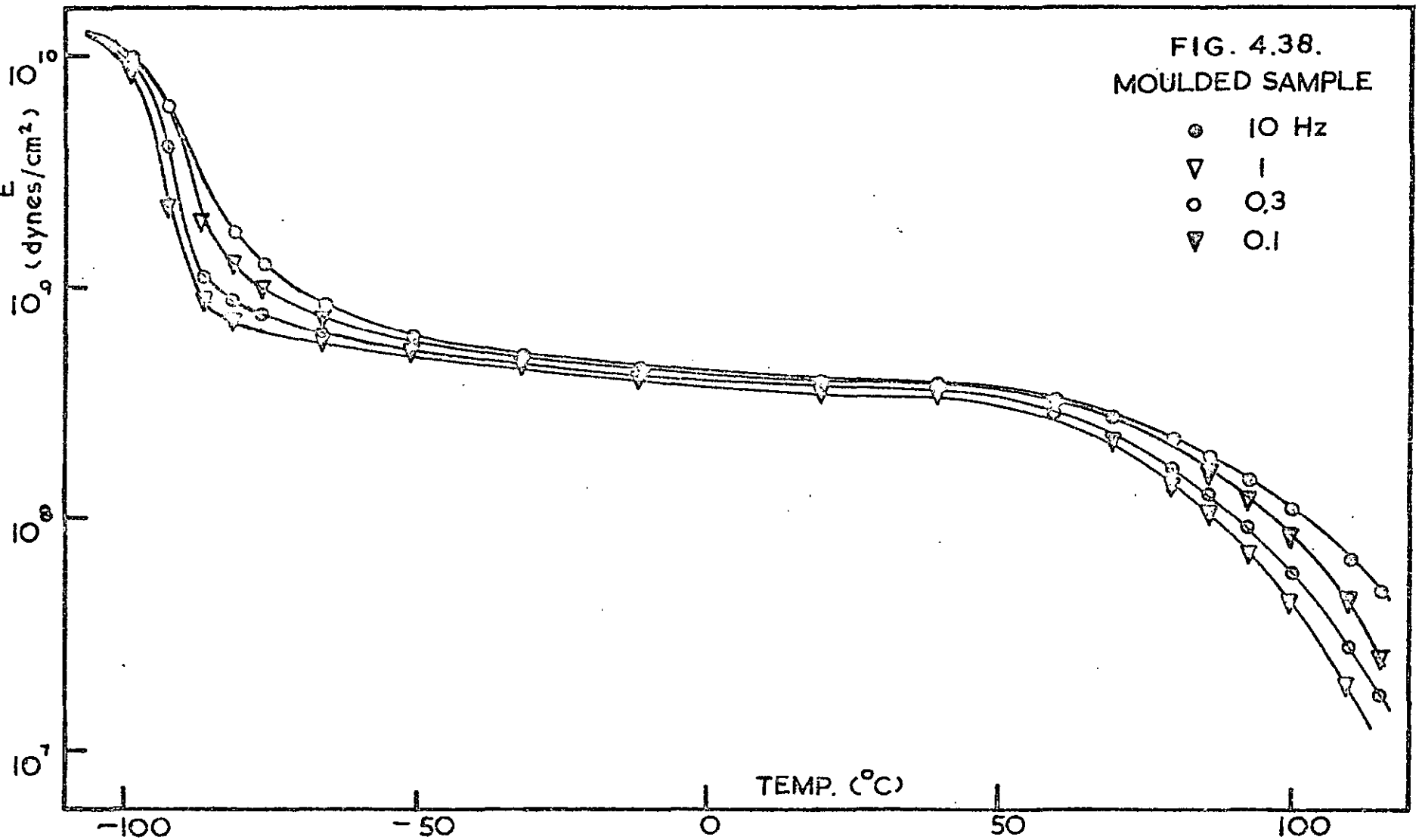
FIG. 4.38.
MOULDED SAMPLE
10 Hz
1
0.3
0.1
E' (dynes/cm²)
10¹⁰
10⁹
10⁸
10⁷
TEMP. (°C)
−100
−50
0
50
100

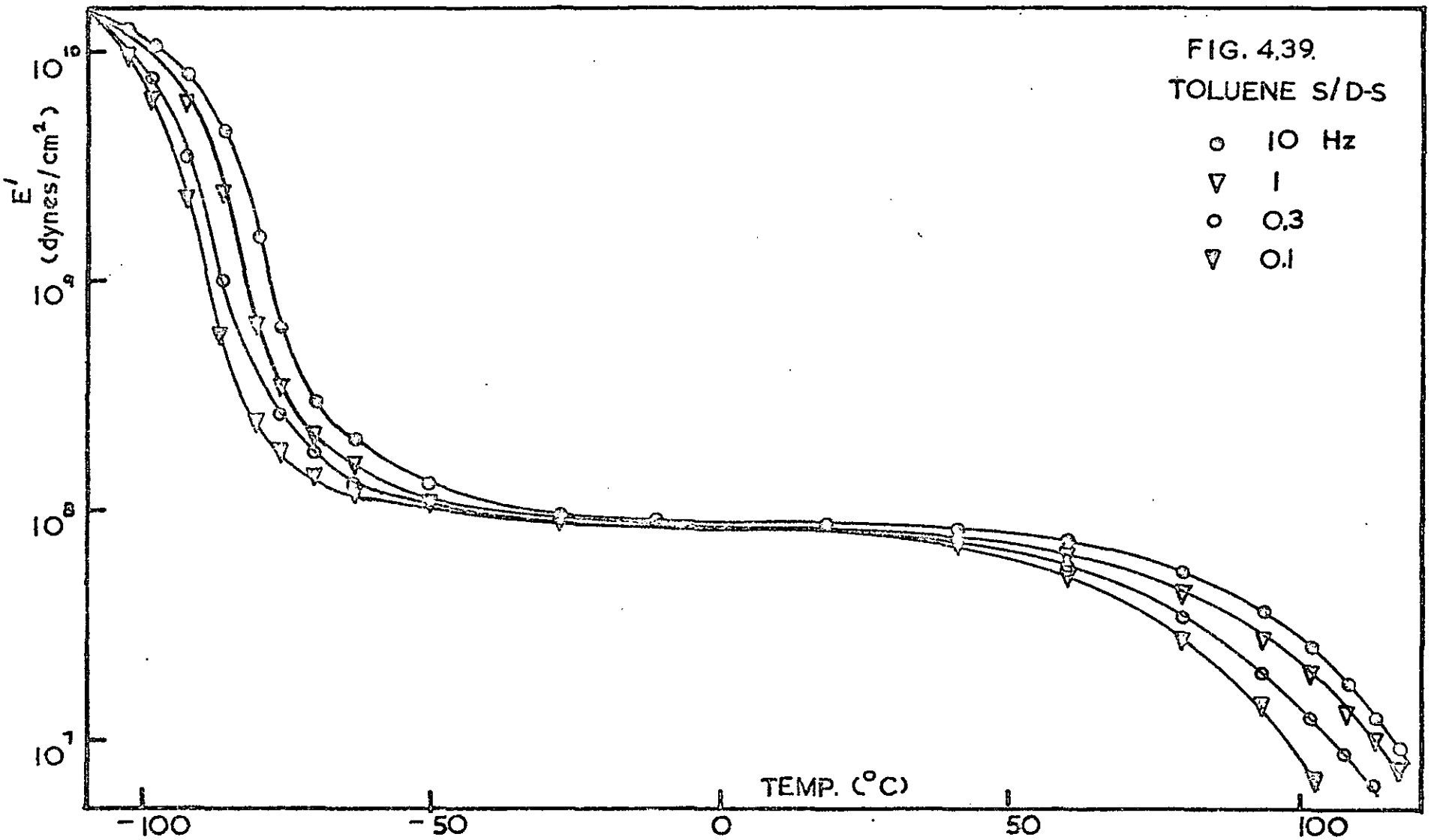
FIG. 4.39.
TOLUENE S/D-S
10 Hz
1
0.3
0.1
E' (dynes/cm²)
10¹⁰
10⁹
10⁸
10⁷
TEMP. (°C)
-100
-50
0
50
100

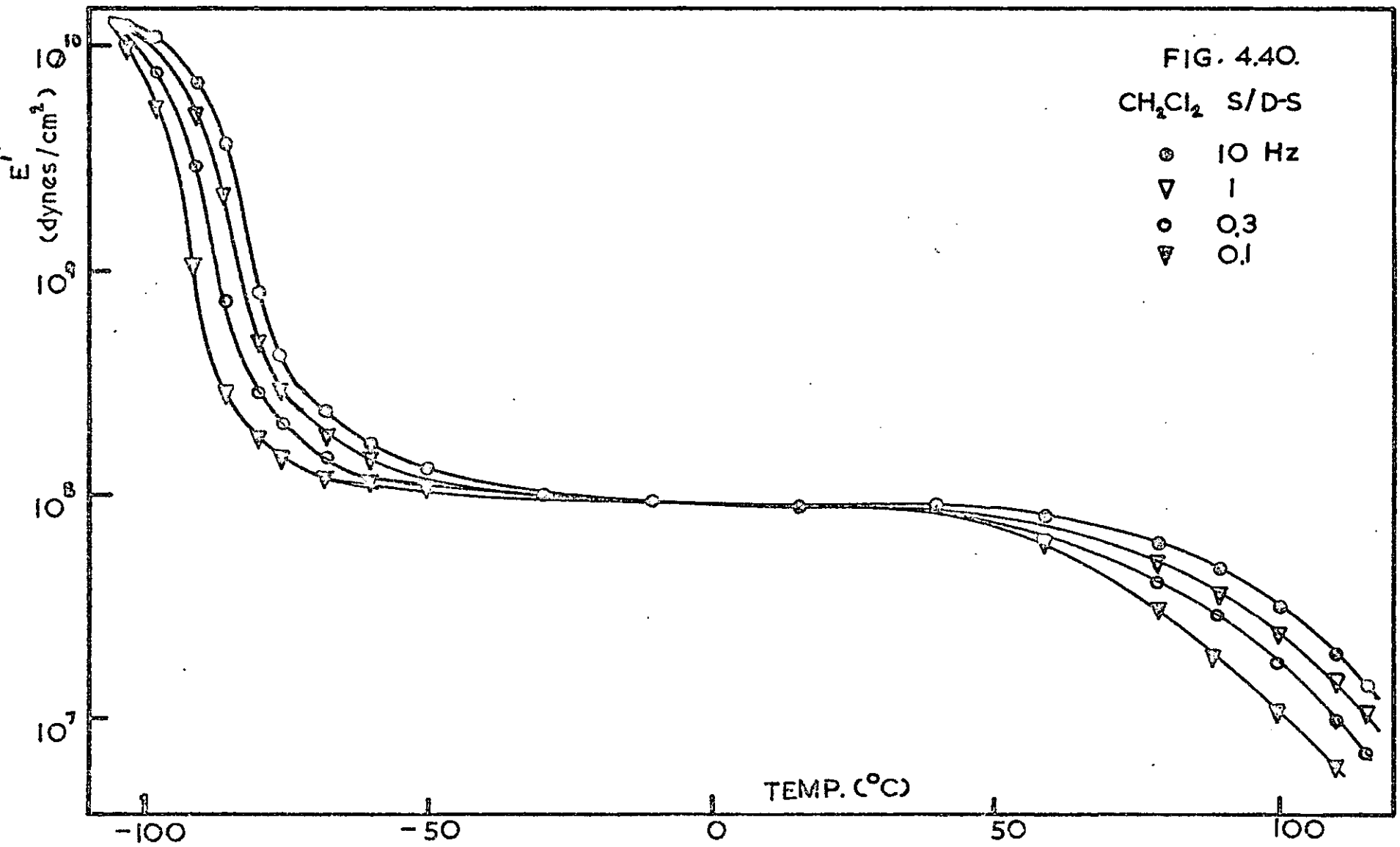
FIG. 4.40.
CH_2Cl_2 S/D-S
10 Hz
1
0.3
0.1
E' (dynes/cm²)
10^{10}
10^{9}
10^{8}
10^{7}
TEMP. (°C)
-100
-50
0
50
100

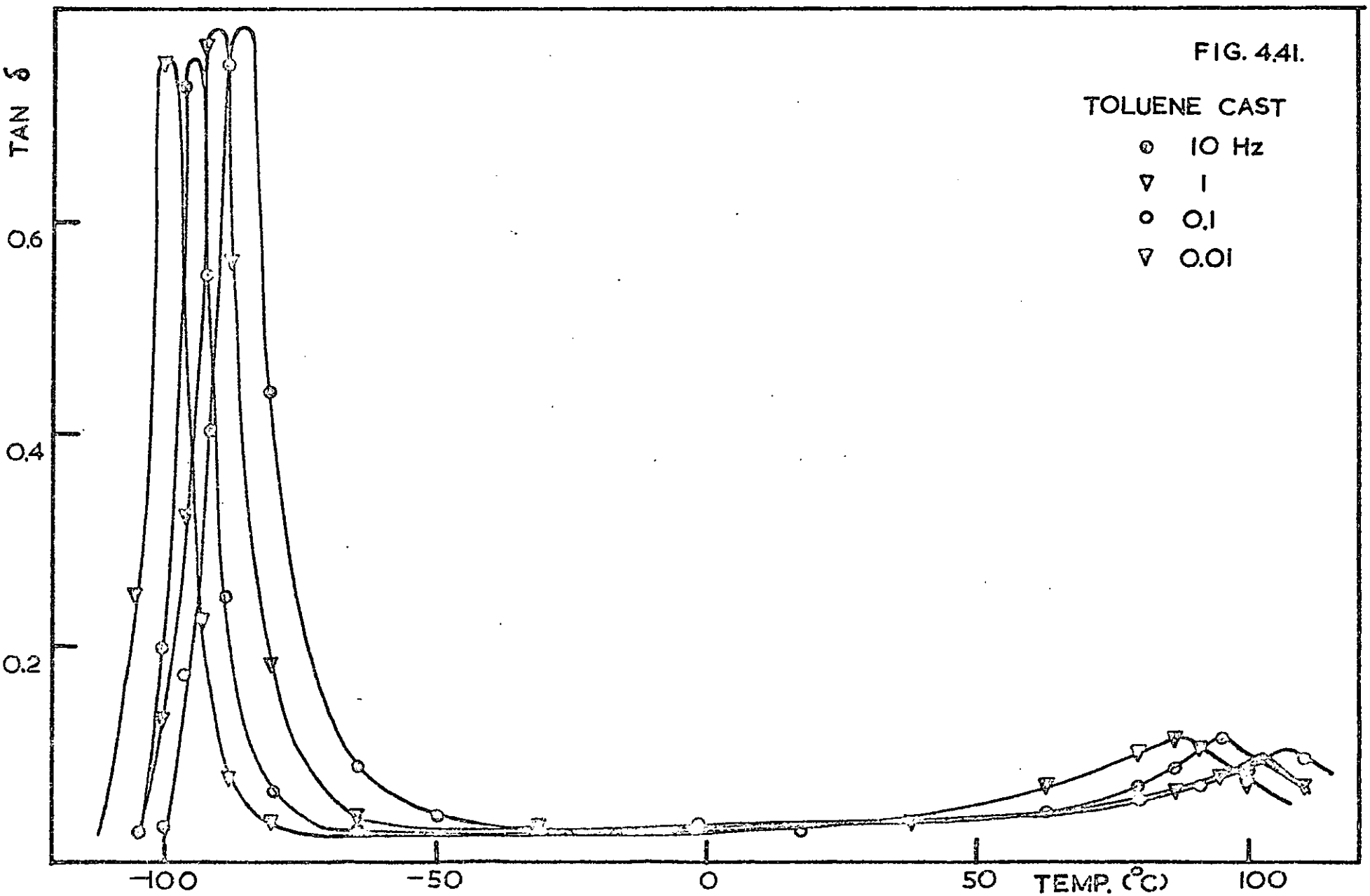
FIG. 4.41.
TOLUENE CAST
10 Hz
1
0.1
0.01
TAN δ
0.6
0.4
0.2
−100
−50
0
50
TEMP. (°C)
100

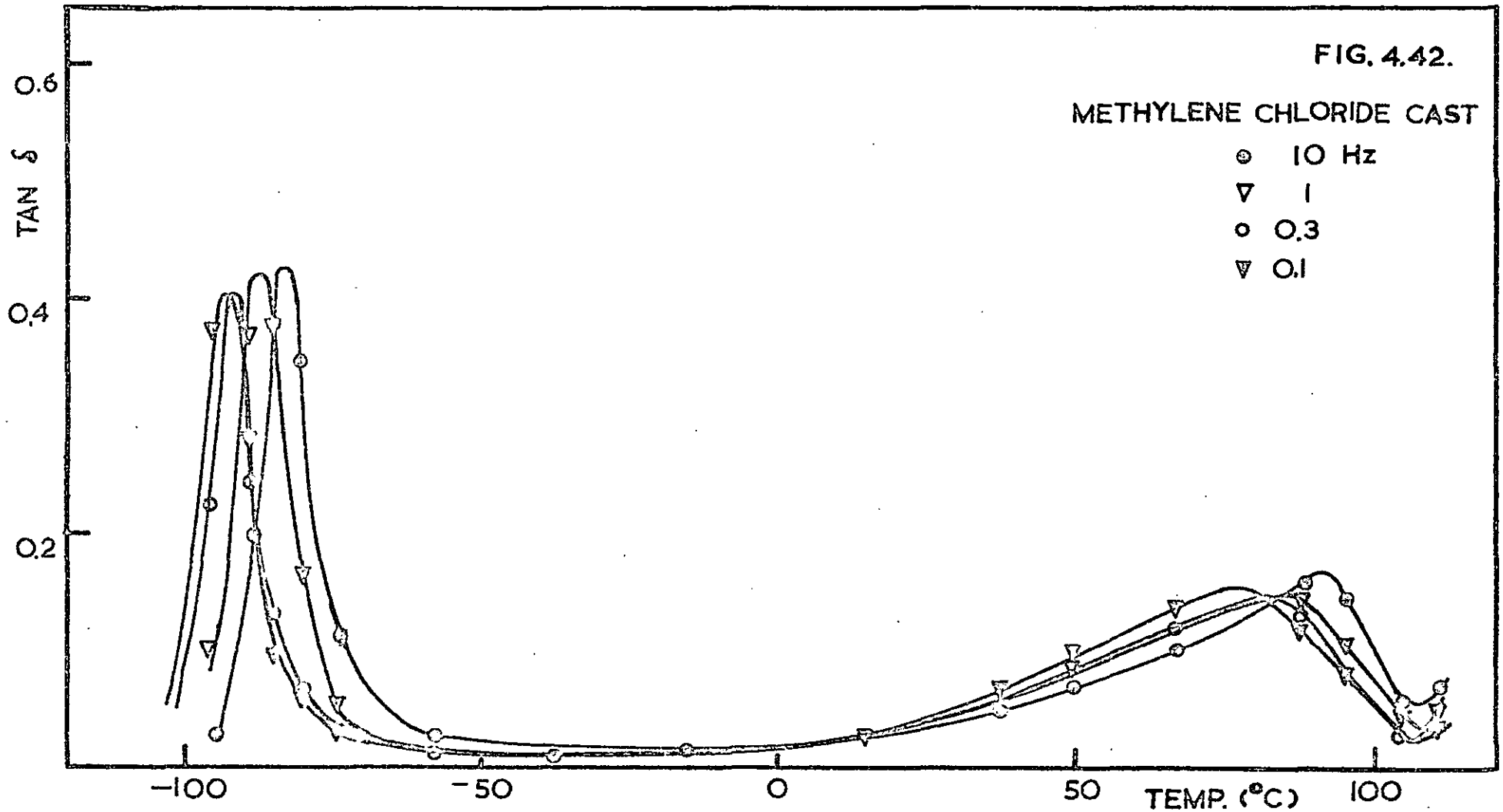
FIG. 4.42.
METHYLENE CHLORIDE CAST
10 Hz
1
0.3
0.1
TAN δ
0.6
0.4
0.2
−100
−50
0
50
100
TEMP. (°C)

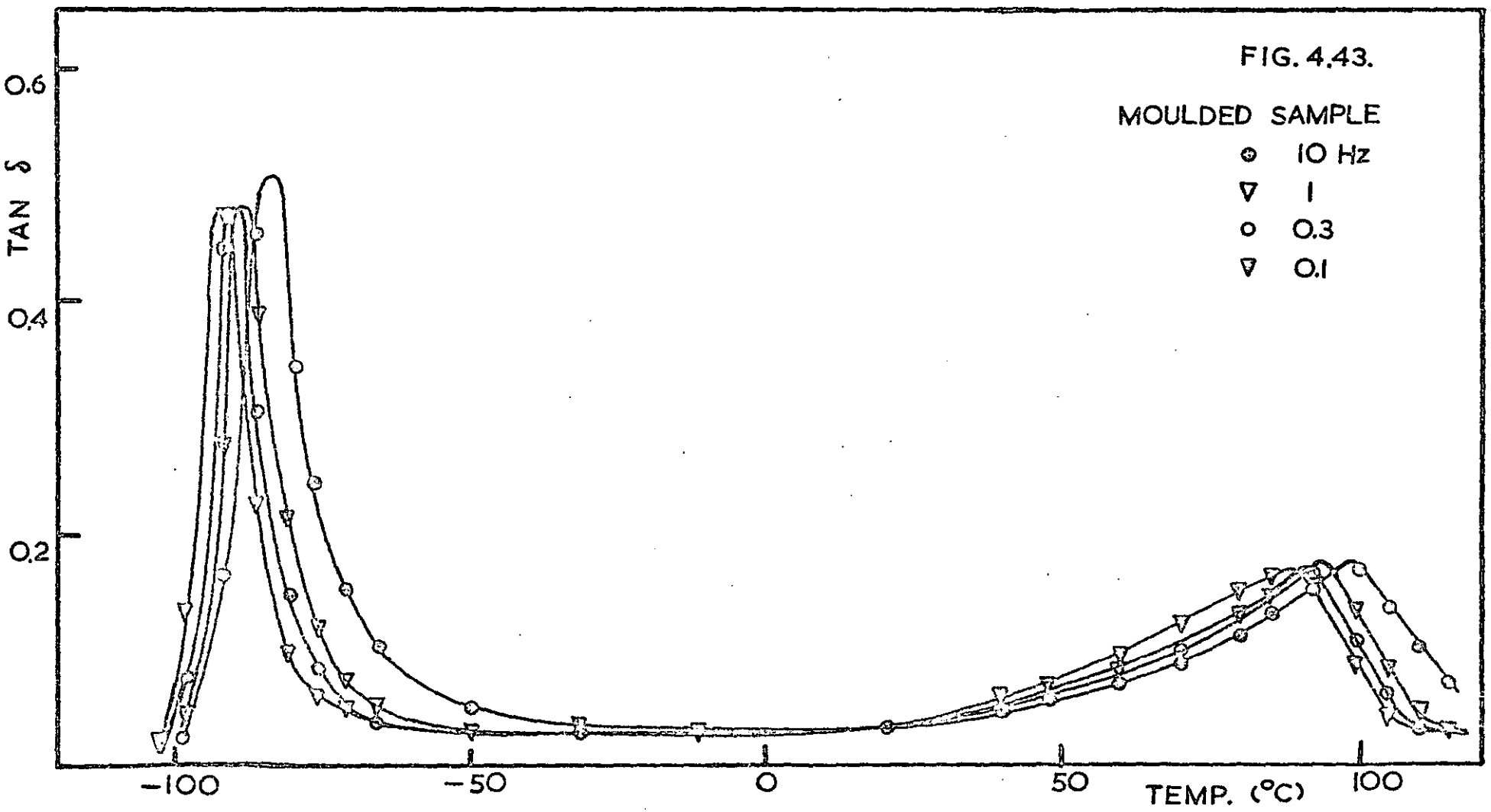
FIG. 4.43.
MOULDED SAMPLE
10 Hz
1
0.3
0.1
TAN δ
0.6
0.4
0.2
−100
−50
0
50
100
TEMP. (°C)

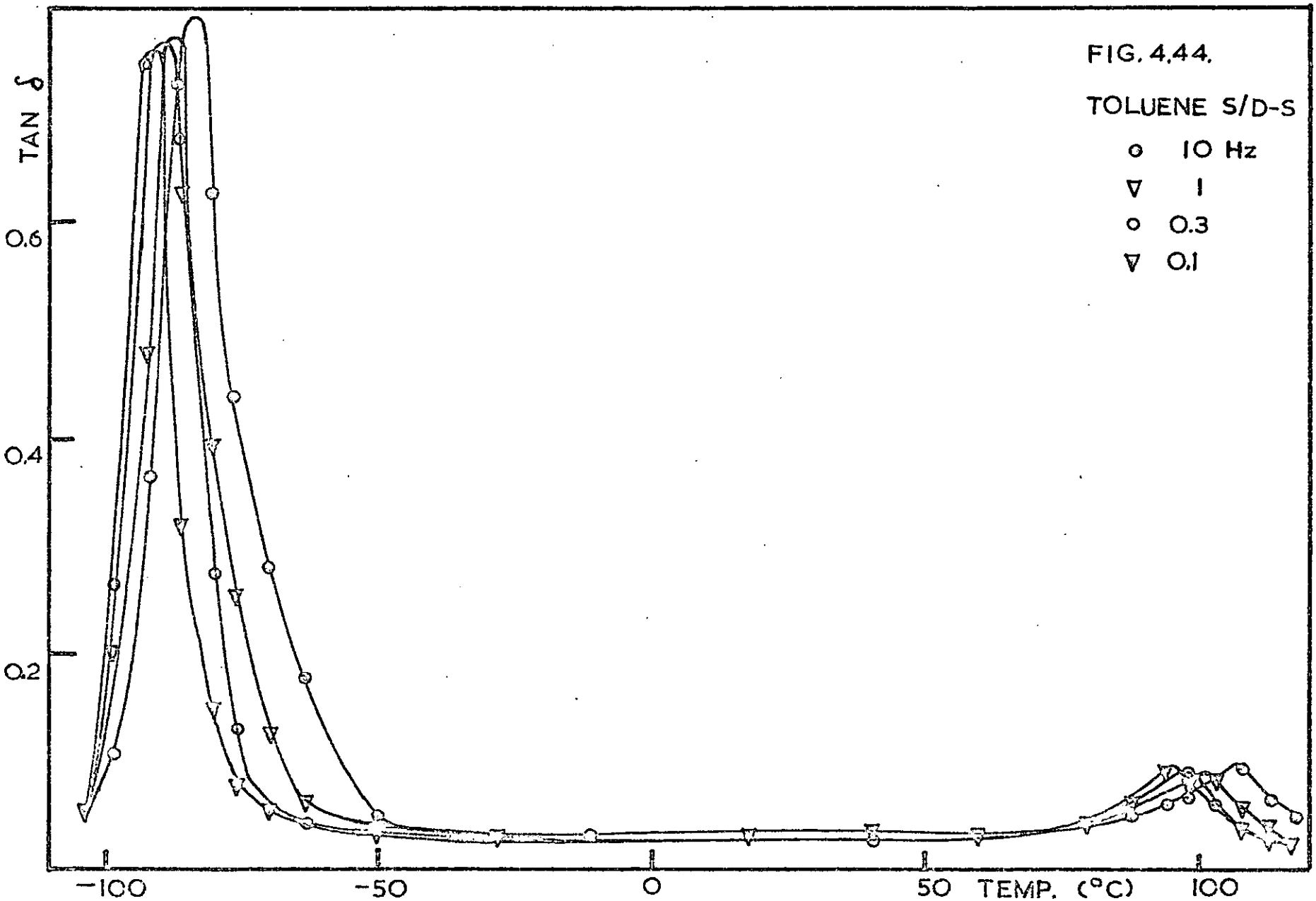
FIG. 4.44.
TOLUENE S/D-S
o 10 Hz
∇ 1
o 0.3
∇ 0.1
TAN δ
0.6
0.4
0.2
−100
−50
0
50
TEMP. (°C)
100

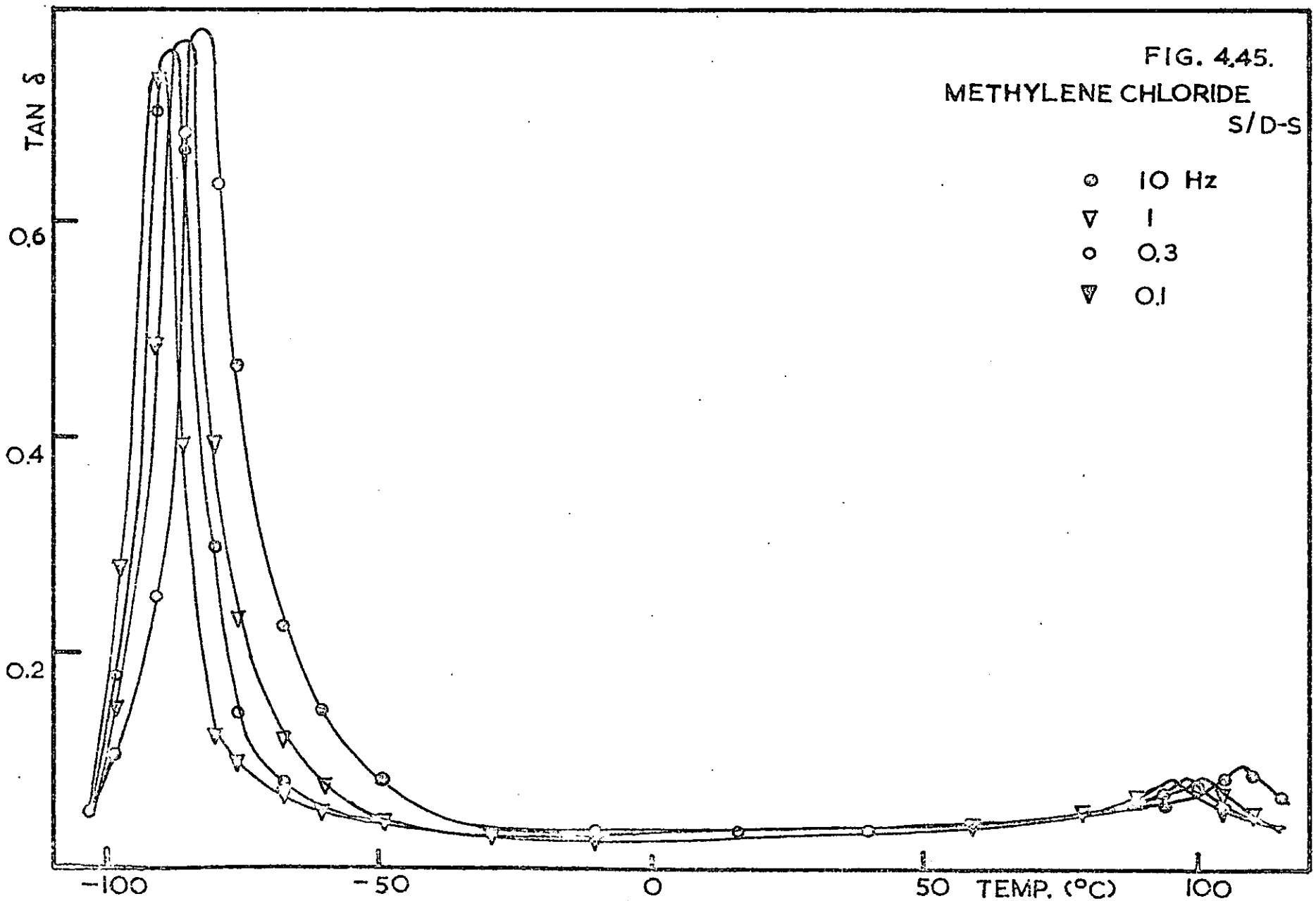
FIG. 4.45.
METHYLENE CHLORIDE
S/D-S
10 Hz
1
0.3
0.1
TAN δ
0.6
0.4
0.2
-100
-50
0
50
TEMP. (°C)
100

4.6. VIBRATING REED MEASUREMENTS

The results of the vibrating reed measurements for the various blends of K101 and polystyrene and of polystyrene and polybutadiene are summarized by the plots of log E' and tan δ against temperatures. (Figures 4.46. to 4.50.)

Sample MI to MVI were obtained by mechanical blending, whereas Samples SI to SIV were obtained by solution blending. (See Section 3.10.). The composition of the blends by weight is given by Table 3.3. (Section 3.10.).

The volume % of polystyrene in K101 is 25%. The densities of polystyrene and polybutadiene are 1.04 and 0.90 gm/c.c. respectively. Using the above data, the volume % composition of the blends in terms of the total polystyrene and polybutadiene contents are given in Table 4.8.

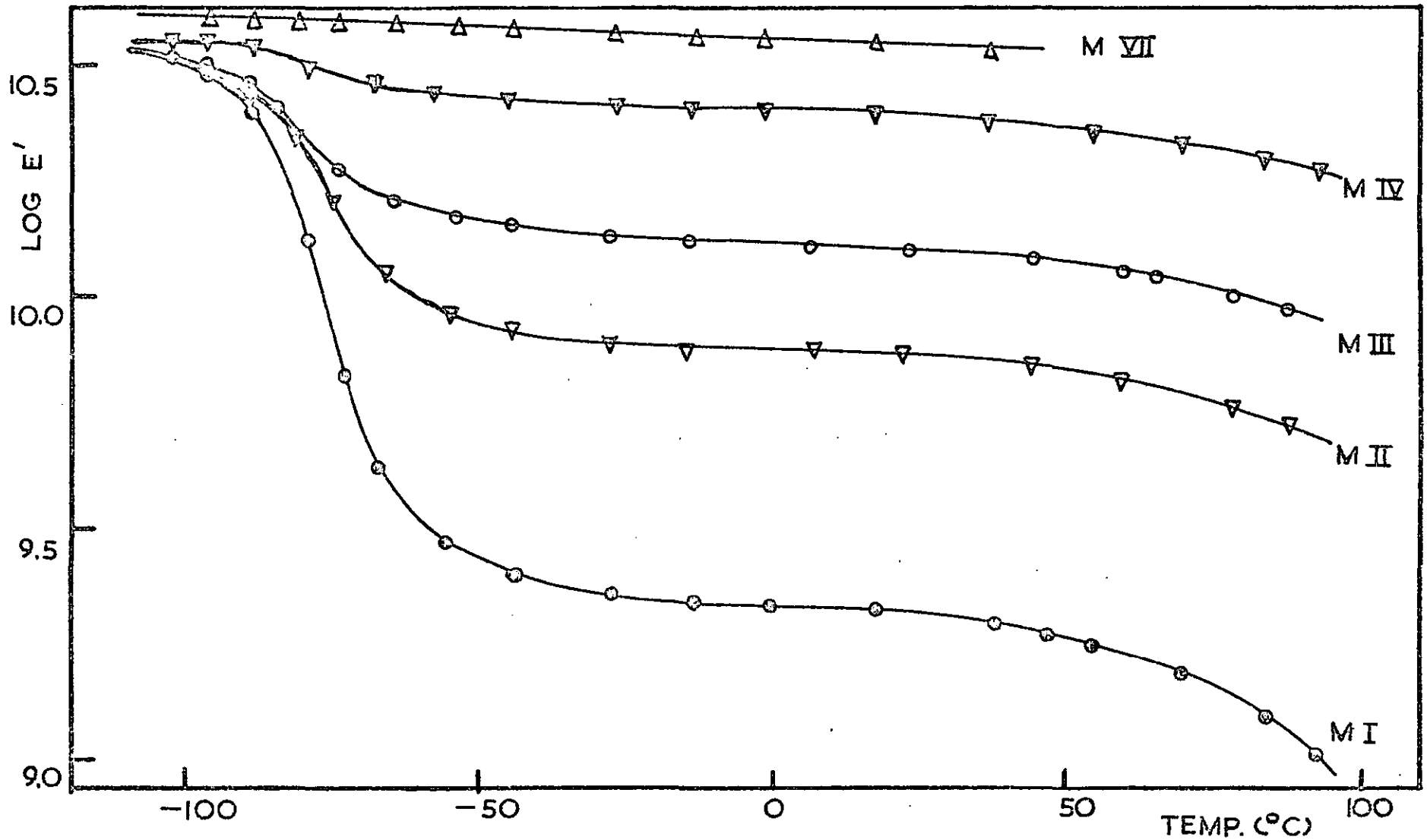

FIG. 4.46.

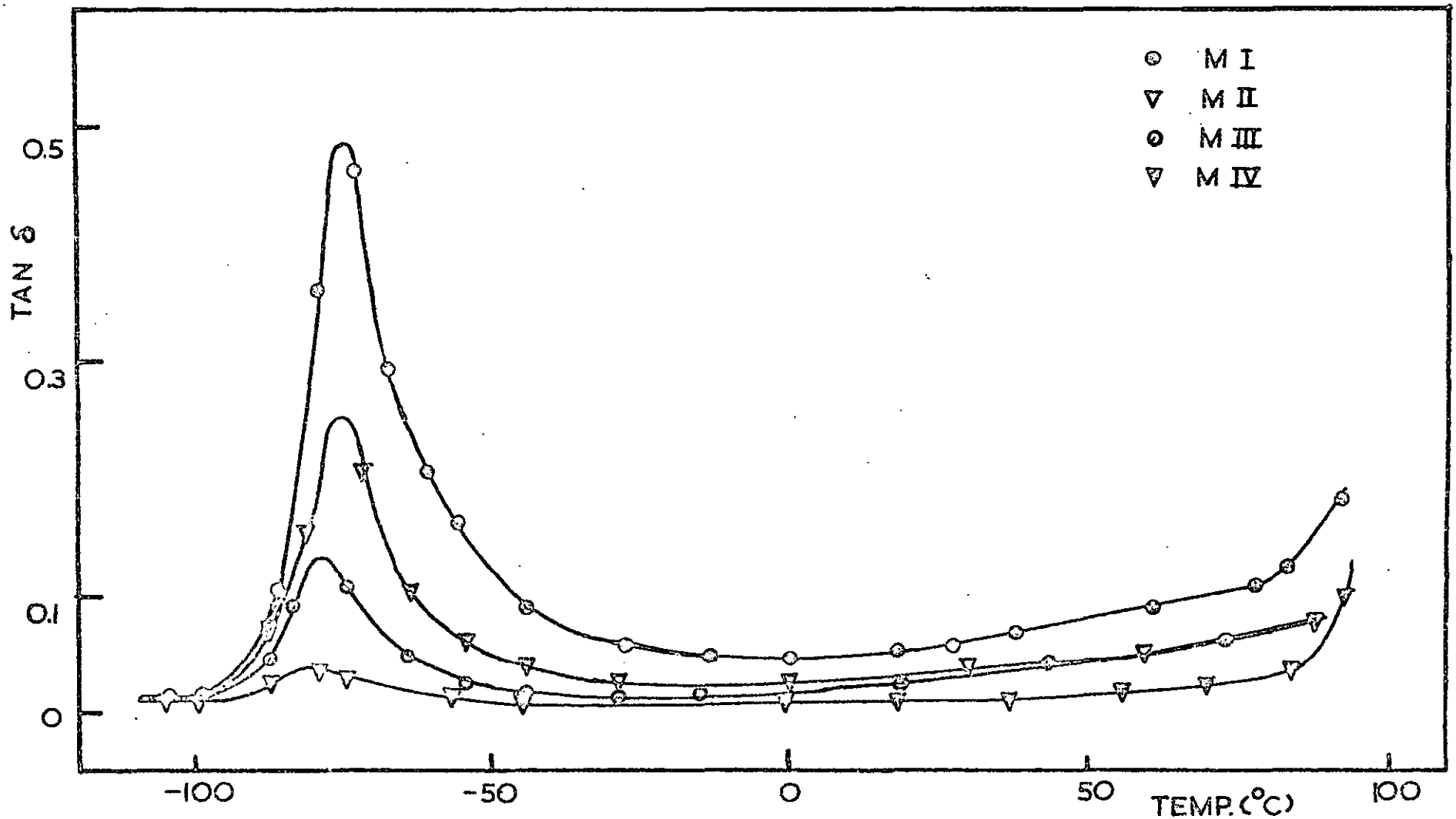

FIG. 4.47.

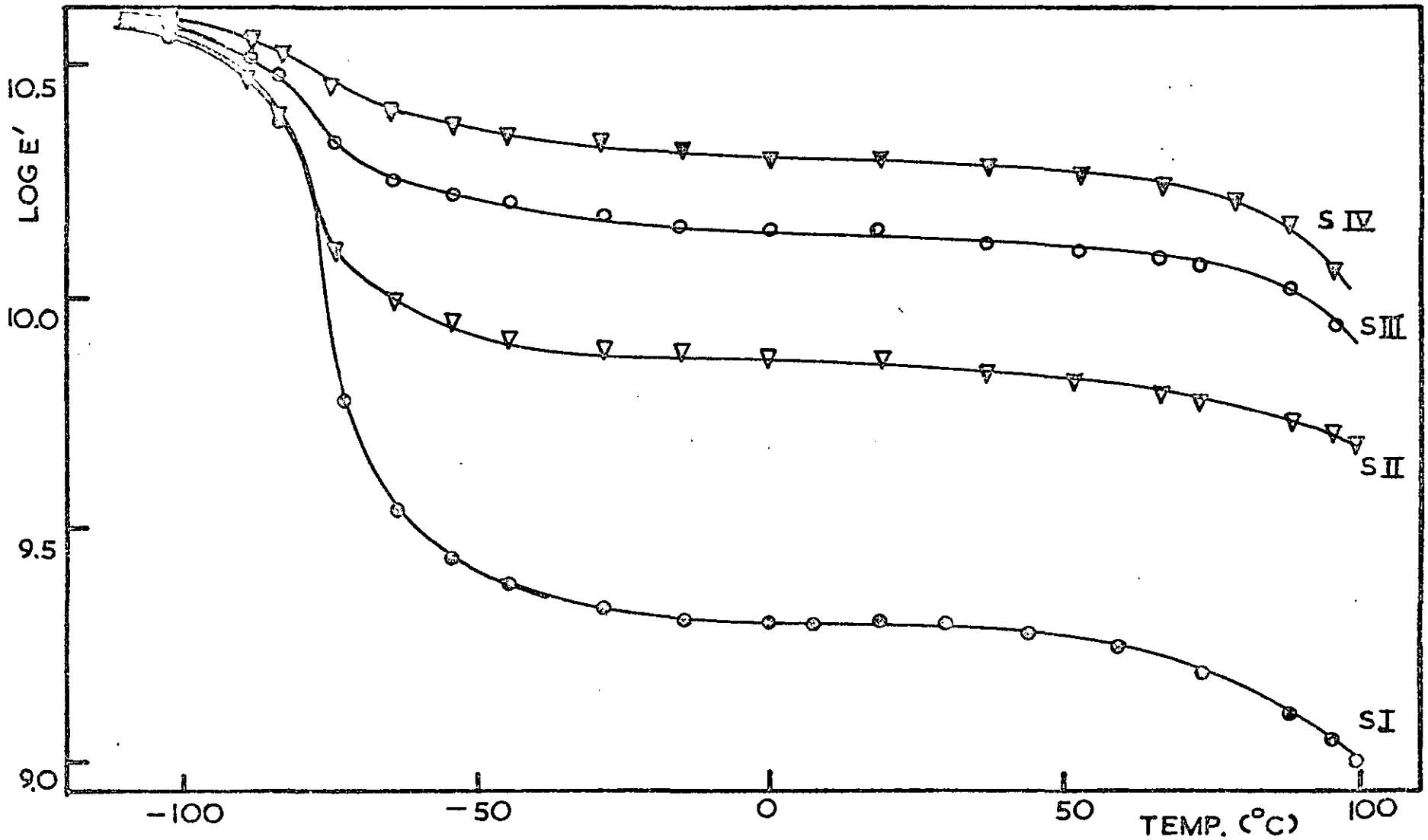

FIG. 4.48.

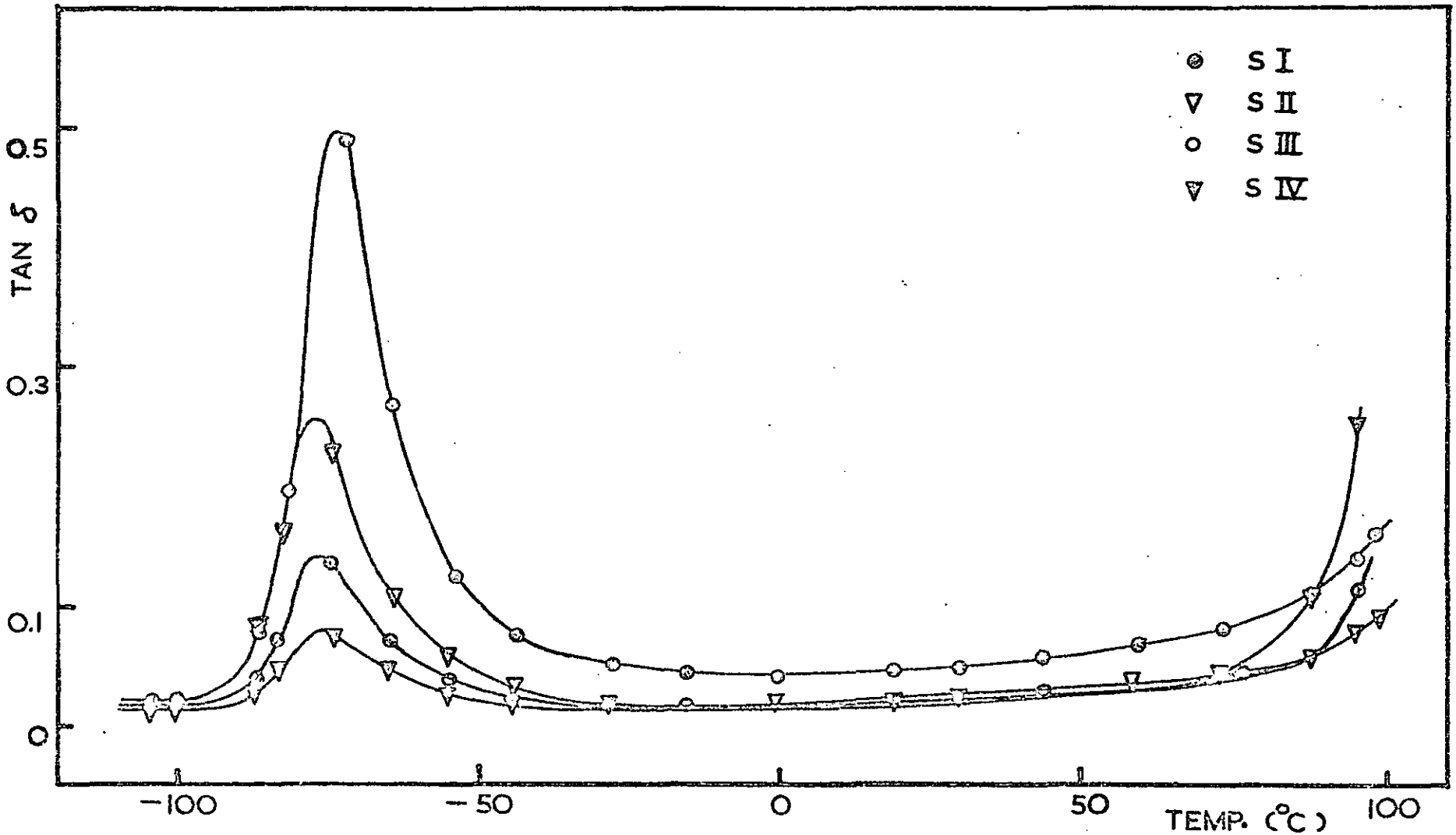

FIG. 4.49.

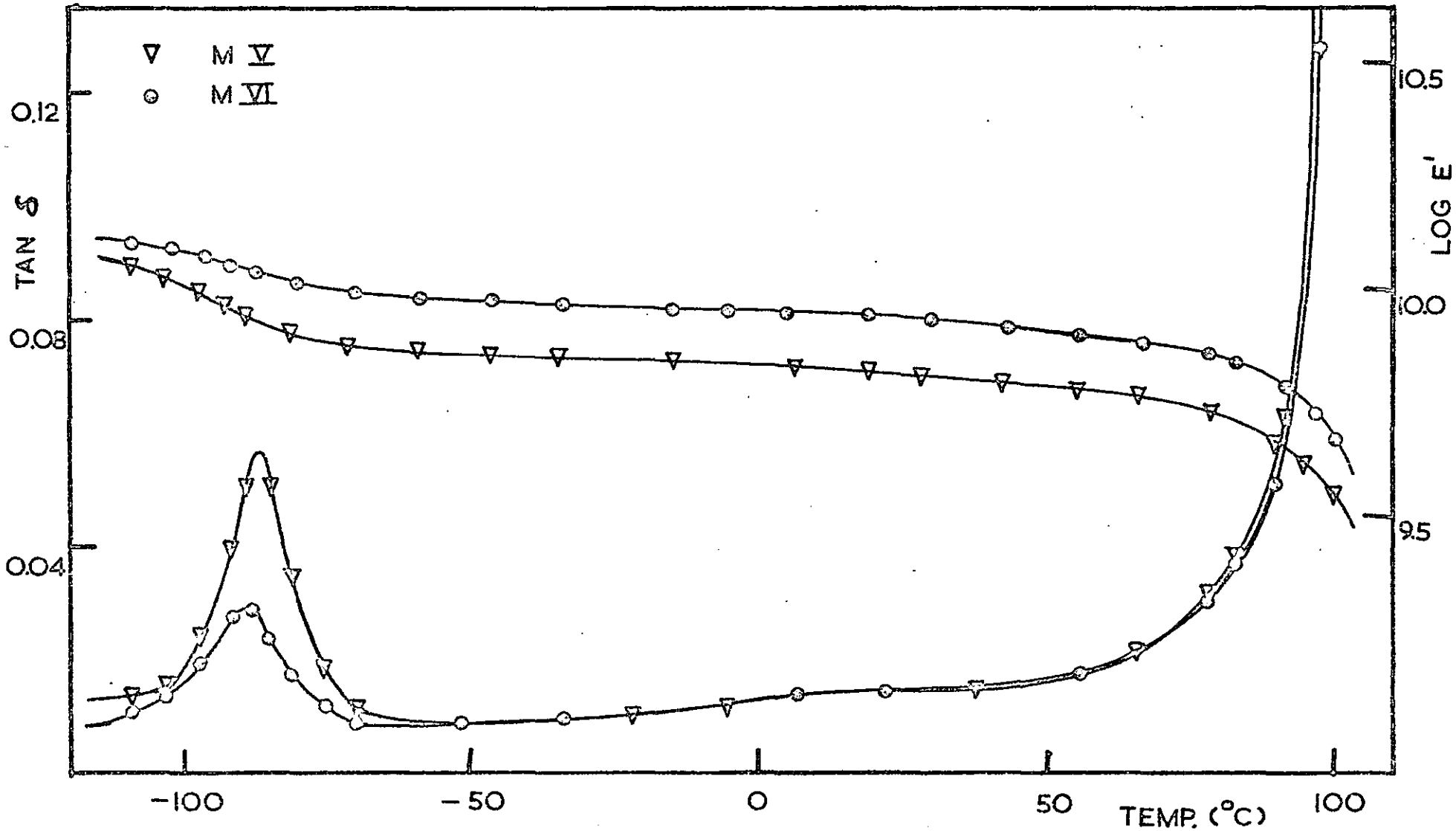

FIG. 4.50.

TABLE 4.8.

Composition of the blends by volume

Sample	Volume %	
	Polybutadiene	Polystyrene
MI	47.2	52.8
MII	32.2	67.2
MIII	21.8	79.2
MIV	13.9	86.1
MV	23.5	76.5
MVI	13.8	86.2
MVII	0	100
SI	47.2	52.8
SII	32.2	67.2
SIII	21.8	79.2
SIV	13.9	86.1

4.7. SYNTHESES OF HOMOPOLYMERS AND COPOLYMERS

The results of the synthese carried out as described in Section 3.11. are given in Tables 4.9. and 4.10.

TABLE 4.9.

Bulk polymerization of THF and BCMO using p-chlorophenyl diazonium hexafluorophosphate as initiator

(Conditions, 25°C for 20 hours)

No.	Monomers (moles)		Initiator Concentration	Conversion (%)
	BCMO	THF		
I	-	0.122	1.83×10^{-3} M	76.4
II	-	0.136	7.35×10^{-3} M	80.2
III	-	0.122	16.21×10^{-3} M	71.0
IV	0.067	-	6.76×10^{-3} M	80.8
V	0.042	-	11.70×10^{-3} M	95.0
VI	0.025	0.086	5.63×10^{-3} M	60.3
VII	0.042	0.061	5.52×10^{-3} M	83.0
VIII	0.054	0.043	5.69×10^{-3} M	87.3

The homopolymerization of THF (I - III) were carried at three different initiator concentrations. The polymerization solution turned pink in colour, after the ampoule containing the monomer and initiator had been heated for 30 minutes at 50°c, and left for about 2 hours at 25°c. Tough, yellowish-brown, crystalline polymers were obtained. The yield is approximately 70 - 80% at the different initiator concentrations.

In the homopolymerization of BCMO (IV and V), the polymer came out of solution as white precipitates, as it was formed. The polymer obtained was white and crystalline. The ampoule (IV) was heated to about 100°c, the product inside remained solid.

The copolymerization of BCMO and THF (VI and VIII) were carried out at three monomer compositions and at approximately the same monomer compositions. The conversion percentage was based on the combined amount of the two monomers. The products from the monomer mixtures containing 40 mole-% and 22 mole-% of BCMO in the monomer are waxy. At about 55 mole-% of BCMO in the monomer mixture, a soft, light brown, rubbery product was obtained. All polymers obtained are completely insoluable in methanol, but are completely soluable in chloroform. Polymer (VIII) is also soluable in o-dichlorobenzene.

TABLE 4.10.

Solution polymerization of BCMO using p-chlorophenyldiazonium hexafluorophosphate as initiator and o-dichlorobenzene as solvent. (Conditions, 60°C for 5 hours; Solvent 60mℓ.)

No	BCMO (moles)	Initiator (moles)	Conversion (%)	$\overline{M}_n$ (Calcd.)	$\overline{M}_v$ (exptal.)
IX	0.050	7.04×10^{-5}	42.0	46,500	98,500
X	0.050	8.80×10^{-5}	51.6	-	-

The initiator did not dissolved completely. The colourless solution turned pink, after 2 hours and the polymer preciptated out of solution. The product, after washing with methanol and vacuum dried, was white and powdery.

The intrinsic viscosity $[\eta]$ of poly(BCMO) (IX) was measured in cyclohexanone at 70°c in the suspended level dilution Ubbelohde viscometer.

$[\eta] = 0.576$, as shown in Figure 4.51. $\overline{M}_r$ (exptal) was calculated according to the equation $\overline{DP}_r = 1230\ [\eta]^{1.195}$, given by Penczek and Kubisa (170) for poly(BCMO) in cyclohexanone at 40°c.

$$\text{Whereas, } \overline{M}_n \text{ (calcd.)} = [\text{BCMO}] \times \frac{\text{conv.(\%)}}{100} \times \frac{155}{[I]}$$

The BCMO/THF copolymer (VIII) was moulded at 35°c for 4 minutes into a rectangular beam of thickness 0.23 cm, width 0.96cm., and length 6.4cm. The density of the sample was determined to be 1.15 gm/c.c. The vibrating reed measurement from room temperature down to -150°c is shown in Figure 4.52. Data from room temperature to about -40°c could not be obtained due to limitation of the apparatus.

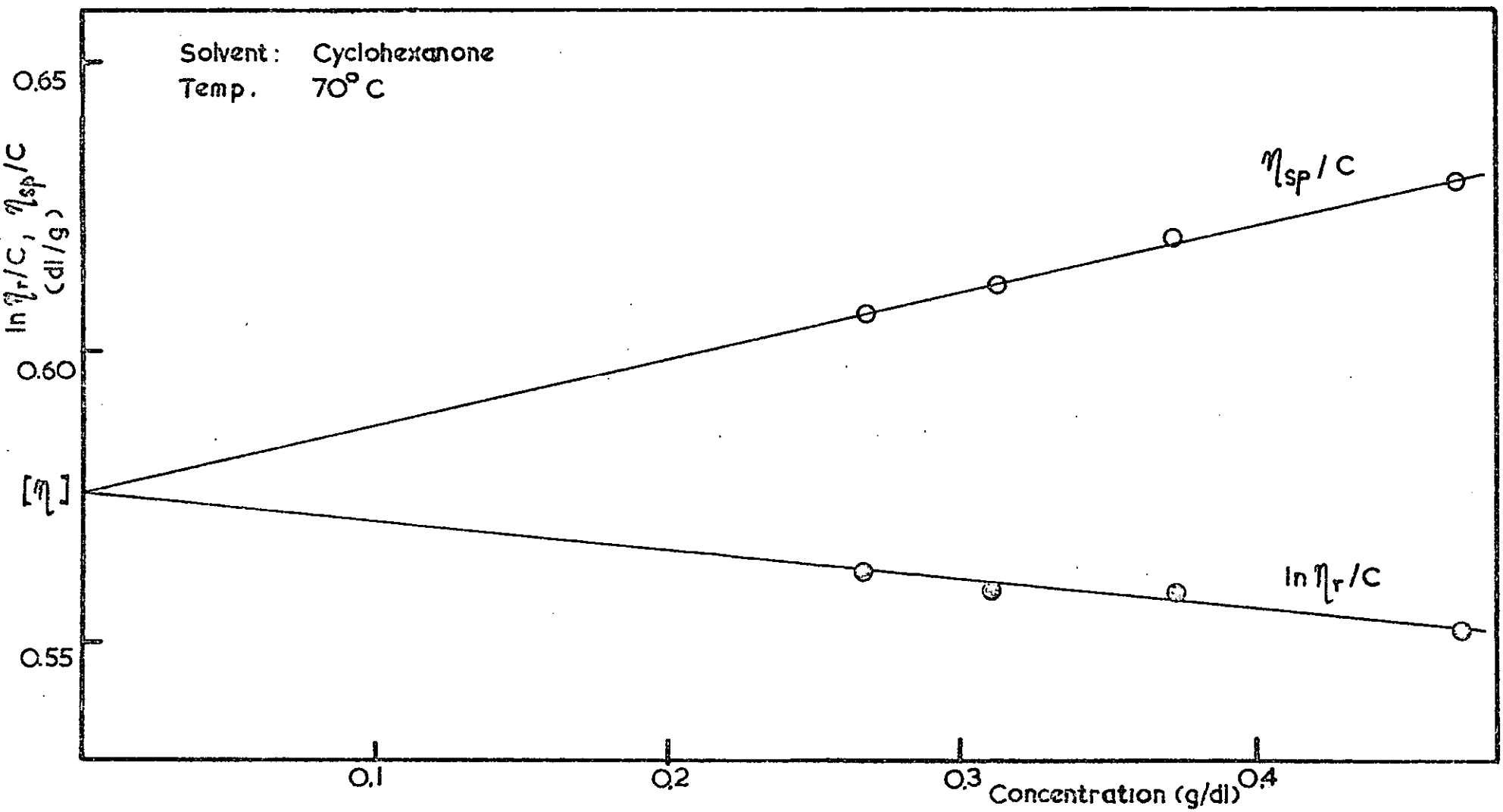

FIG. 4.51. INTRINSIC VISCOSITIES OF POLY (BCMO) (SAMPLE IX)

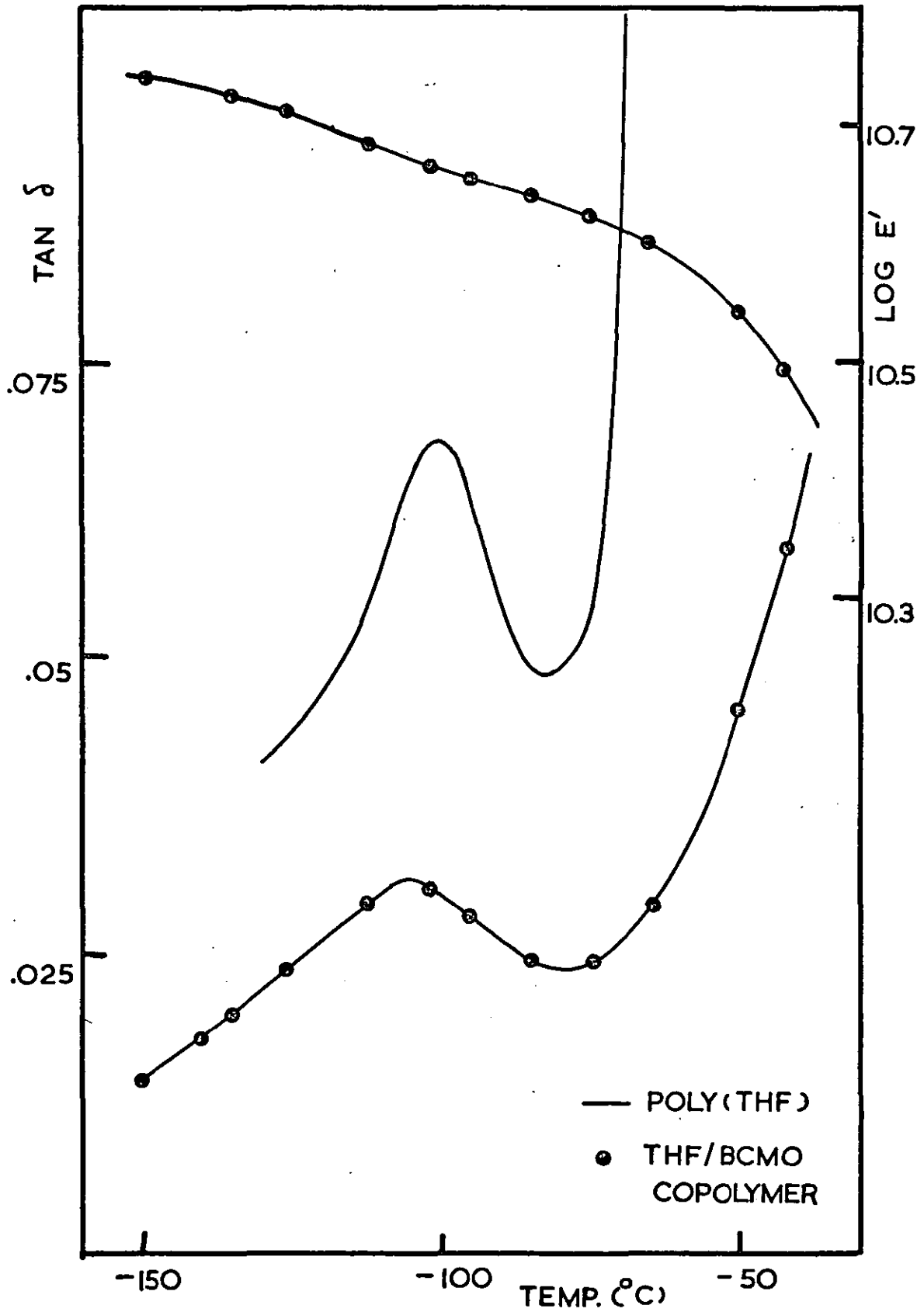
TAN δ
.075
.05
.025
LOG E'
10.7
10.5
10.3
POLY(THF)
THF/BCMO COPOLYMER
-150
-100
-50
TEMP. (°C)

FIG. 4.52.

5.1 MORPHOLOGY OF SBS BLOCK COPOLYMER

The details of the polymer studied, Shell Cariflex K101, and the specimen treatments have been given in Section 3.1. In this section the results of the small angle X-ray scattering studies will be discussed in terms of an adopted model for the polymer system. This adopted model should allow correlation of the phase structure observed with the dynamic mechanical spectra obtained and should also give some insight into the complex large strain properties of these systems.

Figure 4.2a shows the SAXS pattern obtained using pinhole optics and CuK_{α} radiation with the toluene cast specimen. The whole region of diffraction lies within one degree of the main beam, and the fact that a diffraction pattern is observed in this region indicates a periodicity in structure in the 100 Å range. The diffraction pattern is actually a set of rings rather than spots. A very intense first order diffraction, a weak second order, and a stronger third order are visible. This is reminiscent of Debye-Scherrer powder photographs with normal X-ray scattering techniques.

Fortunately, with toluene cast sample, the reflections could be indexed, as shown in Table 5.1.

There is good agreement between the observed d spacing ratio R and that required for a cubic lattice. Some reflections are absent or too weak to be observed. No other theoretical lattice spacings give any satisfactory agreement with the observed ratios. Thus, the adopted model for this system would be one of styrene domains lying on a cubic macro-lattice of 300 Å spacing. There must be different lattice regions in the specimen with random orientations in order to give a powder diagram analogue.

The diffraction pattern for the methylene chloride cast specimen is nearly as sharp as for the toluene cast specimen but, unfortunately, the reflections do not index to a simple Bravais lattice. However, the sharp diffraction pattern indicates an ordered arrangement of

the domains. The SAXS study, by itself, does not give enough data to postulate a model for this system.

TABLE 5.1 CUBIC MACRO-LATTICE PARAMETERS, K101 TOLUENE CAST

Miller indices	d(observed) (Å)	R(observed)	R(theoretical)
100	300		1·000
110	208	1·47	1·414
111			1·732
200			2·000
210	130	2·35	2·236
211			2·449

Figure 5.1 gives a diagrammatic representation of the order in the system. Based on optical analogues, the line broadening would be commensurate with random displacements from lattice positions of magnitude shown. The solid lines represent boundaries between the regions of cubic lattice with different orientations.

The diffraction patterns obtained using pinhole optics for stretched toluene cast specimens up to 400% extension, show intensification on basically elliptical diffraction patterns which intensified into spots at certain regions. (Figure 4.2b). The fact that the diffraction patterns obtained from stretched samples show intense spots rather than lines is evidence in favour of an ordered arrangement of spheres rather than rod or sheet morphology. Precise experimental observation of this fact is not easy with the pinhole system because of the large back-stop size and higher resolution slit optics in conjunction with Geiger counting was employed to determine the exact location and shape of the intensified spots. At each extension of the specimen, the scans at

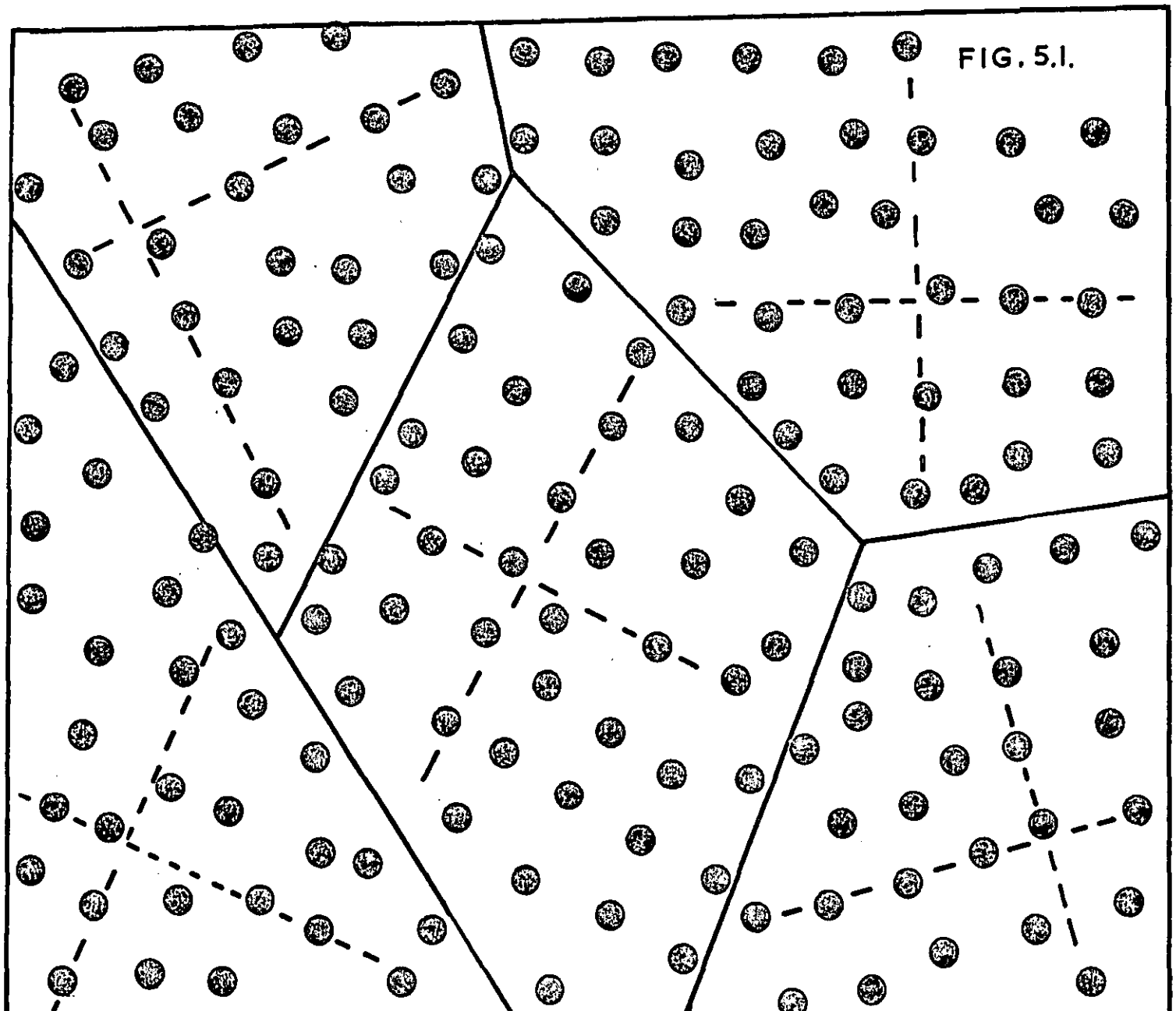

FIG. 5.1.

both 0° and 90° to the stretching direction were observed, as shown typically in Figure 5.2a. The details of the scattering patterns are summarised in Table 5.2. At 0% extension, both 0° and 90° - scans give indentical patterns of 300 Å for the nearest neighbour spacing and 32 Å for the half-width. (An increase in the half-width indicates an increase in the distribution of the interdomain distance.) The half-width of the scattering patterns increase with extensions and similar values are obtained at each extension for both 0° and 90°-scans. This behaviour would be obtained only with a circular intensification, assuming that the peaks in the scans correspond to the intense spots observed in the pin-hole method. A 45° inclination elliptical intensification could give similar half-width in both scans at one extension, but would differ at other extensions.

TABLE 5.2 EFFECT OF EXTENSION ON SAXS PATTERN IN TOLUENE CAST SAMPLE

Extension	Scan at 0°		Scan at 90°	
	N.N.S.*	Half-width	N.N.S.	Half-width
0%	300 Å	32 Å	300 Å	32 Å
15%	310	38	364	50
30%	384	122	530	118
100%	412	133	581	124
250%	416	140	658	156
400%	388	137	-	-

* Nearest neighbour spacing.

From the results given in Table 5.2, at high extensions, the circular intensifications are found to occur at the intersections

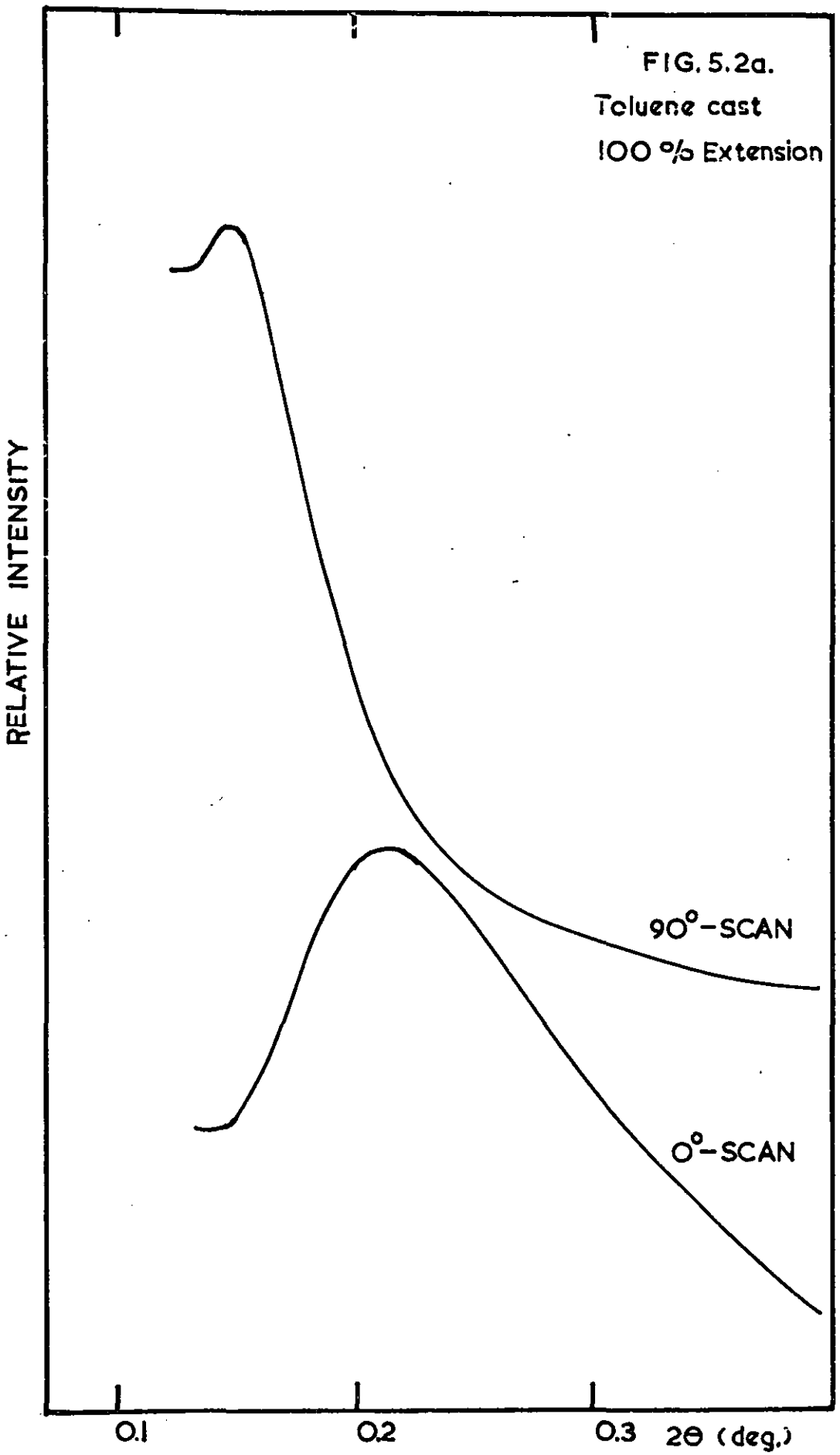
FIG. 5.2a.
Toluene cast
100 % Extension
RELATIVE INTENSITY
90°-SCAN
0°-SCAN
0.1
0.2
0.3
2θ (deg.)

of the diffraction ellipse and the unstrained diffraction circle. However, the results obtained for low extensions is less meaningful, since the ratio of the intensity of the spots caused by orientation to the general intensity of the diffraction ellipse is relatively low. In these cases, the peaks observed for slit optics will not correspond to the exact angular position of the spots, and the width of the peaks will be distorted by contributions from the rest of the diffraction ellipse.

In the unextended state, the cubic lattice regions are randomly orientated. The presence of intense spots in the reciprocal lattices on stretching indicates that the stretching produced preferred orientation of the real lattices, resulting from shear forces acting in the lattices. On stretching, the lattices are orientated initially, such that the unit cell diagonals are parallel to the stretching direction. At low extensions, the unit cell axes will be approximately 45° to the stretching direction, but further extensions will greatly reduce this angle (Figure 5.2).

The elliptical pattern, ignoring the intensification effect is commensurate with affine deformation of randomly oriented cubic lattices. The intersphere spacing will elongate along the stretching direction and will contract perpendicular to it. For a cube originally oriented such that one of its sides is parallel to the stretching axis, an extension of 100% is expected to double the length parallel to the axis with a corresponding contraction by a factor of $1/\sqrt{2}$ in the perpendicular direction, if Poisson's ratio is 0.5. The extended and contracted lengths of the original cube are derived from the reciprocal lengths of the equatorial and polar axes of the 100 diffraction ellipse. Extended and contracted cell lengths obtained in this way are compared with values calculated on the assumption of affine deformation and Poisson's ratio of 0.5 and 0.35 in Table 5.2a for different extensions.

Within experimental errors, there is agreement between calculations

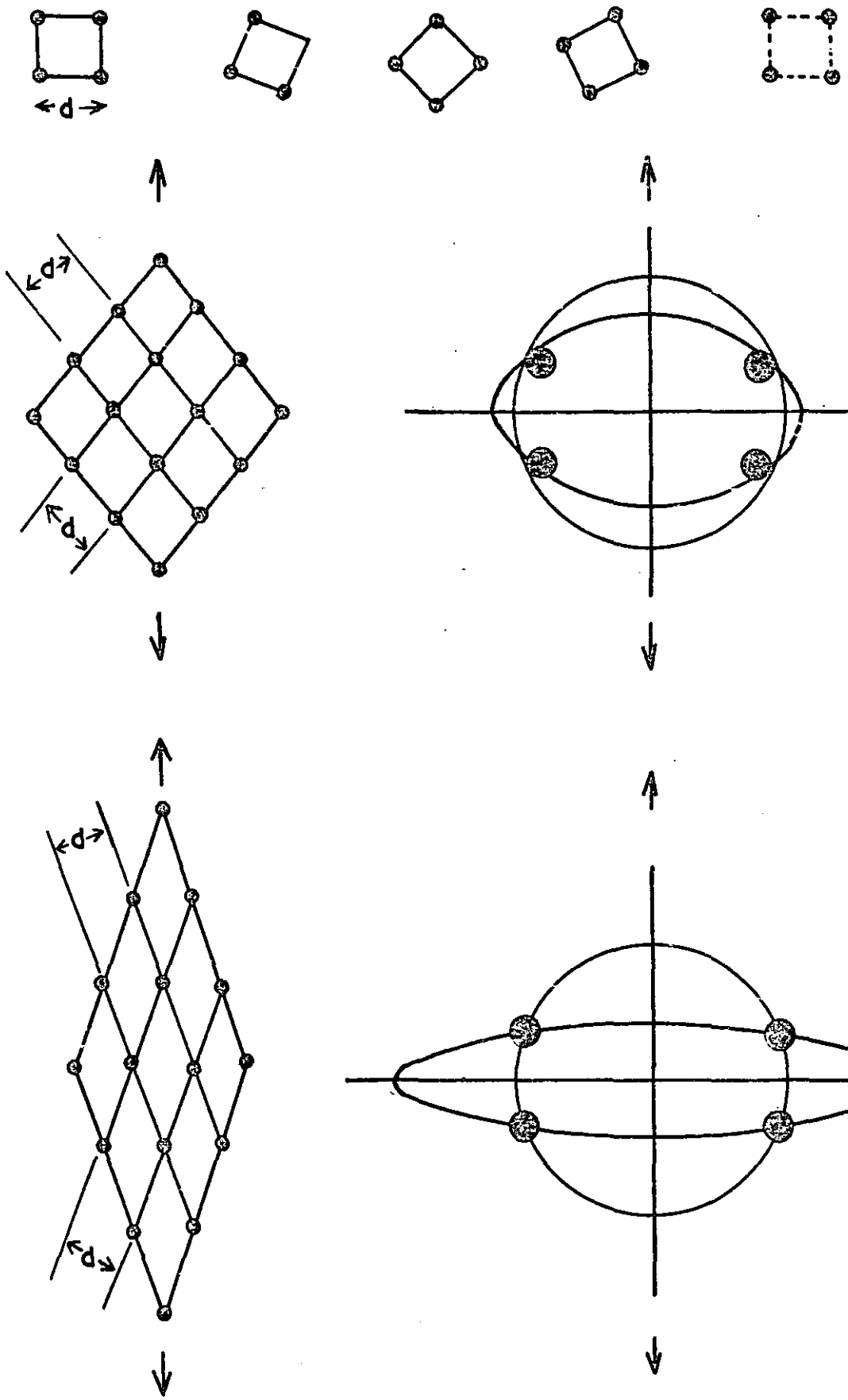

FIG. 5.2. DEFORMATION OF 2-D ANALOGY OF CUBIC ORIENTATION.

based on the cubic model and observed values using Poisson's ratio as a parameter. It is clear that the ideal rubber value of 0.5 does not give as good agreement as average values in the region 0.3 to 0.4.

TABLE 5.2a COMPARISON OF CALCULATED AND OBSERVED CELL LENGTHS (K101, Toluene Cast)

Extension Ratio	Calculated Cell Lengths				Observed Cell Lengths	
	Poisson's Ratio = 0·5		Poisson's Ratio = 0·35			
	Extended Å	Contracted Å	Extended Å	Contracted Å	Extended Å	Contracted Å
2 ± 0·06	600 ±20	212 ±10	600 ±20	236 ±12	685 ±50	236 ±12
4 ± 0·3	1200 ±90	149 ±5	1200 ±90	185 ±10	1000 ±200	208 ±30

The scattering patterns obtained using slit optics in conjunction with Geiger counting of the scattered intensity, show the effect of thermal or solvent treatment in the fabrication of the specimen. An intense, narrow interdomain scattering peak was observed in the scattering patterns of all the specimens except the moulded sample. Such intense scattering peaks could only be associated with a highly ordered arrangement of the domains in the matrix. (Scattering patterns of crystalline polymers only indicate a broad shoulder.) However, the Bragg spacing derived for the principal maximum increases from

290 Å for both of the swollen/deswollen specimens to 300 Å for the toluene and methyl cyclohexane specimens and to 348 Å for the methylene chloride specimen.

The difference in the scattering patterns of the methylene chloride cast and methylene chloride S/D-S specimens give evidence of a change in morphology due to the swelling process. The swelling agent n-hexane (δ = 7·3) is a very poor solvent for polystyrene but it swells the polybutadiene phase. Swelling the methylene chloride cast specimen to an increase of about 50% in each dimension would effectively break any polystyrene link connecting the domains. The resulting morphology is then close to that of a toluene cast specimen. The scattering pattern of both the S/D-S specimens are identical and almost identical to the toluene cast specimen. Such similarity is also observed in the dynamic mechanical spectra discussed in Section 5.2.

For the moulded specimen the scattering pattern exhibits a board peak at the highest scattering angle observed, corresponding to a Bragg spacing of 412 Å. The broad peak is associated with a wide range of distribution in interdomain distance. In their SAXS study of SBS block copolymers, Harpell and Wilkes (174) reported that the morphology of the moulded sample is dependent upon the moulding temperature or time. As such, no specific model could be ascribed to to moulded samples in general.

The effect of temperature in the range -100°C to +125°C is to change the density difference ($\Delta\rho$) between the phases and hence the scattered intensity, since the total intensity is proportional to $(\Delta\rho)^2$. Besides the change in intensity of the scattering peak for the toluene cast sample, there is also a shift in the Bragg spacing from 300 Å at -100°C to 318 Å at +125°C (Table 4.2). Using the 'universal' value of $\alpha = 4 \times 10^{-4}$ deg^{-1} for the thermal expansion coefficient of elastomers (186), the change in Bragg spacing for the toluene cast sample is calculated to be 26 Å. This is close to the observed value within experimental error.

The toluene cast specimen was stretched to various extensions up to 600%, and instantly allowed to relax. The scattering patterns of the specimen in the relaxed state after each extension, show no shift in the Bragg spacing nor any change in the half-width of the curve (Table 4.3). This is possible with the model of domains free of polystyrene links, and dispersed in the rubbery matrix.

Calculations based on a cell spacing (cube length) of 300 Å and volume fraction, 25% polystyrene, show that the average diameter of the spherical domains in such a lattice would be approximately 240 Å.

From the electron micrographs of a toluene cast specimen (Figure 4.3) by Dr. Bowman et al in the I.S.R. laboratories, the patterns observed do not conclusively indicate spherical domains arranged in cubic lattices. There are regions of parallel lines and also regions of ordered particles. This discrepancy could possibly be attributed to the fast evaporation rate of the solvent in casting this sample, as compared to the slow rate of evaporation in the case of the sample in the SAXS study. However, in the regions of ordered particles, the average particle size and average interparticle distance were measured to be 200 Å and 320 Å respectively. Using the volume fraction, 25% polystyrene, and a cubic cell spacing of 320 Å, the average diameter of the particles is calculated to be 250 Å, which differs from the observed value of 200 Å. This indicates that the particles are not spherical in this sample.

However, electron micrographs of K101 cast from good solvents for both polystyrene and polybutadiene, showing spherical domains have been reported by Lewis et al (175) and Beecher et al (154). The latter have also observed that for the sample cast from a THF/MEK solvent system there are thin strands of polystyrene interconnecting the domains.

5.2 DYNAMIC MECHANICAL SPECTRA

All the five specimens of K101 are characterised by two discrete transition regions indicative of relaxation of each polymer segment type. An upper relaxation region of about 100°C corresponds to the glass transition of the polystyrene segments, while a lower relaxation at around -90°C is attributed to the glass transition of polybutadiene segments. (Figures 4.36 to 4.45.)

A plot of tan δ and E', the storage modulus, in the temperature plane for the toluene and methylene chloride cast samples at 10 Hz is shown in Figure 5.3. Both samples show a sharp polybutadiene relaxation at around -85°C, which is in line with that expected for a chain of this microstructure (176). The dramatic distinction is in the strength of the relaxation in this region, remembering that the polymer species are identical. The weaker modulus drop through the transition with the methylene chloride casting is in line with the depressed value of tan δ exhibited. Reciprocal differences at the polystyrene relaxation are also observed. Whereas the toluene cast sample has a precise, small, tan δ peak at 107°C (10 Hz), the methylene chloride casting has a much larger and more protracted relaxation extending down to room temperature.

This indicates that at least some of the polystyrene is in some special condition, such as highly oriented or plasticised. Plasticisation could only reasonably be expected to occur at the polystyrene-polybutadiene interface and would require a large amount of such material to give the observed relaxation strengths. Oriented polystyrene could occur by entrapment of the same polystyrene molecules in different polystyrene spheres during the phase separation process. These intersphere polystyrene links would then dominate the mechanical behaviour. Very few data are available on the dynamic mechanical properties of oriented rigid amorphous polymers. However, Nielsen and Buchdahl (177) have reported that the damping E''/E' obtained from vibrating reed measurements was slightly greater for oriented polystyrene than for isotropic

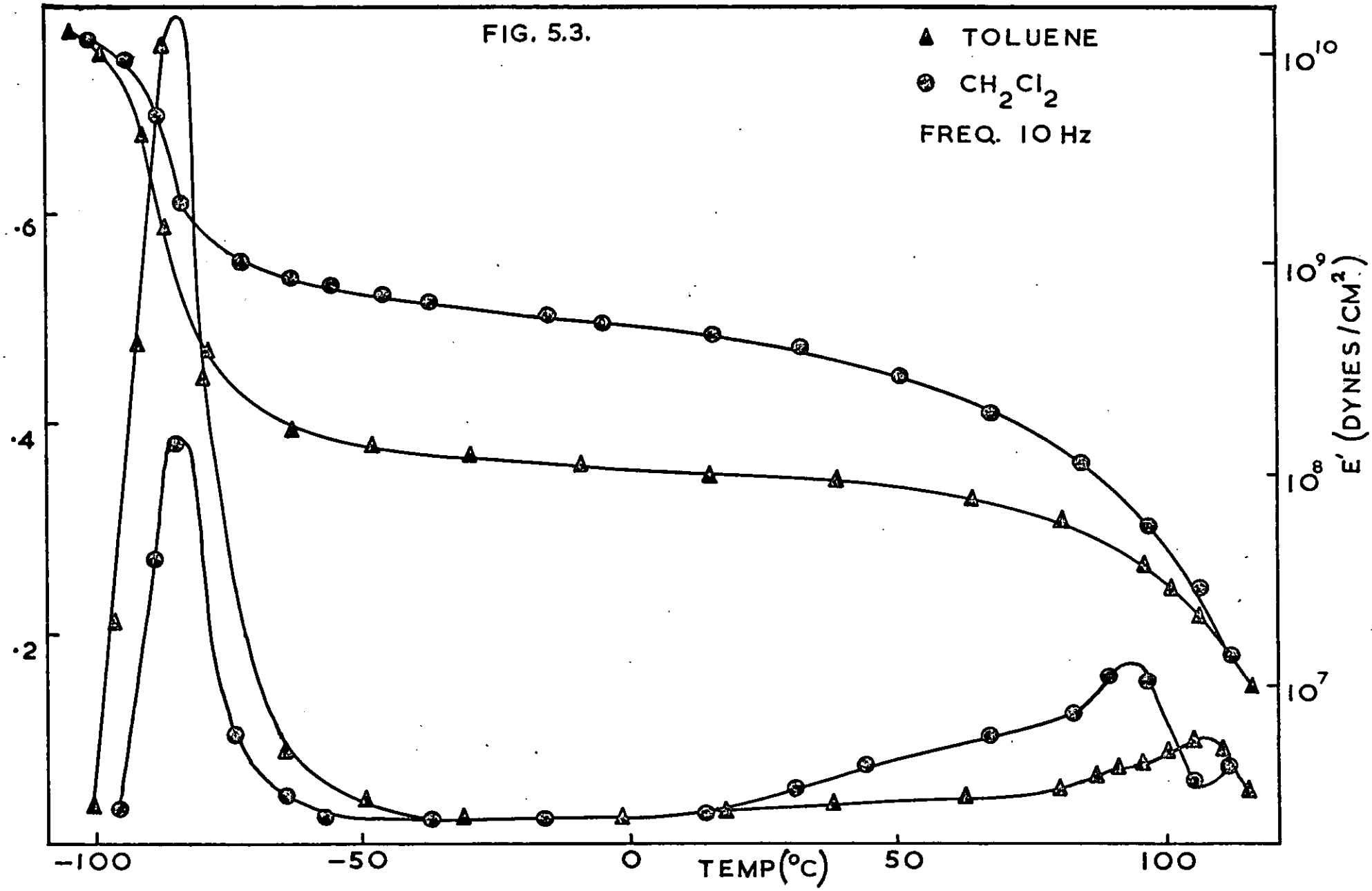
FIG. 5.3.
TOLUENE
CH_2Cl_2
FREQ. 10 Hz
·6
·4
·2
10^{10}
10^{9}
10^{8}
10^{7}
E' (DYNES/CM²)
-100
-50
0
50
100
TEMP(°C)

annealed polystyrene. They also noted that orientation lowers the transition temperature range where the damping increases very rapidly with temperature.

The dynamic mechanical data on a moulded sample shows almost identical features to the methylene chloride cast sample, and therefore one would expect the morphology of the two samples to be similar. But the SAXS patterns indicate that the moulded sample has a more disordered domain structure and a higher average interdomain distance. However, it is reasonable to postulate that in the moulded sample, there are also polystyrene links between domains.

Figure 5.4 shows the tan δ versus temperature plots at 10 Hz for the toluene and methylene chloride S/D-S samples. Both curves are identical within experimental error. The high polybutadiene peak and the small sharp polystyrene relaxation are similar to the toluene cast sample. This is expected, even in the methylene chloride S/D-S case, since swelling to 50% in n-heptane, will effectively break the postulated polystyrene links. If the polystyrene intersphere material contracts back onto the spherical regions, a structure similar to the toluene cast sample will thus result.

Arrhenius activation enthalpy plots (Figure 5.5) based upon the change in location of the damping maximum with frequency indicate the polybutadiene phase molecular motion occurs with an activation enthalpy of 32 kcal./mole in line with the value of 39 kcal./mole obtained for the normal homopolymer and that there is no detectable difference between the samples. The activation enthalpy for the polystyrene relaxation (Figure 5.6) increases from 84 kcal./mole for the methylene chloride cast sample to 96 kcal./mole for the toluene cast and both S/D-S samples to 115 kcal./mole for the moulded sample. For the moulded and methylene chloride cast samples, the polystyrene relaxation is the sum of the relaxation of the polystyrene segments in the domains and in the oriented polystyrene links. The polystyrene relaxation peak in the dynamic mechanical spectra of the toluene cast

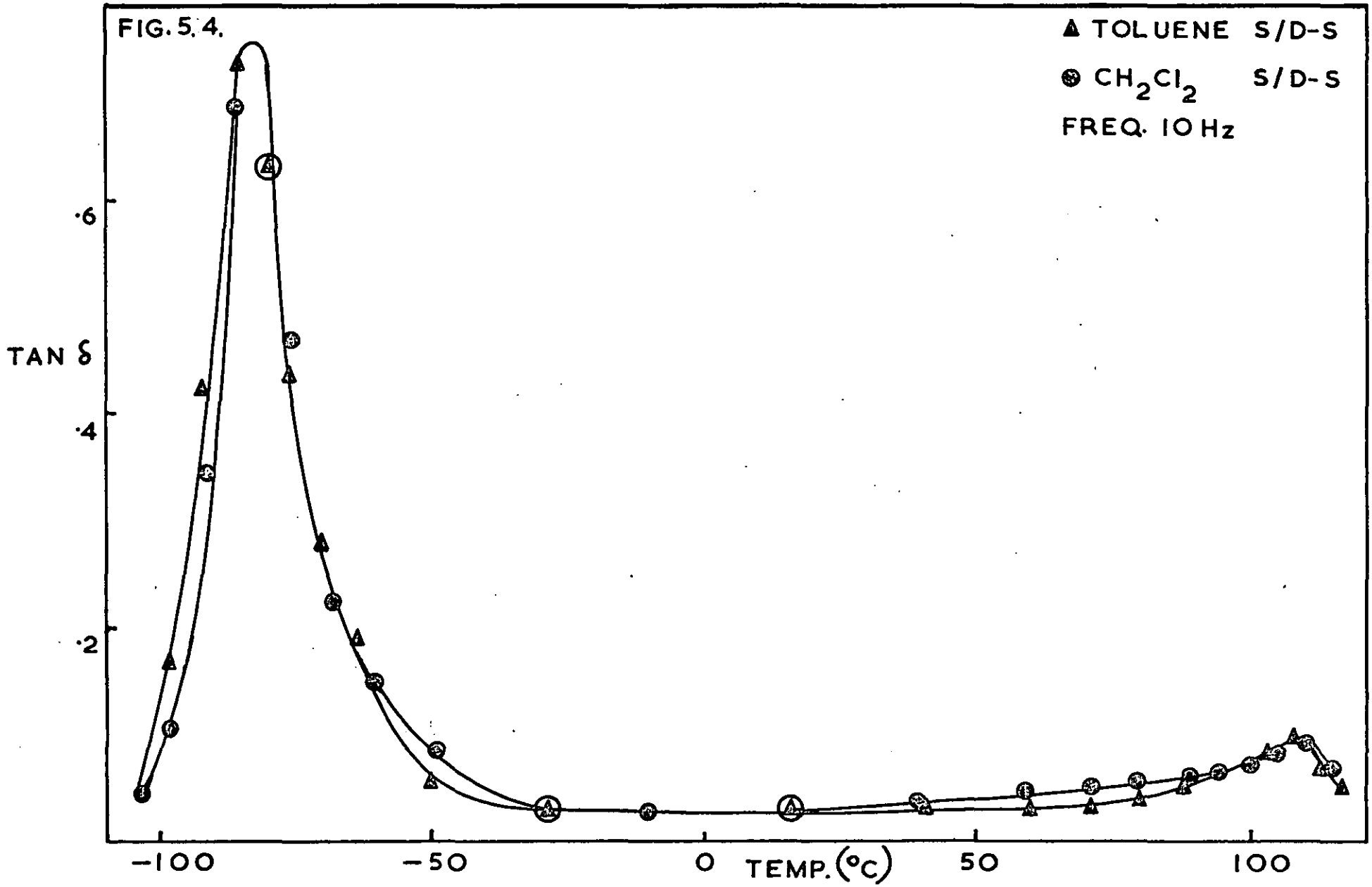
FIG. 5.4.
▲ TOLUENE S/D-S
● CH_2Cl_2 S/D-S
FREQ. 10 Hz
TAN δ
·6
·4
·2
−100
−50
0
TEMP. (°C)
50
100

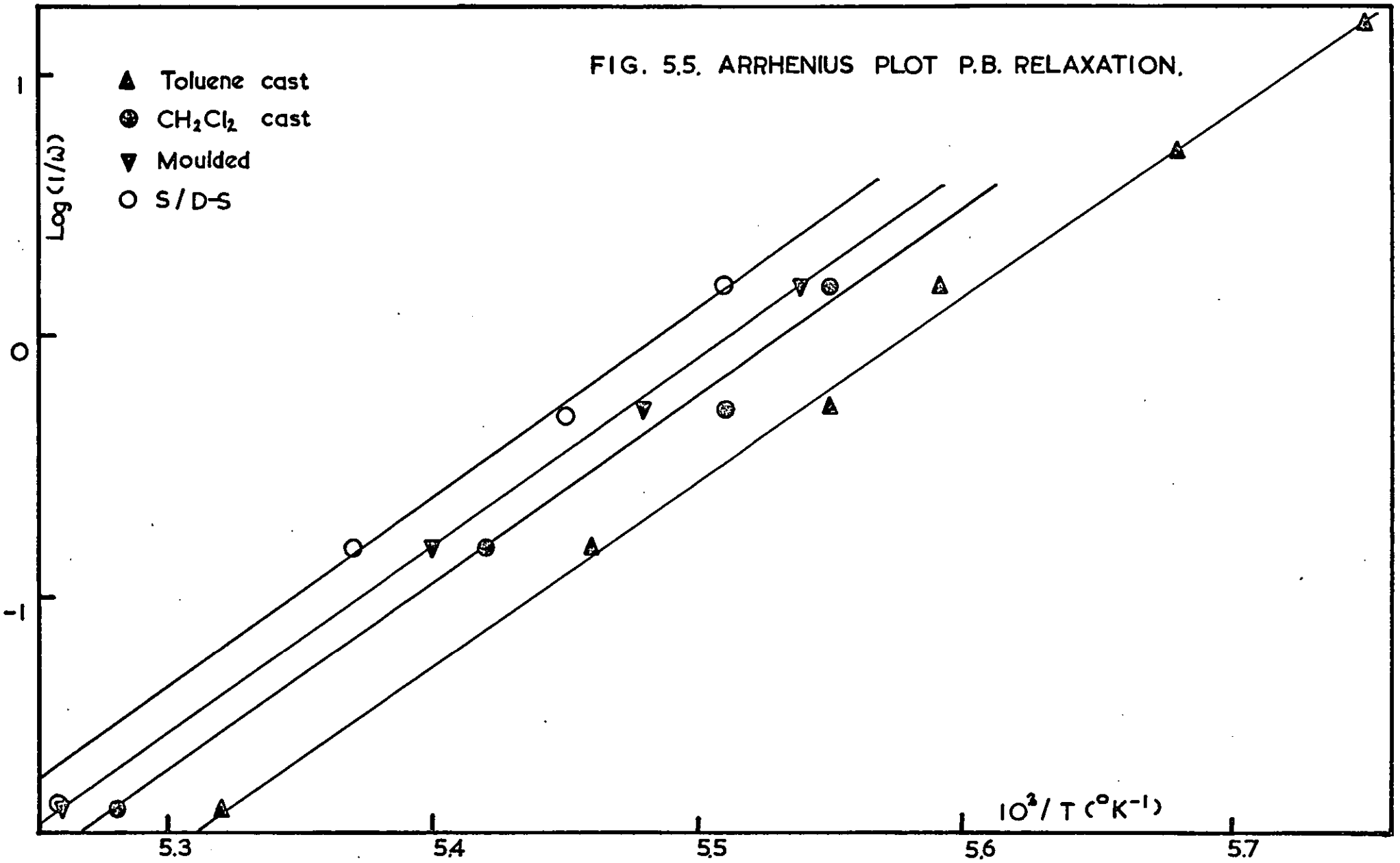
FIG. 5.5. ARRHENIUS PLOT P.B. RELAXATION.
Toluene cast
CH_2Cl_2 cast
Moulded
S / D-S
Log (1/ω)
1
0
-1
10^3 / T (°K^{-1})
5.3
5.4
5.5
5.6
5.7

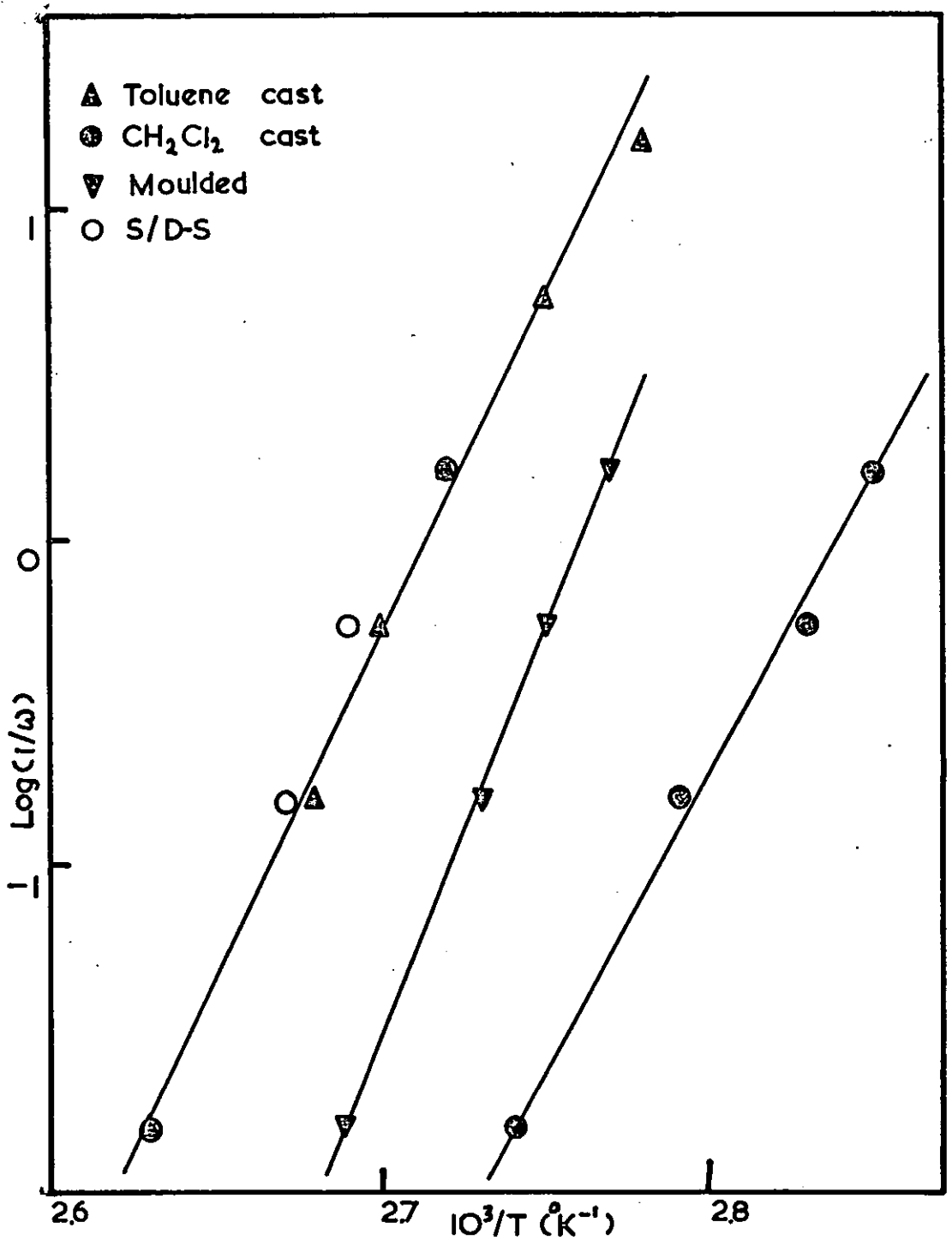

FIG. 5.6. ARRHENIUS PLOT FOR P.S. RELAXATION.

and S/D-S samples is sharp, indicating a pure polystyrene phase. As such the activation enthalpy for the polystyrene relaxation is more accurately given by the toluene cast and S/D-S samples than by the other samples. Smith (178) has reported a value of 45·5 kcal./mole for the activation enthalpy of a moulded K101 sample. The value was obtained by plotting the shift factor log a_T against 1/T using stress-strain data in the temperature range of -40° to $+60^{\circ}$C. This activation enthalpy is for the relaxation processes occurring in the test temperature range, which would include the breaking of the polystyrene links and the desorption of the polybutadiene chains off the domain surface. Also, the activation enthalpy calculated using the time-temperature reduction schemes of Ferry et al. (75) and other authors, (221,222) is subjected to errors due to the arbitrary choice of the factors used in the vertical shifting of the modulus or compliance curves.

In order to assess the mechanical coupling in these specimens, the modulus in the plateau region of the dynamic mechanical spectra is compared with Young's modulus values calculated using Guth-Gold equation (2.43) and Kerner's equation (2.45) (See Section 2.6).

$$E = E_1(1 + 2{\cdot}5\phi + 14{\cdot}1\phi^2) \tag{2.43}$$

$$E = E_1 \left[\frac{\dfrac{V_2E_2}{(7 - 5\nu_1)E_1 + (8 - 10\nu_1)E_2} + \dfrac{V_1}{15(1 - \nu_1)}}{\dfrac{V_2E_1}{(7 - 5\nu_1)E_1 + (8 - 10\nu_1)E_2} + \dfrac{V_1}{15(1 - \nu_1)}} \right] \tag{2.45}$$

where E, E_1 and E_2 are the moduli of the filled system, the matrix and the filler respectively. The modulus E_1 for the matrix is calculated from the kinetic theory of rubber elasticity from an entanglement molecular weight of 3000 (as determined by Ferry on bulk polybutadiene) (179).

However, as can be seen in Table 5.3, dropping the molecular weight between entanglements to 2000 gives a close agreement to the experimental values obtained from the toluene cast sample. It should be noted that the experimental values obtained from the dynamic mechanical measurements, take into account the temporary and permanent entanglements of the polybutadiene chains, the polystyrene-polybutadiene links at the domain surface and also the physical adsorption of polybutadiene chains on to the domains. As such, it is reasonable to assume a lower value of M_e for the toluene cast K101 sample, than the M_e value given by Ferry for the bulk polybutadiene. The close agreement in the toluene case, is thus in line with the model of spherical domains, dispersed in a rubbery matrix, with perfect bonding between the two phases. Such a model is also assumed for both the Guth-Gold equation and Kerner's equation.

Table 5.3 also shows that the modulus slightly decreases with increasing temperature in the plateau region of the dynamic mechanical spectra. This is in contrast to the behaviour of ideal rubber networks as predicted by the kinetic theory of rubber elasticity. This slight decrease is due to the relaxation processes, such as the desorption of the polybutadiene chains off the domain surface with increased temperature, which is greater than the entrophy effect considered by the kinetic theory.

The methylene chloride cast sample has a far higher modulus. In this sample, at low strains and at ambient temperatures, the mechanical behaviour is apparently dominated by the polystyrene links between the domains.

A better appreciation of the methylene chloride cast sample is obtained by fitting the data with Takayanagi's series and parallel coupled phases. The circle points in Figure 5.7 are calculated from Takayanagi's data (88) on polybutadiene (lightly cross-linked) with a constant modulus of 3×10^{10} dynes/cm^2 for the polystyrene spheres.

TABLE 5.3 MODULUS OF TOLUENE AND METHYLENE CHLORIDE CAST SAMPLES

Dynamic Modulus E'(10 Hz)		
Temperature ^{o}C	Toluene Cast	Methylene Chloride Cast
-30	1.05×10^{8} d/cm^2	6.2×10^{8} d/cm^2
+30	9.0×10^{7} d/cm^2	4.0×10^{8} d/cm^2
M_e	Guth-Gold Equation	Kerner's Equation
3000	5.7×10^{7} d/cm^2	4.8×10^{7} d/cm^2
2000	8.5×10^{7} d/cm^2	7.2×10^{7} d/cm^2

FIG. 5.7

$$E^* = \left[\frac{\phi}{\lambda E_s^* + (1-\lambda) E_B^*} + \frac{1-\phi}{E_B^*} \right]^{-1}$$

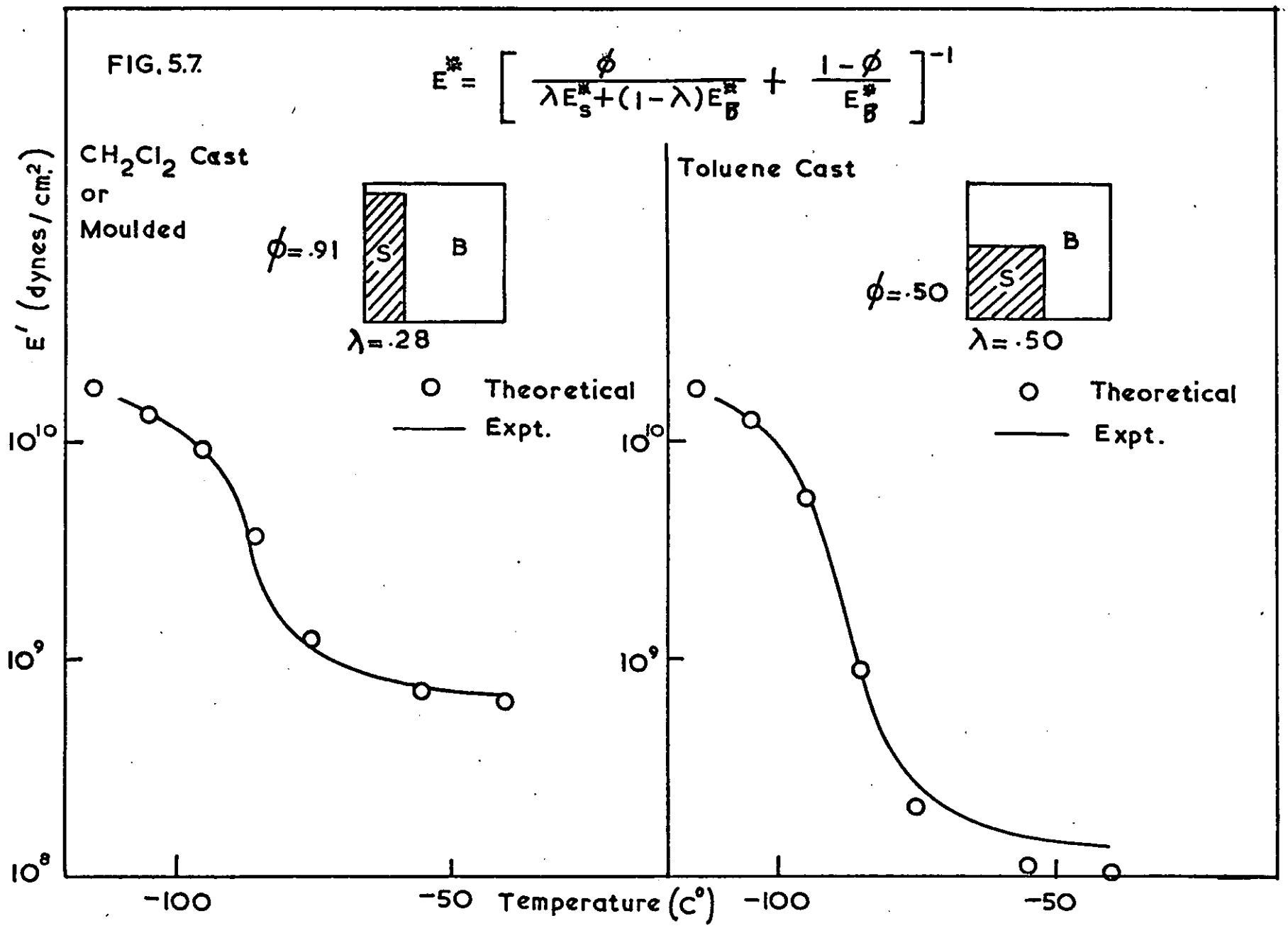

There is good agreement with the experimental values. In this model, $\lambda = \phi = 0{\cdot}50$ to give a product of 0·25 as the known volume fraction of polystyrene. The deviation present indicates that perhaps the polybutadiene in the three block system is more highly entangled than the homopolybutadiene, and also that the physical adsorption of the polybutadiene chains onto the domain surface would contribute as effective crosslinks.

In the methylene chloride case, λ and ϕ are varied to give the best fit to the experimental data. A good fit can only be achieved with almost complete parallel coupling $\phi = 0{\cdot}91$ and $\lambda = 0{\cdot}28$, of the polybutadiene and polystyrene phases. The results indicate that the stress is transmitted more through the polystyrene phase in the methylene chloride cast sample than in the toluene cast sample.

5.3 PROPOSED MODELS FOR TOLUENE AND METHYLENE CHLORIDE CAST SAMPLES

The model that emerges from the SAXS studies of the toluene cast sample is that of an ideally dispersed spherical domain system. The domains are arranged in simple cubic lattices, randomly oriented in the matrix. The interdomain spacing is 300 Å and the spheres are of diameter 240 Å. The polybutadiene matrix is more entangled than in the homopolymer.

In the methylene chloride case, the structure is still highly ordered as evidenced by SAXS but no longer cubic. Further, the mechanical properties demand that the polystyrene phase is highly coupled. The interdomain distance is measured at 345 Å, but its size cannot be calculated without a knowledge of the amount of polystyrene linking phase. The polybutadiene may be less entangled in this system because of its more highly coiled state in the poor solvent. If the polystyrene links were broken by mechanical stretching, then the methylene chloride system should become more like the toluene casting with a slightly lower modulus. This is true for the SAXS data as given in Table 4.1; and the dynamic mechanical properties for the toluene and methylene chloride swelling/deswelling samples is very similar and the same as the original toluene casting with a high polybutadiene mechanical tan δ and a small, sharp polystyrene relaxation peak. (Figures 5.3 and 5.4)

Figure 5.8 gives diagrammatic representations of the adopted models for the toluene and methylene chloride cast samples.

The effect on morphology due to the solvent may be explained by the following mechanism. The two-phase structure of block copolymers in the solid state is influenced by the configurations of the polymer chains in solution and originates even in relatively dilute solutions - at a critical concentration of about 10%, (32-34, 118, 180). Methylene chloride is a good solvent for polystyrene and a very poor solvent for polybutadiene. As the solvent is evaporated, a critical concentration

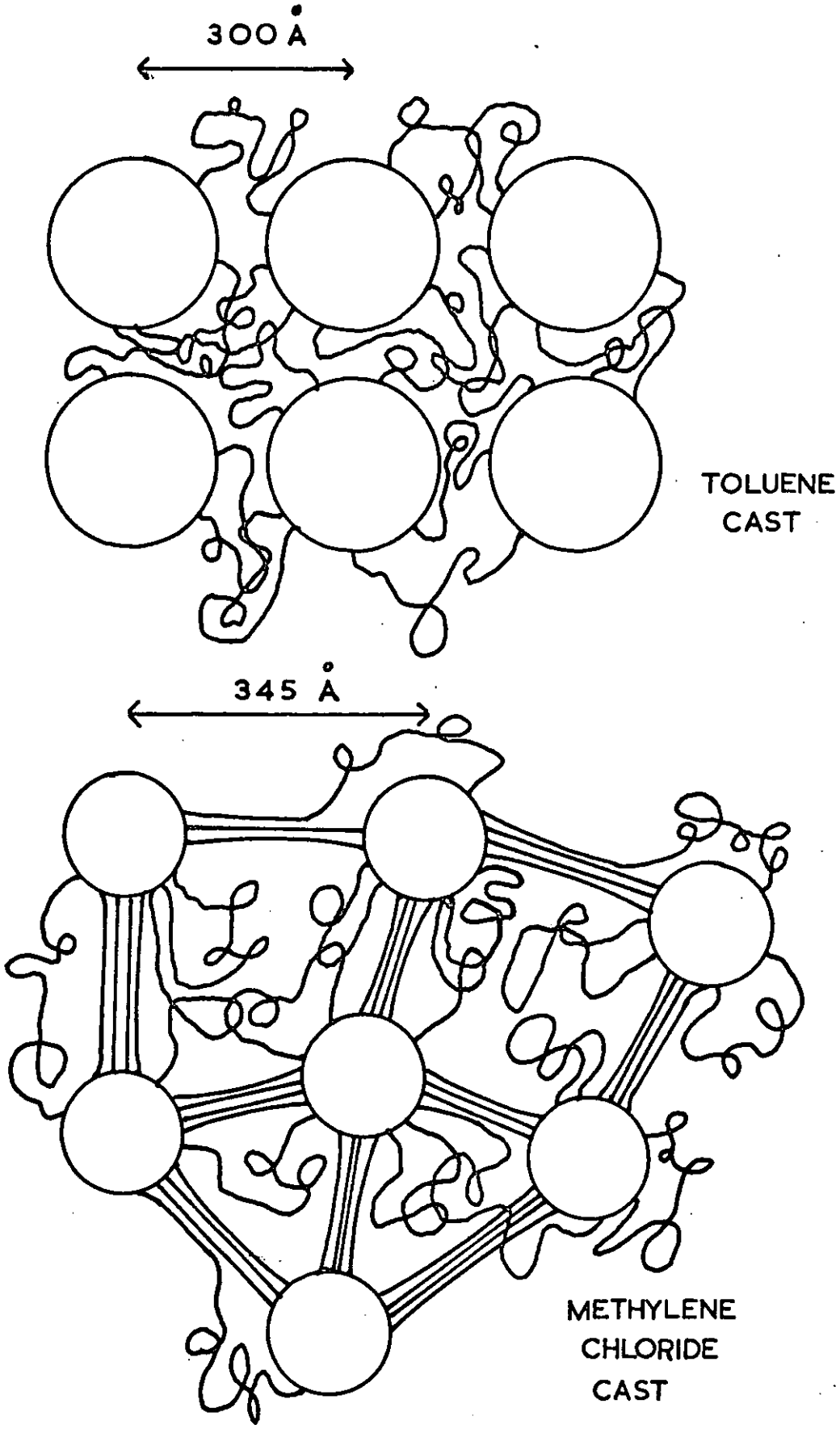

FIG. 5.8.

is attained. At such a concentration the polybutadiene will be unswollen while the polystyrene end blocks aggregated in near spherical domains will be swollen with methylene chloride. The swollen polystyrene will occupy a large proportion of the system volume. This will lead to a high probability of impingement between the polystyrene domains. As the methylene chloride evaporates completely, the polystyrene domains contract, and the entanglements caused by domain contacts would remain to give rise to the thin paths of polystyrene connecting domains. In this way, a three-dimensional network results.

In the toluene solution, at the critical concentration, both the polystyrene and the polybutadiene phases are swollen since toluene is a good solvent for both polymers. However, the volume of polybutadiene in K101 is 75% of the total polymer volume. Hence the swollen polystyrene spherical domains are kept well apart. As the solvent completely evaporated, each of the phases contracts without contact between polystyrene domains which then exist in a polybutadiene matrix, with no polystyrene links.

For the methyl cyclohexane solution, at a critical concentration, the polystyrene domains are less swollen and are kept apart by the swollen polybutadiene phase. Again a free system of spherical domains in a highly entangled polybutadiene matrix is formed on complete evaporation of the solvent. There is no observable difference in the SAXS patterns and stress-strain curves of the toluene and methyl cyclohexane samples, and because of difficulties of methyl cyclohexane casting only the toluene cast specimens have been studied in detail.

5.4 ELASTIC MODULUS OF SBS BLOCK COPOLYMERS

As discussed in Section 5.3 the adopted model for the toluene cast sample is that of an ideally dispersed spherical domain system. In order to obtain from this model, some insight of the large strain properties of the block copolymer, the model needs to be expanded with finer details.

The junction points between the polystyrene and the polybutadiene segments are at or near the domain surface. Each domain is the terminal point for many elastomer chains. From the known dimensions of the polystyrene domains, the average molecular weight of the polystyrene segments, and assuming the density of the domains to be the same as that of the homopolystyrene, the average number of chains emanating from each domain is calculated to be about 400 for the K101 block copolymer. The domains therefore serve as multifunctional crosslinks and give the elastomeric chains a continuous three-dimensional network character.

Interchain loopings or entanglements in the rubbery phase are an important feature of this network. Some of these entanglements disentangle upon extension of the network - temporary entanglements. On the other hand, many entanglements are topologically trapped and serve as tetrafunctional crosslinks for the network - permanent entanglements.

In addition, physical adsorption of polybutadiene chains on to the domain surface would increase the number of crosslinks in the network. Such adsorption are physically feasible because the interfacial tensions are not extremely repulsive. Also there is likely to be a very large diffuse interface. The cross-sectional area of the polystyrene-polybutadiene junctions is assumed to be approximately that for the orientated molecules of the straignt-chain unsaturated acids, like oleic acid. This value is reported to be 20·5 $\mathring{A}$ (185). The total area occupied by the 400 junctions is calculated to be less

than one-twentieth of the surface area of each domain. As such the domains would have several points at which there are surface adsorptions of a polybutadiene chain.

According to the concept of 'domain formation' (10, 181-183) the dominant factors contributing to the elastic modulus of the ABA type of thermoplastic elastomers, are the permanent entanglements in the polybutadiene phase and the filler effect of the polystyrene domains. Both factors contributing to the elastic modulus of these polymers are accounted for in Equation 3.1, from equilibrium swelling measurements,

$$M_c = \frac{\rho_2 \bar{V}_1 (V_r^{1/3} - 2V_r/f)}{\ell n(1 - V_r) + V_r + \chi V_r^2} \qquad (3.1)$$

and from tensile properties of unswollen and swollen samples in Equations 3.2 and 3.3 (See Section 3.3).

$$\sigma = \frac{\rho RT}{M_c}(\lambda - \lambda^{-2})(1 + 2{\cdot}5\phi_s + 14{\cdot}1\phi_s^2) \qquad (3.2)$$

$$\sigma = \frac{\rho RT}{M_c} V_r^{-1/3}(\lambda - \lambda^{-2})(1 + 2{\cdot}5\phi_f + 14{\cdot}1\phi_f^2) \qquad (3.3)$$

In Equations 3.2 and 3.3, the polystyrene domains are regarded as an inert filler and the increase in modulus to the elastomer network is accounted for by the application of the Guth-Gold equation (84).

$$\sigma = \sigma_o(1 + 2{\cdot}5\phi + 14{\cdot}1\phi^2) \qquad (2.43)$$

where σ, σ_o are the stresses required to extend the filled and unfilled polymers respectively. $\phi = \phi_s$ or ϕ_f, are the volume fractions occupied

by the domains in the unswollen and swollen networks respectively.

In Equation 3.1 the network is assumed to contain no free chain ends and to have a crosslink functionality, f, of four. (A permanent entanglement crosslink also has a functionality of four.) The quantity V_r is the volume fraction of the rubbery phase in the swollen network.

The M_c value in all three equations thus referred to the molecular weights between entanglements of the elastomeric chains.

Table 5.4 gives the values of M_c calculated from Equations 3.1 to 3.3 using data obtained from stress-strain measurements on swollen and unswollen samples and equilibrium swelling measurements.

TABLE 5.4

Method	M_c
Tensile measurements:	
unswollen sample (moulded)	$2{\cdot}64 \times 10^3$
swollen sample (toluene cast)	$6{\cdot}60 \times 10^3$
Equilibrium swelling (toluene cast)	$2{\cdot}80 \times 10^4$

Ferry (179) obtained a value of 3000 for the average molecular weight between entanglements, M_c, of bulk polybutadiene having $\bar{M}_W$ = 524,000. He calculated the M_e value using the data obtained from the master curve for the creep compliance, at the reduced temperature of 300 K^o. Kraus and Gruver (184) reported a value of 5600 for the M_e of polybutadiene. This value is the critical molecular weight

corresponding to the break in the logarithmic plot of viscosity against molecular weight. As such it can be considered as the maximum value for the entanglement molecular weight of polybutadiene.

In the equilibrium swelling measurements, any polybutadiene chains adsorbed onto the domain surface would be desorbed by replacement with n-heptane during the swelling process. These adsorption sites would thus no longer contribute as effective crosslink sites. Also, all temporary entanglements would be disentangled. However, the experimental value obtained is about half that of the number-average molecular weight of the polybutadiene segments. The high value indicates experimental errors. Adsorption of the swelling agent by the interphase material would give a decrease in V_r and, as such, would obscure any meaningful interpretation of M_c.

In the tensile measurement on the unswollen moulded samples, the samples were first stretched to about 30% extension. Stress-strain measurements were then taken at decreasing loads. The initial stretching process would break any polystyrene links between the domains. The resulting system would then be close to that of the toluene cast sample. As such one would expect the 'M_c' value obtained to be of the same magnitude as the 'M_e' value calculated from E' of the dynamic mechanical measurements for the toluene cast sample. ($M_e \sim 1900$). The slightly higher value from the tensile measurements suggest, possibly, that most of the physical adsorption entanglements have been desorbed in the initial stretching process. Whereas, because of the minute strain levels used in the dynamic mechanical measurements, all the different types of entanglements discussed earlier in this section would contribute as effective crosslinks to the network.

The sample is swollen with Nujol, which is a non-solvent for polystyrene, but swells the polybutadiene phase. The volume fraction of the rubbery phase at equilibrium was 0·288 as compared to a value of 0·111 when using n-heptane as the swelling agent. Tensile measure-

ments were then carried on the swollen sample. In this type of measurement only the permanent entanglements and the polystyrene-polybutadiene junctions would contribute as effective crosslinks. The value of M_c obtained would be closer to the maximum entanglement molecular weight for polybutadiene, as is observed to be so.

The elastic modulus of the K101 block copolymer is sensitive to the type of measurement used in its determination. At low strains, as in dynamic mechanical measurements, the domain morphology would be the dominating factor. In the case of spherical domains, as in toluene cast samples, all entanglements would contribute as effective crosslinks. In large strains and swelling measurements, the dominant factors contributing to the elastic modulus would be the permanent entanglements in the rubbery phase and the filler effect of the domains.

5.5 STRESS-STRAIN BEHAVIOUR AND ULTIMATE PROPERTIES

Stress-strain studies indicate that increasing temperature led to large decreases in modulus, tensile strength and elongation at break of K101. Similar patterns of behaviour between stress and strain are observed for the toluene, methylene chloride and methyl cyclohexane cast samples. The loss in strength can be associated with the absence of an upturn in the stress-strain curve at higher temperatures. (Figures 4.6 to 4.12).

The effect of strain rate on the tensile properties is less evidenced at lower temperatures but becomes pronounced at temperatures above 50°C. An increase in strain rate corresponds in effect to a decrease in temperature.

The stress-strain curves of Figures 4.6 to 4.12 also show that as the temperature is increased, at a given strain level, the stress in the K101 block copolymer decreases. This is in direct contrast to the behaviour of an ideal rubber for which stress is proportional to absolute temperature. The negative temperature coefficient of the stress is attributed to the increased desorption of the polybutadiene chains off the domain surface and to the increased mobility of the loosely bound polystyrene regions. At higher temperatures, the loss of tensile strength is due to the onset of the viscoelastic softening of the polystyrene phase, leading to the loss of physical crosslinks. The mechanical tan δ - temperature plot for a toluene cast sample (Figure 4.41) indicates the onset of the relaxation region due to the polystyrene segments at about 60°C (0·01 Hz). Also birefringence measurements reported by Fischer and Henderson (187) indicate that the polystyrene blocks in the SBS block copolymers did not deform at temperatures below 70°C. Similar stress-strain behaviour has been reported by Smith and Dickie (153) in SBS block copolymers, by Estes et al. (188) in polyether-urethane and by Riches and Howard (189) in polyester-polyether block polymers.

The ultimate properties of K101 are comparable to those of a natural rubber gum vulcanizate (Figure 5.9) both being of high tensile strength and high elongation at break as compared to a SBR gum vulcanizate. However, an enchancement in ultimate properties is observed for a SBR gum vulcanizate with reinforcing fillers (190-192). It is noted that the moduli and tensile strength of black reinforced rubbers also decrease markedly with temperature, (193, 194). Consequently, the colloidal domains of glassy polystyrene in SBS block copolymers appear to behave similarly to reinforcing filler particles up to temperatures at which the polystyrene blocks soften.

Both the K101 samples display a high slope at low extensions, followed by a plateau region between $\sim$ 20 to 300% extensions in the stress-strain curves (Figure 5.9). These features are enhanced in the methylene chloride case and are associated largely with the breakdown of the polystyrene network in the direction of the stress. The SAXS and dynamic mechanical studies discussed in Sections 5.1 and 5.2 indicate the absence of a rigid polystyrene network in the toluene cast system. Thus the bending of the stress-strain curve towards the strain axis, giving rise to the plateau region can be attributed to the desorption of the polybutadiene chains off the domain surface, and to the fact that the stress at all extensions is based on the initial cross-sectional area of the sample. It should be noted that the Instron data under-estimated the high modulus of the methylene chloride cast samples, because data is only obtained at high strain levels. In the dynamic mechanical measurement, working at minute strain levels, less than 10^{-3}, the modulus E', in the plateau region, for the methylene chloride cast sample is five times greater than that of the toluene cast sample. After the breakdown of the polystyrene network in the methylene chloride cast sample, the rubbery matrix governs the behaviour and, as this is less entangled than the toluene casting, a softer material is obtained (see Section 5.3).

This is further supported by the hysteresis loops obtained for the

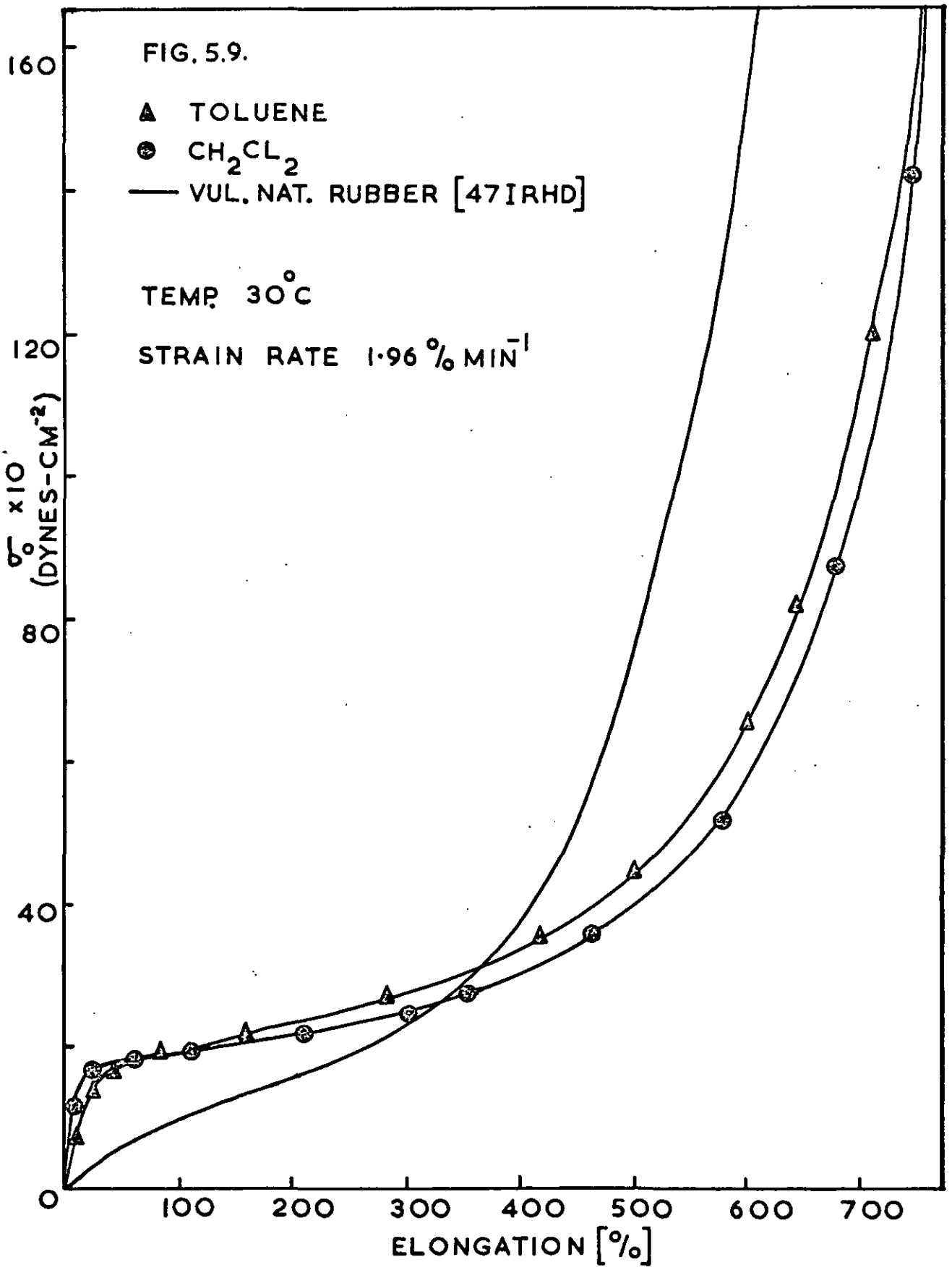
FIG. 5.9.
TOLUENE
CH_2CL_2
VUL. NAT. RUBBER [47 IRHD]
TEMP. 30°C
STRAIN RATE 1·96 % MIN⁻¹
$\sigma_0 \times 10$ (DYNES-CM⁻²)
0
40
80
120
160
100
200
300
400
500
600
700
ELONGATION [%]

toluene and methylene chloride cast samples (Table 4.6, Figures 4.18 and 4.19). The hysteresis (area between the extension and retraction curves) in the second cycle is considerably less than in the first cycle, indicating that the samples have stress-softened through desorption of the polybutadiene chains off the domain surface and thus giving materials with less entanglements. For the methylene chloride cast sample, the break-down of the polystyrene network contributes greatly to the stress-softening process. It is noted that in the second cycle at 30°C the methylene chloride sample is slightly softer throughout. The hysteresis loops at 60°C indicate that both samples occupied almost the same curves in both cycles. At high temperatures and high strains, viscoelastic deformation of polystyrene domains would contribute significantly to the hysteresis observed. When the deforming stress is removed, complete recovery to zero strain was not observed even in the second cycle at lower temperatures. The breakdown of the polystyrene network (in the methylene chloride case), the desorption of the adsorption entanglements and the decrease in mobility of the polybutadiene chains due to the presence of the polystyrene domains all contribute to the observed set in the samples on removal of the load.

The failure envelope (195, 196) for the toluene cast K101 sample is given by the plot of $\log \lambda_b\sigma_b 313/T$ versus $\log (\lambda_b - 1)$ as shown in Figure 5.10. $(\lambda_b\sigma_b 313/T)$ is the temperature-reduced true rupture stress, and $(\lambda_b - 1)$ is the strain at break. From the failure curve, the maximum extension $(\lambda_b)_{max}$ is obtained to be 11·2, the corresponding stress $(\lambda_b\sigma_b 313/T)_{max}$ is approximately $8{\cdot}3 \times 10^8$ dynes/cm^2. Smith and Dickie (153) have also reported similar values of $(\lambda_b)_{max} \simeq 11$ and $(\lambda_b\sigma_b 313/T)_{max} \simeq 1{\cdot}3 \times 10^9$ dynes/cm^2 for K101. Morton et al. (197) reported that polystyrene fillers (a non-reinforcing filler) do not alter the failure envelope of the SBR elastomers. The filler only affects the viscoelastic response of the system. Increasing amounts of the filler simply shift the curves upward along the envelope. Whereas the failure envelopes of SBR elastomers at different carbon black filler loadings do not

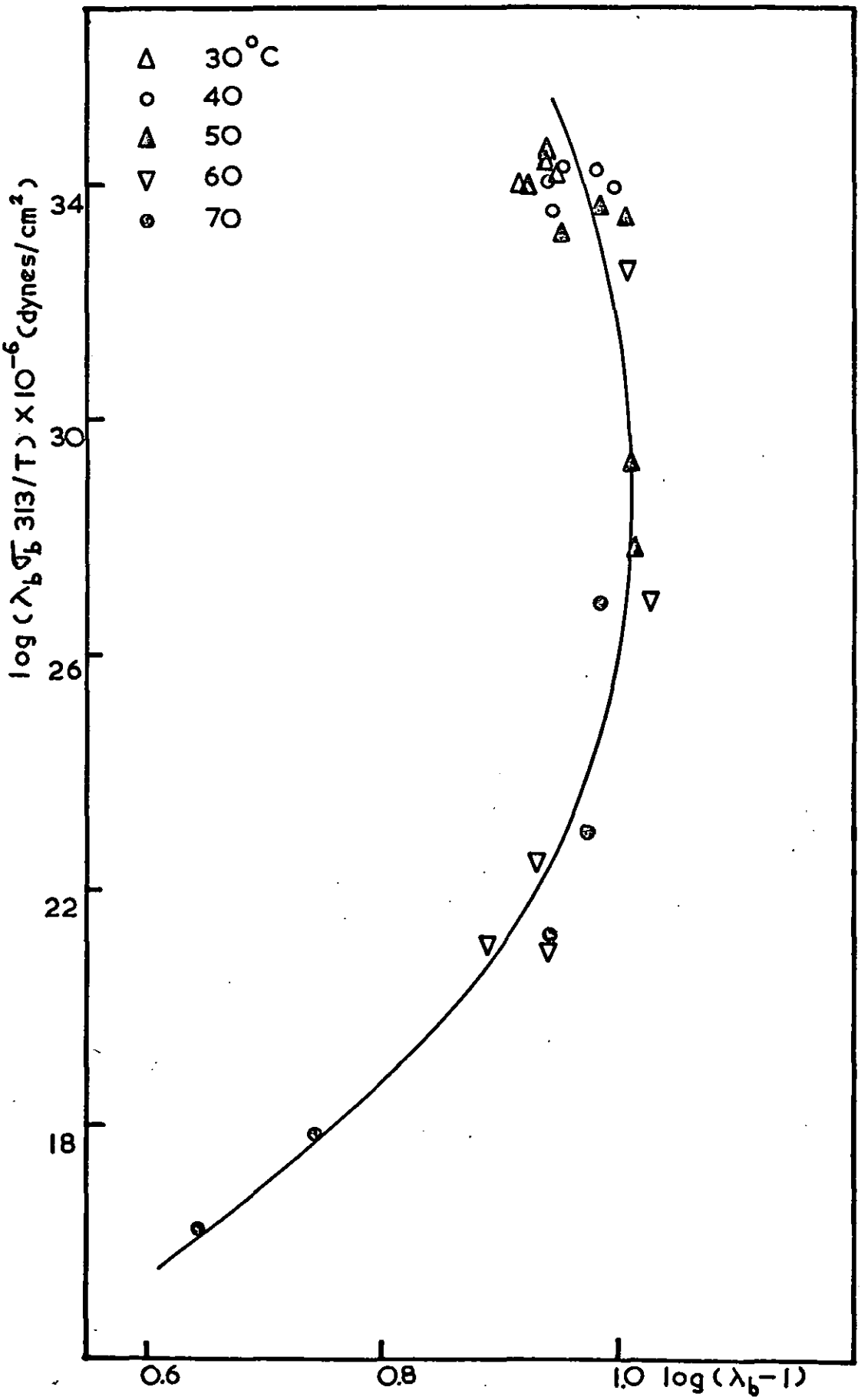

FIG. 5.10. FAILURE ENVELOPE OF K101,

superpose, (192). They show a tendency to go to higher stress values at higher filler loadings. This behaviour was attributed to the dual mechanism by which the carbon black apparently reinforces the tensile strength of elastomers. That is, the carbon black fillers not only affect the viscoelastic response of the network but actually 'increase the crosslink density' resulting in higher failure envelope. Payne et al (198), by applying a 'strain amplification factor' to their data for the SBR-Carbon black systems, showed that the failure curves for the gum and filler loaded vulcanizates superposed. The 'strain amplification factor', X, is given as (223)

$$X = \sigma/E\lambda = E/E_o = 1 + 2{\cdot}5c + 14{\cdot}1c^2$$

where λ is the strain produced by the stress σ, E_o is the modulus of the rubber without filler, and c is the volume concentration of the filler.

It is interesting to speculate that the failure envelopes of polybutadiene elastomer and SBS block copolymer would superpose, after the application of the strain amplification factor for, as discussed earlier in this section, the colloidal domains of glassy polystyrene in SBS block copolymers appear to behave similarly to reinforcing filler particles.

According to Bueche et al (224-226), the maximum extension at break, $(\lambda_b)_{max}$, given by the failure envelope is achieved when the chains between crosslinks or entanglements are fully elongated. Applying this concept of $(\lambda_b)_{max}$ and assuming an affine deformation for the sample, the root mean square end-to-end length for the chain, R, is given as

$$R = L/(\lambda_b)_{max} \quad .$$

The length of the chain when fully extended, L, is defined as

$$L = \ell(M/M_o),$$

where M is the molecular weight between entanglements or crosslinks, M_o is the molecular weight per backbone atom and ℓ is the average length of each backbone bond. Thus, the value for $R/M^{\frac{1}{2}}$ can be calculated from the known values of $(\lambda_b)_{max}$ and L, and can be compared with the experimental value from light scattering measurements. Bueche et al (227) noted that the computed values for $R/M^{\frac{1}{2}}$ is about 0·7 that of the experimental values for the various polymers studied. They attributed the difference in the two sets of values to the invalidity of the assumption that the deformation is affine.

The K101 block copolymer is considered as a filled polybutadiene system with 25% volume of polystyrene fillers. The failure envelope for K101 is shifted in accordance with the strain amplification factor to superpose with the failure envelope of the unfilled polybutadiene, and thus, $(\lambda_b)_{max}$ for the unfilled polybutadiene is obtained.

The polybutadiene phase in K101 has microstructure composition of cis-1,4, 41%, trans-1,4, 51% and 1,2 (vinyl), 8%. For this polybutadiene chain, L is given as (228,229)

$$L = 2{\cdot}12(M/M_o) \text{ angstroms.}$$

The molecular weight between entanglement, M, for the polybutadiene phase has been determined to be 6,600. (See Section 5.4) Thus $R/M^{\frac{1}{2}}$ for the polybutadiene phase in K101 can be computed from the known values of $(\lambda_b)_{max}$, and M and is 0·46. The literature value from light scattering measurement is 0·81 (230). It is observed that within experimental errors the ratio of the two values is reasonably close to that determined for many polymers by Bueche et al. This suggests that the ultimate properties of K101 are dominated by the polybutadiene matrix but are highly enhanced by

the polystyrene domains.

The mechanism by which the SBS block copolymers derive their high tensile strengths has been investigated by several workers (10, 153, 154, 187, 199, 200). Two plausible theories have been advanced to account for the enhancement of tensile strengths of elastomer networks, one attributes to Case (201) and the other to Bueche (202). In the SBS network system the polystyrene domains immobilise the ends of the polybutadiene phase are not able to disengage completely upon extension of the network. However, these entanglement crosslinks are labile in that they could redistribute uneven stresses by allowing slippage of the highly extended chains. The integrity of the overall network is insured by the polystyrene domains.

With such a mechanism one might expect that the toluene S/D-S and methylene chloride S/D-S samples would have a higher tensile strength than the toluene and methylene chloride cast samples for the swelling and deswelling processes would give a more even distribution of entanglement chain lengths. Unfortunately, no data on the tensile properties of the S/D-S samples were obtained.

Bueche theory postulates an enhanced tensile strength if the particulate filler can redistribute the stresses after the rupture of an elastomer chain. By absorbing this energy catastrophic failure of the sample is prevented. Implicit in this theory is the need for elastomer-filler attachments which is a condition uniquely fulfilled by the SBS block copolymers.

The network properties and high tensile strength of K101 can be attributed to the dual action of the dispersed polystyrene phase. The polystyrene domains immobilise the ends of the polybutadiene segments. This effectively results in many permanent entanglements in the rubbery phase. The network structure of the K101 as discussed in Section 5.4 consists of permanent and temporary

entanglement crosslinks in the polybutadiene phase, physical adsorption crosslinks of the polybutadiene chains at the domain surface and also polystyrene-polybutadiene junctions. As noted above in this section, the polystyrene domains behave similarly to reinforcing filler particles and as such they can redistribute the stresses after the rupture of an elastomer chain thus prolonging the time for catastrophic failure and increasing the ultimate strength of the sample.

5.6 RELAXATION PROCESSES

The main features of the plots of stress relaxation rate S, versus extension at various temperatures for toluene and methylene chloride cast samples shown in Figures 4.28 and 4.29 are

(a) At 14% extension the toluene cast samples have a lower relaxation rate than the methylene chloride cast samples. This difference is more pronounced at lower temperatures. The higher relaxation rate of the methylene chloride cast samples is associated with the polystyrene network.

(b) At extensions $\geq$ 40% the methylene chloride cast samples have a slightly lower relaxation rate than the toluene cast samples. At temperatures $\leq 40^{\circ}C$ the relaxation rate for both samples is independent of extension from 40% to 300%. Under such conditions the relaxation of the material originates mostly in the polybutadiene matrix.

(c) At temperatures $\geq 50^{\circ}C$ the relaxation rate increases for both samples at higher extensions owing to the increased mobility of the polystyrene domains. In fact, increased temperature gives an increase in relaxation rate at all extensions for both samples.

Gent (100) has reported that the carbon black filled SBR vulcanizates show a sharp decrease in rate of stress relaxation from very low extension to 25% extension and an almost constant low relaxation till about 300% extension at which the relaxation begins to increase again. Natural rubber gum vulcanizates show very low relaxation rates ($\sim$ 2% per decade of time) at extension to 200%. At higher extensions the rate increases to $\sim$ 6% due to increase crystallinity in the sample. The other extreme is evidenced by unfilled Butyl rubber vulcanizates in which the relaxation rates fall

off at higher elongation ($\sim$ 300%). It is thus observed that the stress relaxation behaviour of the SBS block copolymer follows most closely to that of the SBR vulcanizate with reinforcing fillers.

The stress relaxation rate for K101 between extensions of 40% to 300% at 30 and 40°C is determined to be 10-12% per decade of time. Smith and Dickie (153) by plotting the logarithm of the temperature-reduced true stress against logarithmic time derived from stress-strain data of K101 at different extension rates and temperatures arrived at a relaxation rate of 8% per decade of time. This relaxation rate was independent of temperature below 40°C and also independent of extension for $1{\cdot}2 < \lambda \leq 5$. Similarly, Childer and Kraus (203) also reported a relaxation rate of about 10-11% per decade of time from -25° to +25°C for a SBS block copolymer containing 34% by weight of styrene.

The shape of the stress-strain curve suggests that creep in SBS block copolymer will be pronounced under certain conditions. This follows from the fact that after the initial high slope in the stress-strain curve up to an extension of $\sim$ 20% the strain is observed to increase markedly with only a small rise in stress up to an extension of about 300 to 400%. From Table 4.4 it is observed that the rates of creep for temperatures from 30 to 50°C follow a similar pattern when plotted against % elongation after one minute from the application of a load. At an extension $\leq$ 14% and $\geq$ 300% the rate of creep is low. This could be associated with the high slope of the stress-strain curve in these regions. A pronounced high creep rate is observed at extensions in the plateau region of the stress-strain curve.

As discussed in Section 2.7, Gent (93) has derived a relationship between the rate of stress relaxation (S) at a constant deformation and the rate of creep (C) under a constant load

$$C = AS \qquad (2.52)$$

where $A = (\sigma/e)(\partial e/\partial \sigma)_t$ (2.53)

σ is the stress corresponding to the extension e; $(\partial e/\partial \sigma)_t$ is the slope of the stress-extension relation. The factor A may thus be obtained from the experimentally-determined stress-extension relation.

TABLE 5.5 RELATIONSHIP BETWEEN RATES OF STRESS RELAXATION AND CREEP FOR TOLUENE CAST K101 SAMPLES

Temp (°C)	$\lambda = (1 + e)$	Experimental		Calculated
		S,%/dec.	C,%/dec.	C,%/dec.
30	1·13	10·8	20·1	12·6
	1·41	9·0	87·5	13·8
	1·96	8·6	51·8	15·6
	4·14	7·8	23·5	13·0
40	1·14	14·0	27·6	16·8
	1·45	13·2	79·7	20·7
	1·94	12·6	63·8	22·9
	4·42	12·0	25·8	18·2
50	1·13	21·6	46·8	25·2
	1·43	19·2	133 4	29·8
	1·88	19·4	154·8	34·9
	4·13	25·1	45·6	41·9

As shown in Table 5.5, the experimental values of C and the calculated values of C using Equations 2.52 and 2.53 are observed to differ at all extensions and temperatures. Thus it appears that the relaxation processes involved in the K101 block copolymer at the above test conditions are more complicated than that predicted by Gent (93) for conventional gum and filled vulcanizates. However, it is noted

that the rate of creep for the K101 block copolymer is considerably greater than that observed with conventional vulcanizates. Natural rubber gum vulcanizates show a creep rate of about 4% per decade at ambient temperatures (204), whereas K101 has a creep rate of 20% per decade at extensions in the high slope regions and 90-50% per decade at extensions in the plateau region of the stress-strain curve. The high-stress relaxation and creep rates of K101 suggest that the relaxation processes involved the progressive failure of the physical adsorption bonds of the polybutadiene chains at the domain surface and to a lesser intensity the molecular rearrangement of the elastomeric chains and the glassy domains towards equilibrium in the system. At the higher temperatures it would possibly include the deformation of the domains and the slipping of the polystyrene chains from the domains.

Gent (93) has observed that the rates of creep for many vulcanizates very between 5 and 22% per decade, depending upon the type of deformation. The deformation involving simple extension gives the highest value and that involving the sidewise deflection of a clamped strip gives the lowest value. On the other hand, the stress relaxation rate is independent of the type of deformation. In this work the deformation is that of simple extension. This would contribute to the high experimental creep rates obtained as compared to the calculated creep rates from the stress-relaxation rates. There is also error from the experimentally-determined stress-strain relation and the graphical method employed in deriving the quantity A. As such, the conclusion to be drawn from Gent's treatment of the stress relaxation and creep data is subject to uncertainty.

5.7. POLYMERIZATION AND COPOLYMERIZATION OF CYCLIC ETHERS

The polymerizability of cyclic ethers has been discussed in some details in Section 2.9. For three and four membered rings the free energy change of polymerization ΔG is determined primarily by the enthalpy change ΔH which is related to ring strain and crowding of eclipsed adjacent hydrogen atoms. Whereas for the five, six and seven membered rings, the enthalpy and the entrophy (ΔS) contributions are both important. The three thermodynamic parameters are related according to Equation 5.1.

$$\Delta G = \Delta H - T\Delta S \qquad (5.1.)$$

TABLE 5.6. Thermodynamic Parameters involved in the Polymerization of Cyclic Ethers at 298°K.

Monomer	ΔS (e.u.)	ΔH (kcal./mole)	ΔG (kcal./mole)
Ethylene oxide	-18.7	-22.6	-17.0
Oxetane	-15.9	-19.3	-14.6
3,3-bis(chloromethyl) oxetane	-19.9	-20.2	-14.0
Tetrahydrofuran	-10.2	-3.5	- 0.5
Tetrahydropyran	- 1.1	+1.3	+ 1.6
Tetramethylene formal	- 0.7	-4.7	- 4.5
Pentamethylene formal	+ 4.8	-12.8	-14.2

As shown in Table 5.6., the polymerization of three and four membered cyclic oxides has a large negative ΔH and polymerization occurs readily, probably largely due to ring strain. Tetrahydrofuran (THF) also has a negative ΔH but it is much smaller and THF polymerizes less readily than three and four membered rings. Its polymerizability probably results from repulsions of eclipsed hydrogens. (208) Tetrahydropyran which has a positive ΔH, has not been reported to polymerize. ΔH decreases again for rings larger than six members. Both the seven membered and eight membered cyclic formal are known to polymerize. (209, 210)

In this study, the cyclic ethers of interest are THF and a substituted oxetane, namely 3, 3-bis (chloromethyl) oxetane (BCMO). By thermodynamic considerations, both are polymerizable. However in addition to thermodynamic feasibility, in order for polymerization to occur, there must be a suitable reaction mechanism to induce the ring opening process. Many initiators have been reported for the polymerization of BCMO and THF. (40, 121, 123, 211, 212). In general, the polymerization proceeds by a cationic mechanism.

The catalyst p-chlorophenyl diazonium hexafluorophosphate (PCDHP) is found to be an effective initiator for the polymerization both THF and BCMO. It is convenient to handle and easily purified by recrystallization. However it has a limited solubility in both the monomers and also the solvent, o-dichlorobenzene. The upper concentration of PCDHP in THF is about 20×10^{-3}M, as has been reported by Dreyfussand Dreyfuss (38). High molecular weight poly (THF), using PCDHP as initiator was first obtained by Dreyfuss and Dreyfuss (38). The system was apparently free from termination reactions, although the evidence on this issue was not conclusive.

The reaction mechanisms for the THF polymerization have been presented as follows:

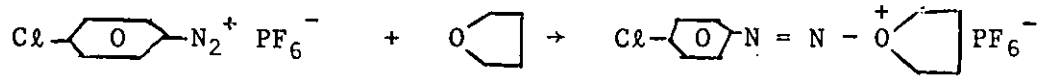

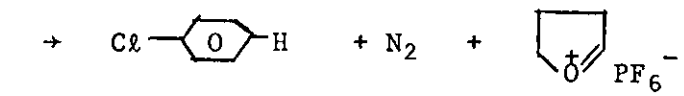

(5.2.)

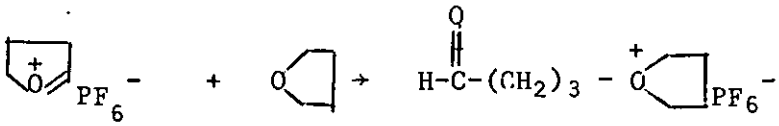

(5.3.)

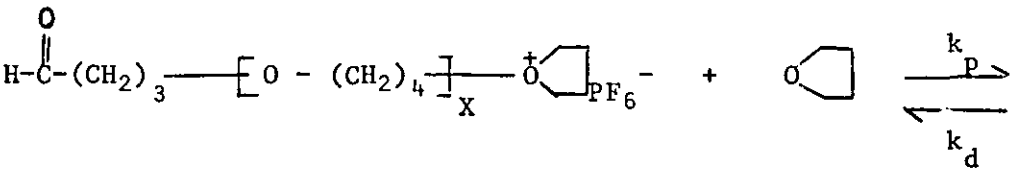

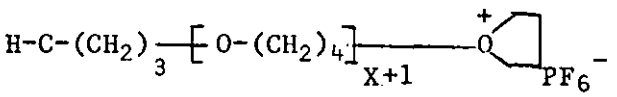

(5.4.)

As has been discussed in Section 2.9., in addition to reaction with monomer oxygen and penultimate polymer chain oxygen, the polymeric cyclic oxonium ion can also react with other ether oxygen atoms distributed randomly in the system. Redistribution reactions of this kind, which occur intermolecularly rather than intramolecularly, would lead to a change in molecular weight distribution for the particular polymeric product.

Termination reactions for this type of system must involve the destruction of active centres. Perhaps the most obvious method for chain termination during polymerization would be by anion recombination e.g.

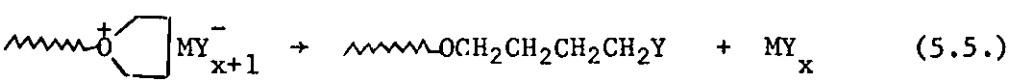

(5.5.)

However polymerization systems having perfluoro anions such as BF_4^-, PF_6^- and SbF_6^- appear to be the most stable and have been reported to demonstrate lack of termination and thus establish a 'living' cationic polymerization. (38,140,141).
Clearly the system must be free of other impurities such as water which could also terminate the reaction.

Szware (213) was the first to give the name 'living' to polymerization systems which are free of termination reactions and in which propagation will continue until the supply of monomer is exhausted. Most of the 'living' systems investigated so far are anionic. One of the consequences of a 'living' system is that when all the chains are initiated more or less simultaneously they will possess a narrow molecular weight distribution. (Poisson distribution) as predicted by Flory (214). This requires a high ratio of initiation to propagation rates, an absence of chain transfer reactions, equilibrium strongly favouring the polymeric species and rigorous exclusion of substances capable of terminating chains. Another consequence of the 'living' system is that upon addition of further monomer to a polymerization at equilibrium, polymerization will continue on the exisiting chains until an equilibrium is again reached at a higher molecular weight. If another monomer is added, polymerization again continues, and a block copolymer is formed.

This is basically the method of production of the SBS thermoplastic elastomers. For the SBS block copolymers, the presence of even 1 to 2% of SB diblocks due to incomplete block polymerization will have a noticeable effect in decreasing the tensile strenght. The SB diblocks presumably leads to 'network defects', in having one free butadiene end. Thus rigorous exclusion of impurities is of utmost important. Also the creep properties of the SBS block copolymers is extremely unsatisfactory. Creep is highly

manifest during substained deformation, at temperatures as low as 60 - 70°c (40 - 30°c below the Tg of the polystyrene). The Tg values of the terminal polymer segments in the block copolymers serve as an approximate guide to the physical behaviour of the network structure. An improvement on the physical properties can be achieved by changing the Tg value of the polymer used in the terminal segment (e.g. poly-α-methylstyrene has Tg$\sim$170°c) or by arranging that the terminal polymer segments are crystalline polymers of more definite melting point. These changes would give rise to better processing characteristics and higher effective service temperatures. Thus it is desirable to synthesize a block copolymer of the type XYX where X is a crystalline segment and Y is an elastomeric segment at ambient temperatures.

Both THF and BCMO are polymerized to reasonable high molecular weight polymers using PCDHP as initiator. Poly(THF) is crystalline and has a Tg$\sim$ - 53°c (100Hz) (163,215) and a Tm$\sim$ 40 - 50°c(126)

Whereas poly (BCMO) has a Tg = + 25°c (89 Hz) (216) and a Tm$\sim$180°c (217). Hence, using poly (BCMO) instead of poly (THF) as the end blocks in the XYX block copolymer would extend the upper limit of the use temperature as an elastomer considerably. The ring strain in BCMO is much higher than in THF and due to this difference, the polymer-monomer equilibrium during polymerization is much less pronounced in the former case than in the later. This would lead to a high conversion of BCMO monomer to polymer, even at relatively high temperature. However BCMO is extremely insoluable in all the usual organic solvents at room temperature. At elevate temperatures, a few highly polar solvents such as cyclohexanone, ethylene acetate, isophorone and diethylene glycol monoethyl ether acetate will dissolve it, at low concentration. It was difficult to find a solvent for solution polymerization of BCMO under homogeneous condition. It was observed during bulk

polymerization, the polymer preciptated out of its own monomer, even at the early stage of the polymerization. Various solvents were found unsuitable.
Cyclohexanone dissolves poly (BCMO) at above 60°c but it reacts with the initiator (PCDHP), giving a brightly red solution. It should be noted that polar solvents would lower the reaction rate and the yield of polymer, in ionic polymerization. The solvent, o-dichlorobenzene, used in this study, dissolves the polymer at low concentration and at high temperature (above 90°c). The boiling point of the solvent is 180 - 3°c. The solution polymerization carried out gave yield of about 50%. The polymer was observed to precipitate out of solution during polymerization at 60°c. Further synthesis works should include the search for a suitable solvent for homogeneous polymerization of BCMO.

Few, if any, homopolymers from cyclic ethers are elastomeric at ambient temperatures. Both poly(BCMO) and poly(THF) show the properties of crystalline materials.

One the other hand, copolymerization of mixtures of cyclic ethers readily produces a whole range of elastomers. Any process which can be used to effect homopolymerization of one or other cyclic ether can in principle - and usually also in practice - be used to bring about copolymerization of mixtures.

Copolymers of THF and BCMO were obtained using PCDHD as initiator. The copolymers obtained were waxy in appearance for monomer mixtures containing 20 and 40 mole-% of BCMO. The waxy appearance and the low conversion -% suggested that the products obtained were of low molecular weight. This is possibly due to low initiator efficiency or presence of impurities. A rubbery product was obtained from a monomer mixture with 55 mole -% of BCMO. All products were completely soluable in chloroform and completely insoluable in methanol. Because the homopolymer of THF is soluable in methanol

and that of BCMO is insoluable in Chloroform, it was concluded that the rubbery products obtained are real copolymers and not mixture of the two homopolymers.

This is also evidenced from the mechanical tan δ- temperature curve (Figure 4.52.) obtained with a vibrating reed apparatus for the rubbery copolymer. As a comparison, the machanical tan δ - temperature curve for poly (THF) obtained by Fielding Russell (163) is included in Figure 4.52. Both the copolymer and poly (THF) display a weak peak at T_{max} 105°c, 102°c respectively. However the dispersion for the poly (THF) is stronger and sharper than that of the copolymer. This dispersion is designated as the γ peak and has been attributed to local mode oscillation of a simple linear polether chain. (163, 215). For poly (BCMO), where the two H atoms at the β-C are replaced by two bulky - $CHC\ell_2$ groups, the γ peak would be suppressed. If the copolymer has long segments of THF, one would expect the γ peak to be of identical strength as that obtained for poly (THF). Thus the weaker and broader peak indicates that the copolymer is random. (Ratio of γ-peak height of the copolymer to the poly(THF) is 4:7).

The glass transition dispersion for the rubbery copolymer is observed to rise slowly at about -50°c. Using the following relation between the Tg's of a random copolymer and the correspodning homopolymers (which have been found to hold in many cases) (218).

$$\frac{1}{T_g} = \frac{W_1}{T_{g_1}} + \frac{W_2}{T_{g_2}} \qquad (5.6.)$$

where T_{g_1} = 220°K for the poly(THF) at 100 Hz (163, 215) and

T_{g_2} = 218°K for poly (BCMO) at 89Hz. (216) W_1 and W_2 are the

weight fractions of poly (THF) and poly (BCMO) respectively. The T_g thus calculated for the rubbery copolymer is $-1^{o}c$. The rubbery copolymer at room temperature has a high damping and the maximum is certainly in the -10 to $+10^{o}c$ region. Increasing the mole-% of the THF monomer in the monomer mixture could lead to a lower T_g for the copolymer, thus giving a more rubbery material at room temperature.

The third stage towards the synthesis of the proposed XYX block copolymer has not been carried out because of lack of time. However it would be of interest to discuss the feasibility of the synthesis. The third stage would involve three steps. Firstly BCMO is homopolymerized to the required molecular weight. The minimum molecular weight for the BCMO segment is that needed by the polymer to form crystalline effectively and to phase separate from the elastomeric phase. Assuming the length of the polymer molecule is about 1000Å for formation of crystallites that could act as effective crosslink for the elastomer chains. The bond lengths for the C-C and C-O links are 1.54 and 1.43 Å respectively. The length of a BCMO molecule is then 5.94 Å . The number of BCMO molecules in a polymer molecule of 1000Å in length is calculated to be 165. So the molecular weight of the required poly(BCMO) is 25,000. The viscosity average molecular weight for the poly (BCMO) prepared by solution polymerization is determined to be about 100,000 (See Section 4.7.), which is a four fold increase over the lower limit set for the effective crystalline of poly (BCMO). It was noted that this polymer precipitated out of solution during polymerization. The solubility of the polymer increases with temperature, dilution and to a certain extent with decreasing molecular weight of the polymer. So possibly an end block having molecular weight of 25,000 - 40,000 would be more suitable.

The second step involves adding THF monomer to the reaction mixture, consisting of 'living' polymeric BCMO chains and unreacted BCMO monomer. The amount of the latter could be calculated from the % conversion - time plots at various conditions. The amount of THF added is such that the resulting monomer composition would produce a rubbery material at ambient temperatures. Since THF monomer has a boiling point of 65^{o}c and the temperature of the polymerizating reactor is 60^{o}c, the upper part of the reactor should be cooled in order to trap the vaporized THF monomer back into the reaction mixture.

According to the mechanism of propagation via tertiary oxonium ions, which was proposed for the homopolymerizations of oxetanes (220) and of THF (219), the following four steps can be formulated for the propagation of the copolymerization of THF and BCMO.

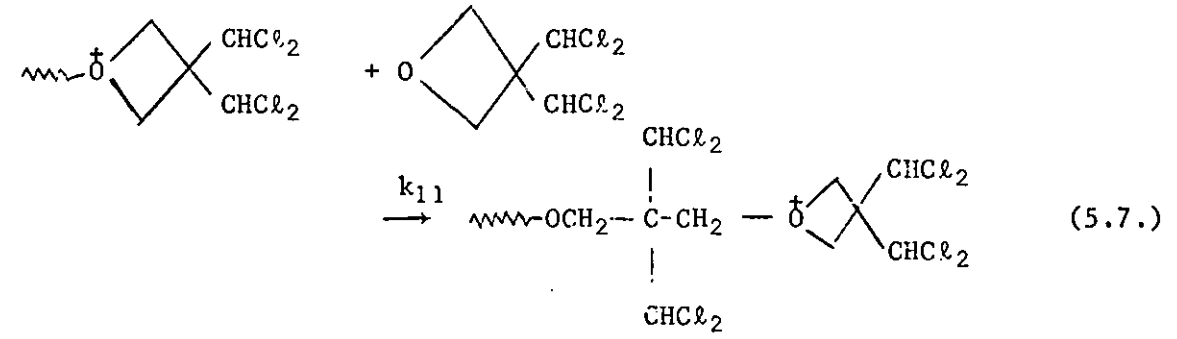

(5.7.)

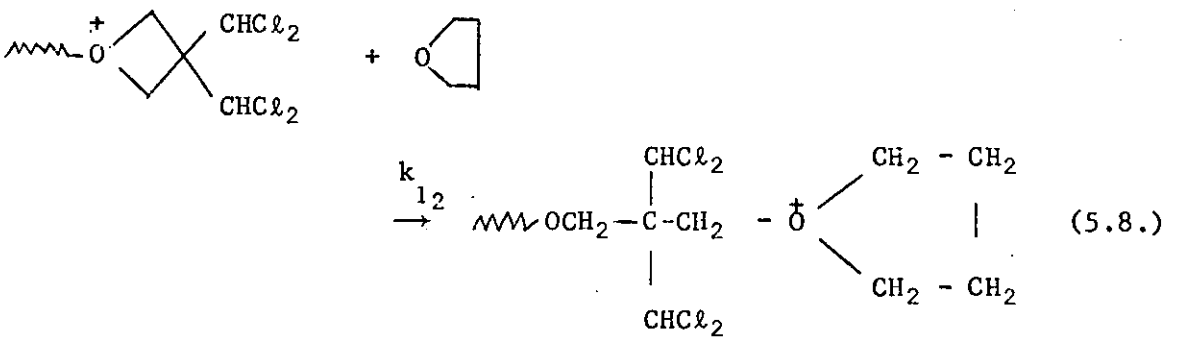

(5.8.)

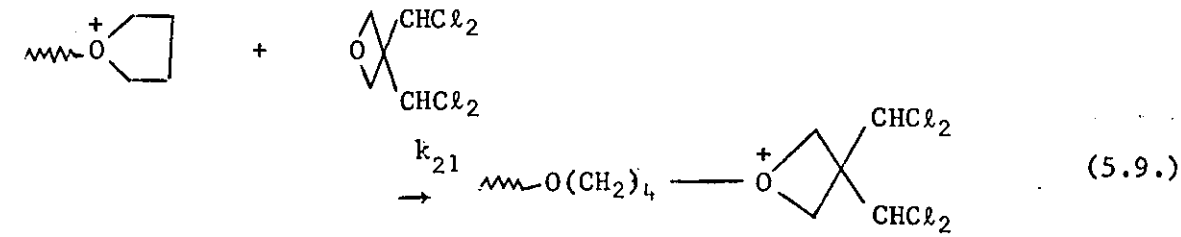

(5.9.)

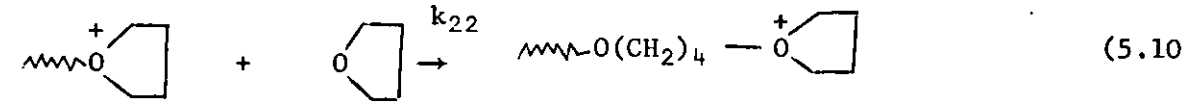

(5.10.)

Further work should include determination of the monomer reactivity ratio k_{11}/k_{12} and k_{22}/k_{21}. Also replacing THF with another cyclic ether, possibly a 7-membered or 8-membered ring which has higher ceiling temperature is worth considering.

The third step is that of adding further BCMO monomer to the 'living' ends of the BCMO/THF segments. The polymerization is terminated by adding methanol to the reaction mixture. Each step is given a designed period of time before proceeding to the next.

The problems involved in the above synthesis would include the difficulty in vacuum distilling the BCMO monomer into ampoule. The monomer has a boiling point of about 196°c and a melting point of 19°c. The distillation is very slow and the distillate tends to solidify along the connecting tubes. This problem is partially solved with the use of apparatus described in Section 3.11. The removal of unreacted THF monomer at the end of the second step would also pose a problem as it will affect the polymerization of the third segment. However, the work done so far indicate that it is feasible to synthesis the proposed XYX block copolymer.

CHAPTER 6. CONCLUSION

The contribution of the two phases to the mechanical properties of the styrene-butadiene-styrene block copolymers is dependent upon their morphology, which is in turn dependent upon the thermal or solution treatment of the polymer.

The model that emerges from the SAXS studies of the toluene cast sample is that of an ideally dispersed system of spherical polystyrene domains. The domains are arranged in simple cubic lattices, randomly oriented in the matrix. The interdomain spacing is 300 Å and the spheres are of diameter 240 Å. The dynamic mechanical properties are in line with those predicted from this model.

For the methylene chloride cast sample, the structure is still highly ordered as evidenced by SAXS studies, but no longer with cubic symmetry. Mechanical properties demand the polystyrene phase is highly coupled, the interdomain distance is increased to 345 Å. The dynamic mechanical spectra and the high strain properties indicate that some of the polystyrene phase exist as oriented links between the domains.

In the toluene and methylene chloride swollen/deswollen samples, in which any polystyrene links originally present were broken by the swelling and deswelling processes, the SAXS patterns and the dynamic mechanical spectra are identical to those of the toluene cast sample. The mechanical properties of the moulded sample are close to those of the methylene chloride cast sample but the SAXS pattern indicates a higher interdomain distance of 412 Å.

The elastic modulus of the SBS block copolymers is sensitive to the type of measurement used in its determination. At low strains,

as in dynamic mechanical measurements, the domain morphology is the dominating factor. For the toluene cast sample, all entanglements in the network contribute as effective crosslinks at low strains. The entanglements in the network structure of K101 are the temporary and permanent entanglements of the polybutadiene chains, the adsorption of the polybutadiene chains onto the domain surface and the polystyrene-polybutadiene junctions. In large strain and swelling measurements, the dominant factors contributing to the elastic modulus are the permanent entanglements in the rubbery phase and the filler effect of the domains.

The stress-strain curves of K101 display a high slope at low extensions, followed by a plateau region between $\sim$ 20 to 300% extension and a sharp upturn in the region immediately preceding the breaking strain. The ultimate properties are dominated by the polybutadiene matrix but are highly enhanced by the polystyrene domains. The polystyrene colloid domains appear to behave similarly to reinforcing filler particles up to temperatures at which the polystyrene blocks soften. The stress-strain behaviour and ultimate properties of K101 are highly temperature dependent, especially at temperatures close to the T_g of polystyrene.

The stress relaxation behaviour of SBS block copolymers follow most closely to that of the SBR vulcanizates with reinforcing fillers. The rate of stress relaxation at low extensions is sensitive to the morphology of the sample. A higher rate is observed for the methylene chloride cast sample than the toluene cast sample at low extensions. The stress relaxation rate for K101 at $1{\cdot}40 \leq \lambda \leq 3{\cdot}00$ is found to be 10-12% per decade of time at ambient temperatures.

The creep behaviour of K101 is extremely unsatisfactory as compared to that of the conventional vulcanizates. Extremely

high creep rate is observed, especially for extensions corresponding to the plateau region of the stress-strain curve.

Poor correlation is found between the rates of stress relaxation and creep as given by the Gent's equation.

The catalyst p-chlorophenyl diazonium hexafluorophosphate is found to be an effective initiator for the polymerisation of both THF and BCMO. A highly viscoelastic random copolymer of THF and BCMO is obtained using PCDHP as initiator. The synthesis of the XYX type block copolymer where X is a crystalline segment (poly BCMO) and Y is an elastomeric segment (THF/BCMO copolymer) is discussed and concluded to be feasible on the evidence of the preliminary synthesis work carried out.

APPENDIX I.

BENDING OF UNIFORM BEAM FIXED AT BOTH ENDS

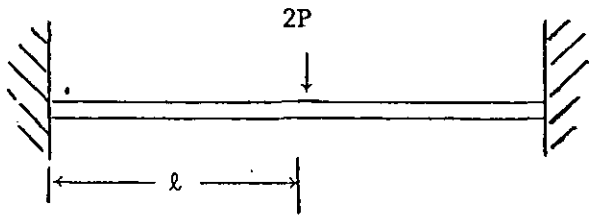

For a uniform beam fixed at both ends and subject to a vertical load at the centre, the Young modulus, E, of the beam is given as (171)

$$E = \frac{P\ell^3}{4\delta I}\,\eta(u), \tag{A.1}$$

where

$$\eta(u) = \frac{u - \tanh u}{u^3} \tag{A.2}$$

$u = \ell/2\sqrt{(S/EI)}$, S is the axial force in the beam and I is the moment of inertia.

δ is the deflection at the centre of the beam.

In the limit of $u = 0$, we have

$$\eta(u) = \lim_{u\to 0}\left\{\frac{u - \tanh u}{u^3}\right\} = \frac{1}{3} \tag{A.3}$$

We measure $E_{effective}$, given as

$$E_e = \frac{P\ell^3}{12\delta I} \tag{A.4}$$

Hence the question is for what ranges of P and δ will E approximate to $\frac{P\ell^3}{12\delta I}$ say, to within 4%.

For different values of u, we have

u	$\eta(u)$	u	$\eta(u)$
0	0·333333	0·20	0·328085
0·01	0·333320	0·30	0·321755
0·02	0·333280	0·40	0·313297
0·05	0·333000	0·50	0·303063
0·10	0·332005	0·60	0·291437
0·15	0·330360	1·00	0·238406

For $u = 0{\cdot}30$, $\eta(u) = 0{\cdot}321755$, which is less than 4% error on 0·333333.

The deflection δ and the load P are defined as follows: (171)

$$\delta = 2\left(\frac{2I}{A}\right)^{\frac{1}{2}}(u - \tanh u)\left(\frac{3}{2} - \frac{1}{2}\tanh u - \frac{3}{2}\frac{\tanh u}{u}\right)^{-\frac{1}{2}} \qquad (A.5)$$

$$P = \frac{8EI(2I/A)^{\frac{1}{2}}}{\ell^3}\, u^3\left(\frac{3}{2} - \frac{1}{2}\tanh^2 u - \frac{3}{2}\frac{\tanh u}{u}\right)^{-\frac{1}{2}} \qquad (A.6)$$

where $I = \frac{bh^3}{12}$, $A = bh$

Hence for $E = 10^6$ dynes/cm^2 (rubbery materials) and $E = 5 \times 10^{10}$ dynes/cm^2 (glassy material) and various dimensions of the test beam, we have

E (dynes/cm^2)	b (cm)	h (cm)	ℓ (cm)	Maximum values for 4% error	
				P (dynes)	δ (cm)
10^6	0·6	0·1	1·5	4·3	0·02342
10^6	1·0	0·1	1·5	7·2	0·02342
10^6	1·0	0·3	1·5	$5·8 \times 10^2$	0·07026
10^6	1·0	0·3	1·0	$2·0 \times 10^3$	0·07026
5×10^{10}	0·6	0·1	1·5	$2·1 \times 10^5$	0·02342
5×10^{10}	1·0	0·1	1·5	$3·6 \times 10^5$	0·02342
5×10^{10}	1·0	0·3	1·5	$2·9 \times 10^7$	0·07026
5×10^{10}	1·0	0·3	1·0	$1·0 \times 10^8$	0·07026

For the beam,

the restoring force $Ek = 2P/\delta$ (A.7)

where k is the geometrical factor for the beam.

Equating (A.7) with (A.4) and substituting $I = bh^3/12$, we have

$$k = \frac{2bh^3}{\ell^3} \quad . \tag{A.8}$$

APPENDIX II

GEOMETRICAL CONDITIONS FOR BENDING

A sample of length 2ℓ, width b, and thickness h, is clamped at both ends to fixed supports. The sample is deformed at its centre by a small static force F, acting perpendicular to its length. The displacement of its centre in the direction of the force is δ. The deflection δ_B, due to bending is, in this case, given by (172):

$$\delta_B = \frac{F\ell^3}{12EAk^2} \tag{A.9}$$

where E is Young's modulus for the material, A the cross-sectional area of the mounting and k is the radius of gyration of the cross-section about the neutral axis of bending.

The deflection δ_S, due to shearing is given by (173):

$$\delta_S = \frac{F\ell}{AG} \tag{A.10}$$

where G is the modulus of rigidity of the sample.

For rubbers, $G = \frac{1}{3}E$, and since the total displacement δ is the superposition of the displacements due to bending and shearing, we have

$$\delta = \delta_B + \delta_S = \frac{F\ell}{AE}\left(\frac{\ell^2}{12k^2} + 3\right) \tag{A.11}$$

Regarding the deformation purely as due to bending, we have

$$\delta = \frac{F\ell^3}{12E'Ak^2} \tag{A.12}$$

where E' is the apparent modulus.

From Equations (A.11) and (A.12), the true and apparent moduli are connected by the relation

$$E' = E\left(\frac{1}{1 + 36k^2/\ell^2}\right) \tag{A.13}$$

$k^2 = h^2/12$ for a rectangular beam sample, thus

$$E' = E\left(\frac{1}{1 + 3h^2/\ell^2}\right) \tag{A.14}$$

If $3h^2/\ell^2 \ll 1$, the conditions in the mounting approximate closely to simple bending and $E' = E$. For Poisson's ratio ν, of 0·35 and 0·20, we have respectively,

$$E' = E\left(\frac{1}{1 + 2{\cdot}7h^2/\ell^2}\right) \tag{A.15}$$

and

$$E' = E\left(\frac{1}{1 + 2{\cdot}4h^2/\ell^2}\right) \tag{A.16}$$

Thus for various values of ℓ, h and ν, the ratio E'/E are given as follows:

ν	h(cm)	ℓ(cm)	E'/E
0·50	0·1	1·5	0·99
	0·1	1·0	0·98
	0·2	1·5	0·95
	0·3	1·5	0·89
0·35	0·1	1·5	0·99
	0·3	1·5	0·90
0·20	0·1	1·5	0·99
	0·3	1·5	0·91

REFERENCES

1. W.J. Burlant and A.S. Hoffman, Block and Graft Copolymers, Reinhold, New York, 1960.

2. R.J. Ceresa, Block and Graft Copolymers, Butterworths, Washington, 1962.

3. H.A.J. Battaerd and G.W. Tregear, Graft Copolymers, Interscience, New York, 1967.

4. M. Szwarc, M. Levy, and R. Milkovich, J.Am.Chem.Soc., 78, 2656 (1965).

5. S. Schlick and M. Levy, J.Phys.Chem., 64, 883 (1960).

6. P. Rempp, V.I. Volkov, J. Parrod and C. Sadron, Bull.Soc. Chim. France, 919 (1960).

7. G. Greber and J. Tölle, Makromol.Chem., 53, 208 (1962).

8. G. Greber, Makromol.Chem., 101, 104 (1967).

9. G. Holden and R. Milkovich, Belg.Pat. 627, 652 (July 29, 1963); Chem.Abstr., 60, 14714f (1964).

10. G. Holden, E.T. Bishop, N.R. Legge, Proceedings of the Internat. Rubb.Conf., Maclaren and Sons, London (1967), p 287.

11. J.T. Bailey, E.T. Bishop, W.R. Hendricks, G. Holden and N.R. Legge, Rubber Age, 98, 69 (1966).

12. R.D. Deanin, S.P.E.J., 23, 45 (1967).

13. S.L. Aggarwal, Ed., Block Polymers, Plenum Press, New York, 1970.

14. S.L. Copper and A. Tobolsky, Textile Res.J., 36, 800 (1966).

15. S.L. Copper and A. Tobolsky, J. Appl.Poly.Sci., 10, 1837 (1966).

16. S.L. Copper and A. Tobolsky, J. Appl.Poly.Sci., 11, 1361 (1967).

17. S.L. Copper, D.S. Huh and W.J. Morris, Ind.Eng.Chem.Res. and Dev., 7, 248 (1968).

18. S. Bonotto and R.K. Walton, Mod.Plastics (5), 143 (1963).

19. C.S. Schollenberg, U.S. Patent 2,871,218, (January, 1959).

20. A.E. Skoulious, G. Tsoulandje and E. Franta, J.Poly.Sci., C-4, 507 (1963).

21. E. Franta, A. Skoulious, P. Rempp and H. Benoit, Die Makromol. Chemie, 87, 271 (1965).

22. C. Sadron, G. Finaz and A. Skoulions, French Patent 1,295,524, (1963).

23. L.J. Fetters and M. Morton, Macromolecules, 2, 453 (1969).

24. G. Karoly, See Reference (13), p. 153.

25. E.P. Goldberg, J.Poly.Sci., C-4, 707 (1963).

26. S.H. Merrill, J.Poly.Sci., 55, 343 (1961).

27. K.P. Perry, W.J. Jackson Jnr., and J.R. Caldwell, J.Appl.Poly. Sci., 9, 3451 (1965).

28. R.L. Merker, M.J. Scott and G.G. Haberland, J.Poly.Sci., A-2, 31 (1964).

29. M. Szwarc, Makromol.Chem., 35, 132 (1960).

30. D.H. Richards and M.Szwarc, Trans.Faraday Soc., 55, 1644 (1959).

31. L.J. Fetters, J.Res.Natl.Bur.Std., 70A, 421 (1966).

32. C. Sadron, Angew Chem., 75, 472 (1963).

33. B. Gallot, B. Mayer and C. Sadron, Compt.Rend.Acad.Sci. Paris, 263C, 42 (1966).

34. E. Vanzo, J.Poly.Sci., A1-4, 1727 (1966).

35. A.V. Tobolsky and A. Rembaum, J.Appl.Poly.Sci., 8, 307 (1964).

36. R.J. Angelo, R.M. Ikeda and M.L. Wallach, Polymer, 4, 141 (1965).

37. M. Bear, J.Poly.Sci., A-2, 417 (1964).

38. M.P. Dreyfuss and P. Dreyfuss, J.Poly.Sci., A1-4, 2179 (1966).

39. T. Saegusa, H. Imai and J. Furakawa, Makromol.Chem., 56, 55 (1962).

40. J. Furukawa and T. Saegusa, Polymerization of Aldehydes and Oxides, Interscience, New York (1963), Chp. IV.

41. A.C. Farthing, J.Appl.Chem. 8, 186 (1958).

42. T. Alfrey, Mechanical Behaviour of High Polymers, Interscience, New York, 1948.

43. P.J. Flory, Principles of Polymer Chemistry, Cornell University Press, New York, 1953.

44. L.R.G. Treloar, The Physics of Rubber Elasticity, 2nd.Ed., Clarendon Press, Oxford, 1958.

45. R.S. Rivlin, Rheology, Vol.I, Academic Press, New York, 1956.

46. L.R.G. Treloar, Proc.Royal Soc. (London), B139, 506 (1952).

47. R.S. Rivlin and D.W. Saunders, Phil.Trans.Roy.Soc., A243, 251 (1951).

48. S.M. Gumbrell, L. Mullins and R.S. Rivlin, Trans.Faraday Soc., 49, 1495 (1953).

49. A. Ciferri and P.J. Flory, J.Appl.Phys., 30, 1498 (1959).

50. A.E.H. Love, A Treatise on the Mathematical Theory of Elasticity, 4th Ed., Cambridge University Press, New York, 1927.

51. H. Lamb, Hydrodynamics, Dover, New York, 1945.

52. L. Boltzmann, Prog.Ann.Erg., 7, 624 (1876).

53. B. Gross, Mathematical Structure of the Theories of Viscoelasticity, Hermann, Paris, 1953.

54. H. Leaderman, Rheology, Theory and Applications, Ed., F. Eirich, Vol. II, Academic Press, New York, (1958), Ch. 1.

55. H. Leaderman, Elastic and Creep Properties of Filamentous Materials, Textile Foundation, Washington, 1943.

56. D.R. Bland, The Theory of Linear Viscoelasticity, Pergamon, London, 1960.

57. E. Wiechert, Ann.d.Phys., 50, 335 (1893).

58. J.J. Thomson, Applications of Dynamics to Physics and Chemistry, Macmillan, London, (1888), Ch.8.

59. J.D. Ferry, Viscoelastic Properties of Polymers, 2nd. Ed., Wiley, New York, 1970.

60. M.G. Sharma, Testing of Polymers, Vol. I, Ed., J. Schmitz, (1965), p. 148.

61. R.B. Blizard, J.Appl.Phys., 22, 730 (1951).

62. B. Gross and R.M. Fuoss, J.Poly.Sci., 19, 39 (1956).

63. B. Gross, J.Poly.Sci., 20, 123 (1956).

64. F. Bueche, J.Chem.Phys., 22, 603 (1954).

65. P.E. Rouse, J.Chem.Phys., 21, 123 (1956).

66. P.E. Rouse and K. Sittel, J.Appl.Phys., 24, 690 (1953).

67. B.H. Zimm, J.Chem.Phys., 24, 269 (1956).

68. R. Cerf, Adv.Poly.Sci., 1, 382 (1959).

69. See Reference (59), p. 247.

60. H. Leaderman, Textile Res.J., 11, 171 (1941).

71. A.V. Tobolsky and R.D. Andrews, J.Chem.Phys., 11, 125 (1943); J.Poly.Sci., 3, 669 (1948).

72. A.V. Tobolsky, Properties and Structures of Polymers, Wiley, New York, 1960.

73. J.D. Ferry, J.Amer.Chem.Soc., 72, 3746 (1950).

74. J.D. Ferry, E.R. Fitzgerald, M.F. Johnson and L.D. Grandine, J.Appl.Phys., 22, 717 (1951).

75. M.L. Williams, R.F. Landel and J.D. Ferry, J.Amer.Chem.Soc., 77, 3701 (1955).

76. E.R. Fitzgerald, L.D. Grandine and J.D. Ferry, J.Appl.Phys., 24, 650 (1953).

77. L.D. Grandine and J.D. Ferry, J.Appl.Phys., 24, 679 (1953).

78. M.L. Williams and J.D. Ferry, J.Colloid Sci., 9, 479 (1954).

79. W.C. Child and J.D. Ferry, J.Colloid Sci., 12, 327 (1957).

80. H. Smallwood, J.Appl.Phys., 15, 758 (1944); Rubb.Chem.Technol., 21, 667 (1948).

81. A Einstein, Ann.Physik, 19, 289 (1906); 34, 1591 (1911).

82. J. Weiss, Trans.Inst.Rubb.Ind., 18, 32 (1942).

83. H. Smallwood, Rubb.Chem.Technol., 18, 892 (1945).

84. E. Guth and O. Gold, Phys.Rev., 53, 322 (1938).

85. L. Cohan, India Rubber World, 117, 343 (1947); Rubb.Chem.Technol., 23, 635 (1950).

86. E. Guth, J.Appl.Phys., 16, 20 (1945); Rubb.Chem.Technol., 18, 596 (1945); Proc.Rubb.Technol.Conf.2nd, Heffer, London, 1948, p 353.

87. E.H. Kerner, Proc.Phys.Soc.London, 69B, 808 (1956).

88. M. Takayanagi, H. Harima and Y. Iwata, Memoirs of the Faculty of Engineering, Kyushu University, 23, 1, August 1963.

89. M. Takayanagi, Proc. 4th.Internat.Cong.on Rheol., Part I, 1965, p. 161.

90. T. Okamoto and M. Takayanagi, J. Appl.Poly.Sci., 23-C, 597 (1968).

91. K. Fujino, Y. Ogawa and H. Kawai, J.Appl.Poly.Sci., 8, 2147 (1964).

92. M. Takayanagi, S. Uemura and S. Minami, J.Poly.Sci., 5-C, 113 (1964).

93. A.N. Gent, J.Appl.Poly.Sci., 6, 433 (1962).

94. R.S. Rivlin and J. Saunders, Trans.Faraday Soc., 48, 200 (1952).

95. D.H. Copper, Ind.Eng.Chem.Ed., 43, 365 (1951).

96. J.H. Dillion and I.B. Prethyman, J.Appl.Phys., 16, 159 (1945).

97. S.H. Hahn and I. Gazdik, India Rubber World, 103, 51 (1951).

98. W. Lethersich, Brit.J.Appl.Phys., 1, 294 (1950).

99. W.J. Lyons, J.Appl.Phys., 17, 472 (1946).

100. A.N. Gent, Proc.Rubb.Technol.Conf., 4th. London 1962.

101. C.J. Derham, E. Southern and A.G. Thomas, Internat.Rubb.Conf., Moscow, 1969.

102. A. Dobry and F. Boyer-Kawenoki, J.Poly.Sci., 2, 90 (1947).

103. R.L. Scott, J.Chem.Phys., 17, 279 (1949).

104. H. Tompa, Trans.Faraday Soc., 45, 1142 (1949).

105. C.H. Bamford and H. Tompa, ibid., 4b, 310 (1950).

106. See Reference (43), Ch. 13.

107. W.H. Stockmayer, L.D. Moore, Jr., M. Finman and B.N. Epstein, J.Poly.Sci., 16, 517 (1955).

108. G.E. Molau, J. Poly.Sci., B-3, 1007 (1965).

109. G.E. Molau, J.Poly.Sci., A-3, 4235 (1965).

110. A. Dondos, P. Rempp and H. Benoit, J.Poly.Sci., B-4, 293 (1966).

111. C.M. Burnett, P. Meares and C. Paton, Trans.Faraday Soc., 58, 737 (1962).

112. J.R. Urwin and J.M. Stearne, Makromol.Chem., 78, 194, 204 (1964).

113. S. Krause, J.Phys.Chem., 68, 1948 (1964).

114. J.R. Urwin and J.M. Stearne, Eur.Poly.J., 1, 227 (1965).

115. H. Inagaki, Makromol.Chem., 86, 289 (1965).

116. H. Inagaki and T. Miyamoto, Makromol.Chem., 87, 166 (1965).

117. F.M. Merrett, J.Poly.Sci., 24, 467 (1957).

118. T. Inoue, T. Soen, T. Hashimoto and H. Kawai, J.Poly.Sci., A2-7, 1283 (1969).

119. M. Matso, S. Sagae and H. Asai, Polymer, London, 10(2), 79 (1969).

120. A.M. Eastham, Fortschr.Hochpolymer Forsch, 2, 1 (1960).

121. J.B. Rose, The Chemistry of Cationic Polymerization, P.H. Plesch, Ed., Pergamon, London (1963), Ch. 11.

122. N.G. Gaylord and H.F. Mark, Linear and Stereoregular Addition Polymers, Interscience, New York, 1959.

123. N.G. Gaylord, Polyethers, Part I, Interscience, New York, (1963).

124. F.S. Dainton, T.R.E. Devlin and P.A. Small, Trans.Faraday Soc., 51, 1710 (1955).

125. P.A. Small, Trans.Faraday Soc., 51, 1717 (1955).

126. H. Meerwein, E. Battenberg, H. Gold, E. Pfeil and G. Wilbfang, J.Prakt.Chem., 154, 83 (1939).

127. H. Meerwin, Angew.Chem., 59, 168 (1947).

128. H. Meerwin, D. Delfs and H. Morschel, Angew.Chem., 72, 927 (1960).

129. K. Hamann, Angew.Chem., 63, 231 (1951).

130. C.E.H. Bawn, R.M. Bell and A. Ledwith, Polymer, 6, 95 (1965).

131. C.E.H. Bawn, R.M. Bell, C. Fitzimmonds and A. Ledwith, Polymer, 6, 661 (1965).

132. M.P. Dreyfuss and P. Dreyfuss, Polymer, 6, 93 (1965).

133. R.C. Burrows and B.F. Crowe, J.Appl.Poly.Sci., 6, 465 (1962).

134. D.B. Miller, A.C.S. Polymer Preprints, No. 2, 613 (1966).

135. E.L. Muetterties, T.A. Bither, M.W. Farlow and D.D. Coffman, J.Inorg.Nucl.Chem., 16, 52 (1960).

136. D. Sims, J.Chem.Soc., 864 (1964).

137. E.B. Lyudvig, B.A. Rozenberg, T.M. Zvereva, A.R. Cantmakhers and S.S. Medvedev, Vysokomolekul,Soedin., 7, 269 (1965).

138. Y. Takeyami, T. Ueno and R. Hirai, Bull.Chem.Soc., Japan, 38, 1222 (1965).

139. H. Rausch, Angew.Chem., 72, 927 (1960).

140. P.R. Johnston, J.Appl.Poly.Sci., 9, 461 (1965).

141. C.C. Price and M. Osgan, J.Am.Chem.Soc., 78, 4787 (1956).

142. Y. Yamashita, T. Tsuda, M. Okada and S. Iwatsuki, J.Poly.Sci., A-4, 2121 (1966).

143. T. Saegusa, H. Imai and J. Furukawa, Makromol.Chem., 56, 55 (1962).

144. A. Ishigaki, T. Shono and Y.Hashihama, Makromol.Chem., 79, 170 (1964).

145. L.A. Dickenson, J.Poly.Sci., 58, 857 (1962).

146. M. Okada, K. Sugana and Y. Yamashita, Tetrahedron Letters, No. 28, 2329 (1965).

147. A. Guiner and G. Fournet, Small Angle Scattering of X-rays, John Wiley, New York, 1955.

148. D. Hosemann and S.N. Bagchi, Direct Analysis of Diffraction by Matter, Interscience, New York, 1962.

149. O. Kratky, Angew.Chem., 72, 467 (1960).

150. G. Porod, Fortschr.Hochpolymer,Forsch, 2, 363 (1961).

151. W.D. Statton, Newer Methods of Polymer Characterization, B.Ke, Ed., John Wiley, New York, 1964, Ch. VI.

152. L.E. Alexander, X-ray Diffraction Methods in Polymer Science, John Wiley, New York, 1969.

153. T.L. Smith and R.A. Dickie, J.Poly.Sci. 26-C, 163 (1969).

154. J.F. Beecher, L. Marker, R.D. Bradford and S.L. Aggarwal, J.Poly.Sci., 26-C, 117 (1969).

155. Z.M. Kolthoff, T.S. Lee and C.W. Carr, J.Poly.Sci., 1, 429 (1946).

156. J.A. Brydson, Plastics, 107 (December 1967).

157. K.U. Fulcher, Ph.D. Thesis, University of Loughborough (1970).

158. P.J. Flory and J. Rehner, J.Chem.Phys., 18, 108 (1943).

159. M. Mooney, J.Appl.Phys., 11, 582 (1940).

160. R.E. Wetton, M.Sc. Thesis, University of Manchester (1960).

161. I.J.W. Bowman, Ph.D. Thesis, University of Loughborough (1968).

162. G.S. Fielding-Russell and R.E. Wetton, Plastics and Polymers, 179, (June 1970).

163. G.S. Fielding-Russell, Ph.D. Thesis, University of Loughborough (1967).

164. L.E. Nielsen, Mechanical Properties of Polymers, Reinhold, New York, 1964.

165. W.T. Thomson, Mechanical Vibration, Allen and Unwin, London 1950.

166. M. Morton, R. Milkovich, D.B. McIntyre and J.L. Bradley, J.Poly. Sci., 1-A, 443 (1963).

167. F. Wenger, J.POly.Sci., 60, 99 (1962).

168. W. Lange and E. Müller, Ber., 63, 1058 (1930).

169. G. Kraus, J.Appl.Poly.Sci., 7, 1257 (1963).

170. S. Penczek and P. Kubisa, Die Makromol.Chem., 130, 186 (1969).

171. R. Frisch-Fay, Flexible Bars, Butterworth, London (1962).

172. See Reference (50), p. 230.

173. R.V. Southwell, An Introduction to the Theory of Elasticity, 2nd Ed., Oxford University Press, p. 191.

174. G.A. Harpell and C.E. Wilkes, See Ref. 13, p. 31.

175. P.R. Lewis and C. Price, Nature, 223, 495 (1969).

176. G. Kraus, C.W. Childers and J.T. Gruver, J.Appl.Poly.Sci., 11, 1581 (1967).

177. L.E. Nielsen and R. Buchdahl, J.Appl.Phys., 21, 488 (1950).

178. T.L. Smith, See Ref. 13, p. 137.

179. J.D. Ferry, Physics of Non-crystalline Solids, J.A. Prins, Ed., North-Holland, Amsterdam, 1965, p. 333.

180. T. Inoue, T. Soen, H. Kawai, M. Fakatou and M. Kurata, J.Poly. Sci., 6-B, 75 (1968).

181. H. Hendus, K.H. Illers and E. Roptes, Kollcid-Z, 216-217, 81 (1969).

182. D.J. Meier, J.Poly.Sci., 26-C, 81 (1969).

183. R.F. Fedors, J.Poly.Sci., 26-C, 189 (1969).

184. J.T. Gruver and G. Kraus, J. Poly.Sci., 2-A, 797 (1964).

185. N.K. Adam, The Physics and Chemistry of Surfaces, Oxford University Press, 3rd Edit., 1941, p. 50.

186. See Ref. 59, p. 226.

187. F. Fischer and J.F. Henderson, J.Poly.Sci., 26-C, 149 (1969).

188. G.M. Estes, D.S. Huh and S.L. Cooper, See Ref. 13, p. 225.

189. K. Riches and R.N. Haward, Polymer, 9, 103 (1968).

190. R.D. Andrews and J.F. Rudd, J.Appl.Phys., 28, 1091 (1957).

191. J.C. Halpin, Rubb.Chem.Tech., 38, 1007 (1965).

192. J.C. Halpin and F. Bueche, J.Appl.Phys., 35, 3142 (1964).

193. B.S.T.T. Boonstra, India Rubber World, 121, 299 (1949).

194. T.J. Dudek and F. Bueche, J.Appl.Poly.Sci., 8, 555 (1964).

195. T.L. Smith, J.Poly.Sci., 1-A, 3597 (1963).

196. T.L. Smith, J.Appl.Phys., 35, 3152 (1964).

197. M. Morton, J.C. Healy and R.L. Denecour, Proc.Internat. Rubb. Conf. May 1967, p. 175.

198. J.A.C. Harwood and A.R. Payne, J.Appl.Poly.Sci., 12, 889 (1968).

199. M. Morton, J.E. McGrath and D.C. Juliano, J.Poly.Sci., 26-C, 99 (1969).

200. E.T. Bishop and S. Davison, J.Poly.Sci., 26-C, 59 (1969).

201. L.C. Case, Makromol.Chem., 37, 243 (1960), 39, 119 (1960).

202. F. Bueche, J.Appl.Poly.Sci., 7, 1165 (1963).

203. C.W. Childer and G. Kraus, Rubb.Chem.Tech., 40, 1183 (1967).

204. E.D. Farlie, J.Appl.Poly.Sci., 14, 1127 (1970).

205. F.S. Dainton and K.J. Ivin, Quart.Rev., 12, 61 (1958).

206. F.S. Dainton, K.J. Ivin and D.A.G. Walmsley, Trans.Faraday Soc., 56, 1784 (1960).

207. F.S. Dainton, D.M. Evans, F.E. Hoare and T.P. Melia, Polymer, 3, 271 (1962).

208. H.K. Hall, Jnr., A.C.S. Polymer Preprints, 6, (2), 535 (1965).

209. J.W. Hill and W.H. Carothers, J.Am.Chem.Soc., 57, 925 (1935).

210. A.A. Strepikheev and A.V. Volokhina, Dokl.Akad.Nauk, S.S.S.R., 99, 407 (1954).

211. P. Dreyfuss and M.P. Dreyfuss, Adv.Poly.Sci., 4, 528 (1967).

212. A. Ledwith and C. Fitzsimmonds, Polymer Chemistry of Synthetic elastomers, Part I, J.P. Kennedy and E.G.M. Törnqvist, Interscience, New York, 1968, Ch. 5.

213. M. Szwarc, Fortschr.Hochpolymer.Forsch., 2, 275 (1960).

214. P.J. Flory, J.Am.Chem.Soc., 62, 1561 (1940).

215. R.E. Wetton, Ph.D. Thesis, University of Manchester, (1962).

216. D.J.H. Sandiford, J.Appl.Chem., 8, 188 (1958).

217. A.C. Farthing, J.Chem.Soc., 3648 (1955).

218. L.A. Wood, J.Poly.Sci., 28, 319 (1958).

219. H. Meerwein, D. Delfs and H. Marschel, Angew.Chem., 72, 927 (1960).

220. J.B. Rose, J.Chem.Soc. (London), 542, 546 (1956).

221. T. Alfrey, Mechanical Behaviour of High Polymers, Interscience, New York, 1948, p. 108.

222. A.V. Tobolsky, J.Appl.Phys., 27, 673 (1956).

223. L. Mullins and N.R. Tobin, J.Appl.Poly.Sci., 9, 2993 (1965).

224. F. Bueche and J. Halpin, J.Appl.Phys., 35, 36 (1964).

225. J. Halpin and F. Bueche, J.Appl.Phys., 35, 3133 (1964).

226. J. Halpin, J.Appl.Phys., 35, 3142 (1964).

227. F. Bueche, B.J. Kinzig and C.J. Coven, Poly.Letters, 3, 399 (1965).

228. C.E.H. Bawn and A. Ledwith, Quart.Rev., 16, 361 (1962).

229. W.J.S. Naunton, Ed., The Applied Science of Rubber, Edward Arnold, London, 1961, p. 63.

230. M. Kurata, M. Iwama and K. Kamada, Polymer Handbook, J. Brandrup and E.H. Immergut, Eds., Interscience, New York, 1966, p IV-56.